METALLOCENE AND ZIEGLER-NATTA CATALYZED POLYPROPYLENE UTILIZING 1-HEPTENE

by

MARIETJIE LUTZ

Thesis presented for the degree of

Master of Science (Polymer Science)

at the

University of Stellenbosch

Study Leader:
Dr. A.J. van Reenen

Stellenbosch
December 2001

DECLARATION

I, the undersigned hereby declare that the work contained in this thesis is my own original work and has not previously, in its entirety or in part, been submitted at any university for a degree.

ABSTRACT

This study concerns the copolymerization of propylene with 1-heptene. The percentage of 1-heptene used as co-monomer in the polymerization reactions was varied from 5% to 20% in order to compare a variety of polymers with different percentages of comonomer incorporated. A variety of different catalysts were used for these polymerizations.

Two metallocene catalysts were used: (A) the isospecific catalyst, *rac*-[ethylene *bis*(1-indenyl)]zirconium dichloride (*rac*-$Et(Ind)_2ZrCl_2$) and (B) the silylene-bridged catalyst, *rac*-$Me_2Si(2\text{-}MeBenz[e]Ind)_2ZrCl_2$. Methylaluminoxane (MAO) was used as cocatalyst for these two metallocene catalysts. Another series of polymerization reactions was done using a Ziegler-Natta catalyst, namely $TiCl_3/AlEt_3/SiO_2$.

Characterization of the copolymers included using high temperature gel permeation chromatography (HTGPC) for molecular mass and molecular mass distributions, differential scanning calorimetry (DSC) and dynamic mechanical analysis (DMA) to investigate the thermal and mechanical properties of the copolymers, nuclear magnetic resonance spectroscopy (NMR) for information concerning the microstructures of the copolymers and crystallization analysis fractionation (CRYSTAF) to investigate the short chain branching of the copolymers.

Comparative studies were done on the different catalysts and the polymer properties. The synthesized polymers were also compared with copolymers of propylene with 1-hexene and 1-octene.

OPSOMMING

Hierdie studie behels die kopolimerisasie van propileen met 1-hepteen. Die persentasie van 1-hepteen wat as komonomeer in die polimerisasie-reaksies gebruik is, is van 5% tot 20% gevarieer. 'n Verskeidenheid van verskillende kataliste is gebruik vir hierdie polimerisasies.

Twee metalloseenkataliste is gebruik: (A) die isospesifieke katalis, *rac*-[etileen *bis*(1-indeniel)]zirconium dichloried (*rac*-$Et(Ind)_2ZrCl_2$) en (B) die silileen-gebrugde katalis, *rac*-$Me_2Si(2\text{-}MeBenz[e]Ind)_2ZrCl_2$. Metielaluminoksaan (MAO) is as ko-katalis gebruik saam met bogenoemde twee metalloseenkataliste. 'n Ander reeks polimerisasie reaksies is gedoen waarin 'n Ziegler-Natta katalis gebruik is as aktiverende katalis, naamlik $TiCl_3/AlEt_3/SiO_2$.

Die karakterisering van die kopolimere sluit in: hoë temperatuur gel deurlatings chromatrografie (HTGPC) vir molekulêre massa en molekulêre massa verspreidings, differensiële skandering kalorimetrie (DSC) en dinamiese meganiese analisering (DMA) om sodoende die termiese en meganiese eienskappe van die polimere te ondersoek, kern magnetiese resonans spektroskopie (KMR) vir inligting in verband met die mikrostrukture van die kopolimere en kristallisasie analise fraksioneringstegniek (CRYSTAF) om die kort-kettingvertakkings van die kopolimere te ondersoek.

Vergelykende studies is op die verskillende katalisatore en die polimeereienskappe gedoen. Die gesintetiseerde polimere is ook met kopolimere van propileen met 1-hekseen en 1-okteen vergelyk.

This thesis is dedicated to my husband, Daniël, for his analyzing comment and advice, to my parents, Jan en Ria, for their unwavering confidence in me over the years, and to Janneman.

ACKNOWLEDGEMENTS

I would like to thank the following people and institutions for their contributions:

Dr. A.J. van Reenen, my study leader, for his advice, guidance and financial support throughout this study.

The following members of our polyolefins research group at the Institute of Polymer Science for their assistance and encouragement: **Liezel Coetzee, Lufuno Siphuma and Madri Smit**.

Elisna Maree, for all the NMR analyses done during this study.

Dr. M.J. Hurndall, for her advice on the proofreading of this thesis.

Derek McCauley, for all the CRYSTAF analyses done during this study.

Charl Morkel, for all the trouble and time he had spend on the DMA analyses.

Marius Pretorius, for all his laboratory assistance and for preparing the copolymer films for the DMA analyses.

Paul Cloete, from Roediger Agencies cc, who carried out the DSC analyses.

Stefan de Goede, from Sasol Polymers, for all the GPC analyses done during this study.

Dawie Joubert, from Sasol Sastech, for providing the Ziegler-Natta catalyzed copolymers.

Daniël, my husband, for tending to the technical aspects of my thesis and for all his patience and support.

God, for holding me in his hands.

LIST OF FIGURES

CHAPTER 2

Figure 2.1 Polypropylene catalyst generations.

Figure 2.2 Preparation of $MgCl_2$-supported catalysts.

Figure 2.3 Schematic representation of the classification of metallocene catalysts according to their symmetry.

Figure 2.4 Comparison of conventional multisite catalysts and modern single site metallocene catalysts in copolymerization.

Figure 2.5 Types of polypropylene chains produced with metallocene catalysts.

Figure 2.6 General features of the Ziegler-Natta polymerization mechanism.

Figure 2.7 Direct insertion mechanism according to Cossee-Arlman for the olefin insertion into a transition metal alkyl bond.

Figure 2.8 Metathesis-mechanism according to Green-Rooney for the olefin insertion into a transition metal alkyl bond.

Figure 2.9 Schematic representation of the suggested features for the modified Green-Rooney mechanism for the insertion of an olefin in a transition metal alkyl bond in Ziegler-Natta polymerization.

Figure 2.10 Formation of a metallocene alkyl cation by reaction between a metallocene and methylaluminoxane.

Figure 2.11 Primary and secondary insertion of an α-olefin in the metal-carbon bond.

Figure 2.12 2,1- and 1,3 insertion for α-olefins.

Figure 2.13 (a) β-hydride elimination reaction.

(b) β-Me elimination reaction.

(c) Transfer to aluminium.

(d) Transfer to the comonomer.

CHAPTER 3

Figure 3.1 Metallocene catalyst, *rac*-Et(Ind)$_2$ZrCl$_2$.

Figure 3.2 ^{13}C NMR spectrum of isotactic polypropylene (Sample A1).

Figure 3.3 ^{13}C NMR spectrum of the methyl region of Sample A1.

Figure 3.4 APT ^{13}C NMR spectrum of a propylene/1-hexene copolymer (Sample A2).

Figure 3.5 ^{13}C NMR spectrum of a propylene/1-hexene copolymer (Sample A2).

Figure 3.6 Numbering of carbon atoms of propylene/1-hexene copolymers for chemical shift predictions.

Figure 3.7 ^{13}C NMR spectrum of a propylene/1-octene copolymer (Sample A9).

Figure 3.8 Numbering of carbon atoms of propylene/1-octene copolymers for chemical shift predictions.

Figure 3.9 The distribution of the molecular mass, w(logM), against the molecular mass of propylene/1-hexene (Sample A4, 3.53% 1-hexene).

Figure 3.10 Folded chain lamellar morphology in semi-crystalline polymers.

Figure 3.11 DSC melting curve of propylene/1-hexene (Sample A2, 1.20 mol%) copolymer.

Figure 3.12 DSC melting curve of propylene/1-hexene (Sample A6, 6.36 mol%) copolymer.

Figure 3.13 Melting temperatures of propylene/1-hexene copolymers as a function of 1-hexene content.

Figure 3.14 Melting temperatures of propylene/1-octene copolymers as a function of 1-octene content.

Figure 3.15 Percentage crystallinity of propylene/1-hexene copolymers as a function of 1-hexene content.

Figure 3.16 Percentage crystallinity of propylene/1-octene copolymers as a function of 1-octene content.

Figure 3.17 The relationship of free volume to transitions.

Figure 3.18 The crankshaft model showing various motions of a polymer chain.

Figure 3.19 Cumulative and differential SCBD of polypropylene homopolymer (Sample A1) as obtained by crystallization fractionation analysis at 10°C/min crystallization rate.

CHAPTER 4

Figure 4.1 The metallocene catalyst, *rac*-$Me_2Si(2\text{-}MeBenz[e]Ind)_2ZrCl_2$.

Figure 4.2 ^{13}C NMR spectrum of isotactic polypropylene (Sample B1).

Figure 4.3 ^{13}C NMR spectrum of the methyl region of Sample B1.

Figure 4.4 Numbering of carbon atoms of propylene/1-hexene copolymers for chemical shift predictions.

Figure 4.5 ^{13}C NMR spectrum of a propylene/1-hexene copolymer (Sample B3).

Figure 4.6 Numbering of carbon atoms of propylene/1-octene copolymers for chemical shift predictions.

Figure 4.7 ^{13}C NMR spectrum of a propylene/1-octene copolymer (Sample B5).

Figure 4.8 Numbering of carbon atoms of propylene/1-heptene copolymers for chemical shift predictions.

Figure 4.9 ^{13}C NMR spectrum of a propylene/1-heptene copolymer (Sample B9).

Figure 4.10 Tacticity of propylene/1-heptene copolymers as a function of 1-heptene content.

Figure 4.11 The distribution of the molecular mass, w(logM), against the molecular mass of propylene/1-heptene (Sample B7, 3.98 % 1-heptene).

Figure 4.12 Melting temperatures of propylene/1-heptene copolymers as a function of 1-heptene content.

Figure 4.13 DSC melting curves of polypropylene homopolymer (B1) and a propylene/1-heptene copolymer (Sample B9, 5.78 mol% heptene).

Figure 4.14 Glass transition temperatures of propylene/1-heptene copolymers as a function of 1-heptene content.

Figure 4.15 Cumulative and differential SCBD of a propylene/1-hexene copolymer (Sample B2, 4.42% 1-hexene) as obtained by CRYSTAF.

Figure 4.16 Cumulative and differential SCBD of a propylene/1-octene copolymer (Sample B5, 4.70% 1-octene) as obtained by CRYSTAF.

Figure 4.17 Cumulative and differential SCBD of a propylene/1-heptene copolymer (Sample B9, 5.79% 1-heptene) as obtained by CRYSTAF.

Figure 4.18 Graph of crystallization temperature, T_c, versus the 1-heptene content of the propylene/1-heptene copolymers produced.

CHAPTER 5

Figure 5.1 Numbering of carbon atoms of propylene/1-heptene copolymers for chemical shift predictions.

Figure 5.2 ^{13}C NMR spectrum of a propylene/1-heptene copolymer (Sample Z2).

Figure 5.3 ^{13}C NMR spectrum of the methyl region of Sample Z2.

Figure 5.4 The distribution of the molecular mass, w(logM), against the molecular mass of propylene/1-heptene (Sample Z2, 1.66% 1-heptene).

Figure 5.5 DSC melting curve of propylene/1-heptene (Sample Z2, 1.66 mol% 1-heptene) copolymer.

Figure 5.6 Cumulative and differential SCBD of propylene/1-heptene copolymer (Sample Z1) as obtained by crystallization fractionation analysis at 10°C/min crystallization rate.

Figure 5.7 Melting temperature as a function of comonomer content for the propylene/1-hexene copolymers (Samples A2-A6), the propylene/1-octene copolymers (Samples A7-A11) and the propylene/1-heptene copolymers (Samples B6-B10).

LIST OF TABLES

CHAPTER 2

Table 2.1 Timetable of the historical developments in the field of metallocene research.

Table 2.2 Worldwide metallocene polyolefins capacity.

Table 2.3 Metallocene-aluminoxane catalyst systems used for copolymerization of propylene with olefins.

Table 2.4 Examples of Ziegler-Natta catalyst systems used for copolymerization of propylene with olefins.

CHAPTER 3

Table 3.1 Experimental information of propylene/1-hexene and propylene/1-octene copolymers produced by *rac*-Et(Ind)$_2$ZrCl$_2$.

Table 3.2 Summary of comonomer content of propylene/1-hexene (sample A2-A6) and propylene/1-octene (Sample A7-A11) copolymers.

Table 3.3 Chemical shift prediction for propylene / (α-olefin) copolymers utilizing the Grant and Paul additivity rules.

Table 3.4 Comparison of observed and calculated chemical shifts of propylene / 1-hexene (Samples A2–A6) copolymers.

Table 3.5 Comparison of observed and calculated chemical shifts of propylene / 1-octene (Samples A7–A11) copolymers.

Table 3.6 Tacticity values of propylene/1-hexene (Samples A2-A6) and propylene/1-octene (Samples A7-A11) copolymers.

Table 3.7 GPC results of propylene homopolymer (Sample A1) and propylene/1-hexene (Samples A2-A6) and propylene/1-octene copolymers (Samples A7-A11).

Table 3.8 DSC results of propylene homopolymer (Sample A1) and propylene/1-hexene (Samples A2-A6) and propylene/1-octene copolymers (Samples A7-A11).

Table 3.9 DMA results of propylene/1-hexene (Samples A2-A6) and propylene/1-octene copolymers (Samples A7-A11).

Table 3.10 CRYSTAF results of the propylene homopolymer (Sample A1) and the propylene/1-hexene (Samples A2-A6) and propylene/1-octene (Samples A7-A11) copolymers.

Table 3.11 CRYSTAF results of the crystallized fractions in specific temperature intervals of the propylene homopolymer (Sample A1) and the propylene/1-hexene (Samples A2-A6) and propylene/1-octene (Samples A7-A11) copolymers.

CHAPTER 4

Table 4.1 Experimental information of propylene/1-hexene, propylene/1-octene and propylene/1-heptene copolymers produced by *rac*-Me_2Si(2-MeBenz[e]Ind)$_2ZrCl_2$.

Table 4.2 Summary of comonomer content of propylene/1-hexene (Sample B2-B3), propylene/1-octene (Sample B4-B5) and propylene/1-heptene (sample B6-B10) copolymers.

Table 4.3 Chemical shift prediction for propylene / 1-heptene copolymers utilizing the Grant and Paul additivity rules.

Table 4.4 Comparison of observed and calculated chemical shifts of propylene / 1-hexene (Samples B2 – B3) copolymers.

Table 4.5 Comparison of observed and calculated chemical shifts of propylene / 1-octene (Samples B4 – B5) copolymers.

Table 4.6 Comparison of observed and calculated chemical shifts of propylene / 1-heptene (Samples B6 – B10) copolymers.

Table 4.7 Tacticity values of propylene homopolymer (Sample B1) propylene/1-hexene (Samples B2-B3), propylene/1-octene (Samples B4-B5) and propylene/1-heptene (Samples B6-B10) copolymers.

Table 4.8 GPC results of propylene homopolymer (Sample A1) and propylene/1-hexene (Samples A2-A6) and propylene/1-octene copolymers (Samples A7-A11).

Table 4.9 DSC results of propylene homopolymer (Sample B1) and propylene/1-hexene (Samples B2-B3), propylene/1-octene (Samples B4-B5) and propylene/1-heptene (Samples B6-B10) copolymers.

Table 4.10 DMA results of the propylene/1-hexene (Samples B2-B3), propylene/1-octene (Samples B4-B5) and propylene/1-heptene (Samples B6-B10) copolymers.

Table 4.11 CRYSTAF results of the propylene homopolymer (Sample B1) and the propylene/1-hexene (Samples B2-B3), propylene/1-octene (Samples B4-B5) and propylene/1-heptene (Samples B6-B10) copolymers.

Table 4.12 CRYSTAF results of the crystallized fractions in specific temperature intervals of the propylene homopolymer (Sample B1) and the propylene/1-hexene (Samples B2-B3), propylene/1-octene (Samples B4-B5) and propylene/1-heptene (Samples B6-B10) copolymers.

CHAPTER 5

Table 5.1 Summary of assignments of peaks in the methyl region of propylene/1-heptene copolymer (Sample Z1, 1.66% 1-heptene).

Table 5.2 Summary of comonomer content of propylene/1-heptene (Samples Z1-Z2) copolymers.

Table 5.3 Comparison of observed and calculated chemical shifts of propylene /1-heptene (Samples Z1–Z2) copolymers.

Table 5.4 GPC results of propylene/1-heptene copolymers (Samples Z1-Z2).

Table 5.5 DSC results of propylene/1-heptene (Samples Z1-Z2) copolymers.

Table 5.6 DMA results of propylene/1-heptene copolymers (Samples Z1-Z2).

Table 5.7 CRYSTAF results of the propylene/1-heptene (Samples Z1-Z2) copolymers.

Table 5.8 CRYSTAF results of the crystallized fractions in specific temperature intervals of the propylene/1-heptene (Samples Z1-Z2) copolymers.

Table 5.9 Summary of assignments of peaks in the methyl region of different polymer series.

Table 5.10 Summary of tacticities of different polymer series.

Table 5.11 Summary of molecular mass and molecular mass distribution of different polymer series.

LIST OF ABBREVIATIONS

br	Branching carbon
^{13}C	Carbon thirteen
CCD	Chemical composition distributions
Cp_2ZrCl_2	Bis(cyclopentadienyl)zirconium dichloride
CRYSTAF	Crystallization analysis fractionation
DMA	Dynamic mechanical analysis
DSC	Differential scanning calorimetry
$Et(Ind)_2ZrCl_2$	Ethylenebis(Indenyl)zirconium dichloride
$Et(Me_4Cp)(Ind)TiCl_2$	Ethylene(2, 3, 4, 5 tetramethyl cyclopentadienyl)(Indenyl)titanium dichloride
GPC	Gel permeation chromatography
HTGPC	High temperature gel permeation chromatography
$iPr(Cp)(Ind)ZrCl_2$	Isopropyl(cyclopentadienyl)(indenyl)zirconium dichloride
$iPr(Flu)(Cp)HfCl_2$	Isopropyl(fluorenyl)(cyclopentadienyl)hafnium dichloride
MAO	Methylaluminoxane / Methylalumoxane
MBI	*rac*-Dimethylsilyl-bis(2-Methylbenz[e]indenyl)zirconium dichloride
MWD	Molecular weight distribution
NMR	Nuclear magnetic resonance spectroscopy
PP	Polypropylene
M_n	Number average molecular mass
M_w	Weight average molecular mass
SCBD	Short-chain branching distribution
T_c	Crystallization temperature
T_n	Number average temperature
T_g	Glass transition temperature
T_m	Melting temperature
T_w	Weight average temperature
TREF	Temperature elution fractionation

CONTENTS

LIST OF FIGURES I

LIST OF TABLES V

LIST OF ABBREVIATIONS IX

CONTENTS X

CHAPTER 1: Introduction and Objectives 1

1.1 INTRODUCTION 1

1.2 OBJECTIVES 2

CHAPTER 2 Ziegler-Natta and metallocene catalysed polymerizations: Historical and theoretical background 3

2.1 HISTORICAL BACKGROUND 3

2.1.1 Introduction 3

2.1.2 Ziegler-Natta Catalysts 4

2.1.3 Metallocene Catalysts 7

2.1.4 Comparison of Ziegler-Natta and metallocene catalysts 9

2.1.5 Propylene copolymers 14

2.2 REACTION MECHANISM OF THE PREPARATION OF POLYMERS PRODUCED BY ZIEGLER-NATTA CATALYSTS 17

2.3 REACTION MECHANISM OF THE PREPARATION OF POLYMERS PRODUCED BY METALLOCENE CATALYSTS 20

2.3.1. The cocatalyst 20

2.3.2. Catalyst activation 21

2.3.3 Propagation 21

2.3.4. Termination 23

2.4 CONCLUSIONS 24

2.5 REFERENCES 24

CHAPTER 3 Polymerization and characterization of propylene/1-hexene and propylene/1-octene copolymers produced with *rac*-Et(Ind)$_2$ZrCl$_2$/MAO

SUMMARY 31

3.1 INTRODUCTION 31

3.2 EXPERIMENTAL 33

3.3 EQUIPMENT 34

3.3.1 Polymerization Equipment 34

3.3.2 Analytical Equipment 34

3.3.2.1 Nuclear magnetic resonance (NMR) 34

3.3.2.2 Differential scanning calorimetry (DSC) 34

3.3.2.3 High temperature gel permeation chromatography (HTGPC) 35

3.3.2.4 Crystallization analysis fractionation (CRYSTAF) 35

3.4 SYNTHESIS OF COPOLYMERS 35

3.4.1 Preparation of the catalyst solution 36

3.4.2 Propylene copolymerization 36

3.5 RESULTS AND DISCUSSION 37

3.5.1 Microstructure 37

3.5.1.1 Polypropylene homopolymer 37

3.5.1.2 Propylene/1-hexene and propylene/1-octene copolymers 40

3.5.2 Molecular mass and molecular mass distributions 48

3.5.3 Thermal properties 51

3.5.3.1 Melting behaviour 51

3.5.3.2 Glass transition temperature 58

3.5.4 Crystallinity 60

3.6 CONCLUSIONS 65

3.7 REFERENCES 66

CHAPTER 4 Polymerization and characterization of propylene/α-olefins copolymers produced with *rac*-Me$_2$Si(2-MeBenz[e]Ind)$_2$/MAO

SUMMARY 70

4.1 INTRODUCTION 70

4.2 EXPERIMENTAL 73

4.3 EQUIPMENT 73

4.3.1 Polymerization equipment 73

4.3.2 Analytical equipment 73

4.4 SYNTHESIS OF COPOLYMERS 73

4.4.1 Preparation of the catalyst solution 73
4.4.2 Propylene copolymerization 73
4.5 RESULTS AND DISCUSSION 74
4.5.1 Microstructure 74
4.5.1.1 Polypropylene homopolymer 74
4.5.1.2 Propylene/1-hexene, propylene/1-octene and propylene/1-heptene copolymers 76
4.5.2 Molecular mass and molecular mass distributions 85
4.5.3 Thermal properties 87
4.5.3.1 Melting behaviour 87
4.5.3.2 Glass transition temperature 90
4.5.4 Crystallinity 92
4.6 CONCLUSIONS 97
4.7 REFERENCES 98

CHAPTER 5. Polymerization and characterization of propylene/1-heptene copolymers produced with $TiCl_3/AlEt_2/SiO_2$

SUMMARY 100
5.1 INTRODUCTION 100
5.2 EXPERIMENTAL 102
5.3 RESULTS AND DISCUSSION 102
5.3.1 Microstructure 102
5.3.1.1 Polypropylene homopolymer 102
5.3.2 Molecular mass and molecular mass distributions 107
5.3.3 Thermal properties 108
5.3.3.1 Melting behaviour 108
5.3.3.2 Glass transition temperature 109
5.3.4 Crystallinity 110
5.4 COMPARISON OF RESULTS 112
5.4.1 Microstructure 112
5.4.2 Molecular mass and molecular mass distribution 114
5.4.3 Thermal properties 114
5.4.3.1 Melting behaviour 114
5.4.3.2 Glass transition temperature 116
5.4.4 Crystallinity 116
5.5 REFERENCES 117

APPENDIX A ^{13}C NMR CURVES 119

APPENDIX B GPC CURVES 125

APPENDIX C DSC CURVES 136

APPENDIX D DMA CURVES 147

APPENDIX E CRYSTAF CURVES 153

CHAPTER 1

Introduction and Objectives

1.1 INTRODUCTION

"The world market for PP has grown from around 1,5 million tons in the 1970s, to about 13 million tons in the 1990s, and is expected to be over 19 million tons in 1995. In the year 2000 it could exceed 25 million tons. Such explosive and unarrestable growth due to the outstanding combination of cost performance, excellent physical properties, strong and continuous expansion of process versatility, and environmental friendly processes and materials, during manufacturing, use, and recycling stages. This unexpected surge, which started in the early '70s, and is still surprizingly vigorous, was made possible by focusing and investing in the thorough scientific understanding of the catalytic system, and its subsequent development. Where is PP going? The adventure is not over yet."

These words were written by Professor Paolo Galli, then president of Montell Technology Company, in March 1996. In the year 2000 the reported global production volume of polypropylene amounted to 29 million tons in the world market [2].

In the past, polyolefin producers relied heavily on process- and catalyst developments to gain advantage over their competition. For ethylene polymers, 1-butene was initially employed as comonomer, but later 1-hexene and 1-octene was also used. These comonomers are produced by ethylene oligomerization and only even numbered compounds can therefore be obtained. It is clear that the role of the α-olefins with uneven carbon numbers as comonomers has been largely ignored, presumably due to limited availability.

In the Sasol Fischer-Tropsch process, unique α-olefins including 1-pentene, 1-heptene and 1-nonene compounds are produced. These are only byproducts of the process and the way for investigating the influence of these odd numbered α-olefins

as comonomers in polypropylene is still widely unexplored. And so, in the words of Paolo Galli, the "adventure" continues.

1.2 OBJECTIVES

The main objective of this work was to synthesize and characterize propylene/1-heptene copolymers, and to compare these copolymers with propylene-1-hexene and propylene-1-octene copolymers. To this end, the C_2 symmetric ansa metallocenes *rac*-Me_2Si(2-MeBenz[e]Ind)$_2ZrCl_2$ and *rac*-Et(Ind)$_2ZrCl_2$ would be used to synthesize series of copolymers of propylene with 1-hexene, 1-heptene and 1-octene. This would allow a comparison of the metallocene catalysts. In addition, the propylene-1-heptene copolymers prepared with the homogeneous metallocene catalyst, *rac*-Me_2Si(2-MeBenz[e]Ind)$_2ZrCl_2$ will be compared with samples of the same type of copolymer synthesized with a heterogeneous Ziegler-Natta catalyst. In particular, the effect of the 1-heptene comonomer on the microstructure, molecular mass, molecular mass distribution, melting point, glass transition temperature and crystallization behaviour of the copolymers synthesized, would be investigated.

The synthesized polymers will be characterized by nuclear magnetic resonance spectroscopy (NMR), high temperature gel permeation chromatography (HTGPC), differential scanning calorimetry (DSC), dynamic mechanical analysis (DMA), and crystallization analysis fractionation (CRYSTAF).

1.3 REFERENCES

1. Galli P., *Polypropylene Handbook* (ed. Moore E.P., jr.), Hanser Publishers, Munich, 1996, v.
2. Joubert D.J., *Ph.D. Thesis*, University of Stellenbosch, 2000.

CHAPTER 2

Ziegler-Natta and metallocene catalyzed polymerizations: Historical and theoretical background

2.1 HISTORICAL BACKGROUND

2.1.1 Introduction

A Ziegler-Natta catalyst can be defined as a transition metal compound having a metal-carbon bond able to carry out a repeated insertion of olefin units. Usually, though not necessarily, the catalyst consists of two components (i.e., a transition metal salt, most frequently a halide, and a main-group metal alkyl which serves the purpose of generating the active metal-carbon bond). These types of catalysts are heterogeneous and the active metal centre occupies a position on the surface of the crystal. Polymerization at the active site is influenced by the electronic and steric environment of the crystal lattice. Because the active centres can occupy a wide variety of lattice sites, they tend to give products with a broad molecular weight distribution (MWD) and also, for example, non-homogeneous comonomer distribution in olefin copolymers **[1]**.

Metallocene catalysts are often referred to as homogeneous Ziegler-Natta catalysts because all the catalyst components are soluble in aromatic hydrocarbon solvents. These catalysts are also known as single-site catalysts because of the fact that the catalytic sites are shielded to a large extent from the influence of their immediate surroundings. These catalysts therefore yield a sharply defined product with a narrow MWD and other molecular characteristics, as well as a minimum of undesirable byproducts (e.g. atactic polypropylene in isotactic polypropylene). Studies on the effect of producing a narrow MWD ($M_w/M_n \approx 2$) were done by various groups, particularly groups of Zambelli **[2-5]**, Chien **[6-11]**, Soga **[12]** and Kashiwa **[13, 14]** showed that copolymers produced by metallocene-based catalysts consist of uniform chains with narrow molecular mass distributions typical of single-site catalysts.

2.1.2 Ziegler-Natta catalysts

Since Ziegler and Natta's pioneering advances during the early 1950's, polypropylene production was revolutionized in remarkably regular intervals of approximately fifteen years. Important development steps and new catalyst and process generations are shown in Figure 2.1 **[15]**. Innovations have stimulated rapid growth of polypropylene production and enhanced polypropylene's competitiveness with respect to other more expensive or less environmentally friendly polymers. The assignment of numbers for catalyst generations is somewhat arbitrary because of the large number of innovative catalyst systems. The generation numbers are used to characterize quantum-leap progress in catalyst and process technology, instead of measuring significant advances within one specific catalyst family. Advances in Ziegler-Natta catalysis were reviewed by Pino **[16]**, Brintzinger **[17]**, Tait *et al* **[18-20]**, and Corradini *et al* **[21]**.

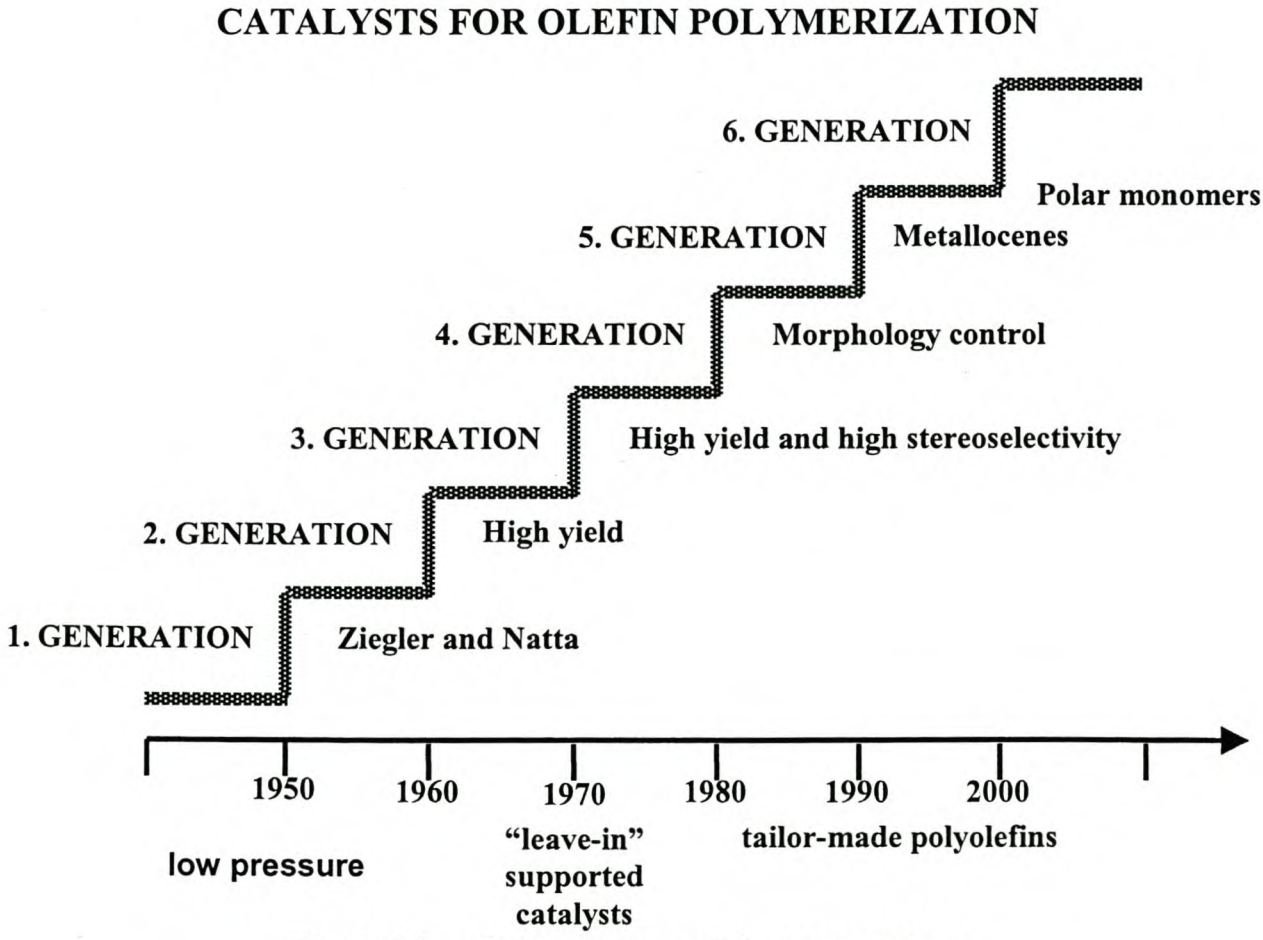

Figure 2.1 Polypropylene catalyst generations.

The first catalyst generation, developed by Natta and his group, was composed of γ-$TiCl_3$ activated with $AlEt_2Cl$. Although the stereoselectivity was improved from 40 to 90% isotactic polypropylene with respect to Ziegler's $TiCl_4/AlR_3$ catalyst systems, extensive polypropylene purification was required to produce commercial isotactic polypropylene. Moreover, propylene polymerization was performed as slurry polymerization in an inert hydrocarbon medium, which required special solvent recycling steps. It was soon recognized that improving the surface area and the presence of anhydrous $AlCl_3$, which can substitute inactive bulk $TiCl_3$, as well as the presence of weak electron donors, such as sterically hindered dialkylethers, during catalyst preparation promoted catalyst performance. The first successful improvements led to the development of the 'Solvay'-type δ-$TiCl_3/AlCl_3$/isoamylether/$AlEt_2Cl$ catalyst system with tenfold catalyst activities and stereoselectivity exceeding 95%. This type of catalyst system was investigated by Nielsen **[22]**. Some of these second generation catalysts and modified systems are still being applied today in conventional isotactic polypropylene slurry processes.

During the late 1980's, third generation supported catalysts were introduced exhibiting significantly improved stereoselectivities without sacrificing high catalyst activities. At Montedison and Shell, it was discovered that highly active catalysts were obtained when $TiCl_4$ was supported on anhydrous high-surface-area magnesium chloride in the presence of electron-donating Lewis bases **[23-27]**. The crystal structure of $MgCl_2$ is an isotype to that of γ-$TiCl_3$. Therefore, $MgCl_2$ can substitute inactive bulk $TiCl_3$ and offers the equivalent coordination site for immobilizing titanium alkyl halide complexes at the $MgCl_2$ surface. Activation of $MgCl_2$ is required to afford high specific surface areas (> 40 m^2/g). This can be achieved by means of mechanical grinding or by *in situ* preparation of $MgCl_2$, e.g. by chlorinating magnesium alkyls.

A typical process for $MgCl_2$-supported catalyst preparation is shown in Figure 2.2 **[28]**. After dehydration, $MgCl_2$ is ground together with $TiCl_4$ and a Lewis base, such as diethylphthalate, as internal electron donor. This internal Lewis base facilitates deagglomeration of primary catalyst particles during propylene polymerization. While conventional $TiCl_3/AlEt_2Cl$ catalysts are encapsulated in an isotactic polypropylene shell, which is highly impermeable to propylene,

deagglomeration during polymerization is responsible for a very high concentration of active sites and less diffusion limitations. In comparison to first generation catalysts, the number of active sites is increased by one or two orders of magnitude. The external Lewis base, which is added together with the activator aluminum alkyl, selectively poisons non-stereospecific sites. Most likely for steric reasons, highly isoselective sites are much less Lewis acidic with respect to the sterically less hindered non-selective sites. In a series of equilibria involving complex formation of Lewis bases with Ti-alkyl sites as well as with the aluminum activator alkyl, the complex formation with highly Lewis acidic nonstereoselective sites is favoured. The selectivity of Lewis bases modifiers with respect to catalytically active sites appears to follow the 'lock-key' principle, which was proposed by several groups in analogy to enzyme/substrate or enzyme/coenzyme complexes, respectively.

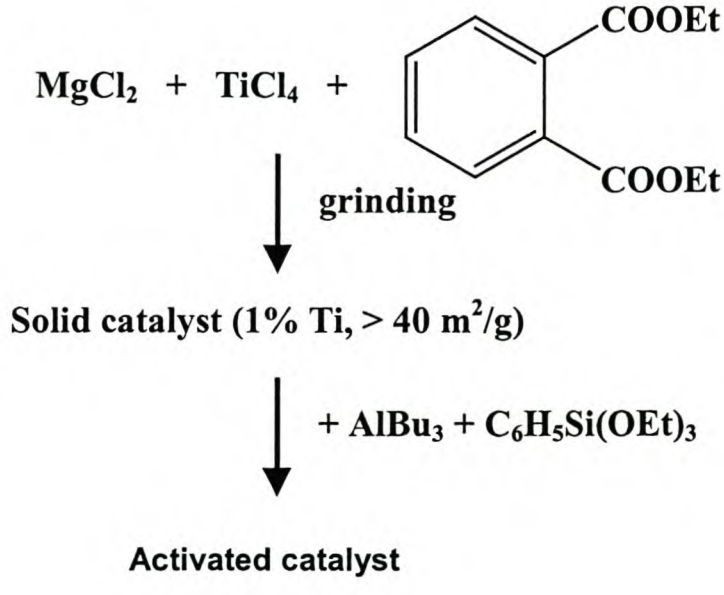

Figure 2.2 Preparation of $MgCl_2$-supported catalysts [28].

Originally esters of aromatic carboxylic acids, such as ethyl benzoate or dialkylphthalate, were used as preferred external and internal Lewis bases. Although esters poisoned nonstereospecific sites selectively, the total catalyst activity decreased markedly with increasing external ester/Al molar ratio and with increasing stereoselectivity **[29]**. In a subsequent improvement during the 1980's, weaker silylether Lewis bases, e.g. phenyltriethoxysilane, were used as external Lewis bases in conjunction with diesters as internal Lewis bases in order to achieve high

stereoselectivities without encountering such pronounced losses of catalyst activity **[30-33]**. During the late 1980's and early 1990's, 1,3-diethers were introduced as a new class of electron-donating Lewis bases **[34]**. When using 1,3-diethers as internal Lewis bases, both the resulting catalyst activities and stereoselectivities were extraordinarily high. Such catalyst systems do not require the use of additional external Lewis bases. In fact, the aluminum alkyl activator does not appear to be able to remove the diether from the solid catalyst component **[35]**. Development of this 'third generation' catalyst is still in progress and illustrates the very attractive potential of Lewis-base-modified $MgCl_2$-supported catalysts for improving polypropylene properties.

Based upon the insight gained from the correlation between catalyst structure and morphology development, Galli and coworkers observed that the catalyst particles can act as templates for the formation of polypropylene polymer particles, when using spherical catalyst particles, which are composed of a large number of agglomerated much smaller primary particles. As a function of the catalyst morphology, dense and microporous polypropylene granules can be obtained. This new catalyst generation, referred to as fourth generation catalysts in Figure 2.1, became known as reactor granule technology **[36-37]**.

During the 1980's, another catalyst generation based upon metallocenes – referred to as fifth generation in Figure 2.1 – became available. This will be reviewed in the next section.

2.1.3 Metallocene catalysts

Metallocene catalysts result from the reaction of metallocenes and a cocatalyst, which is generally an organoaluminium compound. The exact definition of the class of soluble organometallic complexes usually referred to as "metallocene catalysts", is group 4 (titanium, zirconium or hafnium) bent metallocenes. Of the three metals, Zr is the most active **[38]**.

Breslow and Natta discovered metallocene catalysts for olefin polymerization soon after the original discovery of Ziegler Natta catalysts **[39, 40]**. The evolution of metallocene catalyst structures for olefin polymerization until 1984 is tabulated in Table 2.1 **[41]**. Early metallocene catalysts of the type Cp_2TiCl_2/AlR_xCl_{3-x} show poor

reactivity towards ethylene and do not polymerize propylene, although they do copolymerize ethylene with higher α-olefins **[39-40]**. Analogous research with zirconocene dichloride in combination with AlR_3 was started by Breslow **[42]** but with limited success, until the serendipitous discovery in 1973 of the activating effect of small amounts of water on the system $Cp_2MX_2/AlMe_3$ **[43-45]**. The subsequent synthesis of methylaluminoxane (MAO) in 1977 by the group of Sinn and Kaminsky has provided organometallic and polymer chemists with a potent cocatalyst able to activate group 4 metallocenes toward the polymerization of α-olefins **[46]**. In the early 1980s Brintzinger *et al* synthesized racemic ethylene-bridged bis(indenyl)zirconium dichloride, $Et(Ind)_2ZrCl_2$, and racemic ethylene-bridged *bis*(4,5,6,7-tetra-hydroindenyl)zirconium dichloride, $Et(H_4Ind)_2ZrCl_2$ **[47]**, as well as their titanium analogues, $Et(Ind)_2TiCl_2$ and $Et(H_4Ind)_2TiCl_2$ **[48]**, which have both meso and racemic configurations. The *ansa* metallocenes, $Et(Ind)_2ZrCl_2$ and $Et(H_4Ind)_2ZrCl_2$ which were activated by methylaluminoxane (or methylalumoxane, MAO) allowed stereospecific polymerization of propylene for the first time. Ewen synthesized a C_s symmetric zirconocene ($[Me_2C(Flu)(C_p)]ZrCl_2$) in 1988, which allowed the production of syndiotactic polypropylene in high quantities **[49]**. Since 1985 a rapid worldwide industrial and academic development began in the field of metallocene catalysts which continues today.

Table 2.1 Timetable of the historical developments in the field of metallocene research.

1952	Development of the structure of metallocenes (ferrocene) by Fischer and Wilkinson **[50]**.
1955	Metallocene as component of Ziegler-Natta catalysts, low activity with common aluminium alkyls **[39]**.
1973	Addition of small amount of water to increase the activity ($Al:H_2O$ = 1:0.05 up to 1:0.3) (Reichert, Meyer and Breslow) **[43-44]**.
1975	Unusual increase in activity by adding water at the ratio $Al:H_2O$ = 1:2 (Kaminsky, Sinn and Motweiler) **[45]**.
1977	Using separately prepared methylaluminoxane (MAO) as cocatalyst for olefin polymerization. (Kaminsky and Sinn) **[46]**.
1982	Synthesis of *ansa* metallocenes with C_2 symmetry (Brintzinger) **[51]**.
1984	Polymerization of propylene using a *rac/meso* mixture of *ansa* titanocenes led to partially isotactic polypropylene. (Ewen) **[49]**.
1984	Chiral *ansa* zirconocenes produce highly isotactic polypropylene (Kaminsky and Brintzinger) **[52]**.

Metallocenes used in olefin polymerization have been classified on the basis of their symmetry **[53]**. (Figure 2.3) In class I two η^5-cyclopentadienyl ligands (represented by the shaded rectangles) can be bridged or not; in the other classes they are bridged. In classes I and II, the two sites occupied by the η^5-ligands are bisected by a horizontal mirror plane and consequently are achirotopic; they are related by a two-fold rotation axis in class III and are homotopic (equal). In class IV, the two sites are related by a vertical mirror plane and are enantiotopic (mirror image to each other). No symmetry elements are present in class V, and the two sites are diastereotopic (different).

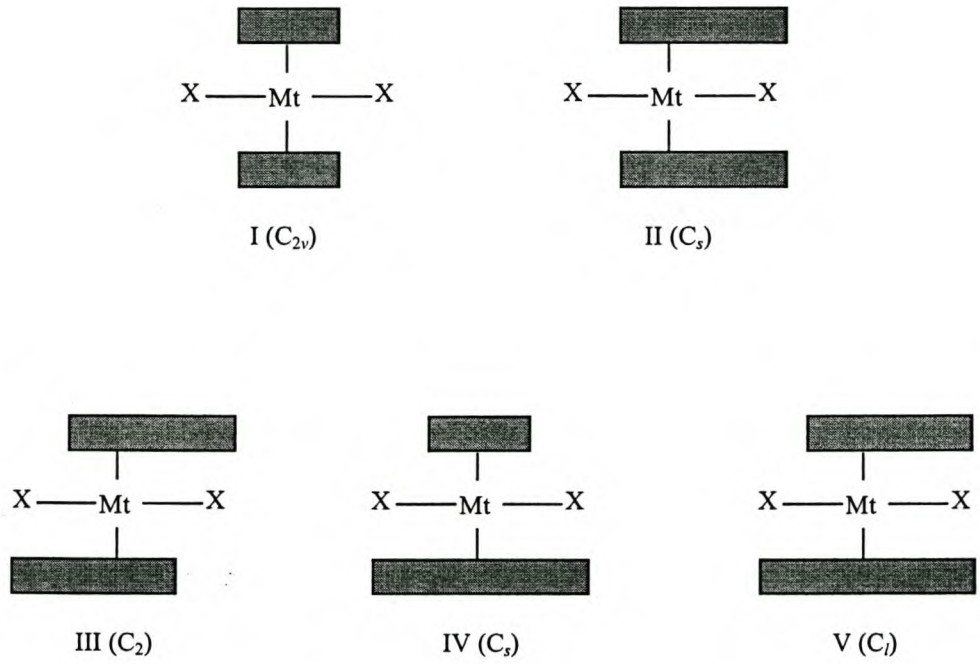

Figure 2.3 Schematic representation of the classification of metallocene catalysts according to their symmetry [53].

2.1.4 Comparison of Ziegler-Natta and metallocene catalysts

One of the most important differences between metallocene catalysts and Ziegler-Natta catalysts is the ability of metallocene catalysts to copolymerize a wide variety of olefins without sacrificing the extraordinary uniformity with respect to narrow molecular weight distribution and especially molecular weight independent comonomer incorporation. Most Ziegler Natta catalysts are multisite catalysts and

contain catalytically active centres with greatly different reactivity towards insertion of propylene and other olefins. This difference between copolymers produced by Ziegler-Natta catalysts on the one hand and metallocene-based catalysts on the other hand is demonstrated in Figure 2.4 **[54]**. In (a) copolymers consist of a complex mixture of homo- and copolymers with comonomers frequently incorporated in the low molar mass fractions and shows a broad molecular mass distribution (M_w/M_n = 5 – 40). And in (b) we see uniform comonomer incorporation, which shows a narrow molar mass distribution ($M_w/M_n \approx 2$).

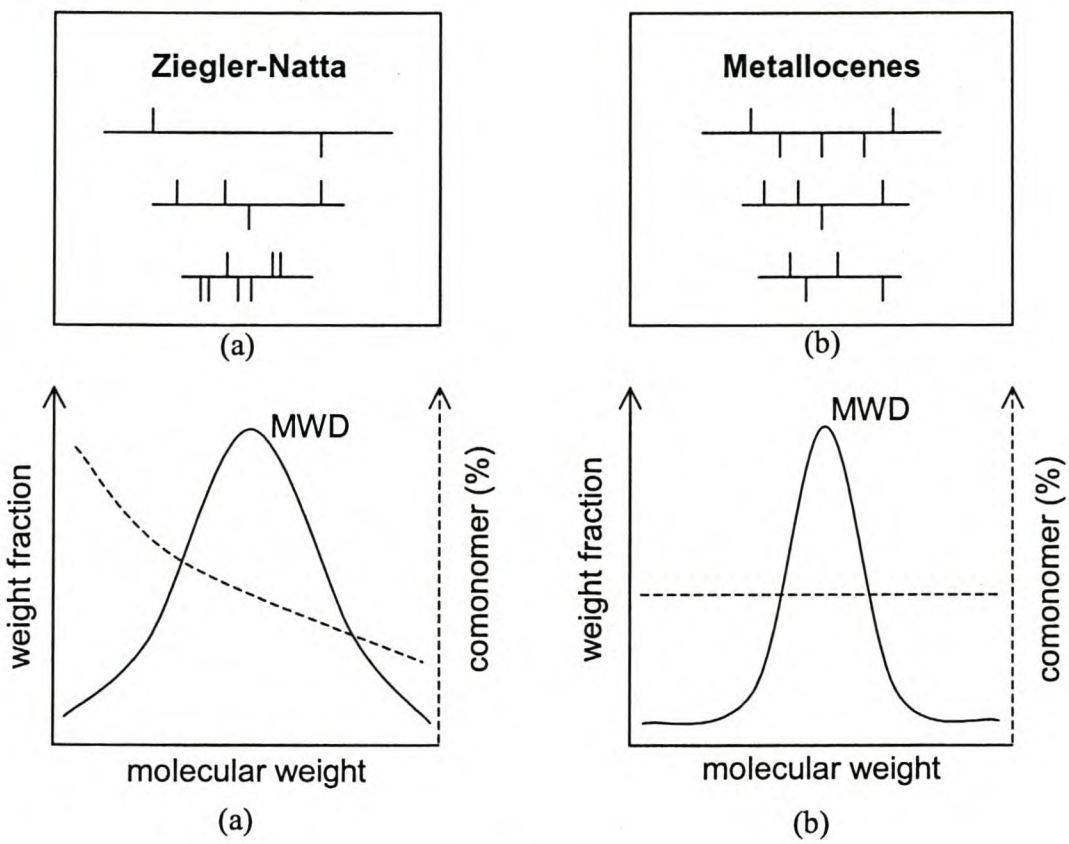

Figure 2.4 Comparison of conventional multi-site catalysts and modern single-site metallocene catalysts in copolymerization [54].

Most polyolefin manufacturing processes today utilize conventional heterogeneous Ziegler-Natta catalysts. Several types of Ziegler-Natta catalysts are stereospecific, i.e. the insertion of asymmetric monomers into the growing polymer chain in a given orientation is favoured over all other possible orientations, leading to the production of isotactic and syndiotactic polypropylene. Because these catalysts

have more than one type of active site, they produce polypropylene with nonuniform stereoregularity. In contrast, metallocenes can be synthesized as single site-type catalysts to produce polymers with uniform stereoregularity. While it is difficult to control the nature of the site types on conventional heterogeneous Ziegler-Natta catalysts, metallocene catalysts can be designed to synthesize polypropylene with different chain microstructures. Polypropylene chains with atactic, isotactic, isotactic-stereoblock, atactic-stereoblock and hemiisotactic configurations can be produced with metallocene catalysts as illustrated in Figure 2.5 **[55]**.

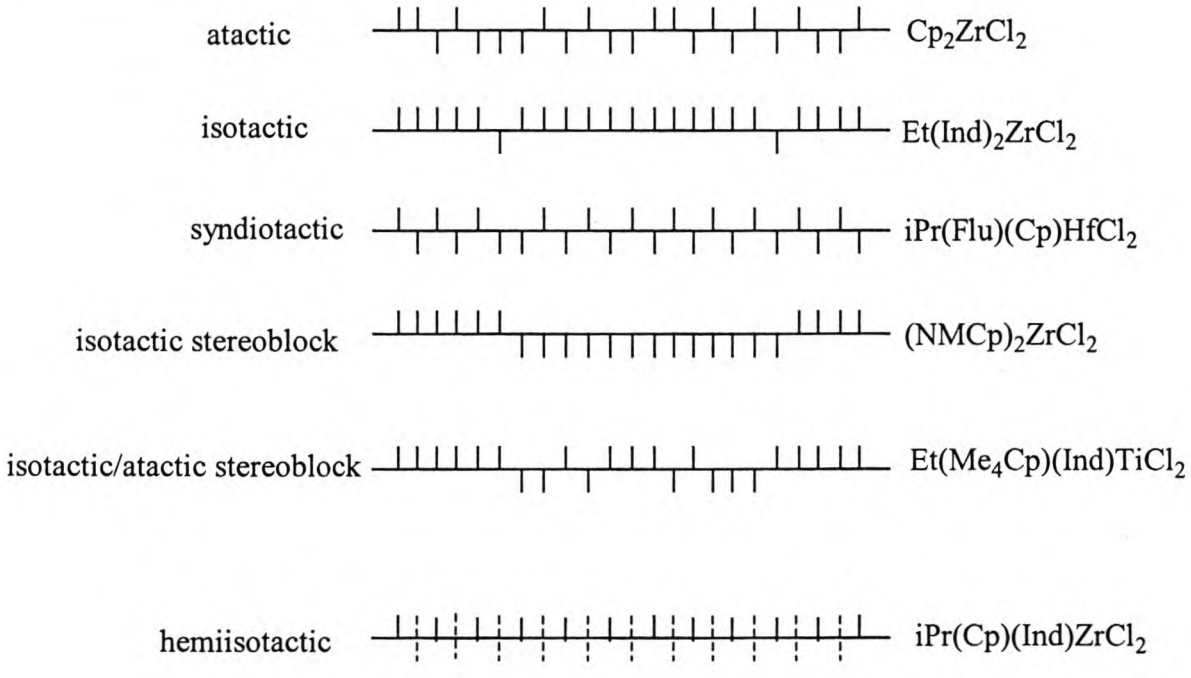

Figure 2.5 Types of polypropylene chains produced with metallocene catalysts [55].

Properties of metallocene-based polypropylene were compared with those of conventional polypropylene **[56]**. Metallocene polypropylene exhibits higher stiffness and improved optical properties. Improved orientation of metallocene-based polypropylene offers opportunities for production of biaxially oriented polypropylene film and fibres. Improved performance of polypropylene films may allow the reduction of film thickness and save weight in packaging applications. The lower melting temperature of polypropylene made possible by metallocene catalysts leads to more "tie" molecules between polypropylene crystallites, thus enhancing tensile

strength and elongation at break. High gloss and excellent optical properties of metallocene-based polypropylene are particularly attractive in injection moulding.

Looking at the properties of metallocene and single site- catalysts it can be inferred that the main advantages of these catalysts over Ziegler-Natta catalysts include:

(a) very high, sustained catalytic activities

(b) small quantities of catalyst required

(c) control over different stereospecificities

(d) controlled comonomer distribution

(e) high comonomer incorporation

(f) copolymerization with a wide variety of monomers, including polar comonomers

(g) block copolymerization possible

(h) produce polymers with narrow molecular mass distributions (approaching the theoretical value of 2.0 as predicted by the Schultz-Flory mechanism)

(i) produce polymers that are easier to recycle

(j) amount of extractables in these polymers is far lower

Disadvantages of these catalyst systems however are:

(a) sometimes extremely laborious preparation procedures

(b) decay type kinetics are evident with ethylene/higher α-olefin mixtures

(c) high Al/Zr ratios are required for obtaining high catalytic activity and a relatively stable kinetic profile

(d) high cost of methylaluminoxane (MAO)

(e) short shelf lifetime of methylaluminoxane

(f) poor control over polymer morphology

(g) incompatibility with slurry and gas-phase processes

(h) narrow molecular weight distribution

Metallocene catalysts have the potential of significantly changing the polyolefin market if production costs (especially those associated with MAO synthesis) can be reduced and if new polymer grades can be implemented without significant processing difficulties. Although metallocene-produced polyolefins can compete with commodity polyolefins synthesized with conventional Ziegler-Natta catalysts, they will not problably be restricted to the polymer commodity market. Because of the better polymer microstructure control obtained with metallocene catalysts, it will be possible to produce specialty polyolefins to compete with non-olefinic polymers, thus opening a completely new market for polyolefin applications. Table 2.2 **[57]** shows the expected production of polyolefins using metallocene catalysts by different polymer companies in North America, Europe and Japan.

Table 2.2 Worldwide metallocene polyolefins capacity [57].

Company	Region	Year of commercialization	Capacity (ton/year)
Polyethylene			
Dow	U.S.	1993	50 000
Exxon	U.S.	1995	100 000
Mitsui	Japan	1995	100 000
Mitsubishi	Japan	1994	100 000
Union Carbide	U.S.	1995	300 000
Polypropylene			
Chisso	Japan		20 000
Exxon	U.S.	1996	100 000
Hoechst	Europe	1995	100 000
Mitsui Toatsu	Japan	1994-1995	75 000 – 100 000

2.1.4 Propylene copolymers

Limited information **[58 - 64]** is available concerning the copolymerization of propylene with other olefins. A list of examples is made in Table 2.3 **[65]** of the metallocene systems used for the copolymerization of propylene with α-olefins.

More recently, copolymers of propylene with 1-octene, 1-decene, 1-tetradecene and 1-octadecene were synthesized using $Me_2Si(2\text{-}MeBenz[e]Ind)_2ZrCl_2$ as activating catalyst **[75-76]**.

In Table 2.4 **[77]** a list of Ziegler-Natta catalyst systems used for the same kind of copolymerizations of propylene and olefins is given.

Table 2.3 Metallocene-alumoxane catalyst systems used for copolymerization of propylene with olefins.

Catalyst	Comonomer	Reference
i-Pr[FluCp]$ZrCl_2$	1-Butene	**[58]**
$Me_2Si(Ind)_2ZrCl_2$	Ethylene	**[59]**
i-Pr(Cp)(Flu)$ZrCl_2$	5-Methyl-2-norborene	**[60]**
rac-$Me_2Si(Ind)_2HfCl_2$	Ethylene	**[61]**
[9,9'-*I*-Pr$(Flu)_2$]$ZrCl_2$	Ethylene	**[62]**
i-Pr(Cp)(Flu)$ZrCl_2$	Norbornene	**[63]**
$C_2H_4(Ind\text{-}H_4)_2ZrCl_2$	1-Hexene	**[64]**
$C_2H_4(Ind)_2HfCl_2$	1-Butene	**[66]**
$C_2H_4(Ind)_2HfCl_2$	1-Hexene	**[66]**
$C_2H_4(Ind)_2HfCl_2$	1-Octene	**[66]**
$C_2H_4(Ind)_2HfCl_2$	1-Dodecene	**[66]**
$C_2H_4(Ind)_2HfCl_2$	1-Hexadecene	**[66]**
i-Pr(Cp)(Flu)$ZrCl_2$	1-Butene	**[67]**
$C_2H_4(Ind)_2ZrCl_2$	1-Hexene	**[68]**
i-Pr(Cp)(Flu)$ZrCl_2$	Ethylene	**[69]**
i-Pr(Cp)(Flu)$ZrCl_2$	1-Butene	**[69]**
i-Pr(Cp)(Flu)$ZrCl_2$	1-Pentene	**[69]**
i-Pr(Cp)(Flu)$ZrCl_2$	1-Hexene	**[69]**
i-Pr(Cp)(Flu)$ZrCl_2$	4-Methyl-1-pentene	**[69]**
$Me_2Si(Ind)_2ZrCl_2$	1-Hexene	**[70]**
i-Pr[CpFlu]$ZrCl_2$	1-Hexene	**[69]**
$Me_2Si(2\text{-}MeBenz[e]Ind)_2ZrCl_2$ [a]	1-Octene	**[71]**
$(C_5H_5)_2ZrCl_2$	Ethylene	**[72]**
$Me_2C(C_5H_4)(Flu)ZrCl_2$	1-Octene	**[73]**
$Me_2C(Fl,Cp)ZrCl_2$	1-Hexene	**[74]**

MAO was used as cocatalyst throughout, except in **a** (**a** = SiO_2/MAO used as support/cocatalyst system).

Table 2.4 Examples of Ziegler-Natta catalyst systems used for copolymerization of propylene with olefins.

Catalyst	Comonomer	Reference
$TiCl_3/AlEt_2Cl$	Ethylene	[78]
$TiCl_3/AlEt_3$	Ethylene	[78]
Solvay-$TiCl_3/Cp_2TiMe_2$	Ethylene	[78]
$TiCl_4/MgCl_2$/PE/$AlEt_3$	Ethylene	[78]
$TiCl_4/MgCl_2$	Ethylene	[78]
Chromocene on silica	Ethylene	[78]
$TiCl_4/MgCl_2$/EB	Ethylene	[78]
$TiCl_4/MgCl_2$/3ROH	Ethylene	[78]
$SiO_2/TiCl_3/MgCl_2$	Ethylene	[78]
$SiO_2/TiCl_4/MgCl_2$	Ethylene	[78]
$TiCl_3/AlEt_2Cl$/HMPTA/H_2	1-Butene	[78]
$TiCl_3/AlEt_2Cl$/HMPTA	1-Butene	[78]
$TiCl_3/AlCl_3/AlEt_2Cl$	1-Butene	[78]
$TiCl_3/AlEt_2Cl$	1-Butene	[78]
$TiCl_3/AlEt_3$	1-Butene	[78]
$TiCl_3$(Stauffer AA)/$AlEt_2Cl$	4-Methyl-1-pentene	[78]
$TiCl_3$(Stauffer AA)/$AlEt_2Cl$	1-Hexene	[78]
$TiCl_3/AlEt_2Cl$	4-Methyl-1,4-hexadiene	[78]
$TiCl_4/MgCl_2$/Al*i*-Bu_3	1-Octene	[79]
$TiCl_4/MgCl_2$/Al*i*-Bu_3	1-Dodecene	[79]
$TiCl_4/MgCl_2$/Al*i*-Bu_3	1-Hexadecene	[79]
$TiCl_4/MgCl_2$/Al*i*-Bu_3	1-Tetradecene	[79]

2.2 REACTION MECHANISM OF THE PREPARATION OF POLYMERS PRODUCED BY ZIEGLER-NATTA CATALYSTS

The essential features for the insertion polymerization used with Ziegler-Natta catalysts are collected in Figure 2.6 **[80]**.

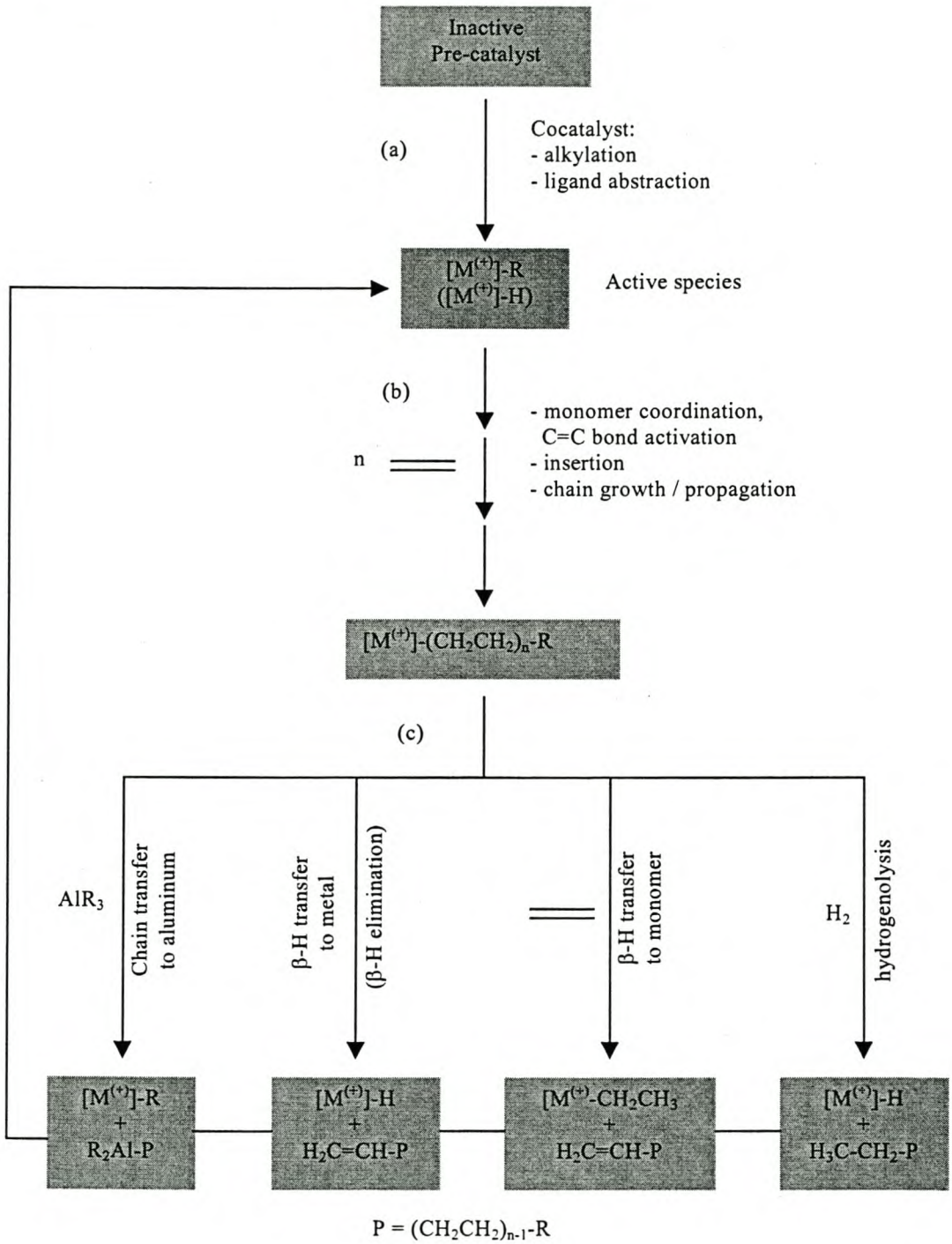

Figure 2.6 General features of the Ziegler-Natta polymerization mechanism.

From the inactive precatalyst, the cocatalyst creates an active metal alkyl species by alkylation (if necessary) and ligand abstraction in (a) to create a vacant coordination site. In (b) repeated monomer coordination and insertion then leads to chain growth/propagation in competition with chain transfer (termination) reactions in (c) to aluminum, by β-hydrogen transfer to metal or to monomer or by hydrogenolysis (if hydrogen is added as a molar mass regulator). The metal-alkyl or metal-hydride species formed from chain transfer are still active and can start a new polymerization process again.

For the insertion of an olefin into a transition metal alkyl bond in Ziegler-Natta polymerization in (b), three basic mechanisms have been suggested, each being supported by experimental evidence: (i) the direct insertion mechanism, proposed by Cossee and Arlman **[81-83]**, involving a loosely coordinated four-center transition state (Figure 2.7); (ii) the metathesis mechanism, proposed by Green and Rooney **[84-85]**, in which an α-hydrogen transfer from the end of the polymer chain and formation of a metal carbene/alkylidene precede the formation of a metallacyclobutane complex (Figure 2.8) and (iii) the 'modified Green-Rooney mechanism' **[86-88]**. There, an α-agostic C-H interaction in a transition state was proposed to assist the insertion of an olefin (Figure 2.9).

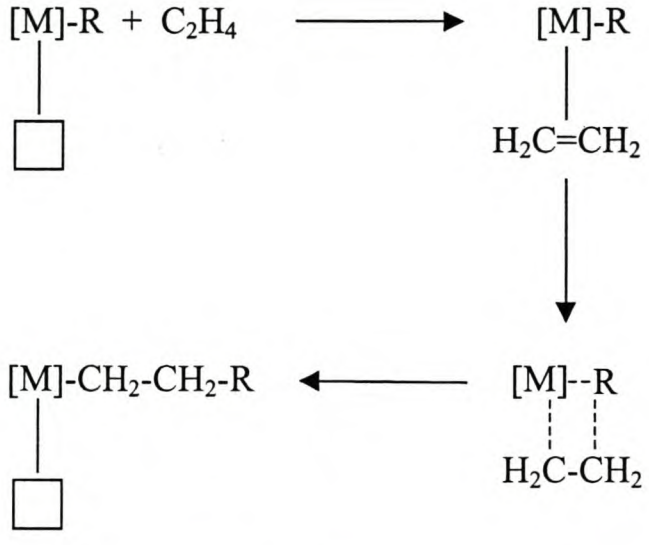

Figure 2.7 Direct insertion mechanism according to Cossee-Arlman for the olefin insertion into a transition metyl alkyl bond [81-83]. (□ = vacant coordination site)

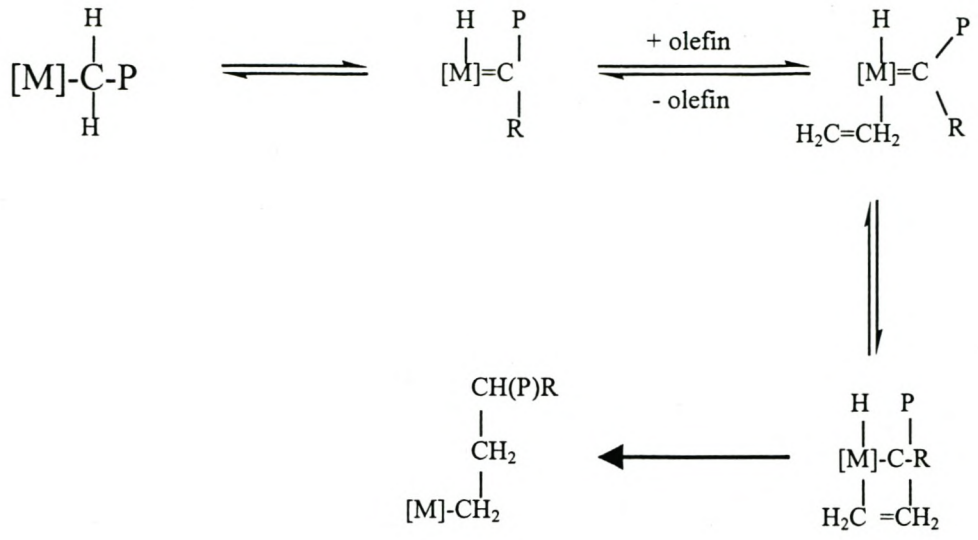

Figure 2.8 **Metathesis-mechanism according to Green-Rooney for the olefin insertion into a transition metal-alkyl bond [84-85].**

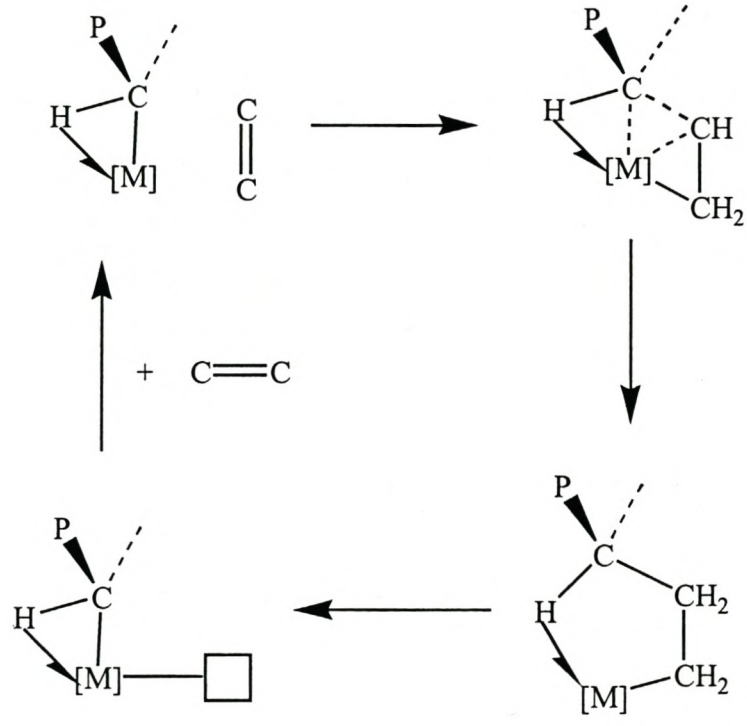

Figure 2.9 **Schematic representation of the suggested features for the modified Green-Rooney mechanism for the insertion of an olefin in a transition metal alkyl bond in Ziegler-Natta polymerization [86-88].**

2.3 REACTION MECHANISM OF THE PREPARATION OF POLYMERS PRODUCED BY METALLOCENE CATALYSTS

2.3.1 The cocatalyst

The most widely used cocatalyst is methylaluminoxane (MAO). The reason for this is its ability to activate the largest number of metallocenes and other soluble transition metal complexes. MAO is obtained by controlled hydrolysis of $AlMe_3$ and consists of oligomers of approximate composition $(MeAlO)_n$, but its true composition is far from known. Various analytical studies (i.e. cryoscopic, GPC and NMR studies) have shown that MAO is a mixture of several different compounds, including residual (coordinated) $AlMe_3$ and possibly AlO_3 units in dynamic equilibrium **[89-93]**. A detailed study was carried out by Barron et al. **[94, 95]** on the hydrolysis products of Al(*t*-Bu)$_3$. In the light of their results, dynamic cage structures seem more likely than linear and cyclic ones.

The main drawbacks of MAO as cocatalyst are:

- its high cost, due to the expensive $AlMe_3$ parent compound,
- the large amount needed (typically Al/Zr = 10^3 to 10^4 molar are used)
- and, as a consequence, the high content of alumina residues in the final product.

A major improvement towards simpler and cheaper metallocene based systems has been the use of boron compounds such as $B(C_6F_5)_3$, $NR_3H^+B(C_6F_5)_4^-$ and $Ph_3C^+B(C_6F_5)_4^-$, in combination with metallocene dialkyls **[96-100]**. As these systems are not able to scavenge impurities, and a large part of the activated catalyst has to be sacrificed for that purpose, much better results have been achieved by adding small amounts of AlR_3 (such as Al(*i*-Bu)$_3$ and $AlEt_3$) to the reaction system with a double advantage: AlR_3 scavenges impurities and alkylates the metallocene so that the simpler metallocene dichloride can be used **[101-102]**.

By using these boron compounds the active metallocene alkyl cation can be generated by means of the following reactions:

$Cp_2MMe_2 + [NHMe_2Ph]^+[B(C_6F_5)_4]^- \longrightarrow Cp_2M^+Me[B(C_6F_5)_4]^- + Me_2NPh + CH_4$

$Cp_2MMe_2 + Ph_3C^+[B(C_6F_5)_4]^- \longrightarrow Cp_2M^+Me[B(C_6F_5)_4]^- + Ph_3CMe$

$CpMMe_2 + B(C_6F_5)_3 \longrightarrow Cp_2M^+Me[B(C_6F_5)_3Me]^-$

2.3.2 Catalyst activation

A catalytically active system develops when hydrocarbon solutions of Cp_2MCl_2 are mixed with MAO. As shown in Figure 2.9 a fast, ligand exchange reaction generates Cp_2MClMe and also Cp_2MMe_2 **[103, 104]** in the presence of excess MAO. Spectroscopic evidence **[105-106]** is consistent with the assumption that Lewis acidic centres present in MAO are able to accept CH_3^- (or Cl^-) anions from the alkylated metallocene, thus generating a metallocene alkyl cation, the active polymerization species **[107-108]**, and a poorly coordinating counterion.

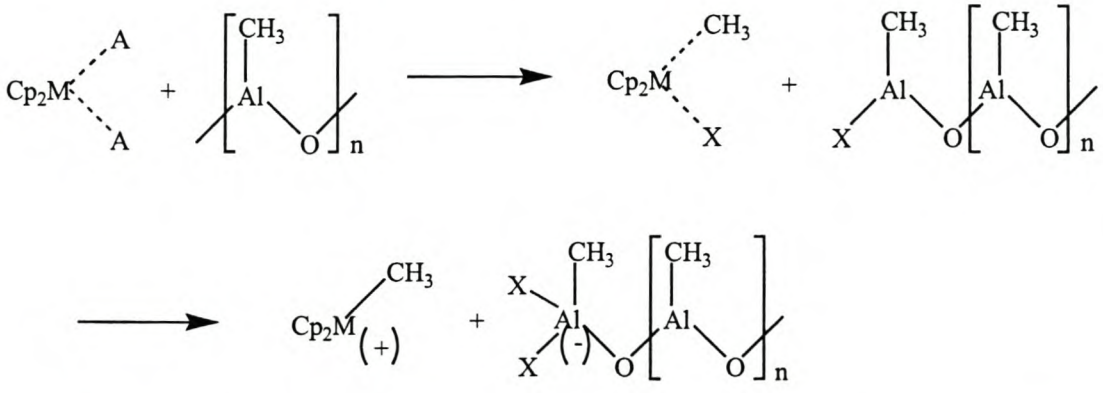

Figure 2.10 Formation of a metallocene alkyl cation by reaction between a metallocene and methylaluminoxane.

2.3.3 Propagation

The insertion of an α-olefin in the metal carbon bond may take place in two different ways, which is shown in Figure 2.11.

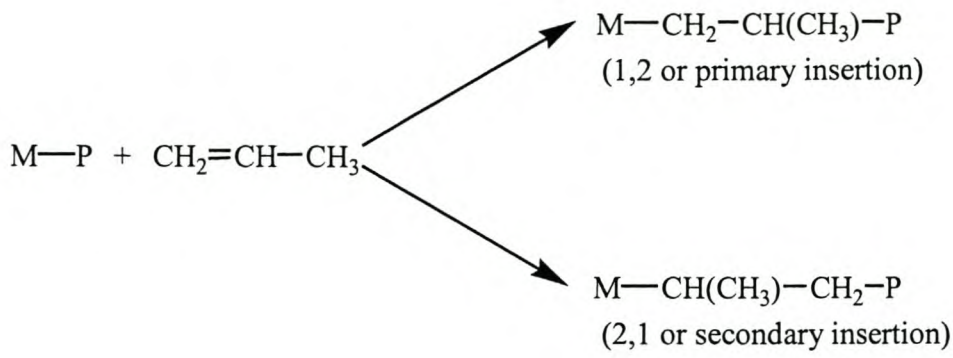

Figure 2.11 Primary and secondary insertion of an α-olefin in the metal-carbon bond.

It was proved by chain end group analysis, that the 1,2 insertion mode is predominent in isospecific polymerization of olefins with both heterogeneous **[109-111]** and metallocene-based **[112-113]** catalysts and in syndiospecific polymerization of propylene with the homogeneous $Me_2C(Cp,F)ZrCl_2$ / MAO catalyst system **[114]**. The 2,1 insertion however is preferred in the syndiotactic propylene polymerization with VCl_4 / Et_2AlCl catalyst and syndiospecific styrene polymerization **[115]**.

Isospecific polypropylene obtained with chiral C_2-symmetry group 4 metallocenes (i.e. $Et(Ind)_2ZrCl_2$) includes a small number (about 1%) of isolated regioirregular structural units resulting from 2,1 and 1,3 insertion of the monomer as shown in Figure 2.12.

—CH_2—CH(CH_3)—CH(CH_3)—CH_2—CH_2—CH(CH_3)— 2,1 insertion

—CH_2—CH(CH_3)—CH_2—CH_2—CH_2—CH_2—CH(CH_3)— 1,3 insertion

Figure 2.12 2,1- and 1,3 insertion for α-olefins.

These insertions are revealed by the presence of $(CH_2)_2$ and $(CH_2)_4$ groups. The content of the two regioirregularities and their relative proportion depends on the π-ligands, polymerization temperature, and monomer concentration **[116]**. In general

regioirregularities are mainly of 2,1 type when the activity of the catalyst is very high **[117-118]**.

2.3.4 Termination

Termination of polypropylene polymerization using metallocene-based catalyst systems usually takes place in four different ways, which are illustrated in Figure 2.13 **[119-121]**.

(a)

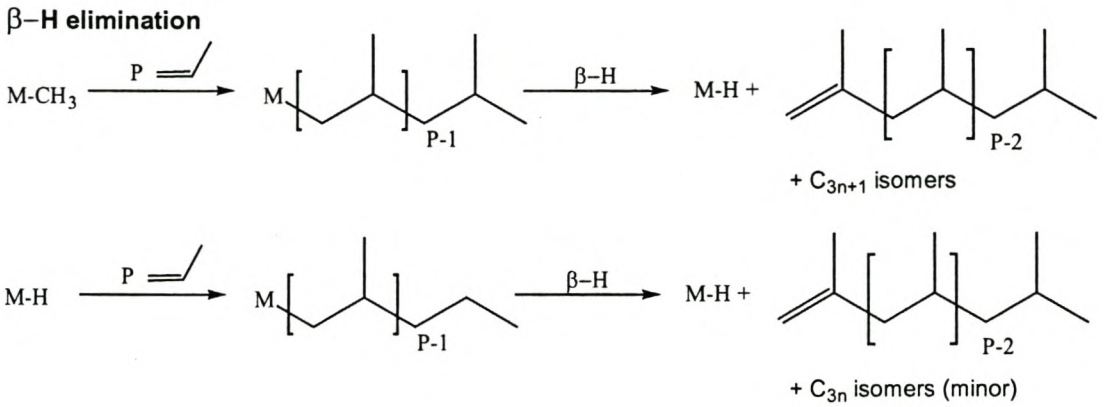

(b)

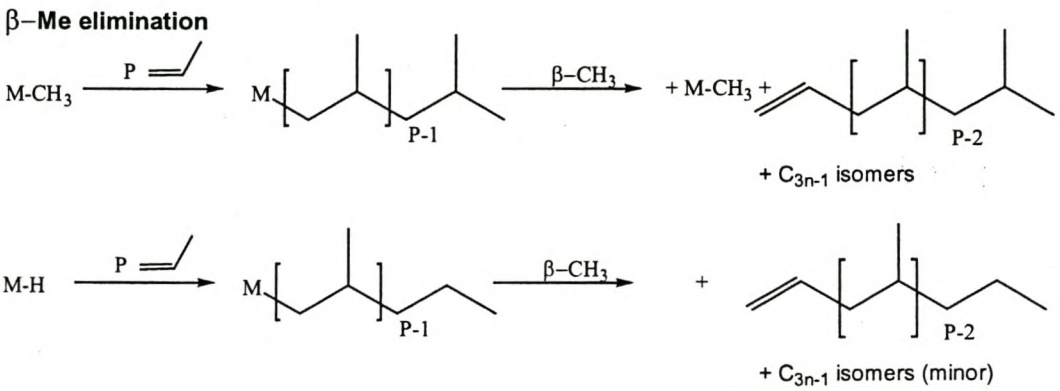

(c)

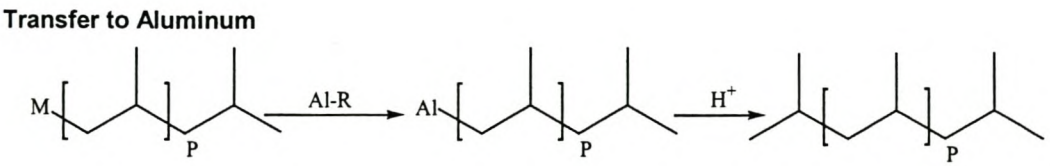

(d)

Transfer to monomer

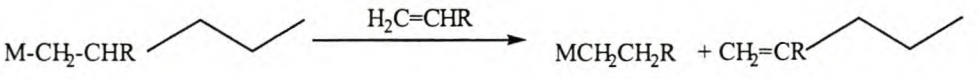

Figure2.13 Termination of polypropylene polymerization through (a) β-H elimination, (b) β-Me elimination, (c) transfer to aluminium and (d) transfer to the comonomer [117-118].

2.4 CONCLUSIONS

One of the most important differences between homogeneous metallocene catalysts and conventional heterogeneous Ziegler-Natta catalysts is the ability of metallocene catalysts to copolymerize a wide variety of olefins without sacrificing the extraordinary uniformity with respect to narrow molecular weight distribution and especially molecular weight independent comonomer incorporation. Polymerization at the active site of Ziegler Natta catalysts is influenced by the electronic and steric environment of the crystal lattice. Because the active centres can occupy a wide variety of lattice sites, they tend to give products with a broad molecular weight distribution (MWD) and also non-homogeneous comonomer distribution in olefin copolymers. This non-homogeneous distribution of comonomer leads to low tacticity in copolymers. In metallocene catalysts however the catalytic sites are shielded to a large extent from the influence of their immediate surroundings. These catalysts therefore yield a sharply defined product with a narrow MWD ($M_w/M_n \approx 2$) and other molecular characteristics, as well as a minimum of undesirable byproducts (e.g. atactic polypropylene in isotactic polypropylene). Metallocene catalysts can therefore produce highly isotactic copolymers.

2.5 REFERENCES

1. Mamielec A.E., Soares J.B.P., *Polypropylene: An A-Z reference*, (Karger-Kocsis J., Ed.) Kluwer Academic Publishers, Dordrecht, 1999, p. 447.
2. Zambelli A., Ammendola P., Grassi A., Longo P., Pronto A., *Macromolecules*, 1986, **19**, 2703.
3. Zambelli A., Longo P., Ammendola P., Grassi A., *Gazz. Chim. Ital.*, 1986, **116**, 731.

3. Zambelli A., Longo P., Ammendola P., Grassi A., *Gazz. Chim. Ital.*, 1986, **116**, 731.
4. Zambelli A., Ammendola P., *Gazz. Chim. Ital.*, 1986, **116**, 329.
5. Grassi A., Zambelli A., Resconi L., Albizatti E., Mazzocchi R., *Macromolecules*, 1988, **21**, 617.
6. Chien J.C.W., He D., *J. Polym. Sci. Part A*, 1991, **29**, 1585.
7. Chien J.C.W., He D., *J. Polym. Sci. Part A*, 1991, **29**, 1595.
8. Chien J.C.W., He D., *J. Polym. Sci. Part A*, 1991, **29**, 1603.
9. Chien J.C.W., He D., *J. Polym. Sci. Part A*, 1991, **29**, 1609.
10. Chien J.C.W., Nozaki T., *J. Polym. Sci. Part A: Polym. Chem.*, 1993. **31**, 227.
11. Chien J.C.W., Xu B., *Makromol. Chem. Rapid Commun.*, 1993, **14**, 109.
12. Uozumi T., Soga K., *Makromol. Chem.*, 1992, **193**, 823.
13. Tsutsui T., Kashiwa N., *Polym. Commun.*, 1988, **29**, 180.
14. Tsutsui T., Mizuno A., Kashiwa N., *Polymer*, 1989, **30**, 428.
15. Mülhaupt R., *Polypropylene: An A-Z reference*, (Karger-Kocsis J., Ed.) Kluwer Academic Publishers, Dordrecht, 1999, p. 910.
16. Pino P., Mülhaupt R., *Angew. Chem. Int. Ed. Engl.*, 1980, **19**, 857.
17. Brintzinger H.H., Fischer D., Mülhaupt R., Rieger B., Waymouth R.M., *Angew. Chem. Int. Ed. Engl.*, 1995, **34**, 1143.
18. Tait P.J.T., *Comprehensive Polymer Science*, Vol. 7, (Allen G., Bevington J.C., Eastmond G.C., Ledwith A., Russo S., Sigwalt P., Eds.), Permagon, Oxford, 1989, p. 1.
19. ibid, p. 533.
20. ibid, p. 575.
21. ibid, p. 29.
22. Nielson R.P., *Transition Metal Catalysts*, (Quirk R.P., Ed.), Harwood, New York, 1983, p. 47.
23. Chadwick J.C., *Ziegler Catalysts*, (Fink G., Mülhaupt R., Brintzinger H.H., Eds.), Springer-Verlag, Berlin, 1995, p. 428.
24. Galli P., Barbe P.C., Noristi L., *Angew. Makromol. Chem.* 1984, **120**, 73.
25. Barbe P.C., Cecchin G., Noristi L., *Adv. Polym. Sci.*, 1987, **81**, 1.

26. Tait P.J.T., Zohuri G.H., Kells A.M., McKenzie I.D., *Ziegler Catalysts*, (Fink G., Mülhaupt R., Brintzinger H.H., Eds.), Springer-Verlag, Berlin, 1987, p. 344.
27. Goodall B.L., *Transition metal catalyzed polymerizations*, Part A, (Quirk T.P., Ed.), Harwood, New York, 1983, p. 355.
28. Mülhaupt R., *Polypropylene: An A-Z reference*, (Karger-Kocsis J., Ed.), Kluwer Academic Publishers, Dordrecht, 1999, p. 913.
29. Kashiwa N., Kojoh S., *Macromol. Symp.*, 1995, **89**, 27.
30. Soga K., Shiono T., Doi Y., *Makromol. Chem.*, 1988, **189**, 1531.
31. Spitz R., Bobichon C., Gugot A., *Makromol. Chem.*, 1989, **190**, 707.
32. Hu Y., Chien J.C.W., *Polymer Sci. Polymer Chem.*, 1988, **26**, 2003.
33. Seppälä J.V., Härkönen M., Luciani L., *Makromol. Chem.*, 1989, **190**, 2535.
34. Albizzati E., Giannini U., Morini G., Smith C.A., Ziegler R.C., *Ziegler Catalysts*, (Fink G., Mülhaupt R., Brintzinger H.H, Eds.), Springer-Verlag, Berlin, 1995, p. 413.
35. Iiskola E., Pelkonen A., Kakkonen H.J., Pursiainen J., Pakkanen T.A., *Makromol. Chem. Rapid Commun.*, 1993, **14**, 133.
36. Galli P., Haylock J.C., Simonazzi T., *Polypropylene, Structure, Blends and Composites*, Vol. 2, (Karger-Kocsis J., Ed.), Chapman & Hall, London, 1995, p. 1.
37. Galli P., Haylock J.C., *Macromol. Symp.*, 1992, **63**, 19.
38. Albizzati E., Giannini U., Collina G., Noristi L., Resconi L., *Polypropylene Handbook*, (Moore E.P., jr., Ed.), Hanser Publishers, Munich, 1996, p. 46.
39. Breslow D.S., Newburg N.R., *J. Am. Chem. Soc.*, 1957, **79**, 5072.
40. Natta G., Pino P., Mazzanti G., Giannini U., *J. Am. Chem. Soc.*, 1957, **79**, 2957.
41. Mashima k., Nakayama Y., Nakamura A., *Adv. Polym. Sci.*, 1997, **133**. 1.
42. U.S. Patent, 4 522 982, 1960, Hercules.
43. Reichart K.M., Meyer K.R., *Makromol. Chem.*, 1973, **169**, 163.
44. Long W.P., Breslow D.S., *Justus Liebigs Ann. Chem.*, 1975, 463.

45. Andresen A., Cordes H.G., Herwig J., Kaminsky K., Merck A., Mottweiler R., Pein J., Sinn H., Vollmer H.J., *Angew. Chem. Int. Ed. Engl.*, 1976, **15**, 630.

46. Sinn H., Kaminsky W., *Adv. Organomet. Chem.*, 1980, **18**, 99.

47. Matkovsky P.E., Belov G.P., Kissin Y.V., Chirkov N.M., *Vysokomol. Soed.*, 1970, **A12**, 2286.

48. Belov G.P., Belova V.N., Raspopov L.N., Kissin Y.V., Birkenshtein K.A., Chirkov N.M., *Polym. J.*, 1972, **3**, 681.

49. Ewen J.A., Jones R.L., Razavi A., Ferrara J.P., *J. Am. Chem. Soc.*, 1988, **110**, 6255.

50. Wilkinson G., Birmingham I.M., *J. Am. Chem. Soc.*, 1954, **76**, 4281.

51. Wild F.R.W.P., Zsolani L., Huttner G., Brintzinger H.H., *J. Organomet. Chem.*, 1982, **232**, 233.

52. Kaminsky W., Kulper K. Brintzinger H.H., Wald F.R., *Angew. Chem. Int. Ed. Engl.*, 1985, **24**, 507.

53. Farina M., Di Silvestro G., Terragni A., *Makromol. Chem. Phys.*, 1995, **196**, 353.

54. Mülhaupt R., *Polypropylene: An A-Z reference*, (Karger-Kocsis J., Ed.) Kluwer Academic Publishers, Dordrecht, 1999, p. 468.

55. ibid, p. 448.

56. ibid, p. 461.

57. Reddy S.S., Sivaram S., *Prog. Polym. Sci.*, 1995, **20**, 309.

58. Tsutsui T., Ishimaru N., Mizuno A., Toyota A., Kashiwa N., *Polymer*, 1989, **30**, 1350.

59. Hirose T., Tsutsui T., Toyota A., (Mitsui Petrochemical Industries, Ltd.) Japanese Kokai 01,173,111, *Chem. Abstr.*, 1991, **114**, 7423w.

60. Winter A., Dolle V., Rohrmann J., Antberg M., Boehm L, Walter S., (Hoechst A-G) German Offen. DE 3,914,468, *Chem. Abstr.*, 1991, **114**, 62977e.

61. Shiomura T., Sanuma T.A., Kouno M., Inoue N., Fukushima S., Sonobe Y., Mizutani K., Iwantani T., Sugimoto R., (Mitsui Toatsu Chemicals, Inc.) PCT Int. Appl. WO 91,15,523(1991), *Chem. Abstr.*, 1992, **116**, 4222r.

62. Schreck M., Winter A., Spaleck W., Kondoch H., Rohrmann J., (Hoechst A-G) European Patent Appl. EP 433,990, *Chem. Abstr.*, 1991, **115**, 160011a.

63. Winter A., Dolle V., Rohrmann J., Spaleck W., Antberg M., (Hoechst A-G) European Patent Appl. EP 433,986, *Chem. Abstr.*, 1991, **115**, 233115z.

64. Asanuma T., Iwantani T., Sugimoto R., Inoue N., Kouno M., Shiomura T., (Mitsui Toatsu Chemical, Inc.) European Patent Appl. 452,763(1991), *Chem. Abstr.*, 1991, **116**, 84387P.

65. Uozumi T., Soga K., Bello A., Perez E., Lacatelli P., Fan Z.Q., Zucchi D., *Polym. Bull.*, 1996, **36**, 249.

66. Arnold M., Henschke O., Knorr J., *Macromol. Chem. Phys.*, 1996, **197**, 563.

67. De Rosa C., Talarico B., Caporaso L., Auriemma F., Galimberti M., Fusco O., *Macromolecules*, 1998, **31**, 9109.

68. Forlini F., Fan Z-Q., Tritto I., Lacatelli P., Sacchi M.C., *Macromol. Chem. Phys.*, 1997, **198**, 2397.

69. Naga N., Mizunuma K., Sadatoshi H., Kakugo M., *Macromolecules*, 1997, **30**, 2197.

70. Fink G., Ojala T.A., *Transition Metal Organometallics as Catalysts for Olefin Polymerization*, (Kaminsky W., Sinn H., Eds.), Springer-Verlag, Berlin, 1988, p. 169.

71. Jüngling S., Koltzenburg S., Mülhaupt R., *J. Polym. Sci. Part A: Polym. Chem.*, 1997, **35**, 1.

72. Banzi V., Angiolini L., Caretti D., Carlini C., *Angew. Makromol. Chem.*, 1995, **229**, 113.

73. Jüngling S., Mülhaupt R., Fischer D., Langhauser F., *Angew. Makromol. Chem.*, 1995, **229**, 93.

74. Herfert N., Montag P., Fink G., *Makromol. Chem.*, 1993, **194**, 3167.

75. Van Reenen A.J., Brull R., Wahner U., Raubenheimer H.G., Sanderson R.D., Pasch H., *J. Polym. Sci., Polymer Chem. Ed.*, 2000, **38**, 4110.

76. Brull R., Wahner U., Van Reenen A.J., Raubenheimer H.G., Sanderson R.D., Pasch H., *J. Macromol. Chem. Phys.*, 2001, **202**, 1281.

77. Albizzati E., Giannini U., Collina G., Noristi L., Resconi L., *Polypropylene Handbook*, (Moore E.P., jr., Ed.), Hanser Publishers, Munich, 1996, p. 91.
78. Van der Ven S., *Propylene and other polyolefins*, Elseriver, 1990.
79. Cheng H.N., Kakugo M., *Macromolecules*, 1991, **24**, 1835.
80. Togni A., Halterman R.L., *Metallocenes*, Vol. 2, Wiley-VCH, Weinheim, 1998, p. 563.
81. Cossee P., *J. Catal.*, 1964, **3**, 80.
82. Arlman E.J., *J. Catal.*, 1964, **3**, 89
83. Arlman E.J., Cossee P., *J. Catal.*, 1964, **3**, 99.
84. Ivin K.J., Rooney J.J., Stewart C.D., Green M.L.H., Mahtab R., *J. Chem. Soc., Chem. Commun.*, 1978, 604.
85. Green M.L.H., *Pure Appl. Chem.*, 1978, **50**, 27.
86. Grubbs R.H., Coates G.W., *Acc. Chem. Res.*, 1996, **29**, 85.
87. Brookhart M., Green M.L.H., Wong L.L., *Prog. Inorg. Chem.*, 1988, **36**, 1.
88. Brookhart M., Green M.L.H., Wong L.L., *J. Organomet. Chem.*, 1983, **250**, 395.
89. Halterman R.L., *Chem. Rev.*, 1992, **92**, 965.
90. Sinn H., Bliemeister J., Clausnitzer D. Tikwe L., Winter H., Zarcke O., *Transition Metals and Organometallics as Catalysts for Olefin Polymerization*, (Kaminsky W., Sinn H., Eds.), Springer-Verlag, Berlin, 1988, p. 257.
91. Cam D., Albizatti E., Giannini U., *Makromol. Chem.*, 1990, **191**, 1641.
92. Resconi L., Bossi S., Abis L., *Makromolecules*, 1990, **23**, 4489.
93. Sugano T., Matsbara K., Fujita T., Takahashi T., *J. Mol. Catal.*, 1993, **82**, 93.
94. Mason M.R., Smith J.M., Bott S.G., Barron A.R., *J Am. Chem. Soc.*, 1993, **115**, 4971.
95. Harlan C.J., Mason M.R., Barron A.R., *Organometallics*, 1994, **13**, 2957.
96. Yang X., Stern O.L., Marks T.J., *J. Am. Chem. Soc.*, 1991, **113**, 3623.
97. Yang X., Stern O.L., Marks T.J., *J. Am. Chem. Soc.*, 1994, **116**, 10015.
98. Bochmann M., Lancaster S.J., *Organometallics*, 1993, **12**, 633.
99. Chien J.C.W., Tsai W., Rausch M.D., *J. Am. Chem. Soc.*, 1991, **113**, 8570.
100. Herfert N., Fink G., *Macromol. Chem. Rapid Commun.*, 1993, **14**, 91.

101. European Patent Appl. 513 380, 1992, Idemitsu.

102. Tsai W., Rausch M.D., Chien J.C.W., *Appl. Organomet. Chem.*, 1993, **7**, 71.

103. Kaminsky W., Burk A., Steiger R., *J. Mol. Catal.*, 1992, **74**, 109.

104. Tritto I., Li S., Sacchi M.C., Zannoni G., *Macromolecules*, 1993, **26**, 7111.

105. Siedle A.R., Lamanna W.M., Newmark R.A., *Makromol. Chem. Makromol. Symp.*, 1993, **66**, 215.

106. Shista C., Hatorn R.M., Marks T.J., *J. Am. Chem. Soc.*, 1992, **114**, 1112.

107. Jordan R.F., Bajyur C.S., Willet R., Scott B., *J. Am. Chem. Soc.*, 1986, **108**, 7410.

108. Jordan R.F., *Adv. Organomet. Chem.*,1991, **32**, 325.

109. Natta G., Pino P., Mantica E., Danusso F., Mazzanti G., Peraldo M., *Chim. Id. (Milan)*, 1956, **38**, 124.

110. Zambelli A., Locatelli P., Sacchi M.C., Tritto I., *Macromolecules*, 1982, **15**, 831.

111. Sacchi M.C., Tritto I., Locatelli P., *Prog. Polym. Sci.*, 1991, **16**, 331.

112. Ewen J.A., *J. Am.Chem. Soc.*, 1984, **106**, 6355.

113. Zambelli A., Ammendola P., Grassi A., Longo P., Proto A., *Macromolecules*, 1986, **19**, 2703.

114. Ewen J.A., Jones R.L., Razavi A., Ferrara J.D., *J. Am. Chem. Soc.*, 1988, **110**, 6255.

115. Zambelli A., Longo P., Pellecchia C., Grassi A., *Macromolecules*, 1987, **20**, 2035.

116. Busico V., Cipullo R., Chadwick J.C., Modder J.F., Sudweijer O., *Macromolecules*, 1994, **27**, 7538.

117. Spaleck W., Küber F., Winter A., Rohrmann J., Bachmann B., Antberg M., Doll V., Paulus E.F., *Organometallics*, 1994, **13**, 954.

118. Stehling U., Diebold J., Kirsten R., Röll W., Brintzinger H.H., Jüngling S., Mülhaupt R., Langhauser F., *Organometallics*,1994, **13**,964.

119. Bassi I.W., Polato F., Calcaterra M., Bart J.C.J., *Z. Crystallogr.*, 1982, **159**, 297.

120. Albizatti E., *Chim. Ind. (Milano)*, 1993, **17**, 107.

121. Resconi L., Cavallo L., Fait A., Piemontesi F., *Chem. Rev.*, 2000, 1253.

CHAPTER 3

Polymerization and characterization of propylene/1-hexene and propylene/1-octene copolymers produced with *rac*-$Et(Ind)_2ZrCl_2$/MAO

Summary

One series each of propylene/1-hexene and propylene/1-octene copolymers were synthesized with different percentages of comonomer incorporated into the propylene backbone. The copolymerizations were carried out using the isospecific, bridged metallocene rac-[ethylene *bis*(1-indenyl)]zirconium dichloride (*rac*-$Et(Ind)_2ZrCl_2$) as activating catalyst. These copolymers were used to investigate the effect of the two α-olefin comonomers on the microstructure, molecular mass, molecular mass distribution, melting point, glass transition temperature and crystallization behaviour of the different series copolymers produced. Characterization methods on the obtained copolymers included differential scanning calorimetry (DSC), high temperature gel permeation chromatography (HTGPC), dynamic mechanical analysis (DMA), nuclear magnetic resonance spectroscopy (NMR) and crystallization analysis fractionation (CRYSTAF). Each series of copolymers was compared within the series itself and also with the other series as entity. The two copolymer series were produced and analyzed mainly to compare with the propylene/1-heptene copolymers which will be discussed in the following two chapters.

3.1 INTRODUCTION

Metallocene catalysts are organometallic coordination compounds in which one or two cyclopentadienyl rings or substituted cyclopentadienyl rings are π-bonded to a central transition metal atom. The most remarkable feature of these catalysts is that their molecular structure can be designed to create active centre types to produce polymers with entirely novel properties.

Currently, there are six review articles published in the literature on metallocene catalysts, covering different aspects of metallocene catalyst synthesis, nature of active sites, polymerization mechanisms, metallocene catalyst patents and polymerization reaction engineering **[1–6]**.

In the last 15 years, the field of polyolefin chemistry has gone through a renaissance with major achievements in control over the polymer microstructures and hence over the bulk properties of this important family of organic polymers. This development was triggered by the synthesis of stereorigid *ansa*-zirconocene dichlorides by Brintzinger's group at the University of Konstanz at the beginning of the 1980's **[7-9]**. The indenyl groups define a certain stereochemistry and the ethylene bridge hinders rotation of these moieties and thus fixes their position relative to each other. In the following years, John Ewen (1984) **[10]** and Walter Kaminsky (1985) **[11]** and their co-workers succeeded in the preparation of isotactic polypropylene by applying the racemic mixture of the S- and R-enantiomers, activated by methylaluminoxane (MAO). For the first time it was possible to correlate a molecularly defined active catalyst species with the microstructure of a stereoregular polymer chain. This opened the way to a new catalyst generation, where all the active species have a uniform structure ('single-site catalysts').

Bis(cyclopentadienyl) group IV metal complexes are currently introduced in industry as a new generation of Ziegler-Natta catalysts for the polymerization of olefins **[12-21]**. Among the group IV metallocenes of titanium, zirconium and hafnium, the zirconocene complexes deserve the most interest both academically and industrially as their combination of properties gears them towards application. Hence the so-called 'metallocene catalysts' are mostly zirconocene derivatives, with zirconocene dichloride being the parent system. Their development as practical polymerization catalysts is the first large-scale industrial application for the long known and well developed class of metallocene complexes **[22-23]**. Of all the fascinating organometallic chemical aspects in metallocene catalysis, the key aspect which earned them their enormous industrial research input is that group IV metallocene catalysts make the synthesis of polymers possible that cannot be produced by conventional Ziegler-Natta catalysts.

The *ansa* metallocene catalysts possess very high polymerization activities over a wide range of comonomer feed compositions. This investigation comprised a study of the effect of the amount of comonomer (1-hexene and 1-octene respectively) on the propylene/α-olefin copolymerization with the isospecific catalyst *rac*-[ethylene *bis*(1-indenyl)]zirconium dichloride (*rac*-Et(Ind)$_2$ZrCl$_2$) (Figure 3.1). The influence of the amount of comonomer incorporated in the copolymer on the copolymer microstructure, molecular mass, molecular mass distribution, melting point, glass transition temperature and crystallization behaviour is reported here.

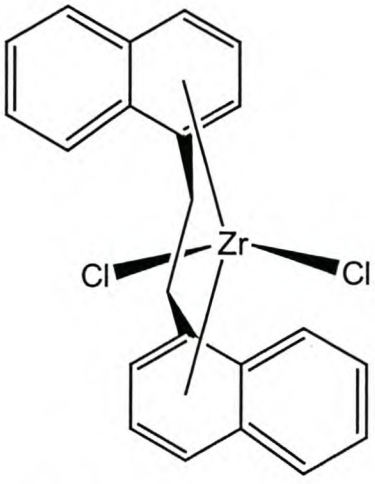

Figure 3.1 *rac*-Et(Ind)$_2$ZrCl$_2$

3.2 EXPERIMENTAL

All catalyst manipulations were carried out in a glovebox in a nitrogen atmosphere. The catalyst used in this study was the stereorigid C_2-symmetric ethylene *bis*(indenyl)zirconium dichloride, *rac*-Et(Ind)$_2$ZrCl$_2$. This metallocene catalyst was obtained from Strem Chemicals and used as received. All reagents were adequately dried and glassware, including syringes, and the steel reactor base were kept in an oven at 110°C prior to use. These precautions were necessary due to the moisture and air sensitivity of the catalyst. Analytical grade toluene was used as solvent in all the reactions and was obtained from Aldrich. Toluene was refluxed over sodium and then distilled onto 3Å molecular sieves which was obtained from Aldrich. The comonomers, 1-hexene and 1-octene, were obtained from Polifin and refluxed over lithium aluminium hydride ($LiAlH_4$) and afterwards also distilled onto 3Å molecular sieves. Propylene (polymerization grade, > 99%) was obtained from

Fedgas and purified by passing through three columns containing BASF catalyst R3-11G and R3-12 and molecular sieves obtained from Polifin. Methylaluminoxane (MAO) was obtained from Aldrich as a 10% wt solution in toluene and was used as received.

3.3 EQUIPMENT

3.3.1 Polymerization equipment

A 350 ml stainless-steel Parr autoclave which was equipped with a fitted seal ring and a pressure gauge was used for the polymerization reactions.

3.3.2 Analytical equipment

The copolymers were analyzed by nuclear magnetic resonance (NMR), high termperature gel permeation chromatography (HTGPC), differential scanning calorimetry (DSC), dynamic mechanical analysis (DMA) and crystallization analysis fractionation (CRYSTAF).

3.3.2.1 Nuclear magnetic resonance (NMR)

Broadband proton decoupled ^{13}C syntheses were conducted at 5.42 MHz, using a Varian VXR 300 NMR spectrometer. By using a pulse angle of 45 degrees and a relatively short repetition time of 0.82 seconds, good sensitivity could be obtained by accumulating only 4 000 transients for each sample. Resolution and accuracy were improved by zero-filling the data once before performing the Fourier transformation. Baseline correction was also applied in order to further enhance the accuracy and repeatability of the integrals measured for selected peaks in the spectra. Samples (~ 80mg) for ^{13}C NMR analyses were dissolved at 110°C in a mixture of 1,2,4,-trichlorobenzene and benzene-d_6 (9:1 volume ratio). The analyses of these samples were executed at 100°C.

3.3.2.2 Differential scanning calorimetry (DSC)

Differential scanning calorimetry (DSC) analyses on the different copolymers were carried out with a (Du Pont 9900 Computer/Thermal analyzer), in order to

determine their different melting points (T_m). The samples (8 – 10 mg) were heated in aluminium pans in a nitrogen atmosphere at a rate of 10°C/min to a temperature of 200°C. Thereafter they were allowed to cool down to room temperature before they were reheated at the same rate. The endothermic peaks of the DSC curves represent the melting temperatures.

3.3.2.3 *High temperature gel permeation chromatoghraphy (HTGPC)*

Samples for high temperature gel permeation chromatoghraphy (HTGPC) were analyzed with a Waters Alkana 2 000 GPC with a flow rate of 1,0 ml/min.. The analyses were carried out in 1,2,4,-trichlorobenzene at 145°C and the molecular mass and molecular mass distributions were obtained from this. Each set of samples include a polystyrene standard and a NBS 1475a standard in order to check the validity of data against the calibration curve data. Polystyrene standards, varying in molecular weight from 31 000 000 – 1 000 g/mol were used for calibration. Differential Refractive Index was used for detection.

3.3.2.4 *Crystallization analysis fractionation (CRYSTAF)*

For CRYSTAF analyses of the different samples, a Hewlett Packard 5890 II was used for the crystallization temperature program. Crystallization of the polymers was carried out in 5 stainless steel reactors of 60 mL capacity each in which dissolution and filtration takes place automatically. Each of these reactors is also fitted with a stirrer. A dual wave length optoelectronic infrared detector together with a heated flow-through micro cell was used to measure the polymer concentration in solution at each sampling step during the crystallization. The microcell operates at 150°C and uses 3.5 μ as the measuring wavelength. Samples were dissolved in trichlorobenzene (commercial grade) at a concentration of 0.1% w/v. The samples were stabilized at 110°C for one hour after dissolving them at 140°C. After this crystallization took place at a rate of 0.10°C/min. until the temperature reached 30°C.

3.4 SYNTHESIS OF COPOLYMERS

3.4.1 Preparation of catalyst solution

The catalyst solution was prepared at least 12 hours prior to use. About 5 mg of ethylene *bis*(indenyl)zirconium dichloride, *rac*-Et(Ind)$_2$ZrCl$_2$ was accurately weighed in a glove box under nitrogen atmosphere and then dissolved in 10 ml of dry toluene. The dissolved catalyst was stored at 4°C.

3.4.2 Propylene copolymerization

All the copolymerizations were carried out in a 350 ml stainless steel pressure reactor fitted with a magnetic stirring bar of which all parts were kept in an oven at 110°C prior to use. Typically, the reactor was first evacuated and then flushed with nitrogen while cooling down to room temperature. Injection of the methylaluminoxane, solvent and comonomer were all completed in a nitrogen atmosphere. 5 ml methylaluminoxane (MAO) was introduced first and stirred for 5 minutes in order to scavenge any impurities present in the reactor. Thereafter 10 ml of toluene was injected as well as the specific comonomer. The reactor was then placed in a dry ice bath (-70°C) while introducing approximately 50 g gaseous propylene. The catalyst solution (1 ml) was then injected to initiate the polymerization reaction. The reactor was then allowed to warm to room temperature and the reaction was allowed to continue for 3½ hours. The reactor was then vented and the copolymer produced was precipitated in 200 ml methanol, acidified with 10 ml (10 wt%) aqueous hydrochloric acid. After stirring overnight, the copolymer was filtered, washed with methanol and dried.

Two different series of copolymers were synthesized varying the amounts of comonomers in each series. The reaction conditions were kept constant for all the copolymerizations. A summary for these two series copolymers can be seen in Table 3.1.

Table 3.1 Experimental information of propylene/1-hexene and propylene/1-octene copolymers produced by *rac*-Et(Ind)$_2$ZrCl$_2$.

Sample	1-hexene (A2-A6)/ 1-octene (A7-A11) feed (mL)
A1	0
A2	7.4
A3	11.1
A4	14.9
A5	22.3
A6	29.7
A7	9.3
A8	14.0
A9	18.7
A10	28.0
A11	37.3

Conversions were kept to below 20% in all reactions.

3.5 RESULTS AND DISCUSSION

3.5.1 Microstructure

Carbon-13 nuclear magnetic resonance (^{13}C-NMR) spectroscopy is used extensively to study the microstructure of polymers. ^{13}C-NMR can be used to determine overall composition and the sequence distribution in copolymers; if two or more monomer units are present, it can provide a quantitative determination of the mixture composition. In this study we investigated the branches formed when 1-hexene and 1-octene were incorporated respectively into polypropylene by using the *rac*-Et(Ind)$_2$ZrCl$_2$/MAO catalyst system.

3.5.1.1 Polypropylene homopolymer

The main advantage of NMR in the characterization of polymers is the unique molecular structural information which can be obtained. For instance, the relative

configurational distribution (tacticity) and regioirregularities (defects) in homopolymers of polypropylene can be mapped out and represent a unique fingerprint of polymer microstructure.

Figure 3.2 shows a typical ^{13}C NMR spectrum of sample A1, a relatively highly isotactic polypropylene homopolymer **(I)** synthesized using the isospecific catalyst, *rac*-Et(Ind)$_2$ZrCl$_2$. The spectrum contains three primary resonance signals which can be identified as those of (a) the methylene carbons (δ = 46.04 ppm), of (b) the methine carbons (δ = 28.38 ppm), and of (c) the methyl carbons (δ = 21.47 ppm) of polypropylene **[24]**. Often, the methyl region is chosen for tacticity analysis due to good chemical shift resolution. According to the spectrum the polymer is relatively highly isotactic and the resonances diagnostic of isolated regioirregular units can also be observed. The isotacticity can be inferred from the intense peak at δ = 46.04 ppm **[25]** and the relatively few and small stereoirregularities.

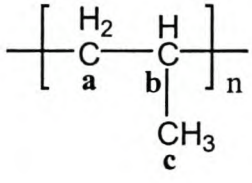

I

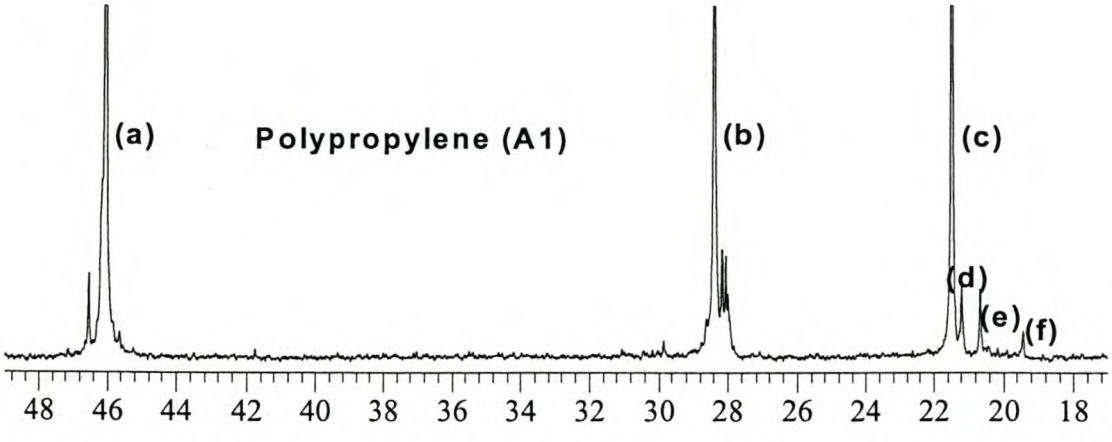

Figure 3.2 ^{13}C NMR spectrum of isotactic polypropylene (Sample A1).

Assuming stereochemical shifts of the methyl pentads are grouped together according to the central triad sequences *mm*, *mr* and *rr*, from low to high field **[26]**, at least ten resonances can be assigned to the unique pentad sequences **[27]**, observed in the order *mmmm*, *mmmr*, *rmmr*, *mmrr*, *mmrm*, *rmrr*, *mrmr*, *rrrr*, *rrrm* and *mrrm*.

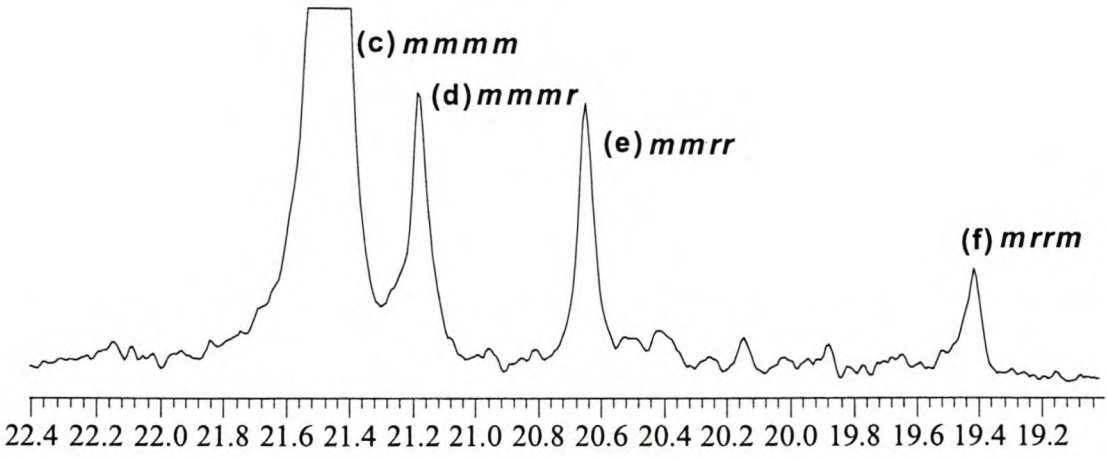

Figure 3.3 ^{13}C NMR spectrum of the methyl region of Sample A1.
Solvent 1,2,4-trichlorobenzene:benzene-d_6 (9:1 volume ratio), temperature 100°C.

The methyl region is chosen for tacticity analysis. The peaks due to the stereoirregular *mmmm* (δ = 21.47 ppm) and the stereoirregular units *mmmr* (δ = 21.18 ppm), *mmrr* (δ = 20.65 ppm) and *mrrm* (δ = 19.42 ppm) of sample A1 can be seen in Figure 3.3 indicated respectively as (c), (d), (e) and (f). These assignments correspond with previous investigations **[28-29]** and the relative intensities of the resonance of the *mmmr*, *mmrr* and *mrrm* stereochemical pentads are roughly 2:2:1 **[24]**, as expected from the statistical model **[30]** of the enantiomorphic site control of the stereospecific propagation **[33]**. The tacticity of this homopolymer was determined by way of integrating the methyl peak region and this shows a 84.5% isotactic polypropylene.

According to Ewen **[31]** the ^{13}C NMR analyses of the steric pentads of this highly isotactic polypropylene are consistent with the polymer having the configurational microstructure represented by the idealized structure **(II) [32-33]**.

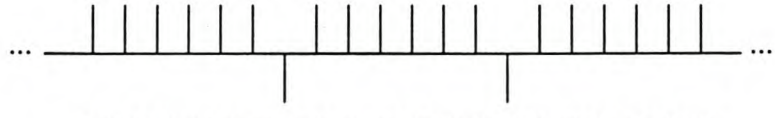

m m m m m m r m m m m m m m r m m m m m m

II

The pseudoasymmetric methine carbon atoms of successive monomer units have the same relative configuration with occasional placements of units with opposite handedness. The relative configuration of the adjacent pseudoasymmetric centers are used in NMR notation **[27]**. The structure **(II)** therefore corresponds to stereosequences of isotactic meso (m) dyads connected by pairs of syndiotactic racemic (r) dyads which results from a catalytic-site mechanism of stereocontrol (enantiomorphic site control).

In addition small peaks can be observed in Figure 3.2 in the areas of 30 ppm and 42 ppm. These regioirregularities result from 2,1-type insertion and produce head-to-head units. The intensities of these peaks however are low and corresponds to approximately 1% of 2,1 and 3,1 misinsertions. These peaks are actually quite significant, because 2,1 misinsertions often lead to chain termination and this limits molecular weight.

3.5.1.2 Propylene/1-hexene and propylene/1-octene copolymers

Assignments of the different peaks appearing in the spectra of the produced propylene/1hexene (Samples A2-A5) and propylene/1-octene (Samples A7-A11) copolymers were done making use of the literature where possible, combined with APT analyses and checked against the chemical shift assignments predicted by the additivity rules described by Grant and Paul **[34]**.

APT analysis converts ^{13}C signals into positive and negative signals **[35]** where the positive amplitudes indicate CH_2- and C-carbon atoms and the negative amplitudes indicate CH_3- and CH-carbon atoms. Figures 3.5 and 3.6 compare the APT ^{13}C NMR spectrum with the normal ^{13}C NMR spectrum of propylene/1-hexene (Sample A2). Carbon atoms are numbered according to the structure in Figure 3.4, counting from the methyl group of the side chain towards the branch carbon (br) and α-carbon of the comonomer. This is followed by the methyl, branch and α-carbons of the propylene unit as demonstrated in Figure 3.4.

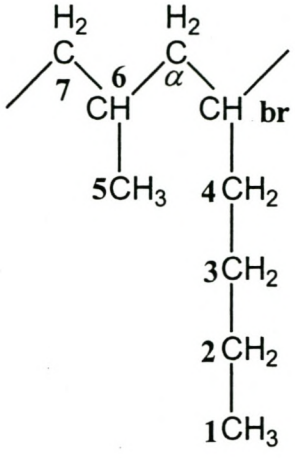

Figure 3.4 **Numbering of carbon atoms of propylene/1-hexene copolymers for chemical shift predictions.**

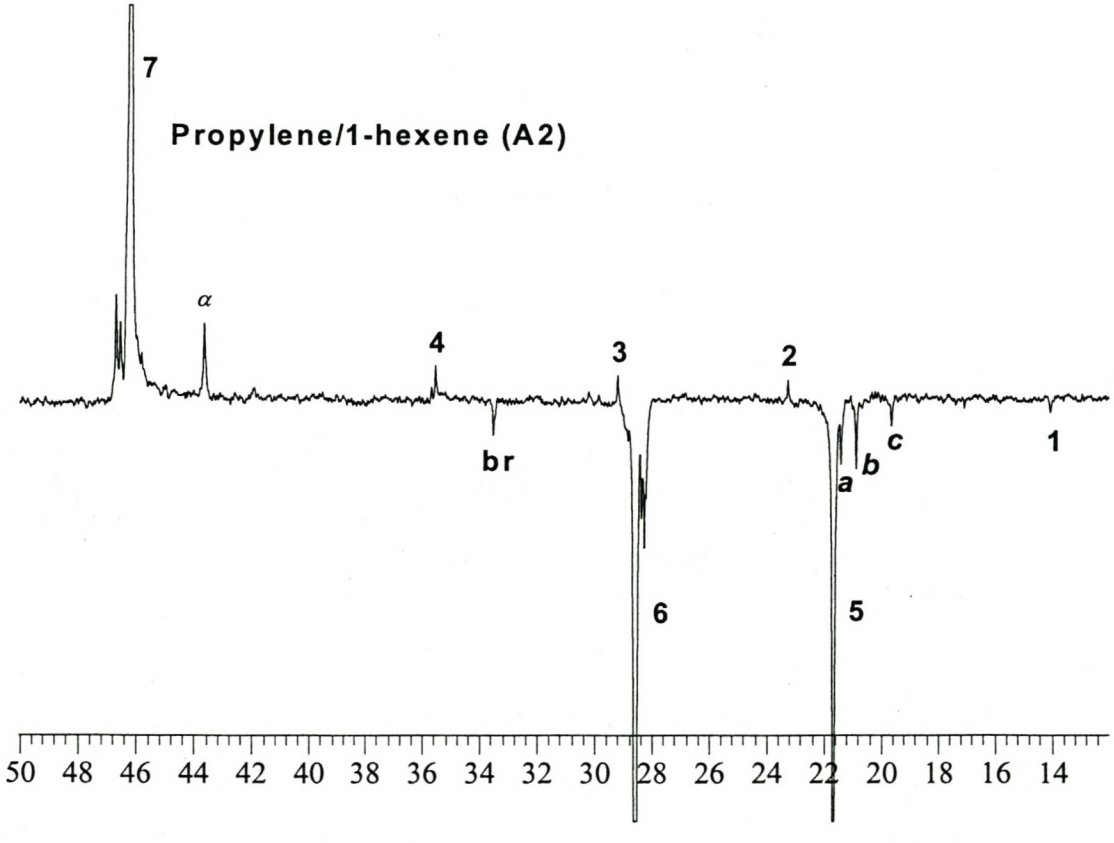

Figure 3.5 **APT ^{13}C NMR spectrum of a propylene/1-hexene copolymer (Sample A2).**

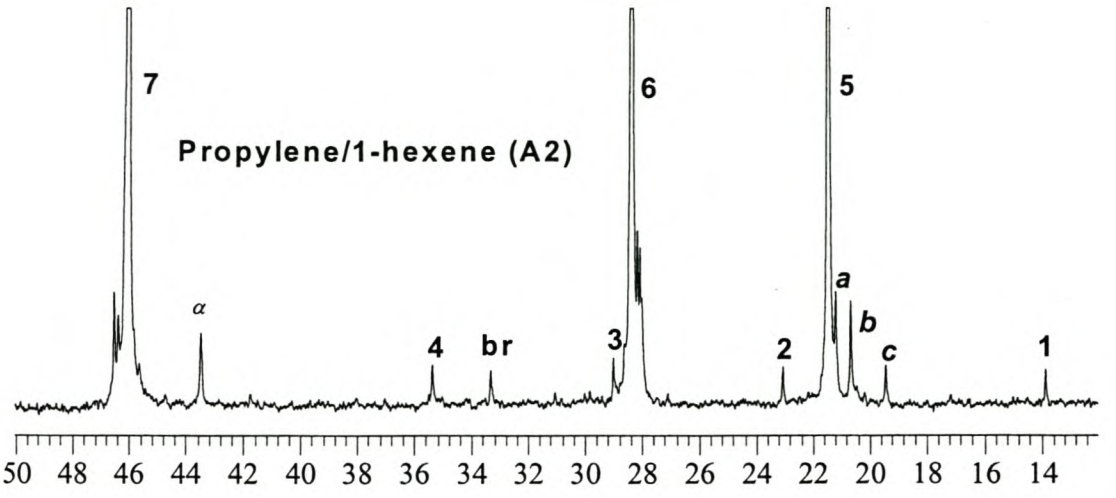

Figure 3.6 **^{13}C NMR spectrum of a propylene/1-hexene copolymer (Sample A2).**

From the spectrum in Figure 3.5 it can be seen that the signals numbered as ***br***, ***5***, ***6*** and ***1*** have negative amplitudes and therefore correspond to CH_3- and CH-carbon atoms. Signals numbered as ***a***, ***b*** and ***c*** also have negative amplitudes and occur because of regioirregularities which were discussed in Section 3.5.1.1. The rest of the signals have positive amplitudes and therefore correspond to CH_2- and C-carbon atoms.

The same method was used to characterize the carbon atoms of the propylene/1-octene copolymers (Samples A7-A11). The ^{13}C NMR spectrum of Sample A9 is shown in Figure 3.8. For consistency carbon atoms are numbered in the same way (shown in Figure 3.7) as with the propylene/1-hexene copolymers.

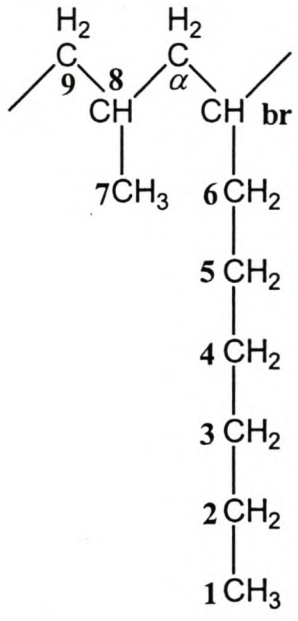

Figure 3.7 Numbering of carbon atoms of propylene/1-octene copolymers for chemical shift predictions.

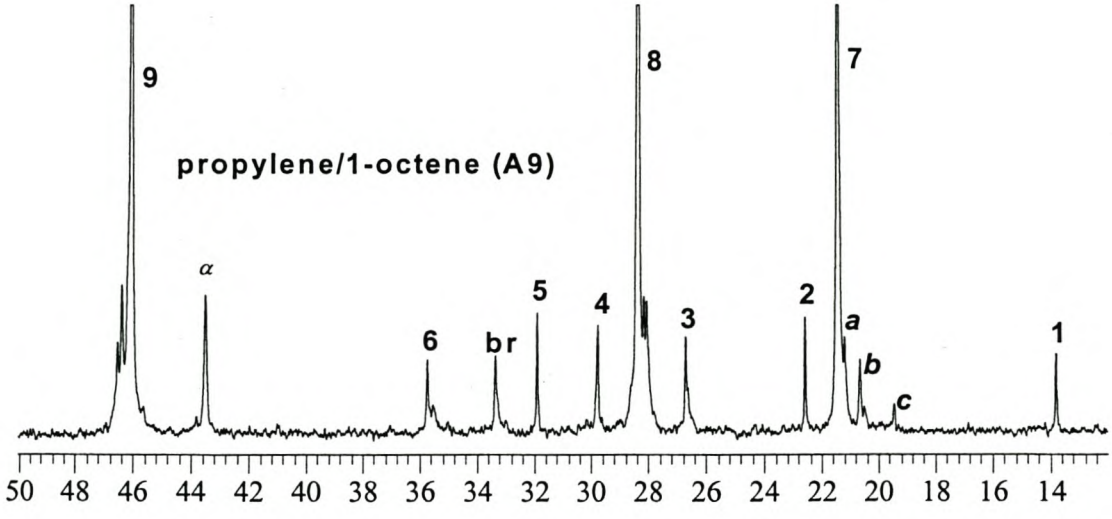

Figure 3.8 ^{13}C NMR spectrum of a propylene/1-octene copolymer (Sample A9).

The different comonomer content in each of the copolymers produced by the bridged *rac*-Et(Ind)$_2$ZrCl$_2$ catalyst are summarized in Table 3.2. In calculating the percentage of comonomer incorporated in each copolymer, the intensities of only the backbone carbon atoms are taken into account. The formulas for calculating the percentage of 1-hexene (**III**) and 1-octene (**IV**) in a specific copolymer respectively are the following **[36]**:

$$C_6 = \frac{\frac{1}{2}(I_\alpha + I_{br})}{I_\alpha + I_{br} + I_6 + I_7} \times 100 \qquad \text{III}$$

$$C_8 = \frac{\frac{1}{2}(I_\alpha + I_{br})}{I_\alpha + I_{br} + I_8 + I_9} \times 100 \qquad \text{IV}$$

C_6 and C_8 represent the percentage of comonomer incorporated and $I_\alpha, I_{br}, I_6, I_7, I_8, I_9$ represent the intensities of the carbon peaks of the backbone of the polymer as numbered in Figure 3.4 and Figure 3.7.

Table 3.2 Summary of comonomer content of propylene/1-hexene (Sample A2-A6) and propylene/1-octene (Sample A7-A11) copolymers.

Sample	Comonomer content (%)
A2	1.20
A3	2.51
A4	3.53
A5	4.10
A6	6.36
A7	2.16
A8	3.89
A9	5.40
A10	6.32
A11	7.08

According to Grant and Paul **[34]** the chemical shift values of the carbons of the copolymers can be calculated by using the following linear equation:

$$\delta_C(k) = B + \sum_l A_l n_{kl} + \sum_l S_l \qquad \text{V}$$

$\delta_C(k)$ is the carbon-13 chemical shift value of the specific k th carbon, B is a regression constant which is equal to –1,87 ppm (the chemical shift of methane), n_{kl} is the number of carbons in the l th position relative to the specific k th carbon, and A_l is the additive chemical shift parameter assigned to the l th carbon atom. The l th

position is counted only for the first five neighbouring carbons. Thus the amount of carbons in the α, β, χ, δ and ε positions relative to the carbon for which the chemical shift is being determined, is counted and each multiplied by its respective correction factor and added together. The last term in the equation is included to account for branching. In this regard, for example, the chemical shift of a tertiary carbon atom having a secondary neighbour, $3^{\circ}(2^{\circ})$, a secondary carbon atom having a tertiary neighbour, $2^{\circ}(3^{\circ})$, and a primary carbon atom having a tertiary neighbour, $1^{\circ}(3^{\circ})$, have different specific influences on chemical shifts.

Table 3.3 demonstrates the calculation of the different chemical shift prediction values for the propylene/α-olefin copolymers investigated in this study. This table represents only values for the isolated comonomer branch, propylene-propylene-comonomer-propylene (ppcp). At higher comonomer concentrations sequences other than ppcp appear and should be included in the calculations of the comonomer content. The predicted chemical shifts for propylene/1-heptene copolymers of the CH_2 and branching CH for the pppp, pppc, cppc, cccc, cccp, pccp, ppcc, cpcc, ppcp, and cpcp sequences were calculated in a previous study **[37]**.

Table 3.3 Chemical shift prediction for propylene / (α-olefin) copolymers utilizing the Grant and Paul additivity rules.

Position	α	β	γ	δ	ε	3°(2°)	2°(3°)	1°(3°)	Constant
Factor	**8.61**	**9.78**	**-2.88**	**0.37**	**0.06**	**-2.65**	**-2.45**	**-1.4**	**-1.87**
Carbon	**Propylene / 1-Hexene**								**Chemical Shift (ppm)**
1	1	1	1	1	2				14.13
2	2	1	1	2	2				23.11
3	2	2	2	2	4				30.13
4	2	3	3	4	2		1		35.20
br	3	3	5	3	4	3			32.30
α	2	4	3	5	3		2		42.96
5	1	2	2	4	3			1	20.80
6	3	2	4	3	5	3			25.46
7	2	4	2	4	3		2		45.47
	Propylene / 1-Octene								
1	1	1	1	1	1				14.07
2	2	1	1	1	1				22.68
3	2	2	1	1	2				32.52
4	2	2	2	2	2				30.01
5	2	2	3	3	4				27.62
6	2	3	3	5	3		1		35.63
br	3	3	5	3	5	3			32.36
α	2	4	3	5	3		2		42.96
7	1	2	2	4	3			1	20.80
8	3	2	4	3	5	3			25.46
9	2	4	2	4	3		2		45.47

In Table 3.4 and Table 3.5 the observed chemical shift values of the produced propylene/1-hexene and propylene/1-octene copolymers respectively are compared with the values calculated above. The observed and calculated values correspond very well overall.

Table 3.4 Comparison of observed and calculated chemical shifts of propylene / 1-hexene (Samples A2–A6) copolymers.

Carbon	1	2	3	4	br	α	5	6	7
Calculated Grant and Paul	**14.13**	**23.11**	**30.13**	**35.20**	**32.30**	**42.96**	**20.80**	**25.46**	**45.47**
Observed A2	13.85	23.04	29.00	35.36	33.32	43.48	21.47	28.40	46.05
Observed A3	13.78	23.05	29.03	35.37	33.34	43.50	21.43	28.39	46.06
Observed A4	13.84	23.05	29.01	35.36	33.31	43.48	21.46	28.37	46.05
Observed A5	13.84	23.04	28.99	35.34	33.31	43.47	21.46	28.38	46.04
Observed A6	13.84	23.07	29.01	35.38	33.33	43.48	21.47	28.39	46.06

Table 3.5 Comparison of observed and calculated chemical shifts of propylene / 1-octene (Samples A7–A11) copolymers.

Carbon	1	2	3	4	5	6	br	α	7	8	9
Calculated Grant and Paul	**14.07**	**22.68**	**32.52**	**30.01**	**27.62**	**35.63**	**32.36**	**42.96**	**20.80**	**25.46**	**45.47**
Observed A7	13.78	22.58	26.71	29.76	31.88	35.97	33.35	43.48	21.45	28.39	46.05
Observed A8	13.79	22.58	26.70	29.76	31.88	35.71	33.36	43.48	21.45	28.39	46.06
Observed A9	13.80	22.59	26.70	29.77	31.89	35.73	33.35	43.49	21.47	28.40	46.06
Observed A10	13.78	22.58	26.71	29.78	31.89	35.73	33.35	43.80	21.45	28.37	46.04
Observed A11	13.80	22.60	26.70	29.77	31.90	35.70	33.32	43.45	21.45	28.34	46.01

The methyl peak regions were integrated in each spectrum in order to calculate the tacticity of the various polymers. These calculations are summarized in Table 3.6 and as with the propylene homopolymer, these copolymers also are shown to be highly isotactic. No real conclusion can be drawn of the effect of the comonomer content on the tacticity of the copolymers. The reason for this is the fact that the copolymers produced by the $Et(Ind)_2ZrCl_2$ catalyst have very low molecular weight as will be discussed next in Section 3.5.2.

Table 3.6 Tacticity values of propylene/1-hexene (Samples A2-A6) and propylene/1-octene (Samples A7-A11) copolymers.

Sample	1-hexene (A2-A6)/ 1-octene (A7-A11) content (mol %)	Tacticity (%)
A2	1.20	81.7
A3	2.51	83.2
A4	3.53	90.9
A5	4.10	78.0
A6	6.36	80.4
A7	2.16	82.1
A8	3.89	72.1
A9	5.40	79.9
A10	6.32	85.7
A11	7.08	87.5

3.5.2 Molecular mass and molecular mass distributions

The fundamental measure of MWD is gel permeation chromatography, currently known as size exclusion chromatrography, which responds to the physical size of the different molecules in dilute solution. In this technique, the polymer solution is passed over a porous medium from which the different sized molecules elute at different times. Assuming the column was properly calibrated, which is not a

simple task, the curve of the eluted material versus time becomes the molecular weight distribution. From that curve, it is possible to calculate the weight-average molecular weight, M_w, and the number-average molecular weight, M_n. The ratio of these two, M_w/M_n, the polydispersity, is a widely used term to describe molecular weight distribution (MWD).

The molecular weight distribution of metallocene-based polypropylene is narrow ($M_w/M_n \approx 2\text{-}2.5$) compared to $M_w/M_n \approx 6\text{-}8$ for conventional polypropylene. Metallocene catalysts also provide a very uniform distribution of comonomers, which is particulary important in random copolymers. In conventional copolymers (produced by heterogeneous Ziegler-Natta catalysts), the comonomer content varies with molecular weight, which, together with the atactic fraction, contributes to stickiness and difficulties in production and handling. Metallocene copolymers show a virtually constant composition with molecular weight. This eliminates the most sticky fraction, the highly substituted low molecular weight end. Consequently, it is possible to prepare copolymers with higher average comonomer concentrations, and therefore lower melting points, without problems with plugging and agglomeration in polymerization.

From Figure3.9 it can be seen that the GPC curves of the copolymers have a characteristic shape, predicted by Flory's distribution law. The molecular mass distributions of such copolymers do not change with polymerization time. The molecular mass at the maximum is related to the weight-average molecular mass of the polymer.

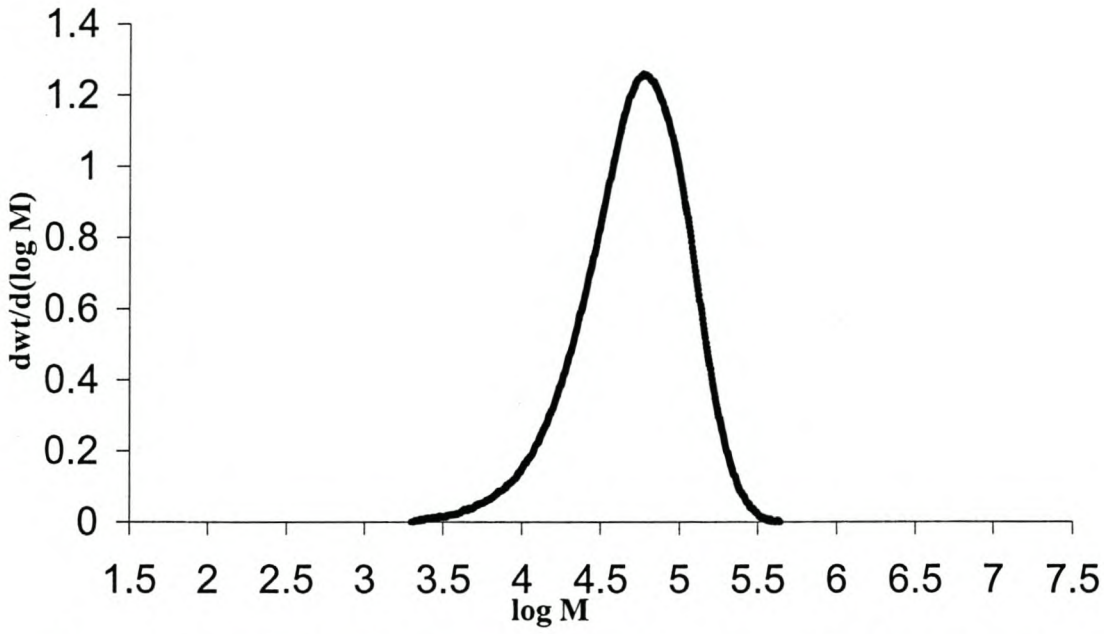

Figure 3.9 The distribution of the molecular mass, w(logM), against the molecular mass of propylene/1-hexene (Sample A4, 3.53% 1-hexene).

Table 3.7 represents the molecular mass results of the GPC analyses carried out on the propylene homopolymer and on the propylene/1-hexene and propylene/1-octene copolymers. Because of the nature of the bridged metallocene *rac*-$Et(Ind)_2ZrCl_2$ catalyst, which was used as polymerizing catalyst for these polymers, the number-average (M_n) as well as the weight average (M_w) molecular masses of the all these polymers are very low. These low molecular masses are the reason why copolymers which were polymerized by the $Et(Ind)_2ZrCl_2$ catalyst are not suitable for industrial use. As expected the polydispersity of the polymers in Table 3.7 were all in the region of 2. This feature is very characteristic of single site catalysts which produces copolymers with uniform comonomer incorporation.

Table 3.7 GPC results of propylene homopolymer (Sample A1) and propylene/1-hexene (Samples A2-A6) and propylene/1-octene copolymers (Samples A7-A11).

Sample	1-hexene (A2-A6)/ 1-octene (A7-A11) content (mol %)	Number-Average Molecular Mass (M_n, g/mole)	Weight-Average Molecular Mass (M_w, g/mole)	Polydispersity (M_w/M_n)
A1	0	11 949	44 504	3.72
A2	1.20	15 881	42 169	2.66
A3	2.51	11 732	26 332	2.24
A4	3.53	37 321	68 325	1.83
A5	4.10	8 373	28 257	3.37
A6	6.36	27 145	52 308	1.93
A7	2.16	13 569	36 969	2.72
A8	3.89	10 078	35 655	3.54
A9	5.40	14 004	36 479	2.60
A10	6.32	36 186	65 771	1.82
A11	7.08	20 242	38 501	1.90

3.5.3 Thermal properties

3.5.3.1 Melting behaviour

The most popular method to study thermal properties of semi-crystalline polymers is by differential scanning calorimetry (DSC). Detailed structural information can be uncovered by a careful interpretation of DSC thermograms generated under different conditions (cooling and heating at various rates, multiple cooling and heating conditions, etc.). Owing to the narrow intermolecular comonomer distribution in metallocene-catalyzed copolymers, they usually have a much broader melting peak than their heterogeneous counterparts produced by multiple site Z-N catalysts as we will discuss in Chapter 5.

Homogeneous semi-crystalline polymers chain-fold to form lamellae with a distribution of thickness during crystallization under a standard set of conditions and these lamellae melt at different temperatures **[38]**. The thicknesses of the lamellae are directly related to the crystallization temperature or degree of supercooling **[39]**.

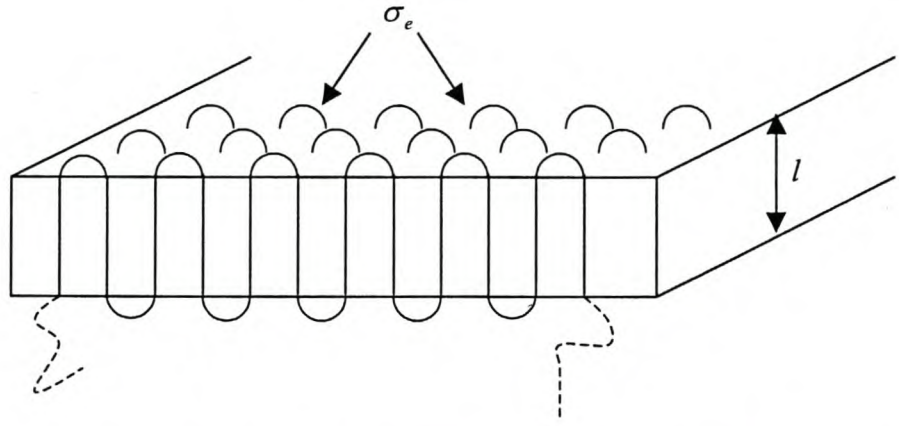

Figure 3.10 Folded chain lamellar morphology in semi-crystalline polymers (l is the lamellar thickness and σ_e is the fold surface interfacial energy).

A particular lamellar thickness, l, is kinetically favoured at a given crystallization temperature, resulting in a folded conformation of chains with lamellae as demonstrated in Figure 3.10. It can readily be shown **[40-41]** that a thin lamellar dimension results in a melting point depression as given by equation **VI**.

$$T_m = T_m^o\left\{1-\left(\frac{2\sigma_e}{\Delta h_f l}\right)\right\} \qquad \textbf{VI}$$

With reference to Figure 3.10, σ_e is the fold surface interfacial energy, Δh_f is the heat of fusion per unit volume of crystal, l is the lamellar thickness, T_m is the observed melting point and T_m^o is the theoretical equilibrium melting point of a perfect and infinitely large crystal. Equation **VI** relates the melting point to the lamellar thickness and predicts that thick crystals melt at high temperature and, conversely, thin crystals melt at lower temperature.

Table 3.8 represents the results of the DSC analyses of the propylene homopolymer and the propylene/1-hexene and propylene/1-octene copolymers

produced with the bridged *rac*-Et(Ind)$_2$ZrCl$_2$ catalyst. The measured fusion enthalpy given in the table was converted to the degree of crystallinity by taking the ratio of the measured heat of fusion to that of a standard of known crystallinity. The heat of fusion of a perfect polypropylene crystal, used in the determination of the crystallinity, was taken as 209 J/g **[42]**.

Table 3.8 DSC results of propylene homopolymer (Sample A1) and propylene/1-hexene (Samples A2-A6) and propylene/1-octene copolymers (Samples A7-A11).

Sample	1-hexene (A2-A6)/ 1-octene (A7-A11) content (mol %)	Melting Temperature (°C)	FUSION ENTHALPY (J/G)	CRYSTALLINITY (%)
A1	0	134.2	50.8	24.3
A2	1.20	121.6	35.4	16.9
A3	2.51	100.3	19.9	9.5
A4	3.53	102.9	24.8	11.9
A5	4.10	93.0	14.0	6.7
A6	6.36	77.0	12.9	6.2
A7	2.16	106.3	23.4	11.2
A8	3.89	106.3	25.1	12.0
A9	5.40	93.0	17.6	8.4
A10	6.32	79.0	13.8	6.6
A11	7.08	60.3	7.0	3.3

Comonomer incorporated into the polymer will lead to defects in an otherwise regular chain and will hinder the chain-folding process of forming lamellae to a certain extent. In Table 3.8 and Figure 3.13 it can be seen that even the smallest amount of 1-hexene comonomer incorporated (Sample A2, 1.20 mol%) into the polypropylene backbone caused a decrease of 12.6°C in the melting point peak of the propylene homopolymer which was produced with the same bridged catalyst. The more comonomer branches present in a chain, the broader its melting peak will be and

the lower the height of the peak will be **[43]**. This effect can clearly be seen when comparing the two DSC melting exotherms of Figure 3.11 (1.20 mol% 1-hexene) and Figure 3.12 (6.36 mol% 1-hexene).

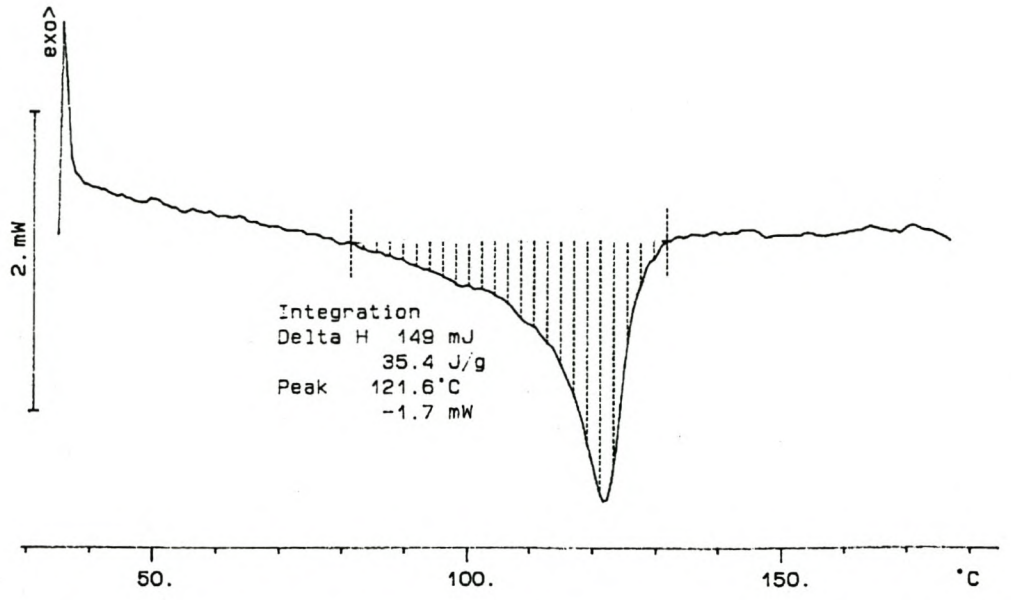

Figure 3.11 DSC melting curve of propylene/1-hexene (Sample A2, 1.20 mol%) copolymer.

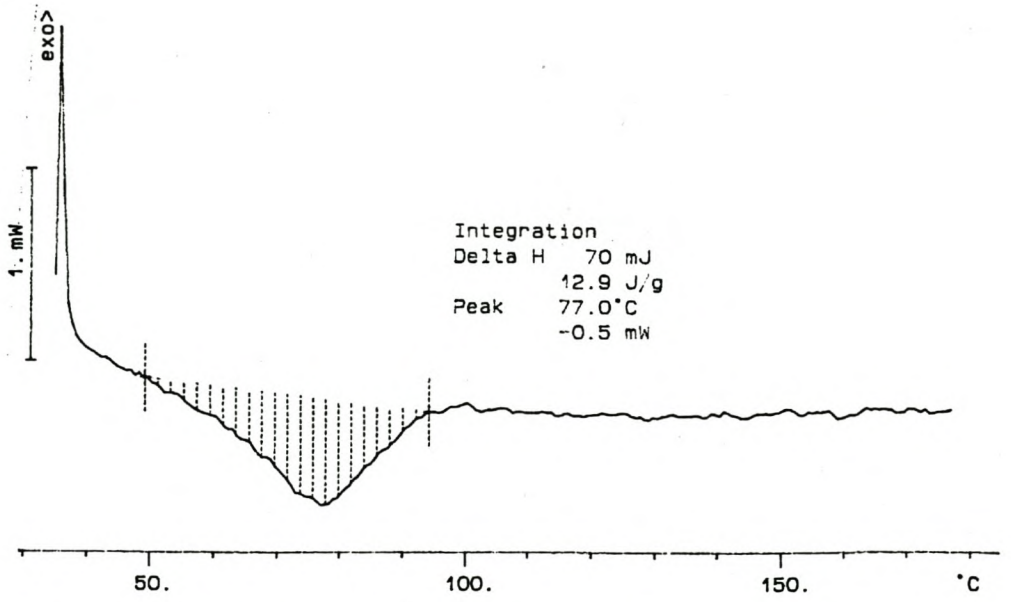

Figure 3.12 DSC melting curve of propylene/1-hexene (Sample A6, 6.36 mol%) copolymer.

When the amount of comonomer increases, the sequence length of the crystallizable units decreases. As the comonomer content increases above a critical value, the amount of thinner lamellae of lower melting crystallites increases at the expense of the thicker high-melting crystallites, resulting in a decrease in the melting temperature **[44]**. This effect of a decrease in the melting temperature with increase in comonomer content is being reflected in Figure 3.13 for the propylene/1-hexene copolymers and Figure 3.14 for the propylene/1-octene copolymers.

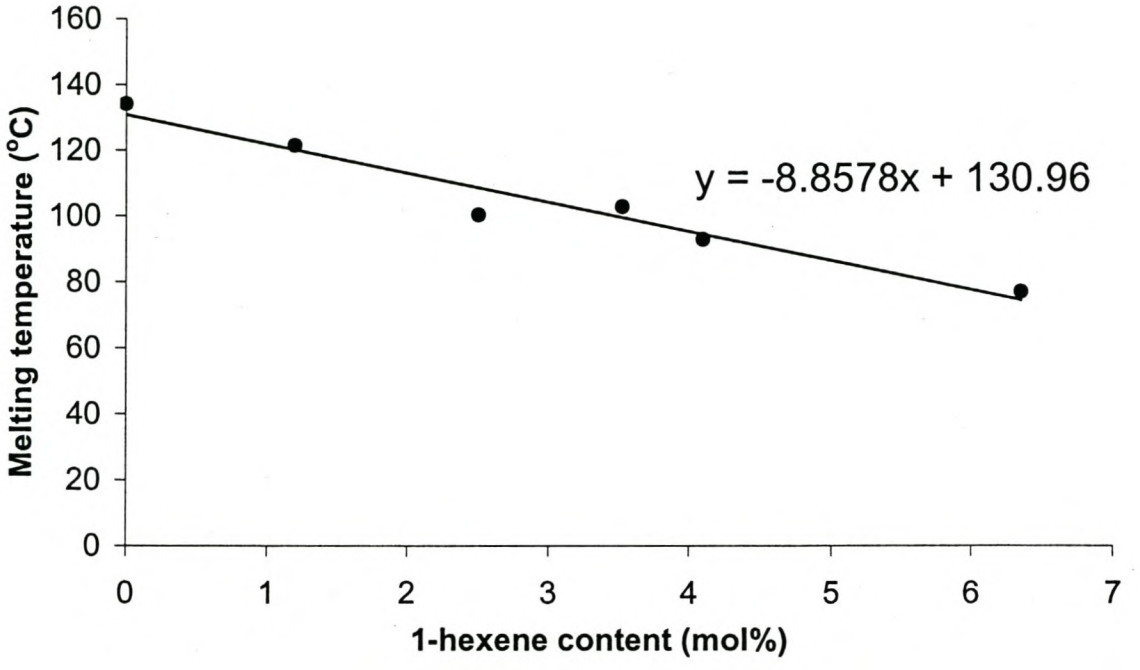

Figure 3.13 Melting temperatures of propylene/1-hexene copolymers as a function of 1-hexene content.

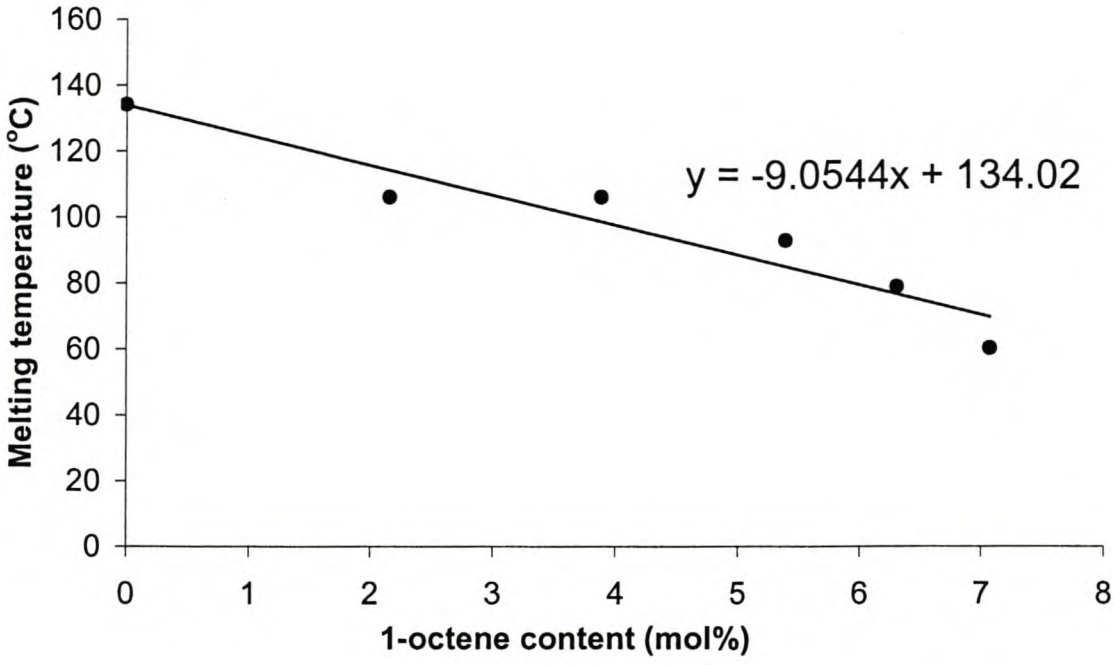

Figure 3.14 Melting temperatures of propylene/1-octene copolymers as a function of 1-octene content.

For both of the graphs in Figure 3.13 and Figure 3.14 a trendline through the datapoints is shown. The equations of these straight lines are given as well and correspond very well as the gradients are both very near to –9 which indicates that the value of melting point depression is virtually independent of comonomer type for these two series.

Figure 3.15 and Figure 3.16 illustrates that the crystallinity of the copolymers also decreases with an increase in the comonomer content. According to Sequela and Rietsch **[45-46]**, even small amounts of branches are not able to enter the crystalline phase and this results in a smaller crystal size and imperfections which again lead to a lower melting temperature and crystallinity. The introduction of the α-olefin comonomer into the polymeric chain creates a discontinuity that sharply reduces the crystallization tendency. This results in a decrease in the rate of crystallization, a lower level of crystallinity, and also a reduction in the melting point.

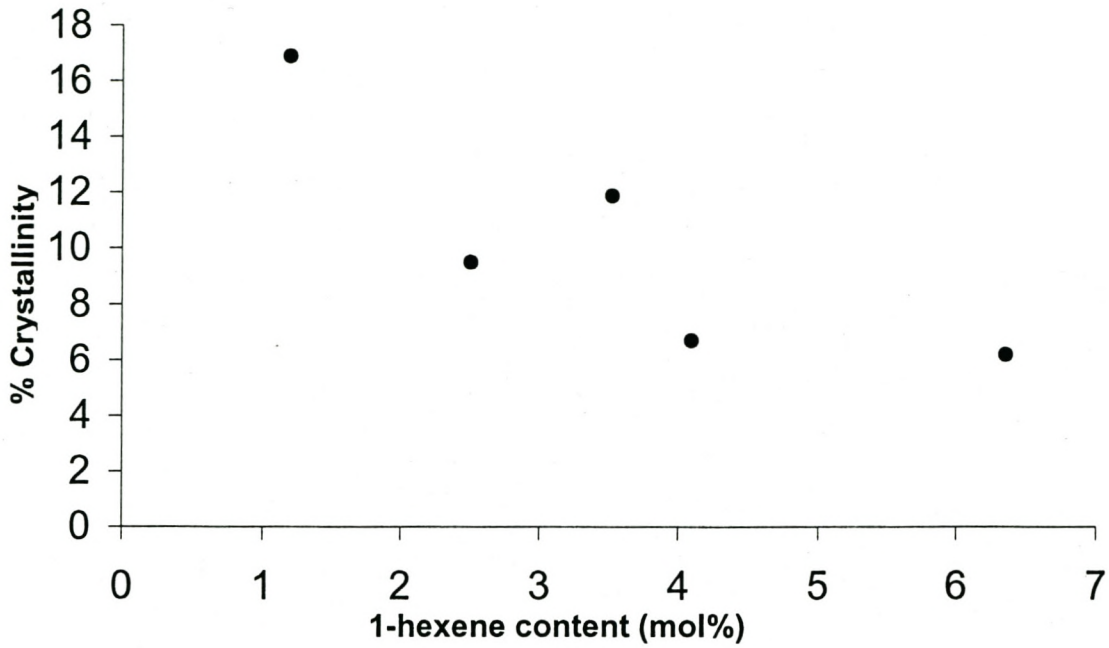

Figure 3.15 Percentage crystallinity of propylene/1-hexene copolymers as a function of 1-hexene content.

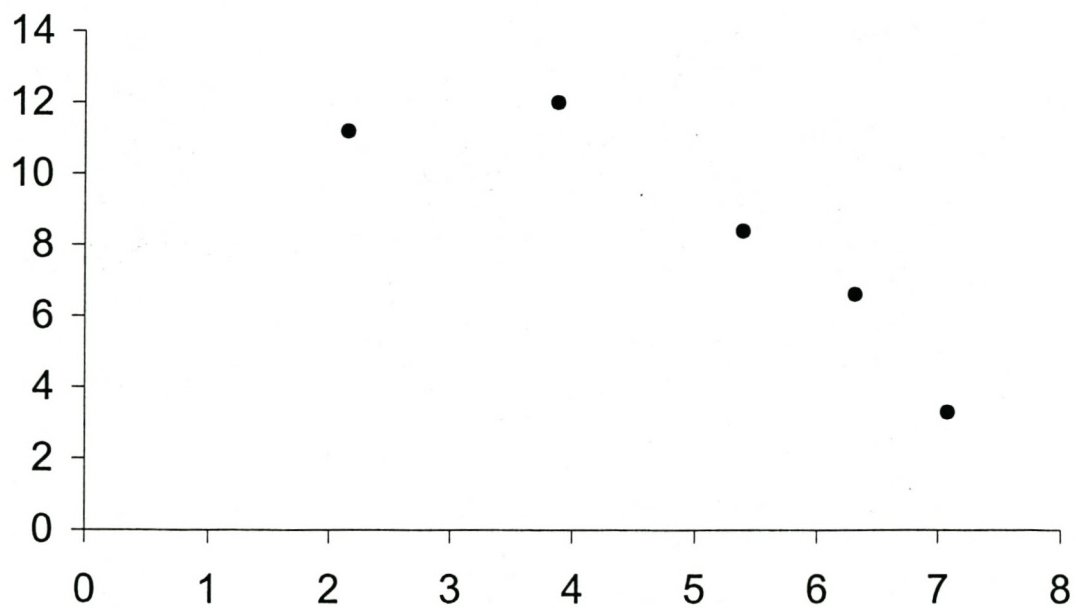

Figure 3.16 Percentage crystallinity of propylene/1-octene copolymers as a function of 1-octene content.

3.5.3.2 *Glass transition temperature*

Dynamic mechanical analysis (DMA) is commonly used to measure various transitions in a polymer, for example the glass transition temperature (T_g).

The thermal transitions of a polymer can be described in terms of either free volume changes **[47]** or relaxation times **[48]**. Changes in free volume, V_f, can be monitored as a volumetric change of the polymer; by the change in heat capacity associated with that change; the loss of stiffness; increased flow; or by a change in relaxation time. Defined also as the change in free volume a molecule has for internal movement, it is schematically shown in Figure 3.17.

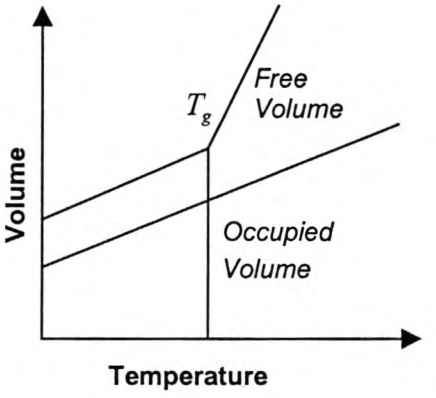

Figure 3.17 The relationship of free volume to transitions.

A simple approach to looking at free volume is the crankshaft mechanism **[49]** where the molecule is imagined as a series of jointed segments. The crankshaft module treats the molecule as a collection of mobile segments that have some degree of free movement. As the free volume of a chain segment increases, its ability to move in varioius directions also increases as demonstrated in Figure 3.18.

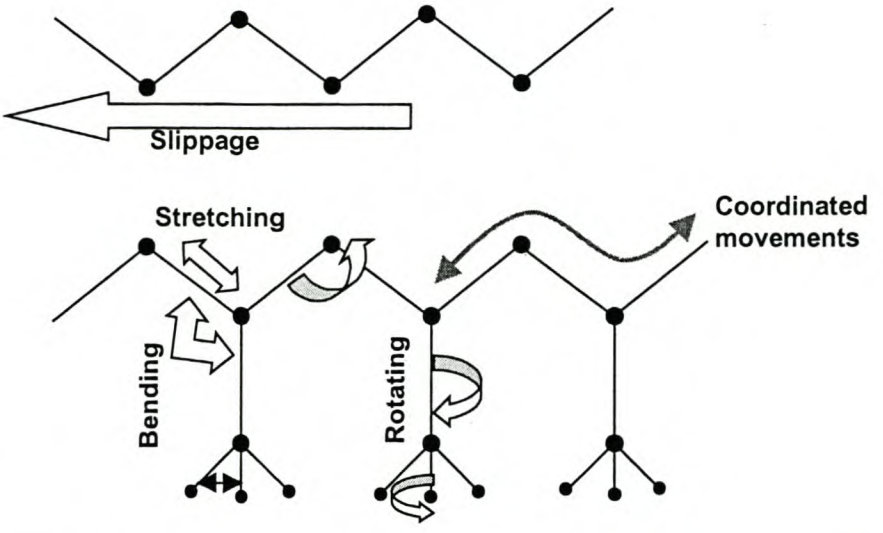

Figure 3.18 The crankshaft model showing various motions of a polymer chain.

When moving from very low temperture, where the molecule is tightly compressed, the material passes through the solid state transitions. As the material warms and expands, the free volume increases so that localized bond movements (bending and stretching) and side chain movements can occur. This is the gamma transition, T_γ, which may also involve associations with water. As the temperature and free volume continue to increase, a beta transition, T_β, appears which is not very clearly defined. As heating continues, we reach the T_g or glass transition, where the chains in the amorphous regions begin to coordinate large-scale motions. One classical description of this region is that the amorphous regions have begun to flow. The T_g represents a major transition for many polymers, as physical properties changes drastically as the material goes from a hard glassy to a rubbery state.

Table 3.9 reflects the different glass transition temperatures of the propylene/1-hexene and propylene/1-octene copolymers produced with the bridged *rac*-Et(Ind)$_2$ZrCl$_2$ catalyst. Because of the low molecular mass (especially number average molecular mass) of these copolymers (see Section 3.5.2) no valid conclusions can be drawn about the change in glass transition temperature as the comonomer content increases.

Table 3.9 DMA results of propylene/1-hexene (Samples A2-A6) and propylene/1-octene copolymers (Samples A7-A11).

Sample	1-hexene (A2-A6)/ 1-octene (A7-A11) content (mol %)	Glass Transition Temperature (°C)	Number Average Molecular Mass (M_n, g/mole)
A2	1.20	-31.25	15881
A3	2.51	-30.75	11732
A4	3.53	-28.00	37321
A5	4.10	-38.43	8373
A6	6.36	-33.23	27145
A7	2.16	-40.27	13569
A8	3.89	-39.84	10 178
A9	5.40	-	14004
A10	6.32	-40.27	36186
A11	7.08	-	20242

3.5.4 Crystallinity

Crystallization analysis fractionation (CRYSTAF) is a relatively new technique, based on a stepwise precipitation approach, to analyze the short-chain branching distribution (SCBD) of a specific polymer. We used this technique to gather information on the crystallinity tendencies of the various polymers synthesized.

The chemical composition distributions (CCD), also referred to as short chain branching distribution (SCBD), has been shown to be a critical structural parameter with strong impact on product performance **[50-61]**, and considerable work has been done in the industrial laboratories to understand the influence of catalyst formulation and polymerization process conditions on SCBD **[62]**. The analysis of the SCBD, however, is not a simple task, and to achieve proper resolution, fractionation of the polymer is required. The most common technique used for the SCBD analysis in polymers is temperature elution fractionation (TREF), which was first described by

Desreux and Spiegels **[63]** in 1950, but also been the work of Wild an Ryle **[50, 62-65]** in the late 1970's with the development of analytical TREF, which established the technique in the polyolefins industry.

CRYSTAF analysis has, however, been shown to provide similar results to TREF analysis but in a shorter time and with a simplified apparatus. It also allows simultaneous analysis of various samples. The theoretical basis of polymer fractionation by crystallization in solution and its application to CRYSTAF and TREF have been extensively discussed **[66-67]** on the basis of the Flory-Huggins statistical thermodynamic treatment **[68-69]** and the Flory equilibrium theory **[70]**.

For random copolymers, the classical Flory equation applies:

$$\frac{1}{T_m} - \frac{1}{T_m^0} = -\frac{R}{\Delta H_u}\ln(p) \qquad \textbf{VII}$$

where ΔH_u is the heat of fusion per polymer repeating unit; p is the molar fraction of the crystallizing unit; T_m^0 is the melting temperature of the pure polymer; and T_m is the equilibrium melting temperature of the copolymer. Equation **VII** can be simplified by replacing $p = (1 - N_2)$, where N_2 is the molar fraction of comonomer incorporated (noncrystallizing unit), and for low values of N_2 the following holds: $\ln(1 - N_2) \cong -N_2$; hence,

$$\frac{1}{T_m} - \frac{1}{T_m^0} \cong \frac{R}{\Delta H_u} N_2 \qquad \textbf{VIII}$$

Further simplification is obtained by assuming that $T_m \cdot T_m^0 \cong (T_m^0)^2$, and also that ΔH_u is constant in the considered crystallization temperature range:

$$T_m \cong T_m^0 - \frac{R(T_m^0)^2}{\Delta H_u} N_2 \qquad \textbf{IX}$$

where the presence of solvent, when crystallizing in solution, is just an additional shift factor. Equation **IX** clearly indicates that a linear dependence of melting or crystallization temperature, T_m, with the amount of comonomer incorporated, N_2, is achieved under these conditions.

Crystallization analysis fractionation uses a unique approach to monitor the solution crystallization of the polymer that will allow the calculation of the overall SCBD. The analysis is carried out by monitoring the polymer solution concentration during crystallization by temperature decrease. Aliquots of the solution are filtered and analyzed by a concentration detector. The whole process is similar to a classical stepwise fractionation by precipitation, except for the fact that the focus is on the polymer that remains in solution and not the polymer precipitated.

In this section we will further discuss the CRYSTAF analyses carried out on the polypropylene homopolymer (Sample A1) and propylene/1-hexene (Samples A2-A6) and propylene/1-octene (Samples A7-A11) copolymers produced by the *rac*-$Et(Ind)_2ZrCl_2$/MAO catalyst system. Figure 3.19 shows the SCBD of a polypropylene homopolymer (Sample A1) which was analyzed by CRYSTAF. The first data points in the cumulative curve, taken at a temperature above any crystallization, provide a constant concentration equal to the initial polymer solution concentration (Zone 1 in Figure 3.19). As the temperature decreases, the most crystalline fractions, composed of molecules with zero or very few branches, will precipitate first, resulting in a steep decrease in the solution concentration (Zone 2 in Figure 3.19). This is followed by precipitation of fractions of increasing branch content as temperature continues to decrease (Zone 3 in Figure 3.19). The last data point, corresponding to the lowest temperature of the crystallization cycle, represents the fraction that has not crystallized (mainly highly branched material) and remains soluble. The top curve in Figure 3.19 corresponds to the cumulative SCBD when the temperature scale is calibrated and transformed to number of branches/1000 carbons. The first derivative of this curve can be associated with the SCBD in Figure 3.19.

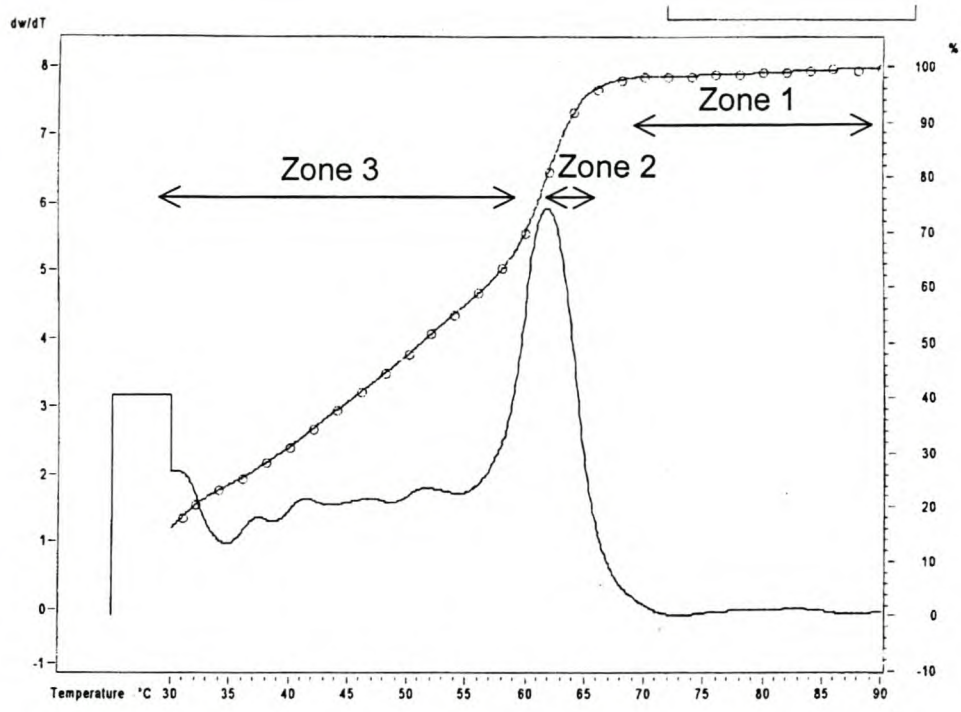

Figure 3.19 Cumulative and differential SCBD of polypropylene homopolymer (Sample A1) as obtained by crystallization fractionation analysis at 10°C/min crystallization rate.

Table 3.10 gives a summary on the CRYSTAF analyses carried out on the propylene homopolymer and the propylene/1-hexene and propylene/1-octene copolymers produced with the *rac*-Et(Ind)$_2$ZrCl$_2$ catalyst. The CRYSTAF curve of the polypropylene homopolymer produced with the *rac*-Et(Ind)$_2$ZrCl$_2$ catalyst shows a clear and definite crystallization temperature peak at 62°C with a soluble fraction of 16.2% left at 30°C. However, the crystallization temperature of most of the propylene/1-heptene and propylene/1-octene copolymers was below 30°C (Table 3.10). The reason for this would be because of the low molecular weight copolymers produced by the bridged *rac*-Et(Ind)$_2$ZrCl$_2$ catalyst. Comparing all the CRYSTAF spectra (Appendix) in each of the two copolymer series (Samples A2-A6 and Samples A7-A11) it can be seen that the start of the crystallization peak decreases in terms of the temperature when the comonomer content is increased. Because of the low crystallization temperatures it is however not relevant interpreting the soluble fraction left at 30°C, weight average temperature (T_w), number average temperature (T_n) or the R and σ parameters indicating the broadness of the crystallization peak.

Table 3.10 CRYSTAF results of the propylene homopolymer (Sample A1) and the propylene/1-hexene (Samples A2-A6) and propylene/1-octene (Samples A7-A11) copolymers.

Sample	Comonomer (mol %)	M_n (g/mole)	Soluble Fraction (%)	T_c (°C)	T_w (°C)	T_n (°C)	R	σ
A1	0.00	11 949	16.2	62.0	47.1	50.6	7.4	12.4
A2	1.20	15 881	34.5	47.2	39.7	41.4	4.2	8.1
A3	2.51	11 732	96.0	<30.0	29.6	29.0	-2.3	-4.9
A4	3.53	37 321	57.7	30.0	32.0	32.0	0.0	-3.4
A5	4.10	8 373	93.9	<30.0	30.5	31.0	1.7	6.1
A6	6.36	27 145	98.9	<30.0	30.1	30.1	-0.2	-3.8
A7	2.16	13 569	76.3	<30.0	31.9	32.2	1.2	4.3
A8	3.89	10 078	3.5	30.0	32.9	33.0	0.2	-2.5
A9	5.40	14 004	95.7	<30.0	30.3	30.3	0.0	-2.8
A10	6.32	36 186	98.6	<30.0	29.8	29.2	-1.9	-7.0
A11	7.08	20 242	94.6	<30.0	30.5	30.5	0.1	-5.7

In Table 3.11 the crystallized fractions of the different polymers are set out in temperature intervals of 9.9°C. From this analysis of the soluble fraction it is clear that in the case of the copolymers most of the crystallization occurs at temperatures lower than 50°C. The last two columns of the table gives an idea of the reliability of the experimental results. The second last column is calculated by adding up all the crystallized fractions given by the CRYSTAF analyses and subtracting it from 100%. This should give the soluble fraction of the polymer left at 30°C and for reliability it must correspond closely with soluble fraction given by the CRYSTAF analyses. Except for the propylene homopolymer, the correlation between the two columns is very good.

Table 3.11 CRYSTAF results of the crystallized fractions in specific temperature intervals of the propylene homopolymer (Sample A1) and the propylene/1-hexene (Samples A2-A6) and propylene/1-octene (Samples A7-A11) copolymers.

Sample	30-39.9°C (%)	40-49.9°C (%)	50-59.9°C (%)	60-69.9°C (%)	70-79.9°C (%)	80-100°C (%)	100%-total (%)	Soluble fraction (%)
A1	-	16.6	10.3	42.7	-	-	30.4	16.2
A2	-	64.2	-	0.5	0.6	-	34.7	34.5
A3	3.3	0.7	-	-	-	-	96.0	96.0
A4	41.6	-	0.4	-	0.2	-	57.8	57.7
A5	4.6	0.2	-	-	-	0.2	95.0	93.9
A6	-	-	0.2	0.5	0.2	-	99.1	98.9
A7	23.5	-	-	0.2	-	0.1	76.2	76.3
A8	95.6	0.3	-	0.4	-	-	3.7	3.5
A9	2.8	0.5	-	0.6	-	-	96.1	95.7
A10	0.6	0.3	-	0.1	-	-	99.0	98.6
A11	1.8	-	-	-	1.6	0.8	95.8	94.6

3.6 CONCLUSIONS

Low molecular mass propylene/1-hexene and propylene/1-octene copolymers (M_w between 26 332 g/mole and 68 325 g/mole) were obtained with the *rac*-Et(Ind)$_2$ZrCl$_2$/MAO catalyst system. The NMR results of these copolymers represent relatively highly isotactic polymers with tacticities in the range of 72.1%-90.9%. Very few and small stereoirregularities are visible in the region of the methyl peak in the ^{13}C spectra. There are also other specific very low intensity regioirregular peaks visible which indicates 2,1-insertion producing head-to-head units. The observed chemical shift values of the carbon peaks in the ^{13}C NMR spectra correspond very well overall with the calculated values.

The GPC curves of the polymers produced by the activating metallocene catalyst have a characteristic shape as predicted by Flory's distribution law. Because of the nature of the specific single-site catalyst that was used, the weight-average molecular masses as well as the number-average molecular masses are very low and

the polymers would therefore not be suitable for industrial use. The polydispersities are in the range of 1.82-3.72 which is typical for metallocene catalyzed polymers. In the DSC analyses a decrease in melting point as well as crystallinity were found for an increase in the comonomer content. The melting peak also became broader and the height lower as the comonomer content was increased. Because of the low molecular mass of the produced copolymers no relevant conclusion could be made on the effect of the comonomer content on the glass transition temperatures as well as on the crystallization temperatures of the polymers, as determined by CRYSTAF.

3.7 REFERENCES

1. Gupta V.K., Satish S., Bhardwaj I.S., *J.M.S.-Rev. Macromol. Chem. Phys.*, 1994, **C34**(3), 439–514.
2. Huang J., Rempel G.L., *Prog. Polymer Sci.*, 1995, **20**, 459-526.
3. Reddy S.S., Sivaram S., *Prog. Polymer Sci.*, 1995, **20**, 309-367.
4. Soares J.B.P., Hamielec A.E., *Polymer React. Engng.*, 1995, **3**(2), 131-200.
5. Hamielec A.E., Soares J.B.P., *Prog. Polymer Sci.*, 1996, **21**, 651-706.
6. Kaminsky W., *Macromol. Chem. Phys.*, 1996, **197**, 3907-3945.
7. Schnutenhaus H., Brintzinger H.H., *Angew. Chem.*, 1979, **91**, 837.
8. Wild F.R.W.P., Zsolani L., Huttner G., Brintzinger H.H., *J. Organomet. Chem.*, 1982, **232**, 233.
9. Wild F.R.W.P., Wasiucionek M., Huttner G., Brintzinger H.H., *J. Organomet. Chem.*, 1985, **288**, 63.
10. Ewen J.A., Jones R., Razavi A., *J. Am. Chem. Soc.*, 1984, **106**, 6355.
11. Kaminsky W., Külper K., Brintzinger H.H., Wild F.R.W.P., *Angew. Chem.*, 1985, **97**, 507.
12. *Chemical and Engineering News*, 1996, **Dec. 16**, p. 15.; **Aug. 12**, p. 9-10; 1995, **Oct. 30**, p. 10, **Sept. 18**, p. 17, **Sept. 11**. p. 15-20, **May 22**, p. 34-38, **May 1**, p. 7-8.
13. *Nachr. Chem. Tech Lab.*, 1995, **43**, p. 701, 1086, 1208.
14. Kaminsky W., *Spektrum der Wissenschaft*, 1997, **Febr.**, p. 85-89.
15. Albauch M., *Chemie heute (Fonds der Chemischen Industrie)*, 1995/96, p. 70-73.
16. Wood A., *Chemical Week*, 1992, **Jul. 1/8**, p. 42-44.

17. Wood A., Chynoweth E., *Chemical Week*, 1992, **May 13**, p. 52-53.
18. Hauthal H.G., *Nachr. Chem. Tech. Lab.*, 1995, **43**, p. 822.
19. Vennen H., *Future (Das Hoechst Magazin)*, 1995, **IV**, p. 48-53.
20. Mülhaupt R., Rieger B., *Chimia*, 1995, **49**, 486.
21. Langhauser F., Kerth J., Kersting M., Kölle P., Lilge D., Müller P., *Angew. Makromol. Chem.*, 1994, **223**, 115.
22. Schnelbach M., Köhler F.H., Blümel J., *J. Organomet. Chem.*, 1996, **8**, 893.
23. Ishirara N., Kuramotot M., Uoi M., *Macromolecules*, 1988, **21**, 3356.
24. Grassi A., Zambelli A., Resconi L., Albizatti E., Mazzochi R., *Macromolecules*, 1988, **21**, 617.
25. Cheng H.N., Statistical modelling and NMR analysis of polyolefins. *Int. Symp. On Transition-Metal Catalyzed Polymerization, 2: Ziegler-Natta and Metathesis Polymerization*, (R.P. Quirk, Ed.), 1986, p. 599.
26. Zambelli A., Dorman D.E., Brewster A.I.R., Bovey F.A., *Macromolecules,* 1973, **6**, 925.
27. The theoretical notation is that proposed by: Frisch I.L., Mallows C.L., Bovey F.A., *J. Chem. Phys.*, 1966, **45**, 156.
28. Hansen E.W., Redford K., *Polypropylene: An A-Z reference*, (Karger-Kocsis J., Ed.) Kluwer Academic Publishers, Dordrecht, 1999, p. 541.
29. Busico V., Cipullo R., Monaco G., Vacatello M., *Macromolecules*, 1997, **30**, 6251.
30. Sheldon R.A., Fueno T., Tsunetsugu T., Furokawa J., *J. Polym. Sci., Part B*, 1966, **45**, 1565.
31. Ewen J.A., *J. Am. Chem. Soc.*, 1984, **106**, 6355.
32. Wolfsgruber C., Zannoni G., Rigamonti E., Zambelli A., *Makromol. Chem.*, 1975, **176**, 2765.
33. Doi Y., Suzuki T., Keii T., *Makromol. Chem. Rapid Commun.*, 1981, **2**, 293.
34. Grant D.M., Paul E.G., *J. Am. Chem. Soc.*, 1904, **86**, 2984.
35. Cheng H.N., *Polym. Bull.*, 1990, **23**, 589.
36. Van Reenen A.J., Institute for Polymer Science, University of Stellenbosch, Stellenbosch, Personal Communication.
37. Joubert D.J., *Ph.D. Thesis*, University of Stellenbosch, 2000.
38. Hingman R., Rieger J., Kersting M., *Macromolecules*, 1995, **28**, 3802.

39. Mandlekern L., *Crystallization and Melting in Comprehensive Polymer Science* (Sir Allen G., Chairman, Ed.), Board, Permagon Press, Oxford, 1989, **2**, p. 363.
40. Lauritzen J.J., Hoffman J.D., *J. Res. Nat. Bur. Std.*, 1960, **64(A)**, 73.
41. Hoffman J.D., Davis G.T., Lauritzen J.I., *Treatis on Solid State Chemistry* (ed. Hannay N.B.), Plenum Press, New York, 1976, 3.
42. Quirk R.P., Alsamarraie M.A.A., *Physical Properties of Poly(propylene)* in *Polymer Handbook*, Third Edition (Brandrup J., Immergut E.H., Eds.), John Wiley & Sons, New York, V/27 (1989).
43. Mathot V.B.F., *The Crystallization and Melting Region in Calorimetry and Thermal Analysis of Polymers* (Mathot. V.B.F., Carl Hanser, Eds.), Verlag, Munich, 1994, **9**, p. 231.
44. Faton J.G., *Crystallization Kinetics, Encyclopedia of Polymer Science and Engineering* (Kroschwitz J.I., Ed.), John Wiley & Sons, New York, Suppl. Vol., 1988, p. 231.
45. Sequela R., Rietsch F., *J. Polym. Sci.: Polym. Lett.*, 1988, **23**, 415.
46. Sakurai K., MacKnight W.J., Lohse D.J., Schulz D.N., Sissano J.A., *Macromolecules*, 1994, **27**, 4941.
47. Flory P., *Principles of Polymer Chemistry*, Cornell University Press, Ithaca, NY, 1953.
48. Bird R., Curtis C., Armstrong R., Hassenger O., *Dynamics of Polymer Fluids*, vol. 1&2, 2nd ed., Wiley, New York, 1987.
49. McCrum N., Williams G., Read B., *Anelastic and Dielectric Effects in Polymeric Solids*, Dover, New York, 1967.
50. Wild L., Ryle T., Knobeloch D., Peat I.R., *J. Polym. Sci. Polym. Phys. Ed.*, 1982, **20**, 441.
51. Cady L.D., *Soc. Plast. Eng.*, 1985, p. 107.
52. Mirabella F.M., Ford E.A., Westphal S.P., Fernando P.L., *Polym. Preprints*, 1985, **26**, 182.
53. Cady L.D., *Plastics Eng.*, 1987, January, p. 25.
54. Dohrer K.K., Hazlit L.G., Whiteman N.F., *J. Plast. Film Sheeting*, 1988, **4**, 214.
55. Mirabella F., Westphal S.P., Fernando P., Ford E., *J. Polym. Sci. Polym. Phys. Ed.*, 1988, **26**, 1995.

56. Brady J.M., Thomas E., *J. Polym. Sci. Polym. Phys. Ed.*, 1988, **26**, 2385.

57. Lustiger A., Ishikawa N., *J. Polym. Sci. Polym. Phys. Ed.*, 1991, **29**, 1047.

58. Hosoda S., *Polym. J.*, 1988, **20**, 383.

59. Hosoda S., Uemura A., *Polym. J.*, 1992, **24**, 939.

60. Hosoda S., *Trends Polym. Sci.*, 1993, **3**, 265.

61. Todo A., Kashiwa N., *Macromol. Symp.*, 1996, **101**, 301.

62. Usami T., Goto Y., Takayama S., *Macromolecules,* 1986, **19**, 2722.

63. Desreux V., Spiegels M.L., *Bull. Soc. Chim. Belg.*, 1950, **59**, 476.

64. Wild L., Ryle T., *Polym. Prepr. Am. Chem. Soc. Polym. Chem. Div.*, 1977, **18**, 182.

65. Wild L., Ryle T., Knobeloch D., *Polym. Prepr. Am. Chem. Soc. Poly. Chem. Div.*, 1982, **23**, 133.

66. Monrabal B.J., *J. Appl. Polym. Sci.*, 1994, **52**, 491.

67. Wild L., *Adv. Polym. Sci.*, 1991, **98**, 1.

68. Flory P., *J. Principles of Polymer Chemistry*, Cornell Univ. Press, Ithaca, NY, 1953.

69. Huggins M.L., Okamoto H., *Polymer Fractionation* (Cantow M.J. Ed.), Academic Press, New York, 1967.

70. Flory P., *J. Trans. Faraday Soc.*, 1948, **51**, 848.

CHAPTER 4

Polymerization and characterization of propylene/α-olefin copolymers produced with *rac*-Me_2Si(2-MeBenz[e]Ind)$_2ZrCl_2$/MAO

Summary

Propylene was copolymerized with 1-hexene (Sample B1-B2), 1-octene (Samples B3-B4) and 1-heptene (Samples B5-B10) respectively differing the comonomer content with each copolymerization. The catalyst used for this production is the homogeneous methylaluminoxane-activated racemic dimethylsilanediyl-bis(2-methylbenzo-[e]indenyl)zirconiumdichloride (*rac*-Me_2Si(2-MeBenz[e]Ind)$_2ZrCl_2$) catalyst. These copolymers were used to investigate the effect of the 1-heptene comonomer on the microstructure, molecular mass, molecular mass distribution, melting point, glass transition temperature and crystallization behaviour of the copolymers produced. Characterization methods included nuclear magnetic resonance spectroscopy (NMR), high temperature gel permeation chromatography (HTGPC), differential scanning calorimetry (DSC), dynamic mechanical analysis (DMA), and crystallization analysis fractionation (CRYSTAF). The series of 1-heptene/propylene copolymers with comonomer content varying between 1% and 8% was investigated in order to compare the different properties and potential performance with the propylene/1-hexene and propylene/1-octene metallocene catalyzed copolymers as well as with the Ziegler-Natta catalyzed propylene/1-heptene copolymers which will be discussed in the next chapter.

4.1 INTRODUCTION

In the previous chapter we concluded that the weight and number average molecular mass of the copolymers obtained from the *rac*-[ethylene *bis*(1-indenyl)]zirconium dichloride (*rac*-Et(Ind)$_2ZrCl_2$) catalyst was too low for industrial use. Most of the first isoselective metallocene catalysts, discovered during the mid-1980's, gave low molecular weights and poor stereoselectivity. The systematic

variation of metallocene molecular architectures led the groups of Brintzinger **[1]** and Spaleck **[2]** independently to the development of 2-methyl substituted silylene-bridged bisindenyl zirconocenes which gave much higher molecular weights and stereoselectivities in propene polymerization.

We also know that most conventional Ziegler-Natta polyolefin manufacturing plants are designed to use heterogeneous catalysts and therefore the commercial application of soluble metallocene catalysts would require the design of new plants or the adaptation of existing ones to operate with soluble catalysts. Metallocene catalysts need to be supported in order to be used in gas phase reactors, such as Union Carbide's fluidized-bed Unipol process, or BASF's stirred-bed Novolen process. For these processes, it is necessary to have a free flowing catalyst powder which will form polymer particles with adequate size distribution, avoiding the formation of fine powder or particle agglomerates. In other words, good replication of the catalyst particle size distribution is essential for the efficient performance of these reactors.

Langhauser *et al.* **[3]** reviewed the industrial production of polypropylene (homopolymer, random copolymer and impact copolymer) using Me_2Si(2-MeBe[e]Ind)$_2ZrCl_2$-supported catalyst and the Novolen-BASF process. This catalyst can produce polypropylene with high molecular weight even at elevated temperatures. The polymer particles replicate well the size distribution of the catalyst particles. This catalyst can produce polypropylene with new properties, such as low extractables for food wrapping and medical applications, which is a consequence of the uniform stereoregularity of polymers produced with a single site-type catalyst. Impact copolymers can also be produced with this catalyst. Impact copolymers made with conventional heterogeneous Ziegler-Natta catalysts show some crystalline domains in the amorphous elastomeric phase, while the elastomeric phase of the metallocene-produced copolymers is entirely amorphous. According to Langhauser *et al.* **[3]**, this catalytic system can be adapted to their existing gas phase polymerization process without any significant technical change.

We chose the *rac*-Me_2Si(2-MeBenz[e]Ind)$_2ZrCl_2$ catalyst (Figure 4.1) as the most suitable homogeneous metallocene catalyst for the purpose of our investigation because of its easy adaptability in the industry. The comonomer content in the propylene/1-heptene (B6-B10) copolymers was varied once again as well as in the

propylene/1-hexene (B2-B3) and propylene/1-octene (B4-B5) copolymers. This chapter reports on the influence of the comonomer content on the copolymer microstructure, molecular mass, molecular mass distribution, melting point, glass transition temperature and crystallization behaviour of the copolymers. A comparison of the properties of the three different types of copolymers synthesized is also drawn.

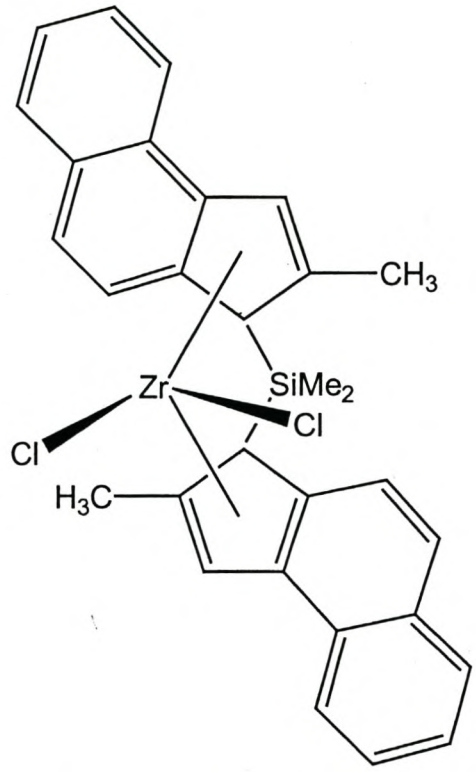

Figure 4.1 ***rac*-$Me_2Si(2\text{-}MeBenz[e]Ind)_2ZrCl_2$**

4.2 EXPERIMENTAL

The experimental conditions were the same as described in Chapter 3 (Section 3.2) except for the change in catalyst to *rac*-$Me_2Si(2\text{-}MeBenz[e]Ind)_2ZrCl_2$. This catalyst, which is also known as MBI, was ordered from Boulder Scientific and used as received.

4.3 EQUIPMENT

4.3.1 Polymerization equipment

A 350 ml stainless-steel Parr autoclave which was equiped with a fitted seal ring and a pressure gauge was used for the polymerization reactions.

4.3.2 Analytical equipment

The copolymers were characterized by NMR, HTGPC, DSC, DMA and CRYSTAF. A description of the analytical equipment used for the analyses is given in Chapter 3 (Section 3.3.2).

4.4 SYNTHESIS OF COPOLYMERS

4.4.1 Preparation of catalyst solution

The catalyst, *rac*-$Me_2Si(2\text{-}MeBenz[e]Ind)_2ZrCl_2$, was dissolved in the same way as the bridged *rac*-$Et(Ind)_2ZrCl_2$ catalyst and stored at 4°C before use.

4.4.2 Propylene copolymerization

All the copolymerizations were carried out in a 350 mL stainless steel pressure reactor fitted with a magnetic stirring bar in the same way as described in the previous chapter (Section 3.3.2). The reaction conditions were once again kept constant and polymerization reactions were conducted for 3½ hours at room temperature.

Three different series of copolymers were synthesized varying the amounts of comonomer (1-hexene, 1-octene and 1-heptene) in each series. The reaction conditions were kept constant for all the copolymerizations. A summary for these three series copolymers can be seen in Table 4.1.

Table 4.1 Experimental information of propylene/1-hexene, propylene/1-octene and propylene/1-octene copolymers produced by *rac*-Me_2Si(2-MeBenz[e]Ind)$_2ZrCl_2$.

Sample	1-hexene (B2-B3)/ 1-octene (B4-B5) 1-heptene (B6-B10) feed (mL)
B1	0
B2	11.1
B3	22.3
B4	14.0
B5	28.0
B6	8.3
B7	8.3
B8	12.5
B9	16.7
B10	25.0

Conversions were kept below 20% in all reactions.

4.5 RESULTS AND DISCUSSION

4.5.1 Microstructure

4.5.1.1 Polypropylene homopolymer

Figure 4.2 shows the ^{13}C spectrum of a polypropylene homopolymer (**I**) produced by the homogeneous *rac*-Me_2Si(2-MeBenz[e]Ind)$_2ZrCl_2$/ MAO) catalyst system.

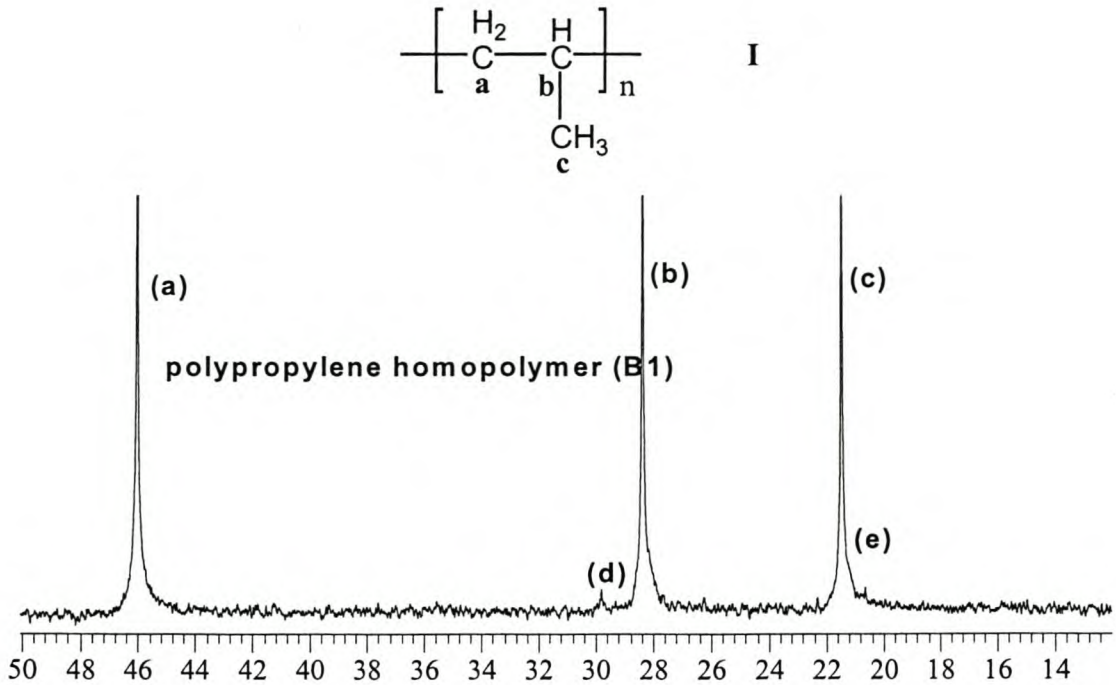

Figure 4.2 **^{13}C NMR spectrum of isotactic polypropylene (Sample B1).**

The primary resonance signals (a), (b) and (c) designate the methylene carbons (δ = 46.03 ppm), the methine carbons (δ = 28.37 ppm), and the methyl carbons (δ = 21.45 ppm) of polypropylene respectively **[4]**. It was shown in the previous chapter (Section 3.5.1.1) that the methyl region is chosen for tacticity analysis. Looking at the methyl region of this spectrum (shown in Figure 4.3) the only stereoirregularities which are clearly visible lies at (e) 20.62 ppm. Comparing the spectrum from Figure 4.3 with the spectrum of the *rac*-Et(Ind)$_2$ZrCl$_2$ catalyzed polypropylene homopolymer from Figure 3.3 we can assign the peak at (e) as *mmrr*. The broad shoulder of the methyl peak in Figure 4.2 may however also hide some of the regioirregularities. Another important regioirregularity appears at (d) 29.79 ppm. This regioirregularity is typical of 3,1-insertion that takes place during polymerization and leads to isolated n-propyl units in the polymer chain. Not only are there very few visible stereoirregularities in the whole of the spectrum but the intensities of these stereoirregular peaks are very low. We can therefore conclude that this homopolymer is very highly isotactic, especially in comparison with Sample A1 (Section 3.5.1.1) which was a polypropylene homopolymer produced under the exact same conditions by the bridged *rac*-Et(Ind)$_2$ZrCl$_2$ catalyst.

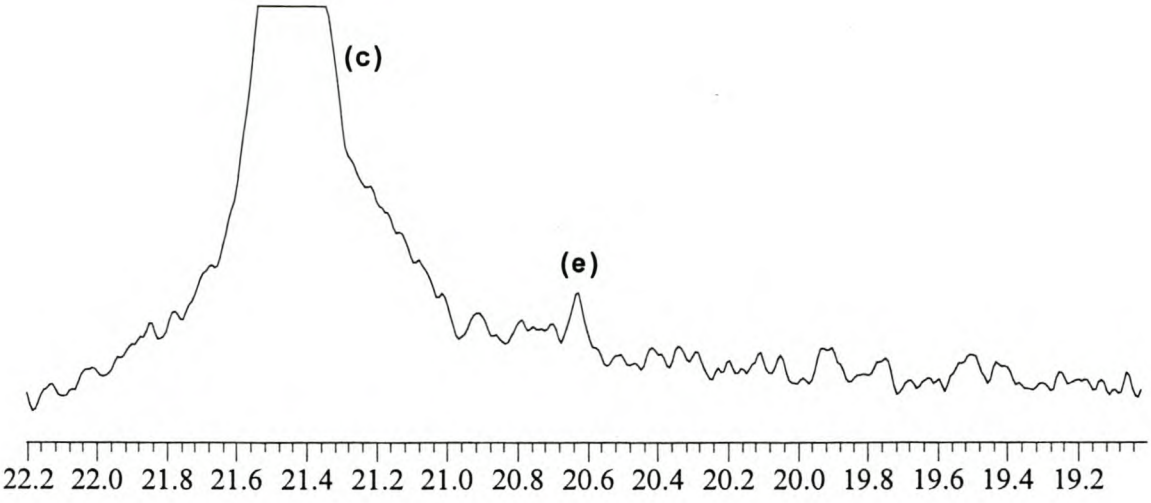

Figure 4.3 ^{13}C NMR spectrum of the methyl region of Sample B1.

4.5.1.2 Propylene/1-hexene, propylene/1-octene and propylene/1-heptene copolymers

Assignments of the different peaks appearing in the ^{13}C NMR spectra of the propylene/1hexene (Samples B2-B3), propylene/1-octene (Samples B4-B5) and propylene/1-heptene (Samples B6-B10) copolymers were done by making use of available literature, combined with APT analysis and checked against the chemical shift assignments predicted by the additivity rules described by Grant and Paul **[5]**.

Figures 4.4, 4.6 and 4.8 show the numbering of the different carbons in the propylene/1-hexene, propylene/1-octene and propylene/1-heptene copolymer structures respectively while Figures 4.5, 4.7 and 4.9 show the ^{13}C NMR spectra of these polymers. As with the propylene homopolymer produced by the *rac*-Me_2Si(2-MeBenz[e]Ind)$_2ZrCl_2$ catalyst, these spectra show almost no visible stereoirregularities. In Figure 4.9 however there is a very clear low intensity peak visible at 40.92 ppm. This peak is visible in almost all the ^{13}C NMR spectra in this study. The reason for this peak is because of 2,1-insertion which results in comonomers connected "head to head". This is also indicated by a broadening of the peak at ~ 35.7 ppm.

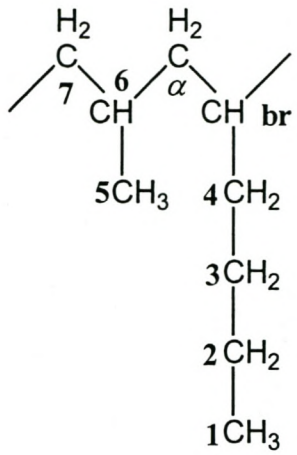

Figure 4.4 **Numbering of carbon atoms of propylene/1-hexene copolymers for chemical shift predictions.**

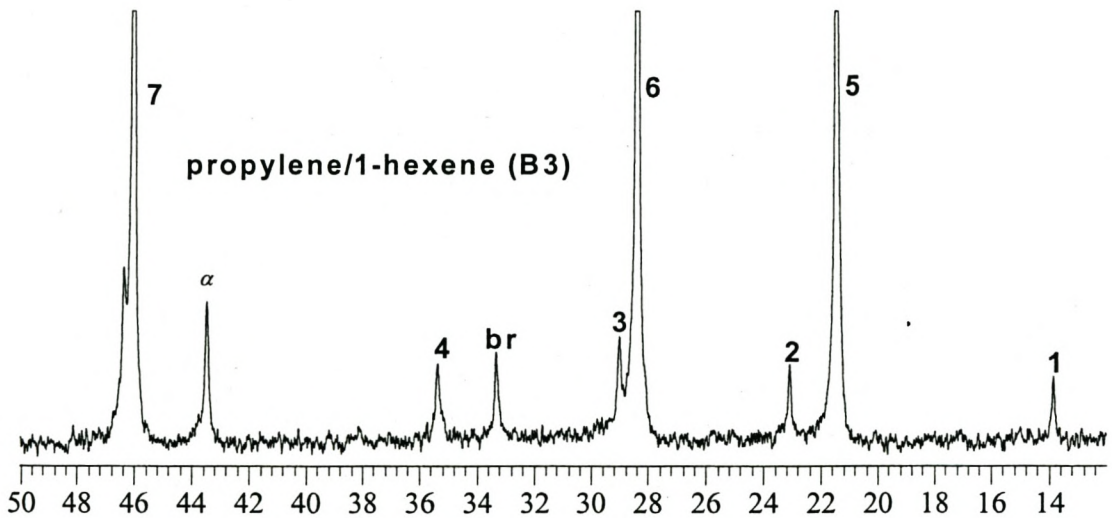

Figure 4.5 **^{13}C NMR spectrum of a propylene/1-hexene copolymer (Sample B3).**

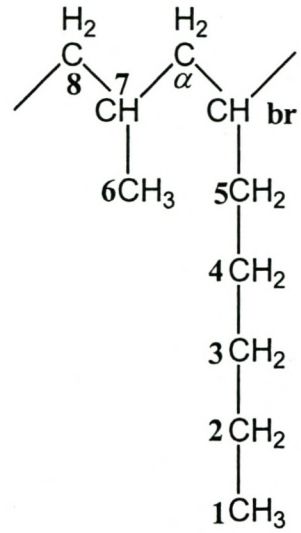

Figure 4.6 **Numbering of carbon atoms of propylene/1-octene copolymers for chemical shift predictions.**

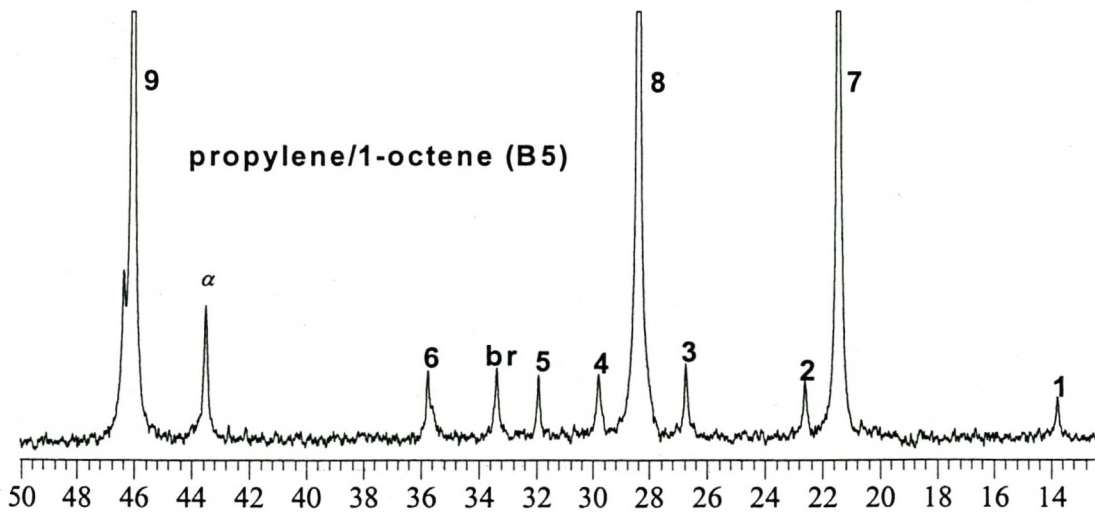

Figure 4.7 **^{13}C NMR spectrum of a propylene/1-octene copolymer (Sample B5).**

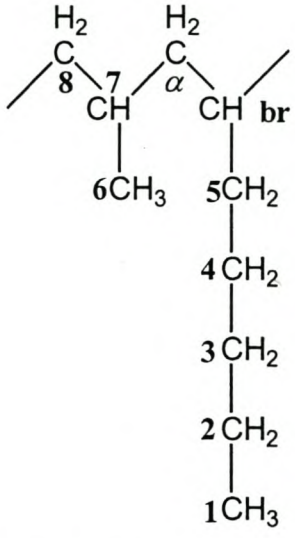

Figure 4.8 Numbering of carbon atoms of propylene/1-heptene copolymers for chemical shift predictions.

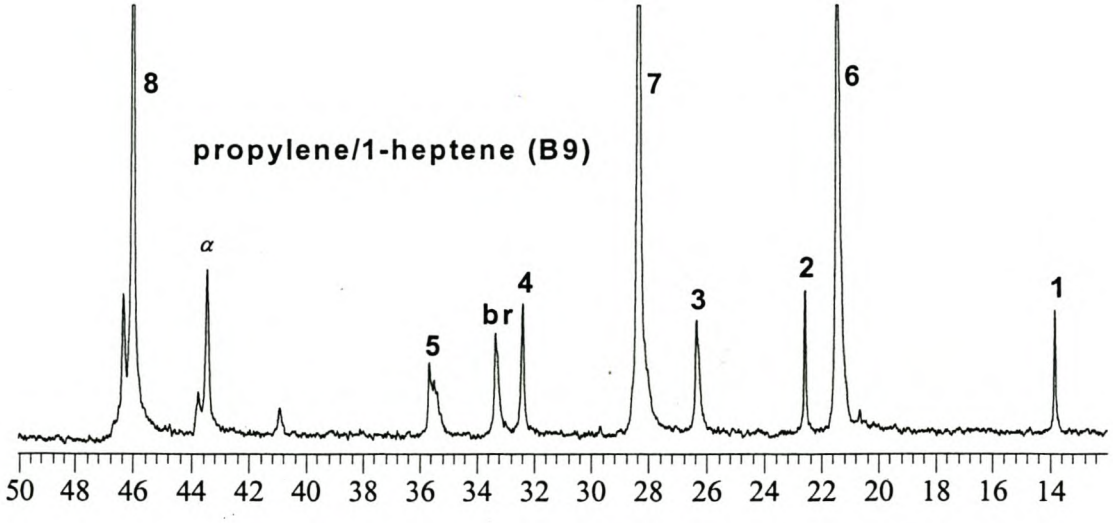

Figure 4.9 ^{13}C NMR spectrum of a propylene/1-heptene copolymer (Sample B9).

The percentages of comonomer incorporated in each of the copolymers produced by the *rac*-Me_2Si(2-MeBenz[e]Ind)$_2ZrCl_2$ catalyst are summarized in Table 4.2 In calculating the comonomer amount of each copolymer, the intensities of only the backbone carbon atoms are taken into account. The formulas for calculating the percentage of 1-hexene (**II**), 1-heptene (**III**) and 1-octene (**IV**) in a specific copolymer respectively are the following **[6]**:

$$C_6 = \frac{\frac{1}{2}(I_\alpha + I_{br})}{I_\alpha + I_{br} + I_6 + I_7} \times 100 \qquad \text{II}$$

$$C_7 = \frac{\frac{1}{2}(I_\alpha + I_{br})}{I_\alpha + I_{br} + I_7 + I_8} \times 100 \qquad \text{III}$$

$$C_8 = \frac{\frac{1}{2}(I_\alpha + I_{br})}{I_\alpha + I_{br} + I_8 + I_9} \times 100 \qquad \text{IV}$$

C_6, C_7, C_8 represent the percentage of comonomer incorporated and $I_\alpha, I_{br}, I_6, I_7, I_8, I_9$ represent the intensities of the carbon peaks of the backbone of the polymer as numbered in Figures 4.4, 4.6 and 4.8.

Table 4.2 Summary of comonomer content of propylene/1-hexene (Samples B2-B3), propylene/1-octene (Samples B4-B5) and propylene/1-heptene (Samples B6-B10) copolymers.

Sample	Comonomer content (%)
B2	4.42
B3	5.73
B4	4.07
B5	4.70
B6	1.03
B7	3.98
B8	5.19
B9	5.79
B10	7.58

Table 4.3 demonstrates the calculation of the different chemical shift prediction values for the propylene/1-heptene copolymers investigated in this study. Prediction values of the propylene/1hexene and propylene/1-octene copolymers were given in the previous chapter (Table 3.3). Table 4.3 represents only values for the

isolated comonomer branch, propylene-propylene-comonomer-propylene (ppcp) and not for any other possible sequences which may appear at higher comonomer concentrations.

Table 4.3 Chemical shift prediction for propylene / 1-heptene copolymers utilizing the Grant and Paul additivity rules.

Position	α	β	γ	δ	ε	3°(2°)	2°(3°)	1°(3°)	Constant
Factor	**8.61**	**9.78**	**-2.88**	**0.37**	**0.06**	**-2.65**	**-2.45**	**-1.4**	**-1.87**
	Propylene / 1-Heptene								
1	1	1	1	1	1				14.07
2	2	1	1	1	2				22.74
3	2	2	1	2	2				32.89
4	2	2	3	2	4				27.25
5	2	3	3	5	2		1		35.57
br	3	3	5	3	5	3			32.36
α	2	4	3	5	3		2		42.96
6	1	2	2	4	3			1	20.8
7	3	2	4	3	5	3			25.46
8	2	4	2	4	3		2		45.47

In Tables 4.4, 4.5 and 4.6 the calculated values of the chemical shift predictions are compared with the observed chemical shift values of the produced propylene/1-hexene, propylene/1-octene and propylene/1-heptene copolymers respectively. The observed and calculated values correspond very well overall. The observed chemical shift values of the propylene/1-hexene (Table 4.4) and propylene/1-octene (Table 4.5) copolymers produced by the *rac*-Me_2Si(2-MeBenz[e]Ind)$_2ZrCl_2$ catalyst also correspond almost exactly with the values of the same copolymers (Table 3.4 and Table 3.5) produced by the *rac*-Et(Ind)$_2ZrCl_2$ catalyst.

Table 4.4 Comparison of observed and calculated chemical shifts of propylene / 1-hexene (Samples B2–B3) copolymers.

Carbon	1	2	3	4	br	α	5	6	7
Calculated Grant and Paul	**14.13**	**23.11**	**30.13**	**35.20**	**32.30**	**42.96**	**20.80**	**25.46**	**45.47**
Observed B2	13.82	23.08	28.98	35.35	33.30	43.47	21.19	28.38	46.04
Observed B3	13.82	23.07	29.00	35.35	33.32	43.47	21.44	28.37	46.04

Table 4.5 Comparison of observed and calculated chemical shifts of propylene / 1-octene (Samples B4–B5) copolymers.

Carbon	1	2	3	4	5	6	br	α	7	8	9
Calculated Grant and Paul	**14.07**	**22.68**	**32.52**	**30.01**	**27.62**	**35.63**	**32.36**	**42.96**	**20.80**	**25.46**	**45.47**
Observed B4	13.77	22.60	26.70	29.77	31.89	35.73	33.33	43.49	21.45	28.38	46.05
Observed B5	13.76	22.60	26.73	29.80	31.90	35.73	33.37	43.50	21.44	28.39	46.04

Table 4.6 Comparison of observed and calculated chemical shifts of propylene / 1-heptene (Samples B6–B10) copolymers.

Carbon	1	2	3	4	5	br	α	6	7	8
Calculated Grant and Paul	**14.07**	**22.74**	**32.89**	**27.25**	**35.57**	**32.36**	**42.96**	**20.80**	**25.46**	**45.47**
Observed B6	13.75	-	26.38	-	35.66	33.35	43.46	21.44	28.37	46.04
Observed B7	13.77	22.56	26.40	32.41	35.68	33.39	43.50	21.44	28.39	46.06
Observed B8	13.79	22.56	26.37	32.37	35.67	33.35	43.48	21.44	28.37	46.04
Observed B9	13.81	22.56	26.35	32.37	35.65	33.33	43.46	21.46	28.36	46.02
Observed B10	13.79	22.56	26.35	32.36	35.65	33.34	43.46	21.45	28.37	46.03

The methyl peak regions were integrated in each spectrum in order to calculate the tacticity of the various polymers. The results are summarized in Table 4.7 and as with the propylene homopolymer. The copolymers are shown to be highly isotactic with all the tacticities above 92%. In the case of the propylene/1-heptene copolymers the tacticity decreases almost linearly as the comonomer amount is increased (Figure 4.10).

Table 4.7 Tacticity values of propylene homopolymer (Sample B1) propylene/1-hexene (Samples B2-B3), propylene/1-octene (Samples B4-B5) and propylene/1-heptene (Samples B6-B10) copolymers.

Sample	1-hexene (B2-B3)/ 1-octene (B4-B5)/ 1-heptene (B6-B10) content (mol %)	Tacticity (%)
B1	0.00	92.5
B2	4.42	92.4
B3	5.73	92.8
B4	4.07	96.0
B5	4.70	96.6
B6	1.03	98.9
B7	3.98	96.4
B8	5.19	95.7
B9	5.79	93.4
B10	7.58	92.6

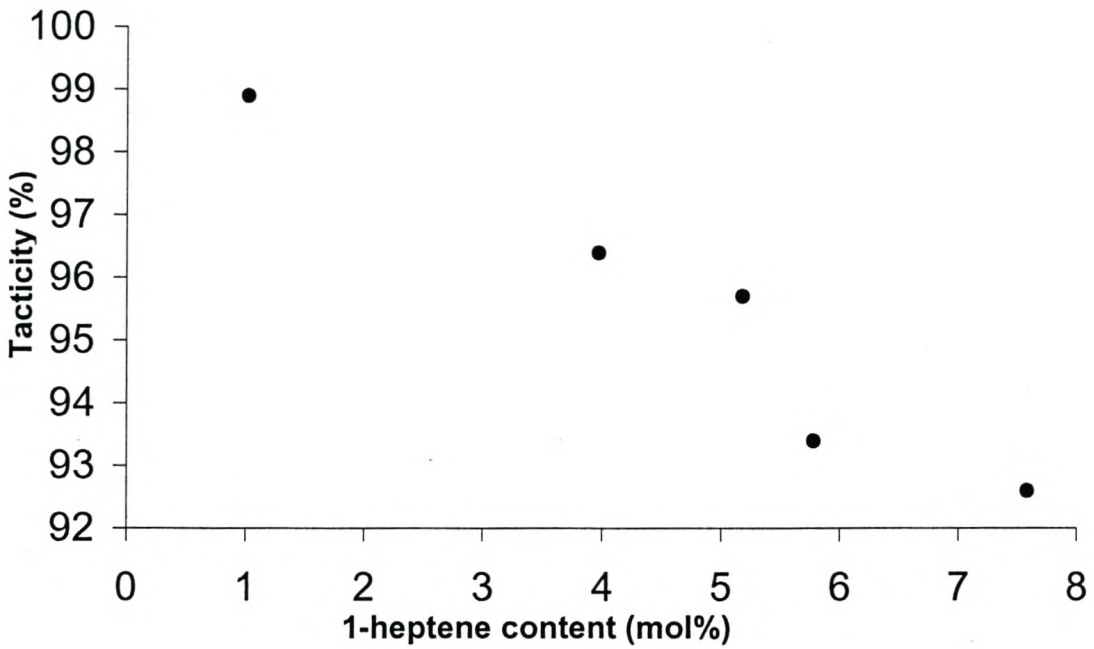

Figure 4.10 Tacticity of propylene/1-heptene copolymers as a function of 1-heptene content.

4.5.2 Molecular mass and molecular mass distributions

From Figure 4.11 it can be seen that the GPC curves of the copolymers have a characteristic shape, predicted by Flory's distribution law. As mentioned in Chapter 3 (Section 3.5.2) the molecular mass distributions of such copolymers do not change with polymerization time. The molecular mass at the maximum corresponds to the weight-average molecular mass of the polymer.

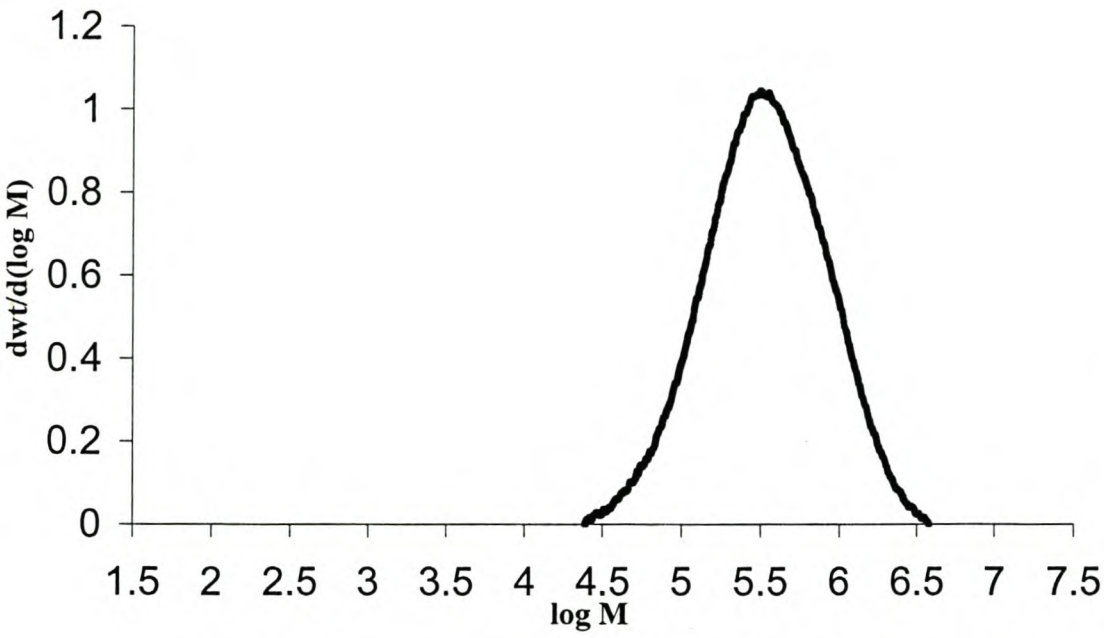

Figure 4.11 The distribution of the molecular mass, w(logM), against the molecular mass of propylene/1-heptene (Sample B7, 3.98% 1-heptene).

Table 4.8 represents the molecular mass results of the GPC analyses carried out on the propylene homopolymer and on the propylene/1-hexene, propylene/1-octene and propylene/1-heptene copolymers. The number-average (M_n) as well as the weight average (M_w) molecular masses of the all these polymers are almost 10 times higher than the *rac*-Et(Ind)$_2$ZrCl$_2$ catalyzed polymers which were discussed in Chapter 3 (Section 3.5.2). As expected the molecular mass distributions of the polymers in Table 3.7 were all in the region of 2. This feature is very characteristic of single site catalysts which produces copolymers with uniform comonomer incorporation.

It is unfortunately difficult to observe and quantify any peaks resulting from 2,1 insertion (which leads to low molecular weight) as these peaks appear in the same region as the peaks due to the CH_2 carbons in the comonomer.

Table 4.8 GPC results of propylene homopolymer (Sample A1) and propylene/1-hexene (Samples A2-A6) and propylene/1-octene copolymers (A7-A11).

Sample	1-hexene (B2-B3)/ 1-octene (B4-B5)/ 1-heptene (B6-B10) content (mol %)	Number-Average Molecular Mass (M_n, g/mole)	Weight - Average Molecular Mass (M_w, g/mole)	Polydispersity (M_w/M_n)
B1	0.00	148 116	346 848	2.34
B2	4.42	213 768	549 762	2.57
B3	5.73	286 781	557 764	1.94
B4	4.07	293 973	619 578	2.11
B5	4.70	255 749	483 245	1.89
B6	1.03	259 577	684 739	2.64
B7	3.98	251 876	594 000	2.36
B8	5.19	188 962	503 049	2.66
B9	5.79	152 926	352 026	2.30
B10	7.58	65 582	221 044	3.37

4.5.3 Thermal properties

4.5.3.1 Melting behaviour

Table 4.9 represents the results of the DSC analyses of the propylene homopolymer and the propylene/1-hexene, propylene/1-octene and propylene/1-heptene copolymers produced with the homogeneous *rac*-Me_2Si(2-MeBenz[e]Ind)$_2ZrCl_2$ catalyst. Crystallinity was calculated from fusion enthalpy based on a value of 209 J/g for 100% crystalline material **[7]**.

Table 4.9 DSC results of propylene homopolymer (Sample B1) and propylene/1-hexene (Samples B2-B3), propylene/1-octene (Samples B4-B5) and propylene/1-heptene (Samples B6-B10) copolymers.

Sample	1-hexene (B2-B3)/ 1-octene (B4-B5)/ 1-heptene (B6-B10) content (mol %)	Melting Temperature (°C)	FUSION ENTHALPY (J/G)	Crystallinity (%)
B1	0	153.4	72.2	34.5
B2	4.42	125.6	8.9	4.3
B3	5.73	85.7	4.9	1.9
B4	4.07	96.3	7.4	3.5
B5	4.70	90.3	12.3	5.9
B6	1.03	129.0	5.4	2.3
B7	3.98	132.3	2.0	1.0
B8	5.19	120.3	2.4	1.1
B9	5.79	114.9	15.9	7.6
B10	7.58	83.5	55.3	26.5

According to the DSC analysis the propylene homopolymer (Sample B1) discussed in this chapter has a much higher melting point (153.4°C) than the propylene homopolymer (Sample A1) produced with the *rac*-Et(Ind)$_2$ZrCl$_2$ catalyst (134.2°C), which was discussed in the previous chapter. When investigating the ^{13}C NMR spectrum (Figure 4.2) of the propylene homopolymer produced with the *rac*-Me$_2$Si(2-MeBenz[e]Ind)$_2$ZrCl$_2$ catalyst, there appears to be very few visible stereoirregularities, especially when comparing with the ^{13}C NMR spectrum (Figure 3.2) of the propylene homopolymer produced with the *rac*-Et(Ind)$_2$ZrCl$_2$ catalyst. This indicates a much higher isotacticity in the first mentioned homopolymer (Sample B1). Because of the very few defects in Sample B1 the chains will fold into much thicker crystals than in the case of Sample A1 when chain-folding to form lamellae.

This causes the higher melting point for Sample B1 (153.4°C) comparing to the melting point of Sample A1 (134.2°C) and corresponds with equation **I [8-9]** which was discussed in Chapter 3 (Section 3.5.3.1):

$$T_m = T_m^o\left\{1-\left(\frac{2\sigma_e}{\Delta h_f l}\right)\right\} \qquad \mathbf{I}$$

As mentioned in Chapter 3 comonomer incorporated into the polymer will lead to defects in an otherwise regular chain and will hinder to a certain extent the chain-folding process of forming lamellae. In Table 4.9 and Figure 4.12 it can be seen that even the smallest amount of 1-heptene comonomer incorporated (Sample B6, 1.03 mol%) into the polypropylene backbone causes a decrease of 24.4°C in the melting point of the propylene homopolymer which was produced with the same homogeneous catalyst.

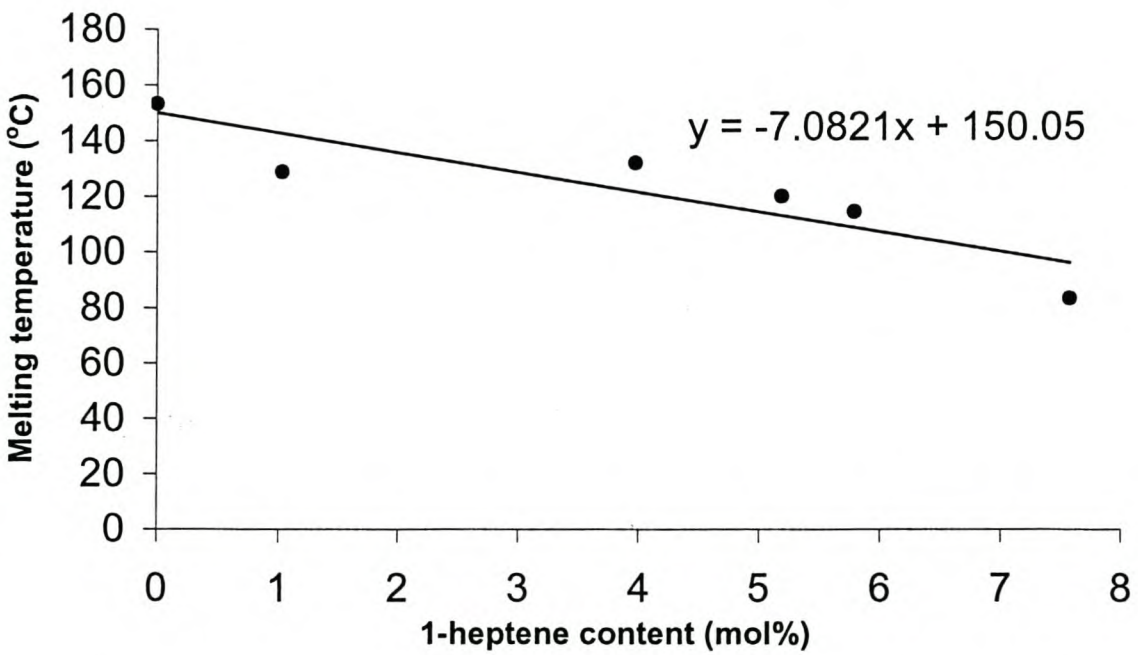

Figure 4.12 Melting temperatures of propylene/1-heptene copolymers as a function of 1-heptene content.

The melting peak also becomes broader and the height decreases as the amount of comonomer branches present in the chain increases **[10]**. This effect can clearly be seen when comparing the two DSC melting exotherms in Figure 4.13 (Comparison of PP homopolymer (B1) and a copolymer sample (B9)).

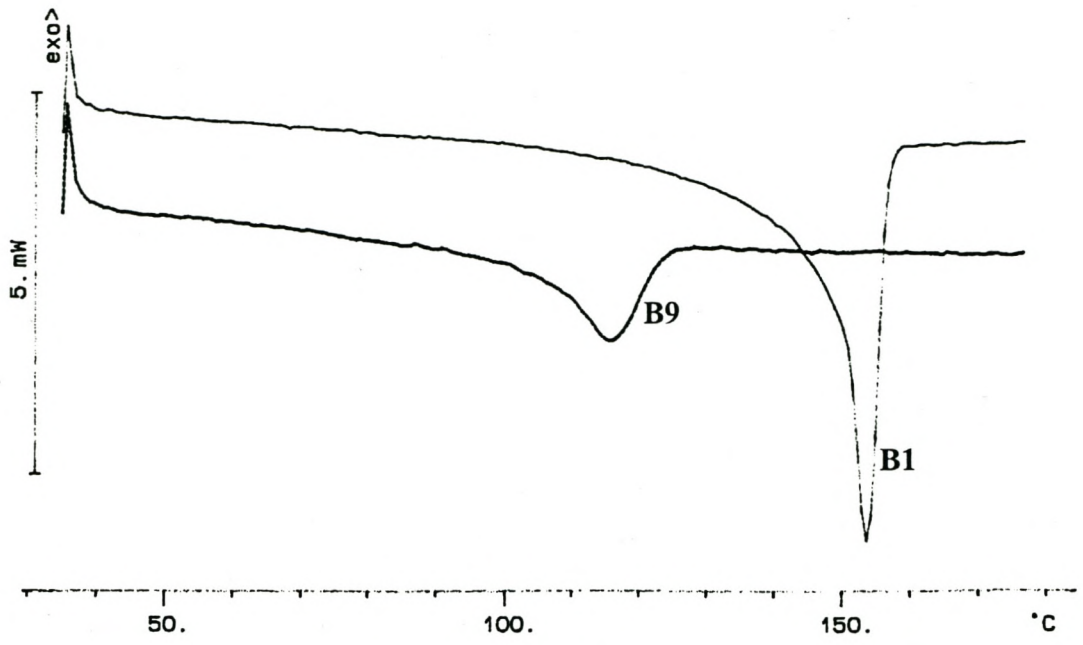

Figure 4.13 DSC melting curves of polypropylene homopolymer (B1) and a propylene/1-heptene copolymer (Sample B9, 5.78 mol% heptene).

4.5.3.2 Glass transition temperature

Table 4.10 reflects the different glass transition temperatures of the propylene/1-hexene, propylene/1-octene and propylene-1-heptene copolymers produced with the *rac*-Me_2Si(2-MeBenz[e]Ind)$_2ZrCl_2$ catalyst.

Table 4.10 DMA results of the propylene/1-hexene (Samples B2-B3), propylene/1-octene (Samples B4-B5) and propylene/1-heptene (Samples B6-B10) copolymers.

Sample	1-hexene (B2-B3)/ 1-octene (B4-B5)/ 1-heptene (B6-B10) content (mol %)	Glass Transition Temperature (°C)
B2	4.42	-35.17
B3	5.73	-35.76
B4	4.07	-33.51
B5	4.70	-33.28
B6	1.03	-
B7	3.98	-35.35
B8	5.19	-37.71
B9	5.79	-39.84
B10	7.58	-41.17

At the glass transtion temperature of the copolymers the chains in the amorphous regions begin to coordinate large-scale motions. With an increase in the comonomer content, there will be an increase in the large-scale motions and therefore also an increase in free volume according to the crankshaft model (Section 3.5.2). An increase in free volume again will lead to a decrease in glass transition temperature. From Table 4.10 and Figure 4.14 it can be seen that there is a definite fast decrease in the glass transition temperatures of the propylene/1-heptene copolymers as the comonomer amount increases.

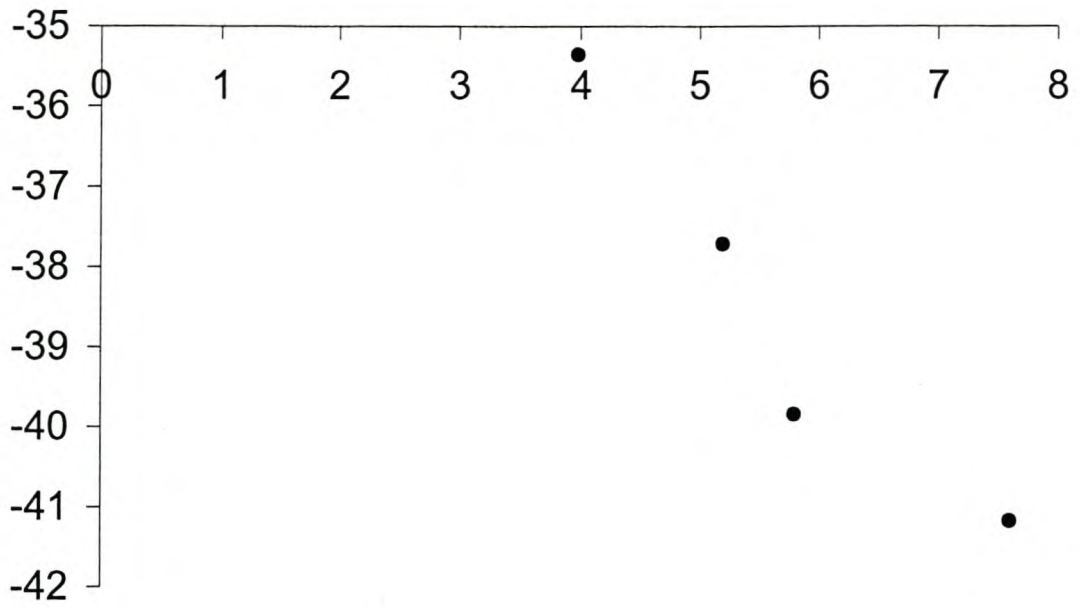

Figure 4.14 Glass transition temperatures of propylene/1-heptene copolymers as a function of 1-heptene content.

4.5.4 Crystallinity

The overall CRYSTAF results are presented in Tables 4.11 and 4.12. The polymers which were produced by the *rac*-Me_2Si(2-MeBenz[e]Ind)$_2ZrCl_2$ catalyst have a much higher molecular mass according to the DSC analysis than the polymers produced by the bridged *rac*-Et(Ind)$_2ZrCl_2$ catalyst which were discussed in the previous chapter. Therefore crystallization peaks of all these *rac*-Me_2Si(2-MeBenz[e]Ind)$_2ZrCl_2$ catalyzed polymers, except for Sample B3 and Sample B10, were clearly visible above 30°C on the CRYSTAF curves. From Table 4.11 it is clear that the crystallization temperature, T_c, as well as the weight average temperature, T_w, and number average temperature, T_n, decreased as the amount of 1-heptene incorporated in the propylene/1-heptene copolymers was increased. A decrease in crystallization temperature therefore indicates an increase in the amount of branches in the copolymer. Sample B10 contains the highest amount of comonomer (7.58 mol%) among the propylene/1-heptene copolymers and therefore has only started to crystallize before the temperature reached 30°C.

The soluble fraction left at the last temperature of the crystallization (30°C) gives an indication of the amount of short-chain branching in the copolymer. Table 4.11 shows a clear increase in the amount of soluble fraction left at 30°C as the amount of comonomer increases in the 1-hexene/1-octene/1-heptene copolymers.

Table 4.12 also compares the soluble fraction values obtained from the CRYSTAF curves with the molecular mass distribution values obtained from GPC analysis. The CRYSTAF results correspond well with the results obtained from GPC analysis. Sample B10 had an amount of 90.3% soluble fraction left in the polymer solution. The number of branches in the copolymer was therefore very high and the copolymer has a very broad SCBD. This result corresponds well with the broad molecular mass distribution of the copolymer obtained from the GPC analysis where the polydispersity of the copolymer, Sample B10, was 3.37.

Table 4.11 CRYSTAF results of the propylene homopolymer (Sample B1) and the propylene/1-hexene (Samples B2-B3), propylene/1-octene (Samples B4-B5) and propylene/1-heptene (Samples B6-B10) copolymers.

Sample	Comonomer (mol %)	M_w/M_n	Soluble Fraction (%)	T_c (°C)	T_w (°C)	T_n (°C)	R	σ
B1	0.00	2.34	-1.9	73.4	73.2	73.0	0.2	3.0
B2	4.42	2.57	41.4	52.9	43.9	41.1	6.9	10.5
B3	5.73	1.94	96.4	<30.0	29.8	30.1	-1.0	-5.8
B4	4.07	2.11	31.9	30.0	33.7	33.6	0.2	-5.8
B5	4.70	1.89	43.2	39.5	36.0	35.5	1.3	1.8
B6	1.03	2.64	11.2	56.6	55.4	53.8	3.0	9.7
B7	3.98	2.36	32.7	54.9	44.8	42.4	5.7	8.2
B8	5.19	2.66	56.5	44.3	37.3	36.2	3.0	4.8
B9	5.79	2.30	57.0	41.6	40.2	38.9	3.2	7.3
B10	7.58	3.37	90.3	<30.0	31.4	30.9	1.7	5.7

The σ and R values given in Table 4.10 are parameters used to measure the broadness of the chemical composition distribution (CCD) and are being calculated as follows **[11]**:

$$\sigma = \sqrt{\frac{\sum c_i \left(T_i^2 - T_w^2\right)}{\sum c_i}} \qquad R = \left(\frac{T_w}{T_n} - 1\right) \cdot 100$$

Figures 4.15, 4.16 and 4.17 show the CRYSTAF curves of Samples B2 (propylene/1-hexene copolymer), B5 (propylene/1-octene copolymer) and B9 (propylene/1-heptene copolymer) respectively. It is clear from these peaks that the metallocene catalyst *rac*-Me_2Si(2-MeBenz[e]Ind)$_2ZrCl_2$ produced copolymers with narrow chemical composition distributions (CCD). If we compare the results obtained from CRYSTAF and the GPC analysis, the CRYSTAF curves confirm the narrow molecular mass distribution of the copolymers.

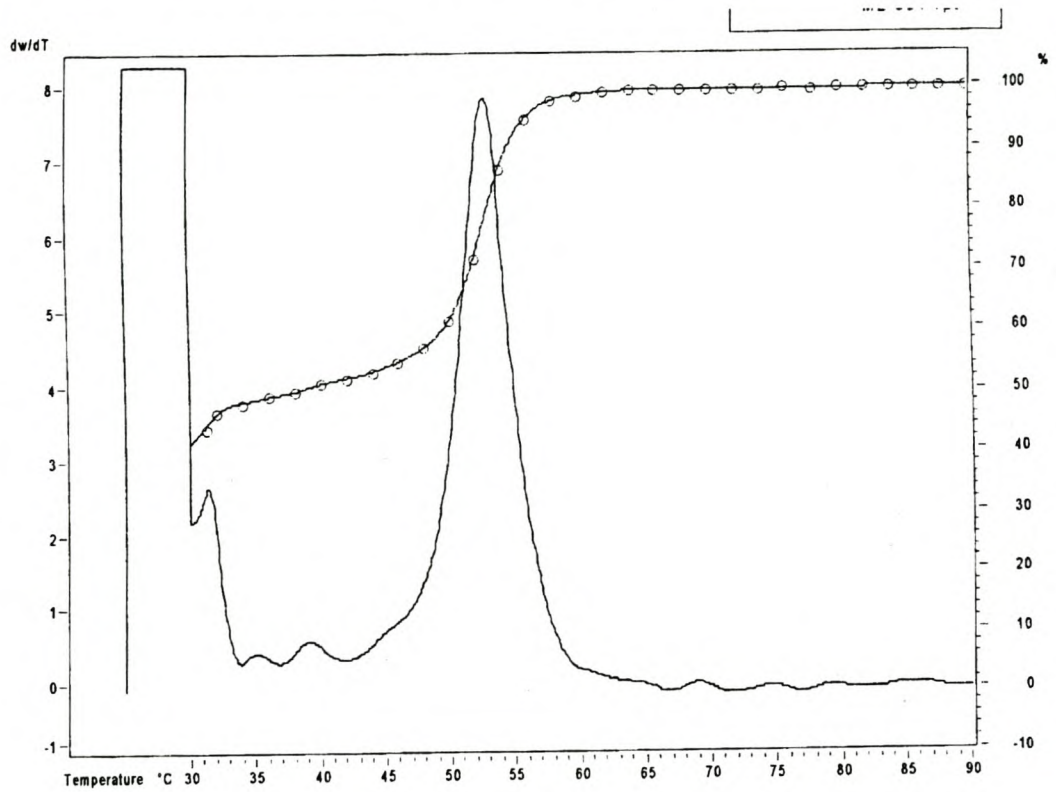

Figure 4.15 Cumulative and differential SCBD of a propylene/1-hexene copolymer (Sample B2, 4.42% 1-hex.) as obtained by CRYSTAF.

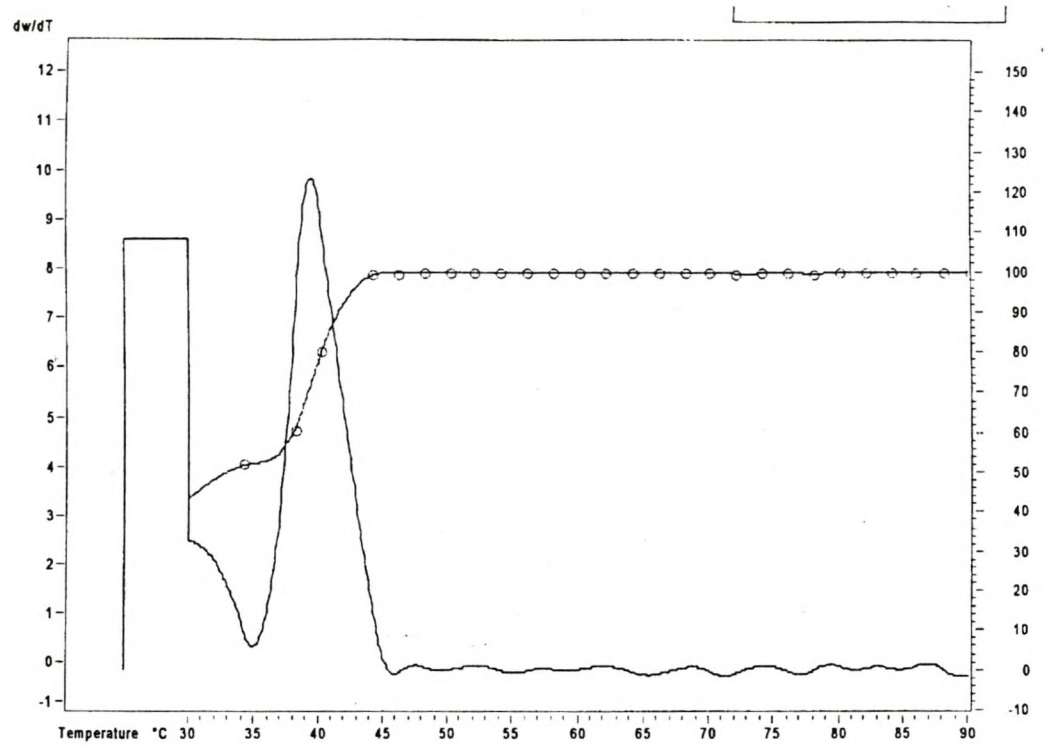

Figure 4.16 Cumulative and differential SCBD of a propylene/1-octene copolymer (Sample B5, 4.70% 1-oct.) as obtained by CRYSTAF.

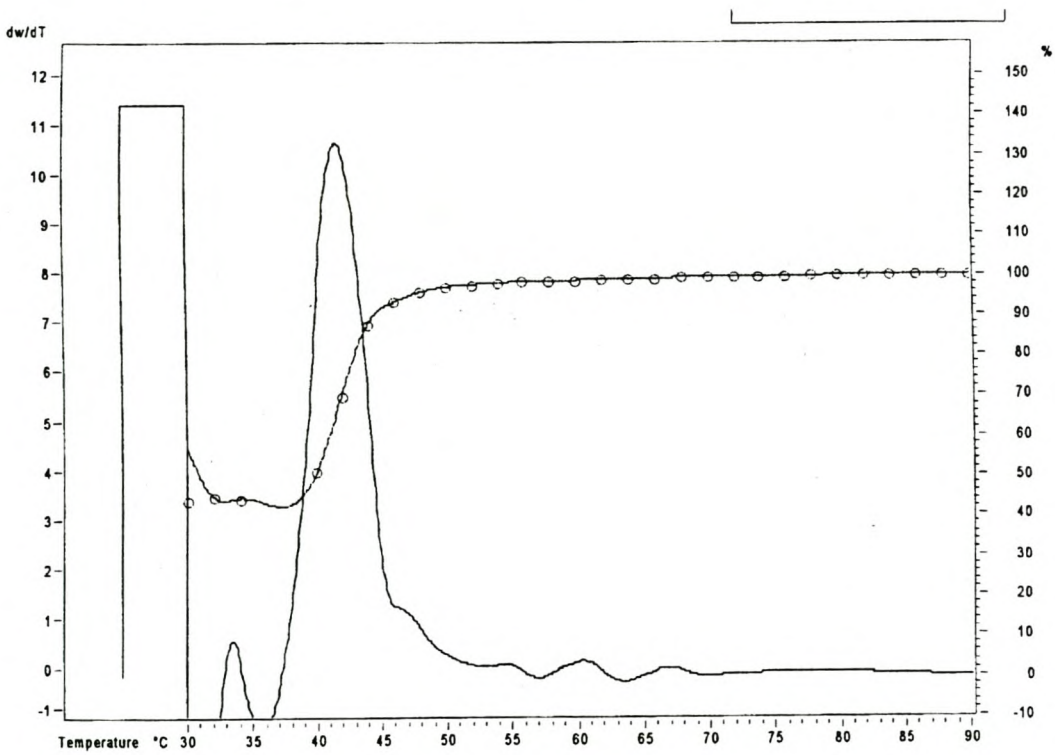

Figure 4.17 Cumulative and differential SCBD of a propylene/1-heptene copolymer (Sample B9, 5.79% 1-hept.) as obtained by CRYSTAF.

Plotting the crystallization temperature, T_c, vs. the comonomer mol% incorporated results in a relatively straight line as shown in Figure 4.18. This seems to indicate a good correlation with Flory's equilibrium theory approach **[12]** and crystallization to be practically independent of molecular weight. The graph also corresponds well with the following equation which was deduced from the classical Flory equation in Chapter 3 (Section 3.5.4):

$$T_m \cong T_m^0 - \frac{R\left(T_m^0\right)^2}{\Delta H_u} N_2$$

The equation clearly indicates that a linear dependence of melting or crystallization temperature, T_m, with the amount of comonomer incorporated, N_2, is achieved.

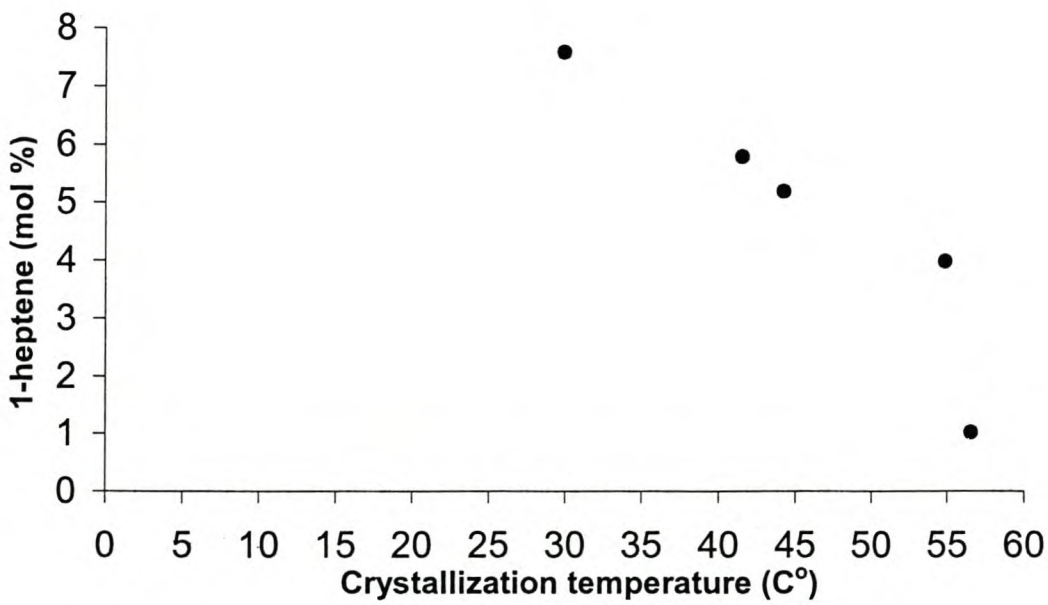

Figure 4.18 Graph of crystallization temperature, T_c, versus the 1-heptene content of the propylene/1-heptene copolymers produced.

In Table 4.11 the crystallized fractions of the different polymers are set out in temperature intervals of 9.9°C. From this analysis of the soluble fraction it is clear that in the case of the copolymers most of the crystallization took place at temperatures lower than 50°C. The last two columns of the table gives an idea of the reliability of the experimental results. The second last column is calculated by adding up all the crystallized fractions given by the CRYSTAF analyses and subtracting it

from 100%. This should give the soluble fraction of the polymer left at 30°C and for reliability it must correspond closely with soluble fraction given by the CRYSTAF analyses. Except for the Sample B9, the correlation between the two columns is very good.

Table 4.12 CRYSTAF results of the crystallized fractions in specific temperature intervals of the propylene homopolymer (Sample B1) and the propylene/1-hexene (Samples B2-B3), propylene/1-octene (Samples B4-B5) and propylene/1-heptene (Samples B6-B10) copolymers.

Sample	30-39.9°C (%)	40-49.9°C (%)	50-59.9°C (%)	60-69.9°C (%)	70-79.9°C (%)	80-100°C (%)	100%-total (%)	Soluble fraction (%)
B1	1.3	-	0.5	-	97.7	1.9	-1.4	-1.9
B2	10.7	-	47.3	-	-	-	42.0	41.4
B3	3.2	-	-	-	0.2	-	96.6	96.4
B4	65.8	-	2.1	-	-	-	32.1	31.9
B5	56.5	-	0.1	-	-	0.1	43.3	43.2
B6	10.3	0.3	80.2	5.8	2.1	-	11.6	11.2
B7	9.0	6.1	52.9	-	-	-	32.9	32.7
B8	-	41.2	-	1.0	1.1	-	56.7	56.5
B9	-	53.0	0.5	0.7	0.5	-	44.0	57.0
B10	7.0	0.7	-	-	0.6	-	91.7	90.3

4.6 CONCLUSIONS

For producing the copolymers discussed in this chapter we used the homogeneous metallocene *rac*-$Me_2Si(2\text{-}MeBenz[e]Ind)_2ZrCl_2$ catalyst. From the ^{13}C NMR spectra we can conclude that these copolymers are extremely isotactic because of the very few and small stereoirregularities present. Some of the regioirregularities are typical of 2,1-insertion but can be ignored because of their low intensities. The tacticities of these polymers were calculated through integration to be between 92-99%. This is almost 10% higher than in the case of the *rac*-$Et(Ind)_2ZrCl_2$ catalyst. The observed chemical shift values of the carbon peaks in the ^{13}C NMR spectra also correspond very well overall with the calculated values.

As in the previous chapter the GPC curves of the polymers produced by the activating metallocene catalyst in this chapter have a characteristic shape as predicted by Flory's distribution law. The polydispersities are in the range of 1.89 - 3.37 which is typical for metallocene catalyzed polymers. The *rac*-Me_2Si(2-MeBenz[e]Ind)$_2ZrCl_2$ catalyst produced copolymers with much higher weight average molecular mass (221 044 - 684 739) as well as number average molecular mass (65 582 - 293 973) as was the case of the bridged metallocene *rac*-Et(Ind)$_2ZrCl_2$ catalyst (M_n: 8 373 – 37 321 g/mol; M_w: 26 332 – 68 325 g/mol). The high molecular mass of the copolymers produced by the MBI catalyst is a very important consequence because it makes these copolymers suitable for industrial use which is not the case with the *rac*-Et(Ind)$_2ZrCl_2$ catalyst.

In the DSC analyses a decrease in melting point as well as crystallinity were found for an increase in the comonomer content. This corresponds well with the findings in Chapter 3. The melting peak also became broader and the height lower as the comonomer content was increased. The DMA analyses showed a fast decrease in glass transition temperature as the comonomer content was increased in the propylene/1-heptene copolymers. This decrease in T_g is caused by an increase in free volume, resulting from comonomer inclusion.

From the CRYSTAF results it is clear that the crystallization temperature, T_c, as well as the weight average temperature, T_w, and number average temperature, T_n, decreased as the amount of 1-heptene incorporated in the propylene/1-heptene copolymers was increased. A decrease in crystallization temperature therefore indicates an increase in the amount of branches in the copolymer. The narrow chemical composition distribution (CCD) of the CRYSTAF curves is in keeping with the narrow molecular mass distribution of the copolymers as obtained by GPC analysis.

4.7 REFERENCES

1. Stehling U., Diebold J., Kirsten R., Röll W., Brintzinger H.H., Jüngling S., Mülhaupt R., Langhauser F., *Organometallics*, 1994, **13**, 964.

2. Spaleck W., Antberg M., Aulbach M., Bachmann B., Dolle V., Haftka S., Küber F., Rohrman J., Winter A., In Fink B., Mülhaupt R., Brintzinger H.H., *Ziegler Catalysts*, Springer, Berlin, 1995, p. 83.
3. Langhauser F., Kerth J., Kersting M., Kölle P., Lilge D., Müller P., *Angew. Makromol. Chem.*, 1994, **223**, 155.
4. Grassi A., Zambelli A., Resconi L., Albizatti E., Mazzochi R., *Macromolecules*, 1988, **21**, 617.
5. Grant D.M., Paul E.G., *J. Am. Chem. Soc.*, 1904, **86**, 2984.
6. Van Reenen A.J., Institute for Polymer Science, University of Stellenbosch, Stellenbosch, Personal Communication.
7. Quirk R.P., Alsamarraie M.A.A., *Physical Properties of Poly(propylene)* in *Polymer Handbook*, Third Edition (Brandrup J., Immergut E.H., Eds.) John Wiley & Sons, New York, V/27 (1989).
8. Lauritzen J.J., Hoffman J.D., *J. Res. Nat. Bur. Std.*, 1960, **64**(A), 73.
9. Hoffman J.D., Davis G.T., Lauritzen J.I., *Treatise on Solid State Chemistry* (Hannay N.B., Ed.), Plenum Press, New York, 1976, p. 3.
10. Mathot V.B.F., *The Crystallization and Melting Region in Calorimetry and Thermal Analysis of Polymers* (Mathot. V.B.F., Carl Hanser, Eds.), Verlag, Munich, 1994, **9**, p. 231.
11. Monrabal, B., Blanco J., Nieto J., Soares J.B.P., *J. of Polym. Sci., PartA; Polym. Chem.*, 1999, **37**, 89.
12. Flory P.J., *Trans Faraday Soc.*, 1984, **51**, 848.

CHAPTER 5

Polymerization and characterization of propylene/1-heptene copolymers produced with $TiCl_3/AlEt_3/SiO_2$

Summary

Two propylene/1-heptene copolymers were synthesized differing in the amount of comonomer incorporated into the propylene backbone. The copolymerizations were carried out using the Ziegler-Natta catalyst, $TiCl_3/AlEt_3/SiO_2$, as activating catalyst. These copolymers were used to investigate the effect of the 1-heptene comonomer on the microstructure, molecular mass, molecular mass distribution, melting point, glass transition temperature and crystallization behaviour of the different copolymers produced. Characterization methods on the obtained copolymers included nuclear magnetic resonance spectroscopy (NMR), high temperature gel permeation chromatography (HTGPC), differential scanning calorimetry (DSC), dynamic mechanical analysis (DMA) and crystallization analysis fractionation (CRYSTAF). The two copolymers produced in this series were compared within the series itself, but the main focus was on comparing the properties of the metallocene, *rac*-$Me_2Si(2\text{-}MeBenz[e]Ind)_2ZrCl_2$, catalyzed propylene/1-heptene copolymers with the properties of the Ziegler-Natta catalyzed propylene/1-heptene copolymers as well as with the *rac*-$Et(Ind)_2ZrCl_2$ catalyzed copolymers.

5.1 INTRODUCTION

When Karl Ziegler and his coworkers investigated the role of transition metal compounds, such as zirconium and titanium halides, in the 1950's, they discovered that group IV transition metal compounds activated with the main group metal alkyls, especially aluminum alkyls, catalyzed the polymerization of ethylene at low pressure **[1]**. In 1954 Giulio Natta polymerized propylene in the Montecatini laboratories by means of a modified Ziegler catalyst and obtained a blend of isotactic and atactic polypropylene **[2-5]**. For this pioneering invention he and Karl Ziegler received the Nobel prize for chemistry in 1963.

The first generation catalysts developed by Natta consisted of δ-$TiCl_3$ with aluminium diethylchloride as activator. The process was very elaborate, since the large quantity of atactic polypropylene had to be removed and furthermore, the low level of activity of the catalyst necessitated deactivation and leaching of the latter **[6-8]**. The second generation was developed by Solvay **[9-11]**. Compared with the first, it was distinguished by a level of activity about four times as high and by a high stereospecifity, obtained through the inclusion of an electron donor in the system. This enabled easier separation of the atactic polypropylene fraction, but not yet the leaching of the catalyst. The decisive breakthrough to the third generation was achieved in 1975 by Montedison and Mitsui Petrochemical. They developed a highly active catalyst system with good stereospecifity. This advance was made possible by supporting the titanium component on magnesium chloride **[12-14]**. This supported catalyst system has the important improvement of eliminating the leaching of the catalyst. Furthermore, due to this improvement the polypropylene process became an extremely environment-friendly technique. A further improvement to the fourth generation in the 1980's was characterized by developing catalysts which retain their spherical and porous morphology during the polymerization process **[15-17]**.

Ziegler-Natta catalysts have a heterogeneous distribution of active sites with different accessibilities and activities and this leads to both the wide molecular weight distribution and the comonomer distributions usually observed. In order to incorporate the higher α-olefins such as 1-heptene, catalyst active sites should thus be "open" enough to allow these bulky monomers to be inserted into the polymer chains. If the active sites are not "open" but rather protected, the bulky comonomers will not be able to come close enough to these active sites to be inserted into the polymer chain. This will result in mainly linear chains. When supporting $TiCl_4$ on an inert support such as $MgCl_2$ the amount of transition metal residues left in the polymer will be decreased and this will lead to an improved product with a better oxidative and colour stability. The activity of these supported catalysts is relative high due to increased seperation between active centres and this improves their accessibility. In order to produce crystalline polypropylene not only accessibility of the active sites is important, but the monomer placement in the chain should also be regular. The active sites should therefore also be able to regulate the coordination of the monomer to ensure a regular chain with as little stereo defects as possible.

We carried out an investigation into the variation of the amount of comonomer (1-heptene) on the propylene/α-olefin copolymerization with the supported Ziegler-Natta catalyst $TiCl_3/AlEt_3/SiO_2$ and will report on the influence of the amount of comonomer incorporated into the copolymer on the copolymer microstructure, molecular mass, molecular mass distribution, melting point, glass transition temperature and crystallization behaviour of the copolymers.

5.2 EXPERIMENTAL

The two Ziegler-Natta catalyzed propylene/1-heptene copolymers which will be discussed in this chapter were synthesized at Sastech and used as received. For a description on the experimental work in connection with these copolymers I refer to reference **18**.

5.3 RESULTS AND DISCUSSION

5.3.1 Microstructure

5.3.1.1 Propylene/1-heptene copolymers

Assignments of the different peaks appearing in the spectra of the synthesized propylene/1-heptene (Samples Z1-Z2) copolymers were done making use of available literature, combined with APT analysis and checked against the chemical shift assignments predicted by the additivity rules described by Grant and Paul **[19]**.

Figure 5.1 shows the numbering of the different carbons in the propylene/1-heptene copolymer structure while Figure 5.2 shows the ^{13}C NMR spectrum of sample Z2. This spectrum of the propylene/1-heptene copolymer containing 1.66 mol% of comonomer shows many visible regioirregularities, especially in the methyl region. These defects are consequences of the multi-site nature of the heterogeneous Ziegler-Natta catalysts.

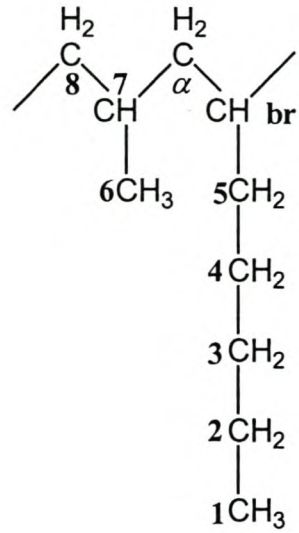

Figure 5.1 Numbering of carbon atoms of propylene/1-heptene copolymers for chemical shift predictions.

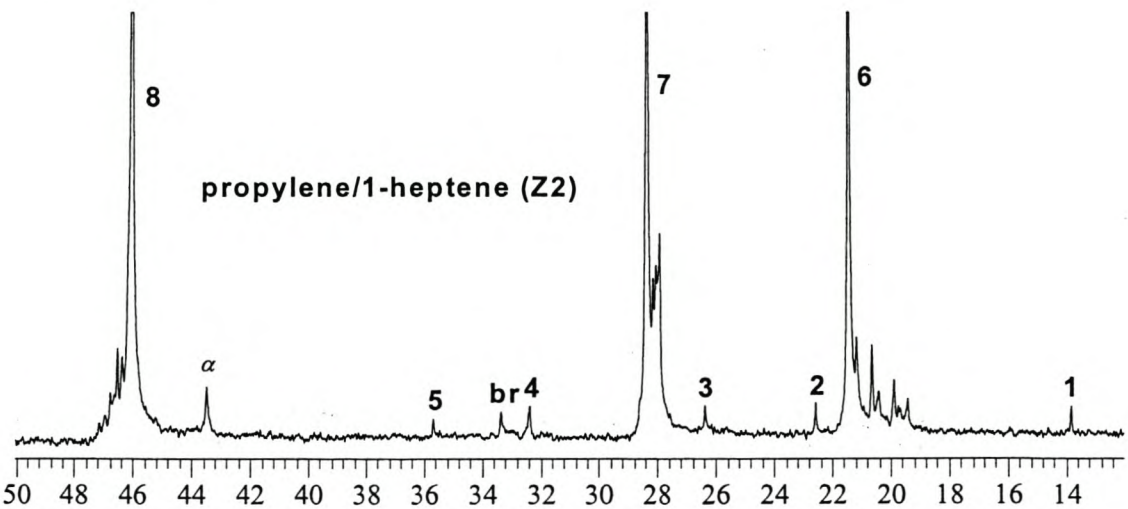

Figure 5.2 ^{13}C NMR spectrum of a propylene/1-heptene copolymer (Sample Z2).

Solvent 1,2,4-trichlorobenzene:benzene-d_6 (9:1 volume ratio), temperature 100°C.

The primary resonance signals (8), (7) and (6) designate the methylene carbons (δ = 46.04 ppm), the methine carbons (δ = 28.37 ppm), and the methyl carbons (δ = 21.46 ppm) of the propylene monomers in the copolymer respectively **[20]**. We mentioned in Chapter 3 (Section 3.5.1.1) that the methyl region is chosen for tacticity analysis. Looking at the methyl region of this spectrum (shown in Figure 5.3) many stereoirregularities can be seen. The stereoirregular units of *mmmm* (δ =

21.46ppm), *mmmr* (δ = 21.17ppm), *mmrr* (δ = 20.64ppm) and *mrrm* (δ = 19.40ppm) of Sample Z2 in Figure 5.3 indicated respectively as (a), (b), (d) and (j) correspond very well with the spectrum of the propylene homopolymer (Sample A1) which was discussed in Chapter 3 (Section 3.5.1). These assignments also correspond with previous investigations **[21-22]** and the relative intensities of the resonance of the *mmmr*, *mmrr* and *mrrm* stereochemical pentads are roughly 2:2:1 **[20]**, as expected from the statistical model **[23]** of the enantiomorphic site control of the stereospecific propagation **[24]**.

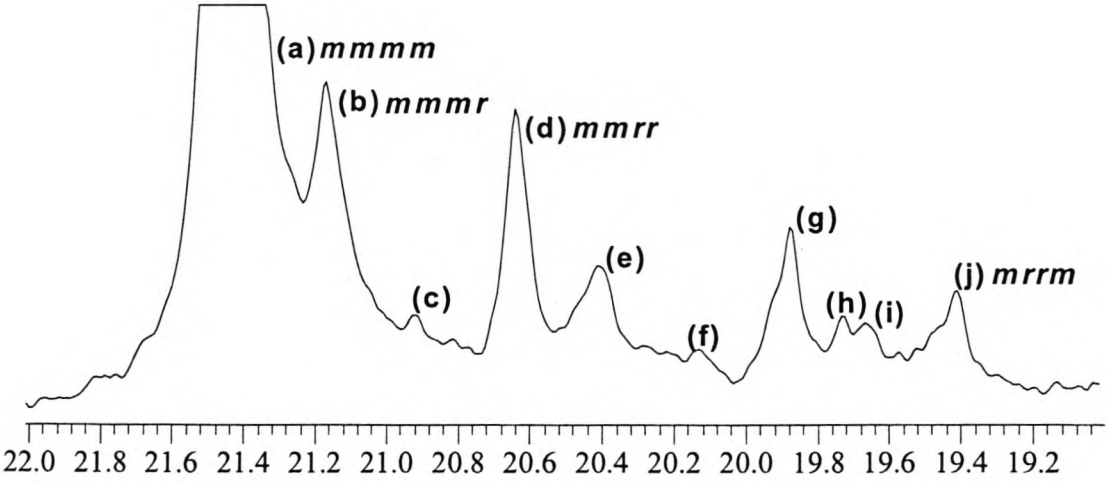

Figure 5.3 ^{13}C NMR spectrum of the methyl region of sample Z2.

Solvent 1,2,4-trichlorobenzene:benzene-d_6 (9:1 volume ratio), temperature 100°C.

Chemical shifts and assignments of the other stereoirregular units in Figure 5.3 are summarized in Table 5.1. Assignments were done using previous investigations **[25-26]**.

Table 5.1 Summary of assignments of peaks in the methyl region of propylene/1-heptene copolymer (Sample Z1, 1.66% 1-heptene).

Peak Number	Chemical shift (ppm)	Assignment
(a)	21.46	*mmmm*
(b)	21.17	*mmmr*
(c)	20.92	*rmmr*
(d)	20.64	*mmrr*
(e)	20.40	*mmrm + rmrr*
(f)	20.13	*rmrm*
(g)	19.88	*rrrr*
(h)	19.73	*rrrm*
(i)	19.67	*mrrr*
(j)	19.40	*mrrm*

The percentages of comonomer incorporated in each of the copolymers produced by the $TiCl_3/AlEt_3/SiO_2$ catalyst are summarized in Table 5.2 In calculating the comonomer amount of each copolymer, the intensities of only the backbone carbon atoms are taken into account. The formula for calculating the percentage of 1-heptene (**I**) in a specific copolymer is the following **[27]**:

$$C_7 = \frac{\frac{1}{2}(I_\alpha + I_{br})}{I_\alpha + I_{br} + I_7 + I_8} \times 100 \qquad \mathbf{I}$$

C_7 represents the percentage of comonomer incorporated and $I_\alpha / I_{br} / I_7 / I_8$ represent the intensities of the carbon peaks of the backbone of the polymer as numbered in Figure 5.1.

Unfortunately we had trouble analyzing Sample Z1 and the baseline of the ^{13}C spectrum of this copolymer was too noisy to be able to read the intensities of the peaks accurately enough for accurate comonomer content calculation. The value quoted for the comonomer content in Sample Z1 is therefore at best an approximation.

Table 5.2 Summary of comonomer content of propylene/1-heptene (Samples Z1-Z2) copolymers.

Sample	Comonomer content (%)
Z1	≈ 1.00
Z2	1.66

Solvent 1,2,4-triclorobenzene:benzene-D_6 (9:1 volume ratio), temperature 100°C.

We calculated the tacticity for sample Z2 by way of integration of the methyl peak region and found it to be a low 61.6%. The low tacticity also corresponds well with the many stereoirregularities found in the methyl region of the ^{13}C NMR spectrum of Sample Z2 (Figure 5.3). Due to the noisy baseline of the ^{13}C spectrum of sample Z1 we could not calculate the tacticity of this sample.

In Table 5.3 the calculated values of the chemical shift predictions are compared with the observed chemical shift values of the produced propylene/1-heptene copolymers respectively. The calculation of the chemical shift values was demonstrated in the previous chapter (Section 4.5.2.2). The observed and calculated values correspond very well overall. The observed chemical shift values of the propylene/1-heptene copolymers produced by the heterogeneous $TiCl_3/AlEt_3/SiO_2$ catalyst also correspond almost exactly to the values of the same copolymers (Table 4.6) produced by the homogeneous *rac*-$Me_2Si(2\text{-}MeBenz[e]Ind)_2ZrCl_2$ catalyst.

Table 5.3 Comparison of observed and calculated chemical shifts of propylene /1-heptene (Samples Z1–Z2) copolymers.

Carbon	1	2	3	4	5	br	α	6	7	8
Calculated Grant and Paul	**14.07**	**22.74**	**32.89**	**27.25**	**35.57**	**32.36**	**42.96**	**20.80**	**25.46**	**45.47**
Observed Z1	14.06	21.45	26.38	32.67	35.66	33.39	43.46	21.45	28.38	46.05
Observed Z2	13.81	22.56	26.36	32.36	35.65	33.35	43.47	21.46	28.37	46.04

5.3.2 Molecular mass and molecular mass distributions

From Figure 5.4 it can be seen that the GPC curves of the copolymers have the characteristic shape, predicted by Flory's distribution law. The molecular mass distributions of such copolymers do not change with polymerization time. The molecular mass at the maximum is closely related to the weight-average molecular mass of the polymer.

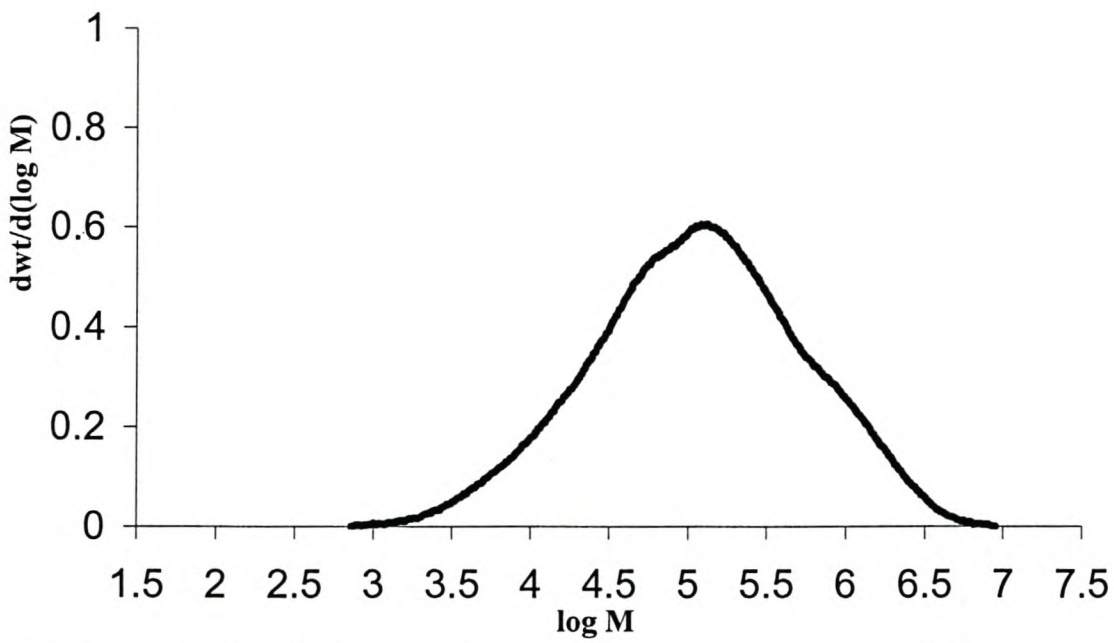

Figure 5.4 The distribution of the molecular mass, w(logM), against the molecular mass of propylene/1-heptene (sample Z2, 1.66% 1-heptene).

Table 5.4 represents the molecular mass results of the GPC analyses carried out on the propylene/1-heptene copolymers. The molecular mass distributions of the polymers in Table 5.4 were very high for both polymers. This feature is very characteristic of multi-site Ziegler-Natta catalysts which produces copolymers with non-uniform comonomer incorporation.

Table 5.4 GPC results of propylene/1-heptene copolymers (Samples Z1-Z2).

Sample	1-heptene (Z1-Z2) content (mol %)	Number-Average Molecular Mass (M_n, g/mole)	Weight - Average Molecular Mass (M_w, g/mole)	Polydispersity (M_w/M_n)
A1	≈1.00	93 809	595 766	6.35
A2	1.66	35 534	333 589	9.39

5.3.3 Thermal properties

5.3.3.1 Melting behaviour

Table 5.5 represents the results of the DSC analyses of the propylene/1-heptene copolymers produced with the heterogeneous $TiCl_3/AlEt_3/SiO_2$ catalyst. Crystallinity was calculated from fusion enthalpy based on a value of 209 J/g for 100% crystalline material **[28]**.

Table 5.5 DSC results of propylene/1-heptene (Samples Z1-Z2) copolymers.

Sample	1-heptene (Z1-Z2) content (mol %)	Melting Temperature (°C)	FUSION ENTHALPY (J/G)	Crystallinity (%)
Z1	≈1.00	148.3	43.0	20.6
Z2	1.66	149.0	41.4	19.8

The melting temperatures of the different comonomers shown in Table 8.3 are relatively insensitive towards comonomer content. This insensitivity corresponds well with previous studies **[18]**. There is however a large drop in melting temperature comparing it to the melting temperature of propylene homopolymer produced by the same heterogeneous catalyst. The propylene homopolymer used for comparison was produced in earlier studies **[18]** with a melting temperature of 166.0°C and it can be seen from Table 5.5 that the introduction of only 1.66% 1-heptene resulted in a

decrease in melting temperature to 149.0°C. The crystallinity has the same relative insensitivity towards comonomer content.

Melting behaviour does not depend directly on comonomer content, but rather on sequence distribution **[29]**. Ziegler-Natta catalysts have a heterogeneous distribution of active sites and will therefore produce heterogeneous copolymers because of differences in copolymerization characteristics of the different active sites **[30]**. A heterogeneous mixture consisting of chains with different lengths and different comonomer content and distribution will be generated. These different chains will crystallize at completely different temperatures, leading to different melting temperatures **[31]**. However, as most of the comonomer is incorporated into the lower molecular weight fractions, the peak crystallization temperature remains essentially unaffected, although a broadening of the melting peak is expected as the comonomer content increases (see Figure 5.5).

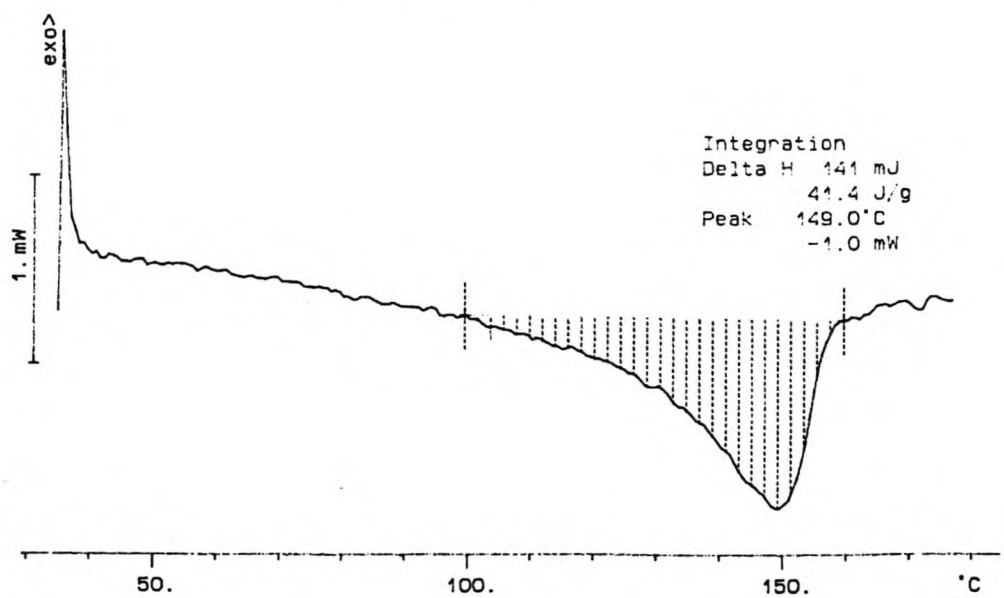

Figure 5.5 DSC melting curve of propylene/1-heptene (Sample Z2, 1.66 mol%) copolymer.

5.3.3.2 Glass transition temperature

Table 5.6 reflects the different glass transition temperature of the propylene-1-heptene copolymers produced with the $TiCl_3/AlEt_3/SiO_2$ catalyst.

Table 5.6 DMA results of propylene/1-heptene copolymers (Samples Z1-Z2).

Sample	1-heptene (Z1-Z2) content (mol %)	Glass Transition Temperature (°C)
Z1	≈1.00	-40.27
Z2	1.66	-

Unfortunately we were unable to determine the T_g of sample Z2.

5.3.4 Crystallinity

The overall CRYSTAF results are presented in Tables 5.7 and 5.8. There is a definite decrease in the weight-average crystallization temperature (T_w) as well as in the number-average crystallization temperature (T_n) with an increase in comonomer content. The crystallization temperature of these two copolymers is however relatively insensitive towards an increase in comonomer content. The σ and R parameters gives an indication of the broadness of the crystallization peak. The σ and R values given in Table 5.7 are relatively big numbers and therefore indicates a broad crystallization peak. The broad crystallization peaks for these two copolymers correspond well with their heterogeneity, which is also indicated by the two smaller crystallization peaks (see Figure 5.6).

Table 5.7 CRYSTAF results of the propylene/1-heptene (Samples Z1-Z2) copolymers.

Sample	Comonomer (mol %)	M_n (g/mole)	Soluble Fraction (%)	T_c (°C)	T_w (°C)	T_n (°C)	R	σ
Z1	≈1.00	93 809	11.0	69.6	63.4	59.5	6.4	12.3
Z2	1.66	35 534	34.6	72.4	56.5	49.8	13.5	17.5

Table 5.8 CRYSTAF results of the crystallized fractions in specific temperature intervals of the propylene/1-heptene (Samples Z1-Z2) copolymers.

Sample	30-39.9°C (%)	40-49.9°C (%)	50-59.9°C (%)	60-69.9°C (%)	70-79.9°C (%)	80-100°C (%)	100%-total (%)	Soluble fraction (%)
Z1	4.1	4.6	-	80.0	-	-	11.3	11.0
Z2	6.3	3.4	-	-	55.7	-	34.6	34.6

Figure 5.6 shows the CRYSTAF curve of Sample Z1 (propylene/1-heptene copolymer). It is clear from this peak that the Ziegler-Natta catalyst, $TiCl_3/AlEt_3/SiO_2$, produced copolymers with wide chemical composition distributions (CCD). If we compare the results obtained from CRYSTAF and the GPC analysis, the CRYSTAF curves confirm the wide molecular mass distribution of the copolymers.

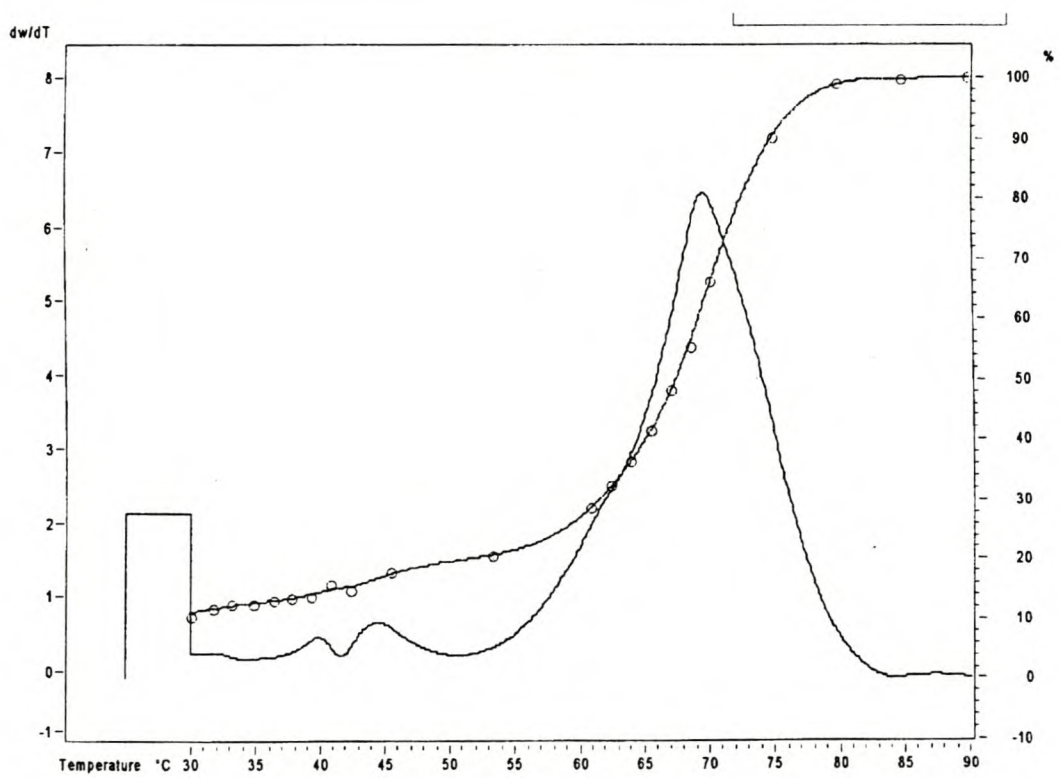

Figure 5.6 Cumulative and differential SCBD of propylene/1-heptene copolymer (Sample Z1) as obtained by crystallization fractionation analysis at 10°C/min crystallization rate.

5.4 COMPARISON OF RESULTS

5.4.1 Microstructure

Stereoirregularities were visible in all three series (A, B and Z) of teh copolymers. The amount of these defects however differs considerably between the different series and are summarized in Table 5.9. From Table 5.9 as well as the ^{13}C NMR spectra of all of the polymers it is clear that the spectra of the MBI catalyzed homopolymer and copolymers contained the least stereoirregularities in the methyl peak region. The B series polymers therefore have by far the highest tacticity according to these results and the Z series the lowest tacticity. Metallocene catalyzed polymers have typically high tacticity because of the fact that the catalytic sites of these single-site catalysts are shielded to a large extent from the influence of their immediate surroundings. These catalysts therefore yield a sharply defined product with a minimum of undesirable products, i.e. atactic polypropylene in isotactic polypropylene. In using a Ziegler-Natta catalyst however, polymerization at the active site is influenced by the electronic and steric environment of the crystal lattice. Because the active centres can occupy a wide variety of lattice sites, they tend to give products with non-homogeneous comonomer distribution in olefin copolymers.

Small regioirregular units typical of 2,1-insertion were visible in all three series of polymers. Tacticity of the polymers were calculated by way of integrating the methyl peak area. The tacticities of the different series of polymers are summarized in Table 5.10. The results of Table 5.10 confirm that the B series polymers have the highest tacticity and the Z series the lowest tacticity.

Table 5.9 Summary of assignments of peaks in the methyl region of different polymer series.

Peak Number	Chemical shift (ppm)	Assignment
	Sample A1 (Figure 3.3)	
(c)	21.47	*mmmm*
(d)	21.18	*mmmr*
(e)	20.65	*mmrr*
(f)	19.42	*mrrm*
	Sample B1 (Figure 4.3)	
(e)	20.62	*mmrr*
	Sample Z2 (Figure 5.3)	
(a)	21.46	*mmmm*
(b)	21.17	*mmmr*
(c)	20.92	*rmmr*
(d)	20.64	*mmrr*
(e)	20.40	*mmrm + rmrr*
(f)	20.13	*rmrm*
(g)	19.88	*rrrr*
(h)	19.73	*rrrm*
(i)	19.67	*mrrr*
(j)	19.40	*mrrm*

Table 5.10 Summary of tacticities of different polymer series.

Series	Tacticity Range (%)
A	72.1-90.9
B	92.4-98.9
Z	≈ 61.6

The chemical shift values of the produced homopolymers and copolymers in the different series were compared with the values calculated according to Grant and Paul **[19]**. The observed and calculated values corresponded very well overall for all the series.

5.4.2 Molecular mass and molecular mass distribution

All the GPC curves of the copolymers have a characteristic shape as predicted by Flory's distribution law. The peaks of the GPC curves of the Z series however are broader when compared to the GPC curves of the A and B series. In Ziegler-Natta catalyzed copolymers, the copolymers consist of a complex mixture of homo- and copolymers with comonomers frequently incorporated in the low molar mass fractions and show a broad molecular mass distribution. In metallocene catalyzed copolymers however we see uniform comonomer incorporation, which shows a narrow molar mass distribution. The GPC results are summarized in Table 5.11 and the difference in molar mass distribution for the metallocene catalyzed polymers (A and B series) and for the Ziegler-Natta catalyzed copolymers (Z series) can clearly be seen.

Table 5.11 Summary of molecular mass and molecular mass distribution of different polymer series.

Series	M_n (g/mole)	M_w (g/mole)	M_w/M_n
A	8 373-37 321	26 332-68 325	1.82-3.72
B	65 582 - 293 973	221 044 - 684 739	1.89-3.37
Z	35 534-93 809	333 589-595 766	6.35-9.39

Another very important conclusion from Table 5.11 is the fact that the MBI catalyzed polymers (B series) have much higher (almost ten times) number average molecular mass (M_n) and weight average molecular mass (M_w) than the $Et(Ind)_2ZrCl_2$ catalyzed polymers (A series). The high molecular mass of the B series makes the polymers suitable for industrial use which is not the case with the A series.

5.4.3 Thermal properties

5.4.3.1 Melting behaviour

Figure 5.7 illustrates the melting temperatures of the propylene/1-hexene copolymers (Samples A2-A6), the propylene/1-octene copolymers (Samples A7-A11) and the propylene/1-heptene copolymers (Samples B6-B10). The gradients of the three different trendlines in Figure 5.7 are almost exactly the same and furthermore the two trendlines for the metallocene catalyzed polymers (Samples A2-A6 and

Samples A7-A11) lie almost on each other. The trendline for the propylene/1-heptene copolymers (Samples B6-B10) however lies far above the the other two. The MBI catalyzed polymers have much higher melting points than the $Et(Ind)_2ZrCl_2$ catalyzed polymers. Because of the very few defects in the polymers of the B series the chains will fold into much thicker crystals than in the case of the polymers of the A series when chain-folding to form lamellae. This causes the higher melting points for the polymers in the B series. The melting temperatures of the Ziegler-Natta catalyzed polymers are 148.3 °C (Sample Z1) and 149.0°C (Sample Z2) which is higher than the T_g of any of the metallocene catalyzed copolymers. The melting temperature is also relatively insensitive towards comonomer content.

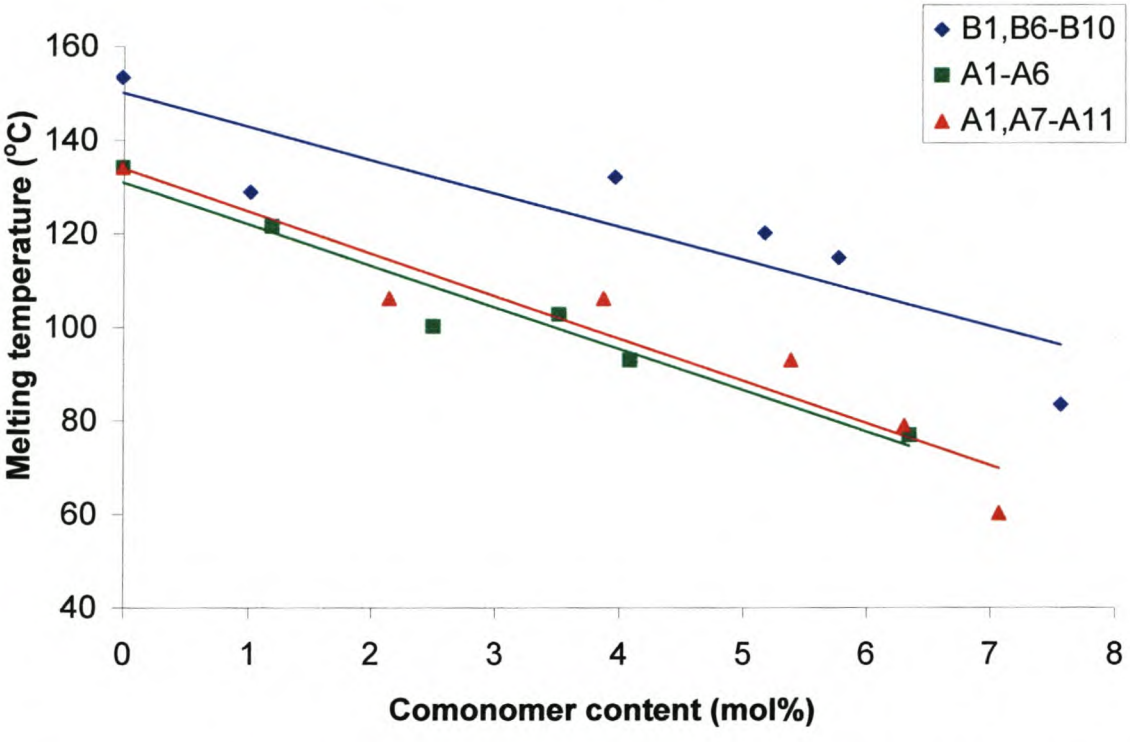

Figure 5.7 Melting temperature as a function of comonomer content for the propylene/1-hexene copolymers (Samples A2-A6), the propylene/1-octene copolymers (Samples A7-A11) and the propylene/1-heptene copolymers (Samples B6-B10).

In the case of the metallocene catalyzed polymers we found that the melting curve became broader and the height decreased as the amount of comonomer branches present in the chain increased. We also observed a decrease in crystallinity in the copolymers of both the A and B series as the comonomer amount was

increased. The crystallinity of the copolymers of the Z series was again relatively insensitive towards a change in comonomer content.

5.4.3.2 Glass Transition Temperature

Because of the very low molecular mass of the polymers from the A series no relevant conclusion could be drawn from the glass transition temperatures of these polymers. In the case of the MBI catalyzed propylene/1heptene copolymers there was a definite decrease in the glass transition temperatures of the propylene/1-heptene copolymers as the comonomer incorporation was increased. This decrease in T_g was caused by an increase in free volume due to an increase in the large-scale motions from the increasing amount of side chains. The T_g of Sample Z1 (-40.27°C) was lower than the T_g's of all the MBI catalyzed copolymers exept for Sample B10 (-41.17°C).

5.4.4 Crystallinity

The crystallization temperatures of almost all of the the A series copolymers were below 30°C. The reason for this is because of the low molecular weight copolymers produced by the bridged *rac*-Et(Ind)$_2$ZrCl$_2$ catalyst. No relevant conclusion could therefore be made of the CRYSTAF analysis of the polymers of the A series. For the copolymers in the B series however the crystallization temperature, T_c, as well as the weight average temperature, T_w, and number average temperature, T_n, increased as the amount of 1-heptene incorporated in the propylene/1-heptene copolymers was increased. The σ and R values, which are parameters used to measure the broadness of the chemical composition distribution (CCD), were relatively low and therefore support the GPC finding of the narrow molecular mass distribution of the copolymers of series B. The σ and R values of the copolymers of series Z were relatively high, indicating a broad chemical composition distribution (CCD) and therefore confirming the broad molecular mass distribution of the copolymers of the Z series.

A plot of the crystallization temperature, T_c, as a function of the comonomer mol% incorporated for the MBI catalyzed propylene/1-heptene copolymers (Samples B6-B10) results in a relative straight line with a negative gradient (Figure 4.13). This

seems to indicate a good correlation with Flory's equilibrium theory approach **[32]** and crystallization to be practically independent of molecular weight.

5.5 REFERENCES

1. German Patent, 973 626, 1953, Ziegler K., Breil H., Martin H., Holzkamp E.
2. Boor J.Jr., *Ziegler-Natta Catalysts and Polymerizations*, Academic Press, New York, NY, 1979, p. 21.
3. Italian Patent 535 712, 1954, Montecatini.
4. Italian Patent 537 425, 1954, Montecatini.
5. Italian Patent 526 101, 1954, Montecatini.
6. U.S.Patent 3 128 252, 1964, Esso Res. & Eng. Co.
7. U.S.Patent 3 032 510, 1964, Esso Res. & Eng. Co.
8. U.S.Patent 3 130 003, 1964, Esso Res. & Eng. Co.
9. German Patent, 2 213 086, 1972, Solvay & CIE.
10. U.S. Patent, 3 769 233, 1973, Solvay & CIE.
11. Bernard A., Fiasse B., *Catalytic Olefin Polymerization* (Keii T., Soga K., Eds.), Kodansha Elsevier, 1990, p 1405.
12. Belgian Patent, 785 332, 1972, Montedison.
13. Belgian Patent, 785 334, 1972, Montedison.
14. German Patent, 2 643 143, 1977, Montedison and Mitsui P.C.
15. U.S. Patent, 4 414 132, 1979, Shell Oil.
16. U.S. Patent, 4 393 182, 1979, Shell Oil.
17. Goodall B.L., *Transition Metal Catalyzed Polymerizations, Alkenes and Dienes* (Quirk R.P., Ed.), Harwood Academic Publishers, New York, 1983, Part A, p. 355.
18. Joubert D.J., *Ph.D. Thesis*, University of Stellenbosch, 2000.
19. Grant D.M., Paul E.G., *J. Am. Chem. Soc.*, 1904, **86**, 2984.
20. Grassi A., Zambelli A., Resconi L., Albizatti E., Mazzochi R., *Macromolecules*, 1988, **21**, 617.
21. Hansen E.W., Redford K., *Polypropylene: An A-Z reference*, (Karger-Kocsis J., Ed.) Kluwer Academic Publishers, Dordrecht, 1999, p. 541.
22. Busico V., Cipullo R., Monaco G., Vacatello M., *Macromolecules*, 1997, **30**, 6251.

23. Sheldon R.A., Fueno T., Tsunetsugu T., Furokawa J., *J. Polym. Sci., Part B*, 1966, **45**, 1565.

24. Doi Y., Suzuki T., Keii T., *Makromol. Chem. Rapid Commun.*, 1981, **2**, 293.

25. Hansen E.W., Redford K., *Polypropylene: An A-Z reference*, (Karger-Kocsis J., Ed.) Kluwer Academic Publishers, Dordrecht, 1999, p. 541.

26. Mülhaupt R., *Polypropylene: An A-Z reference*, (Karger-Kocsis J., Ed.) Kluwer Academic Publishers, Dordrecht, 1999, p. 902.

27. Van Reenen A.J., Institute for Polymer Science, University of Stellenbosch, Stellenbosch, Personal Communication.

28. Quirk R.P., Alsamarraie M.A.A., *Physical Properties of Poly(propylene)* in *Polymer Handbook*, Third Edition (Brandrup J., Immergut E.H.,Eds.), John Wiley & Sons, New York, V/27 (1989).

29. Alamo R., Domszy R., Mandelkern L., *J.Phys. Chem.*, 1984, **88**, 6587.

30. Sacchi M.C., Shan C., Forlini F., Tritto I., Locatelli P., *Makromol. Chem. Rapid Commun.*, 1993, **14**, 231.

31. Mathot V.B.F., *The Crystallization and Melting Region* in *Calorimetry and Thermal Analysis of Polymers* (Mathot V.B.F., Ed.), Carl Hanser Verlag, Munich, 1994, **9**, p. 231.

32. Flory P.J., *Trans Faraday Soc.*, 1984, **51**, 848.

APPENDIX A
(^{13}C NMR Spectra)

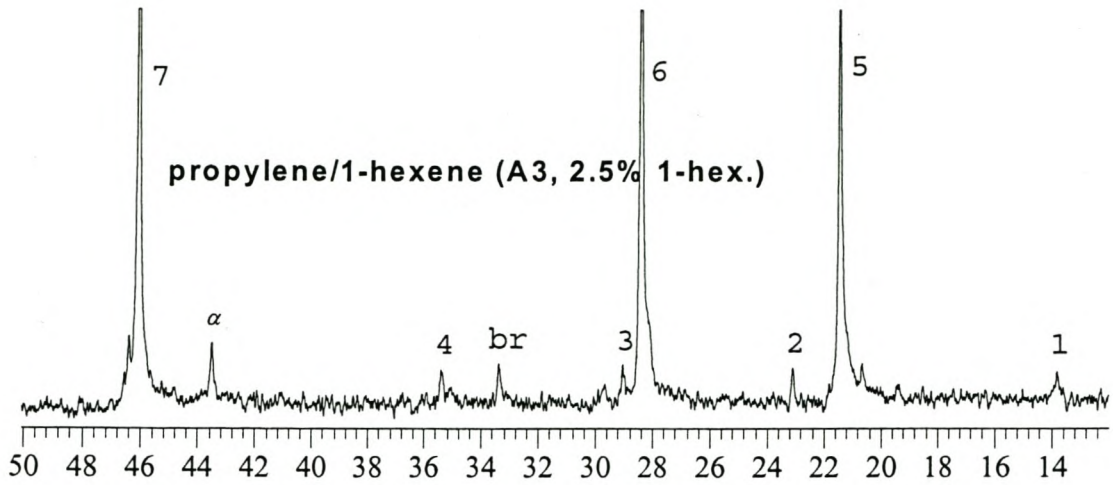

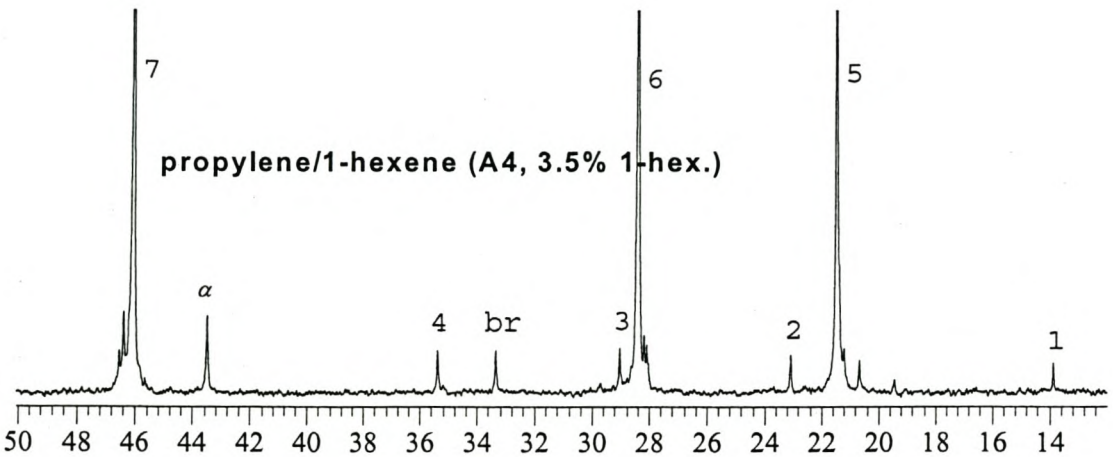

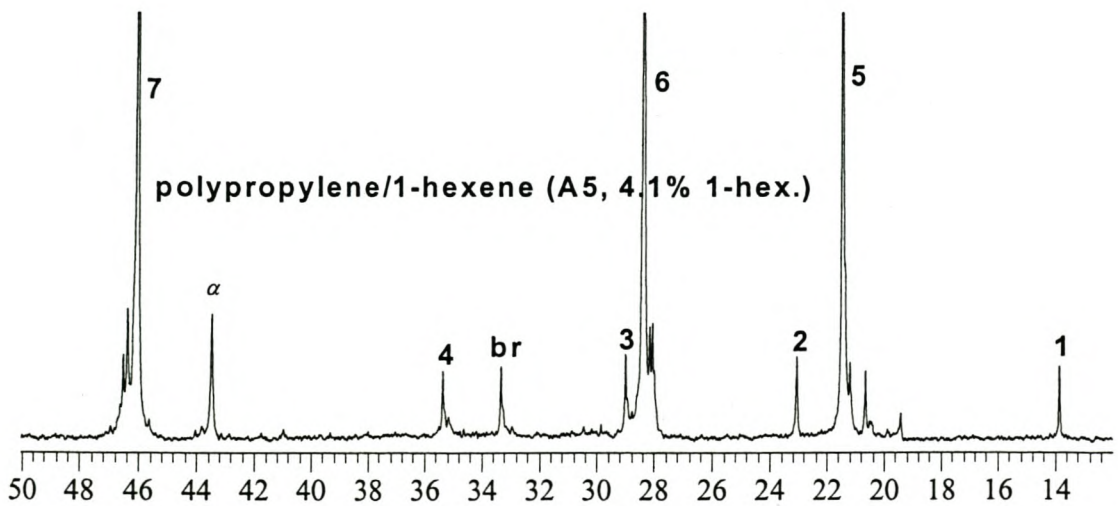

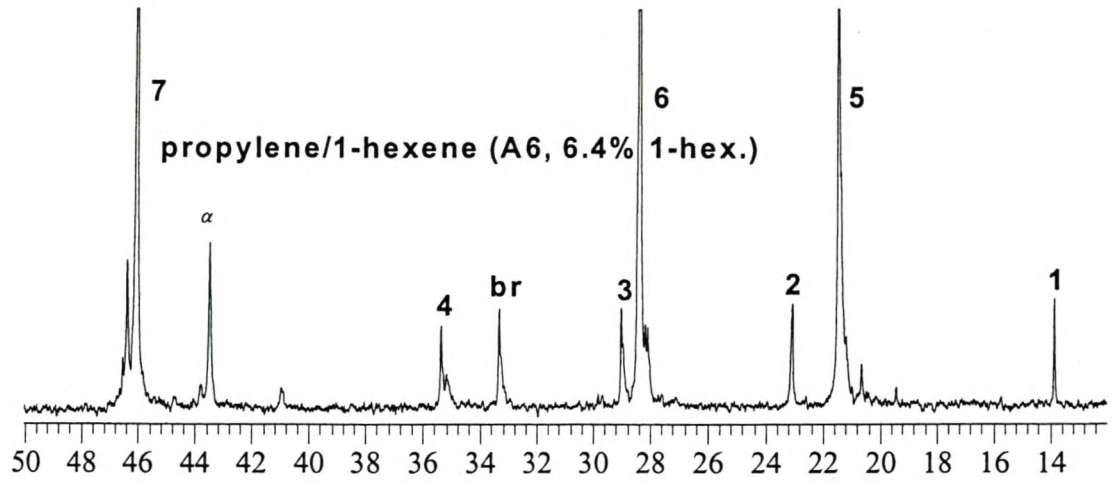

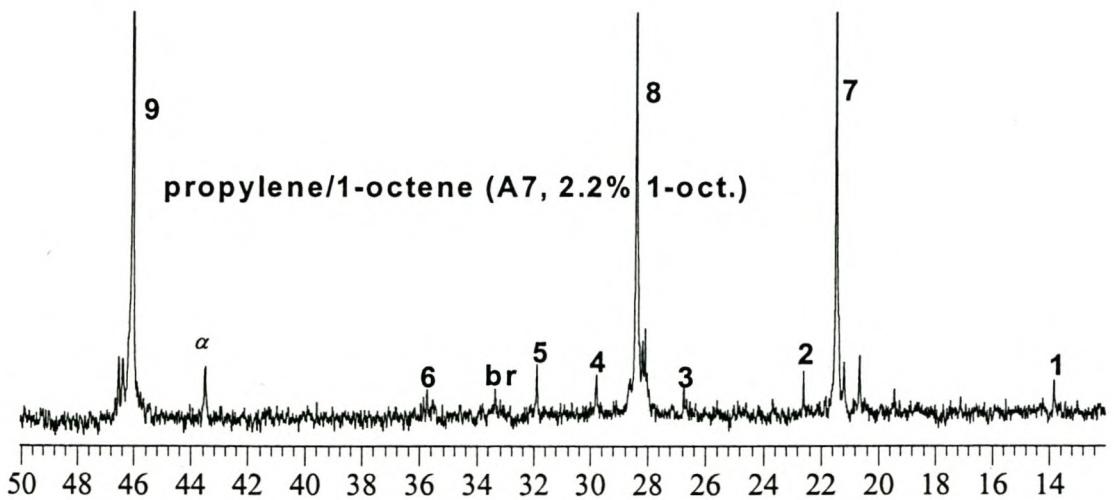

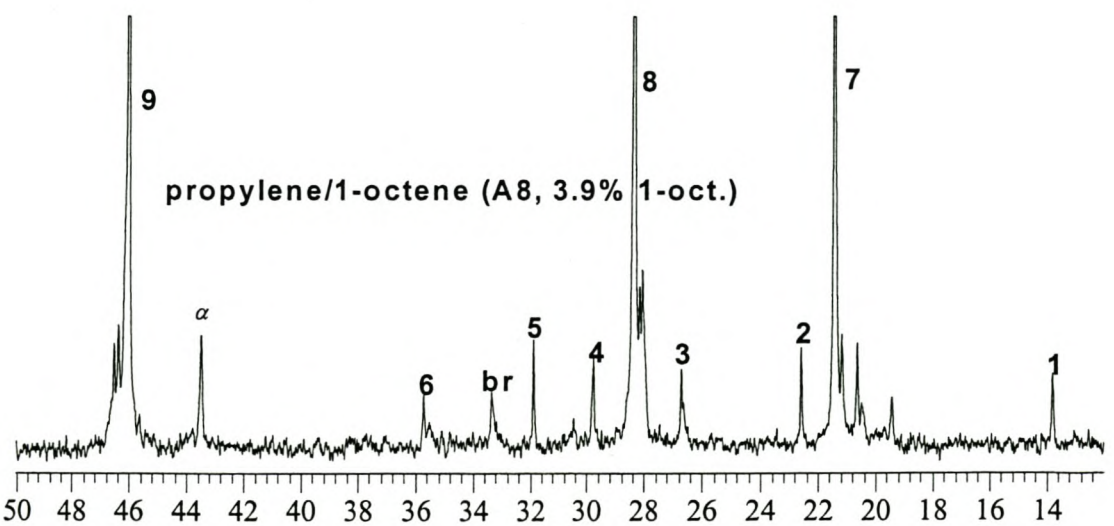

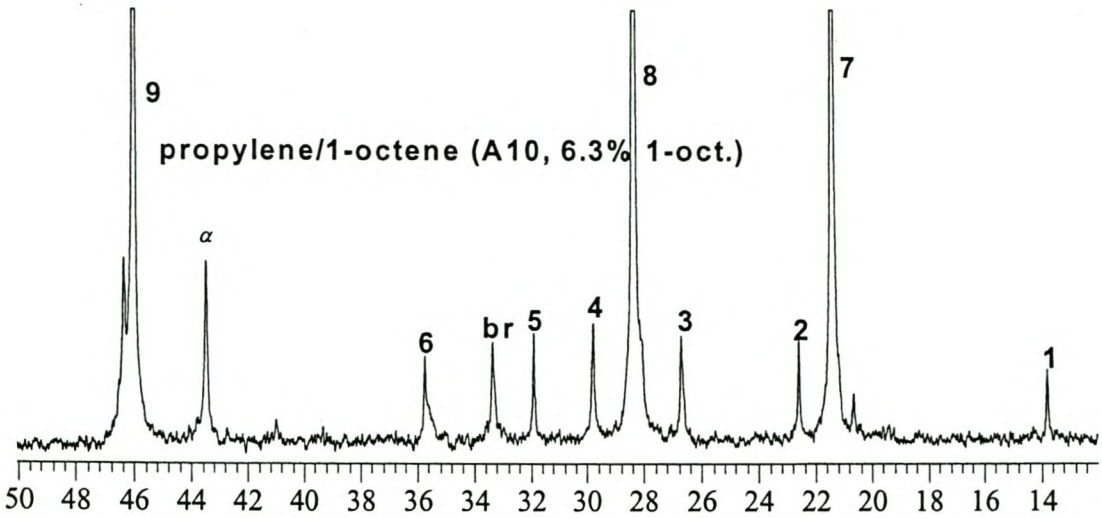

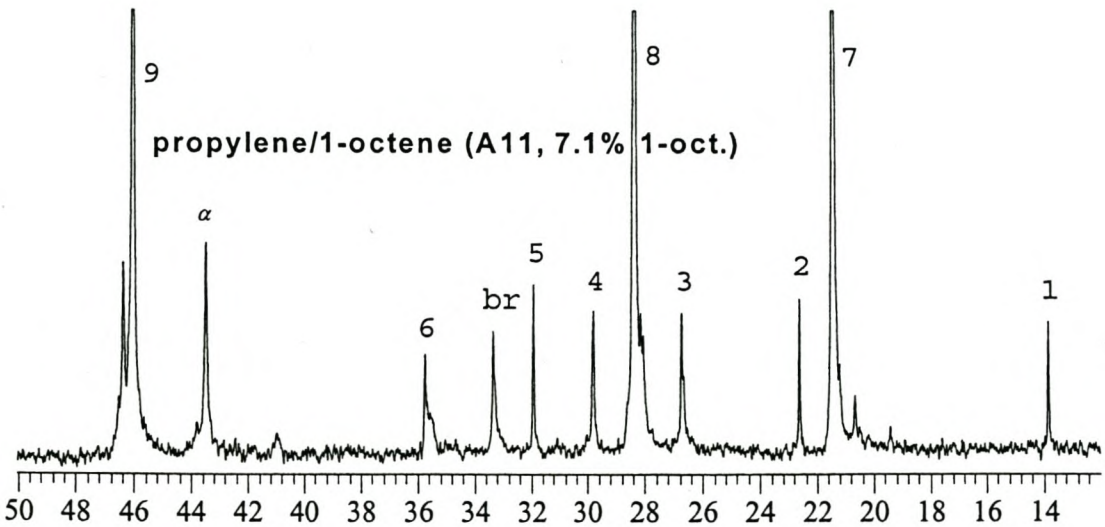

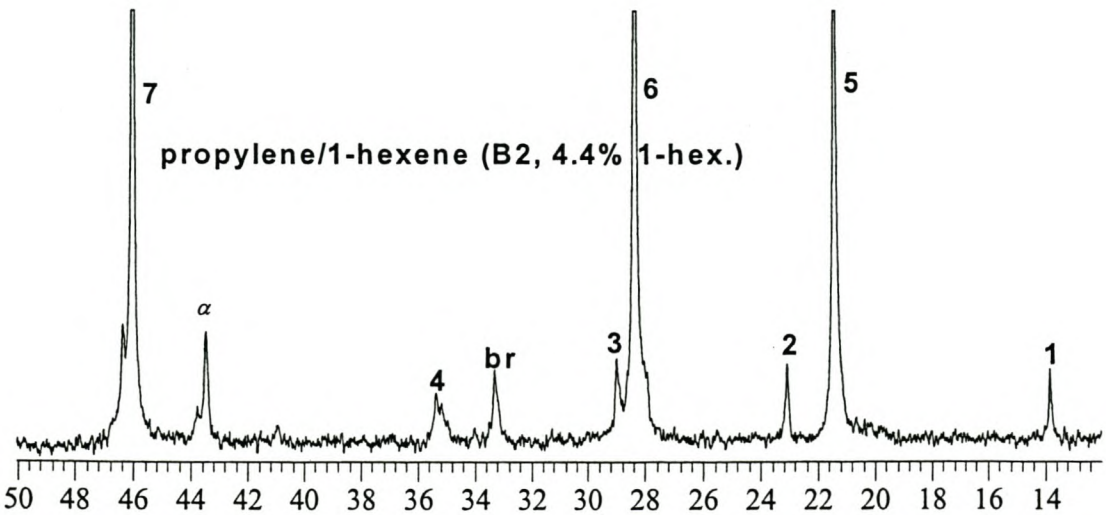

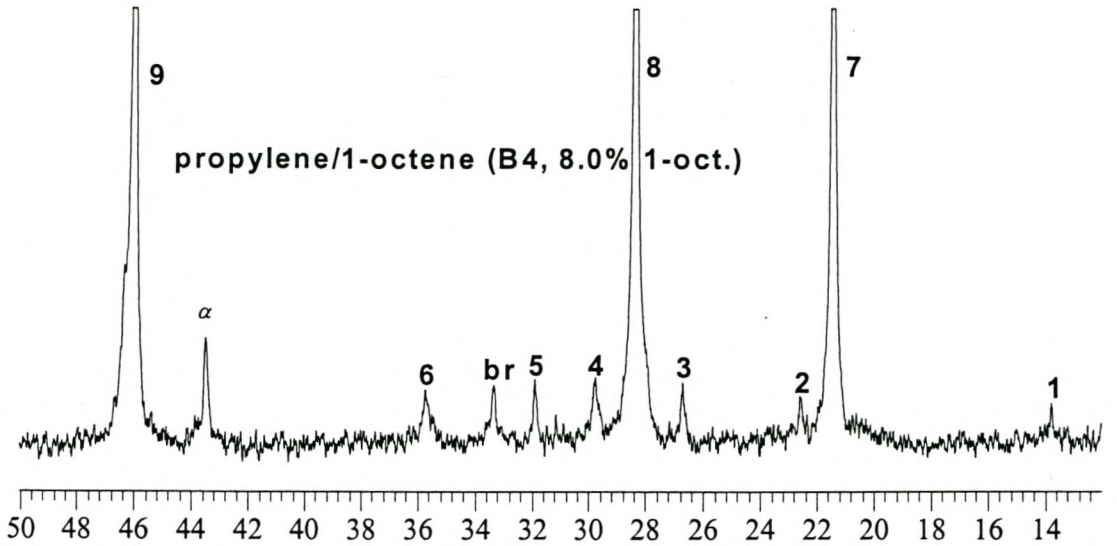

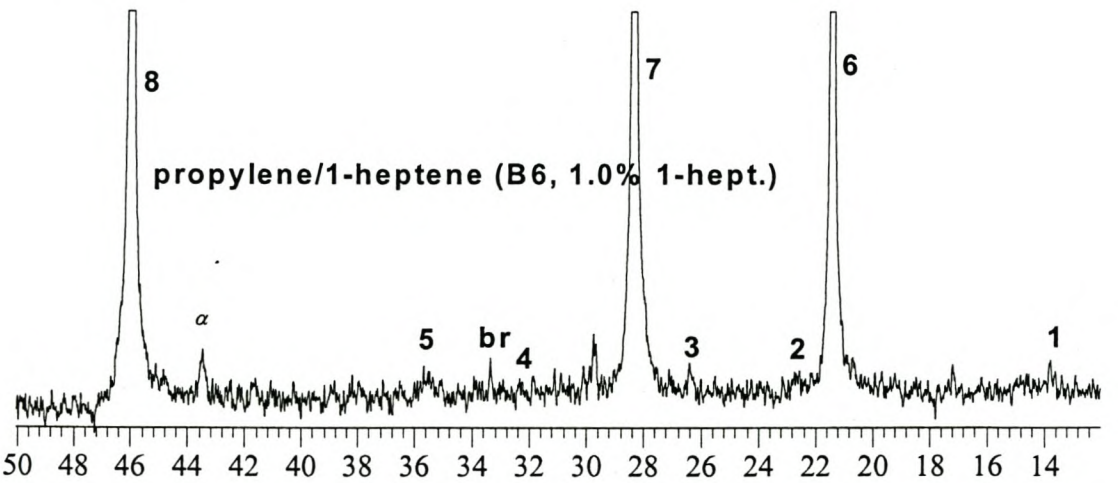

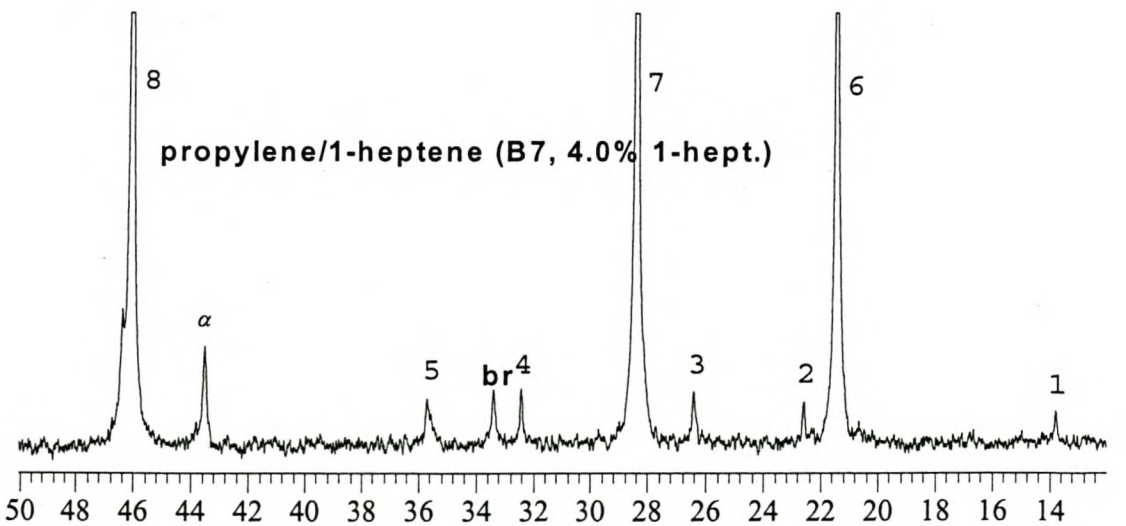

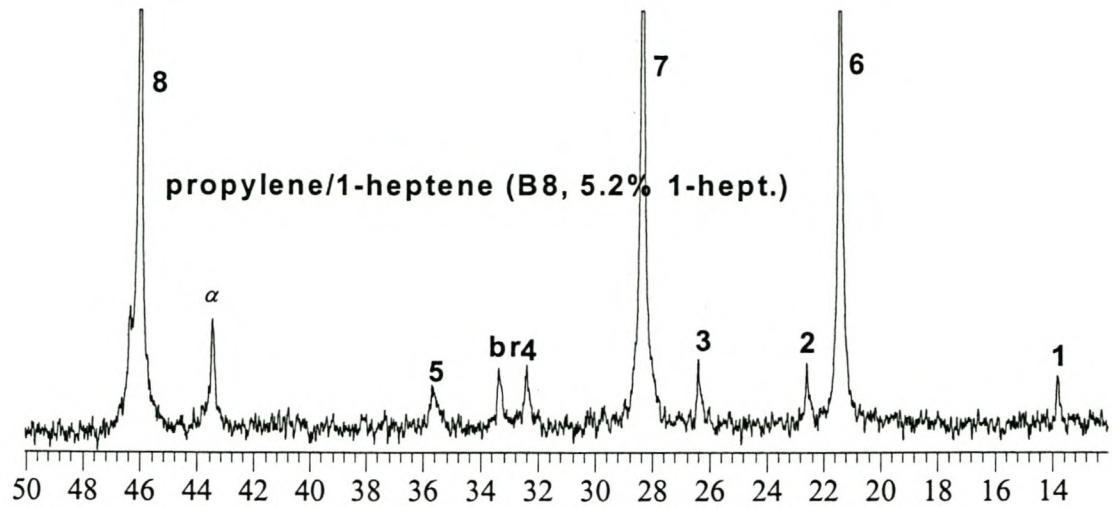

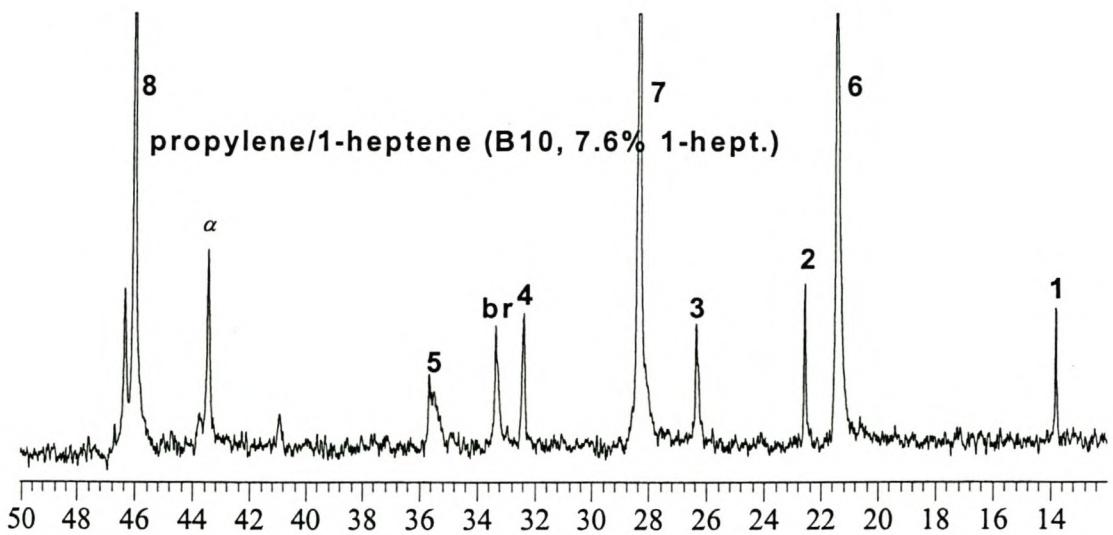

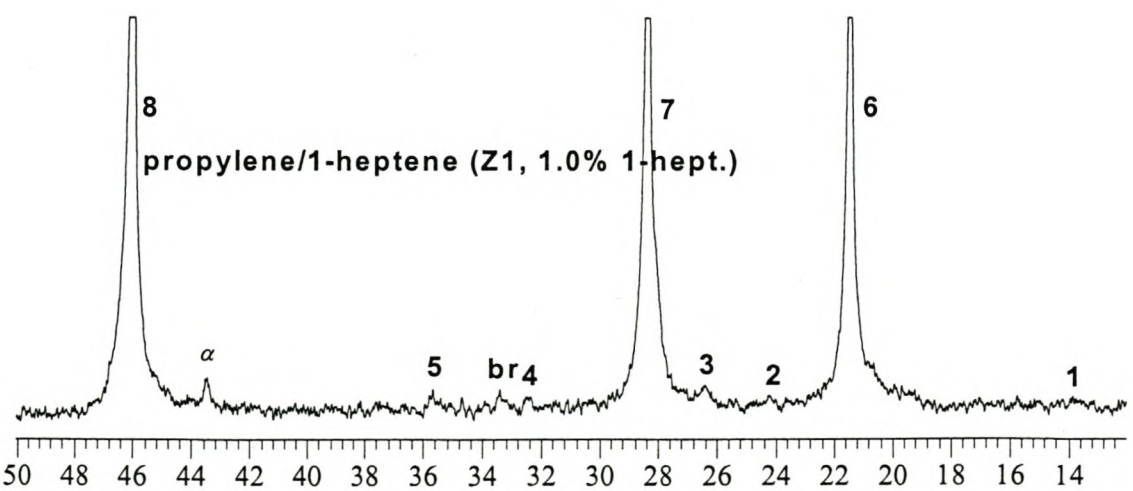

APPENDIX B
(GPC Spectra)

Propylene homopolymer (A1)

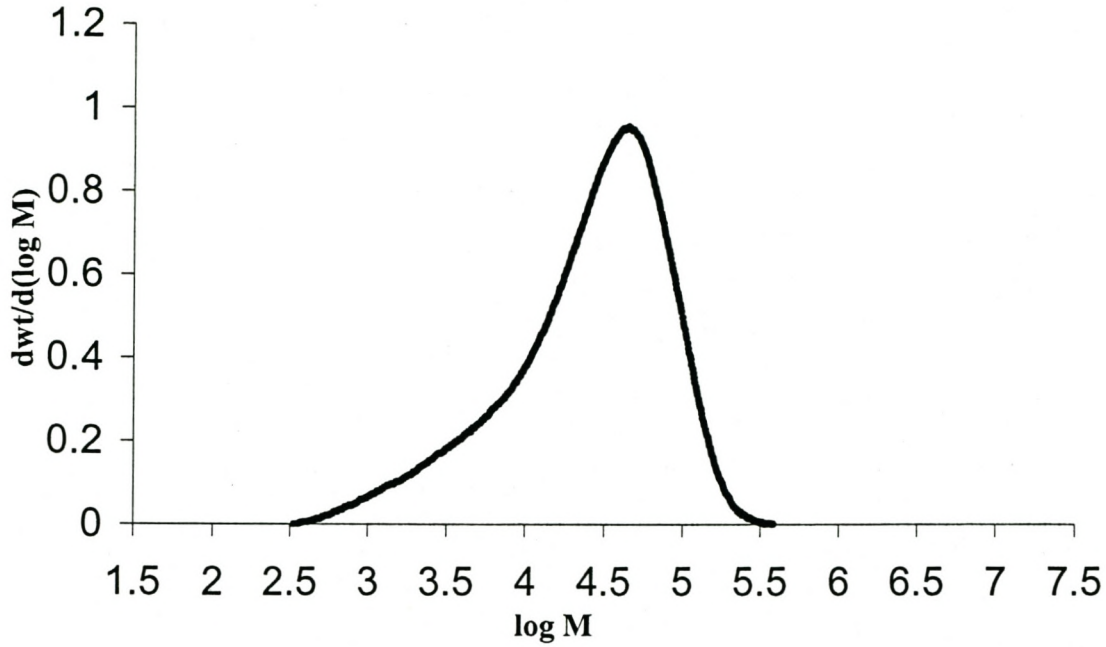

Propylene/1-hexene copolymer (A2, 1.20% 1-hex.)

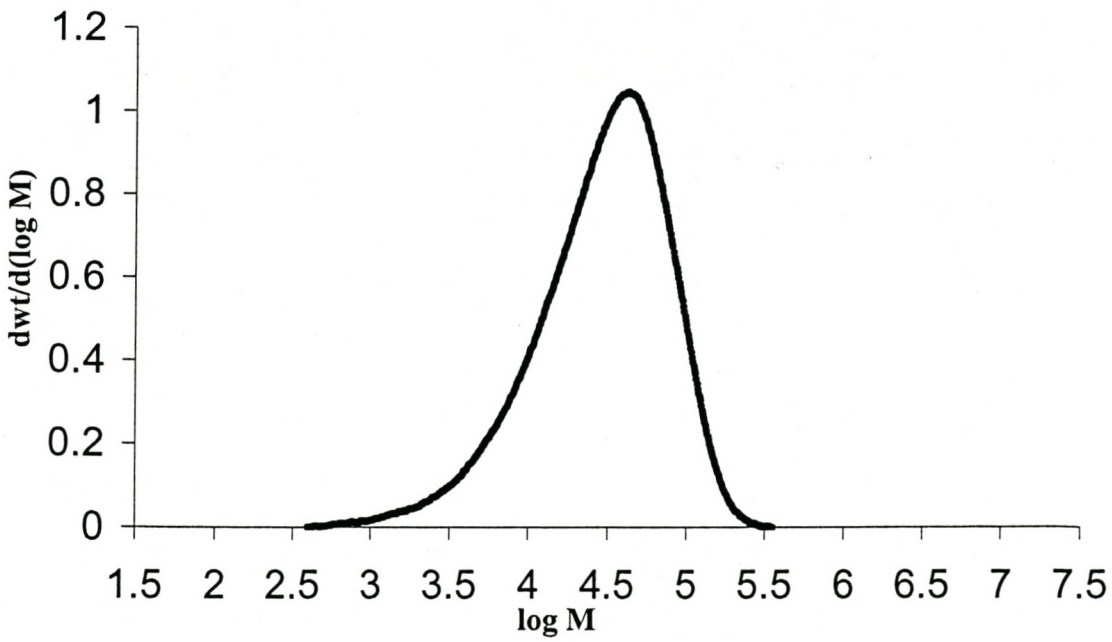

Propylene/1-hexene copolymer (A3, 2.51% 1-hex.)

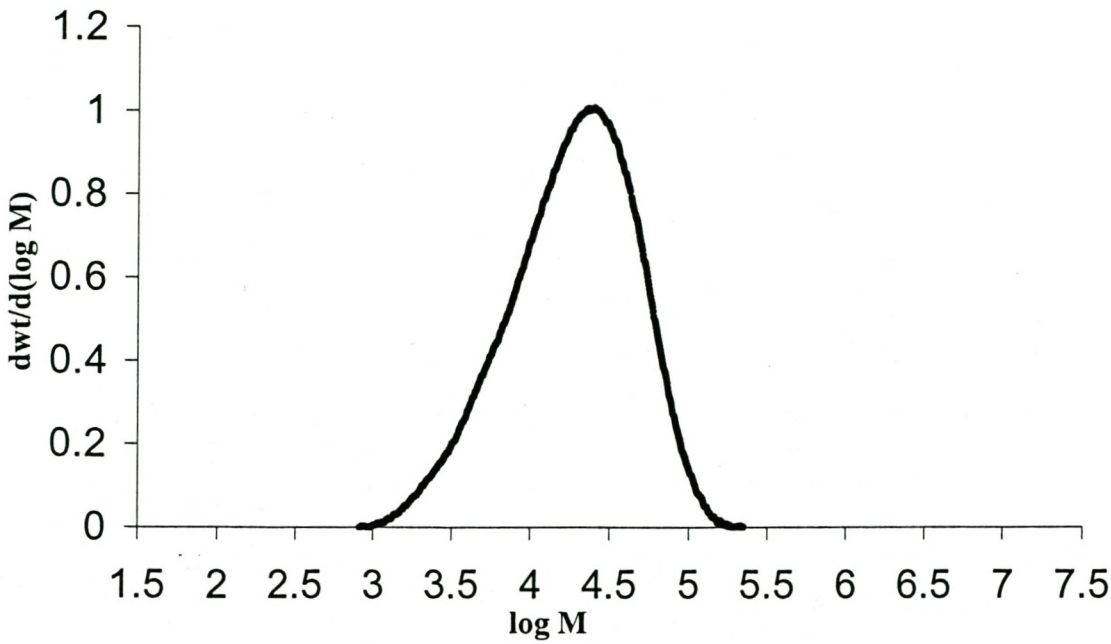

Propylene/1-hexene copolymer (A5, 4.10% 1-hex.)

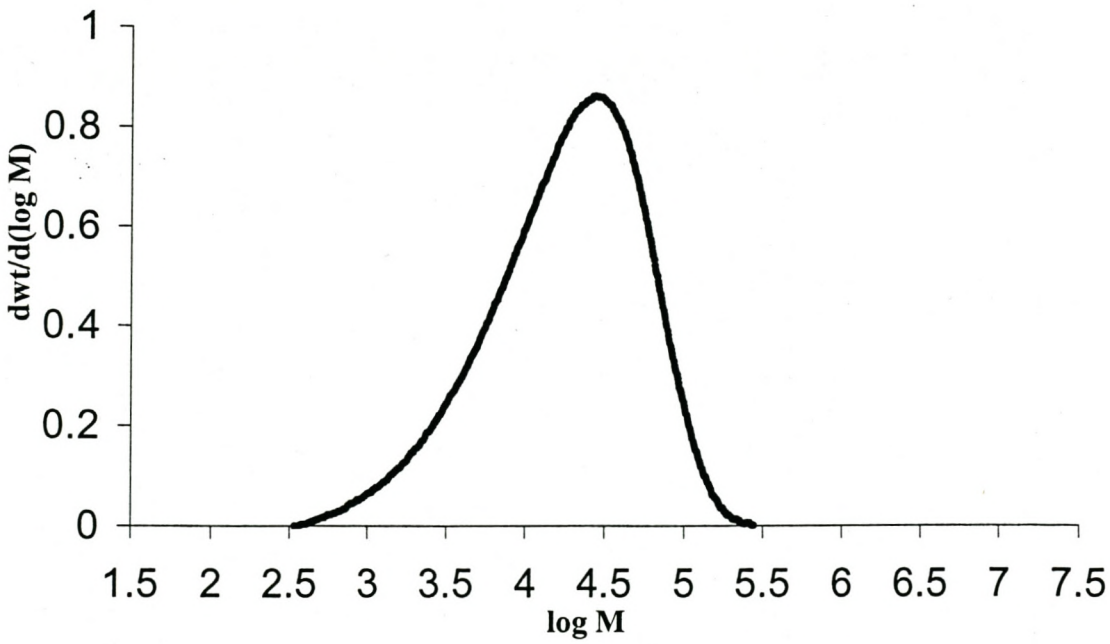

Propylene/1-hexene copolymer (A6, 6.36% 1-hex.)

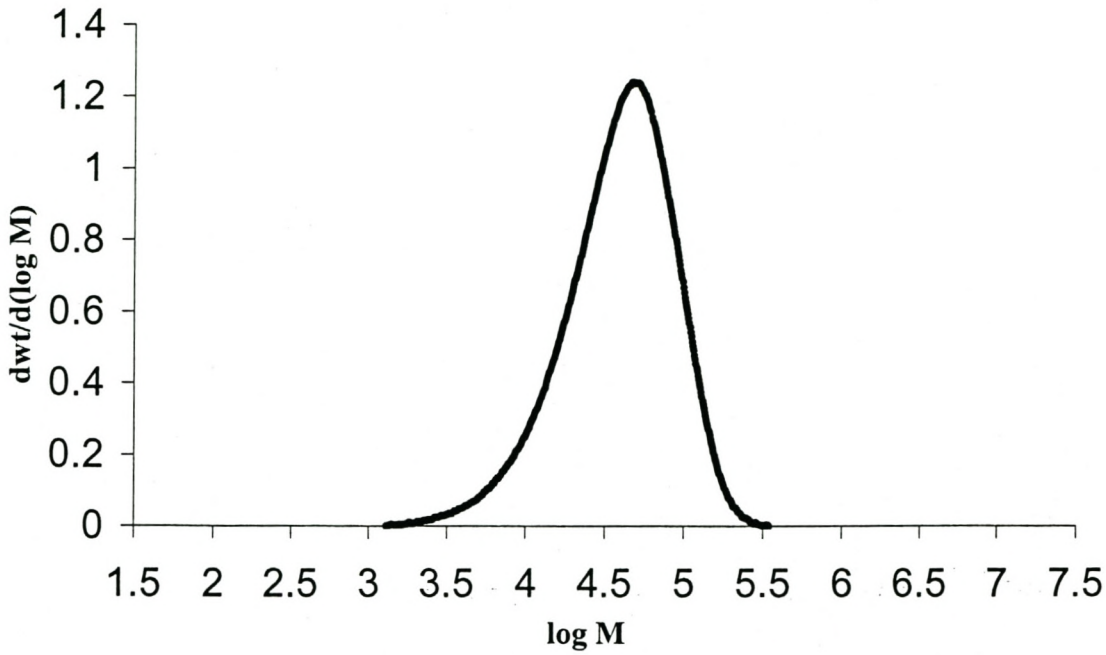

Propylene/1-octene copolymer (A7, 2.16% 1-oct.)

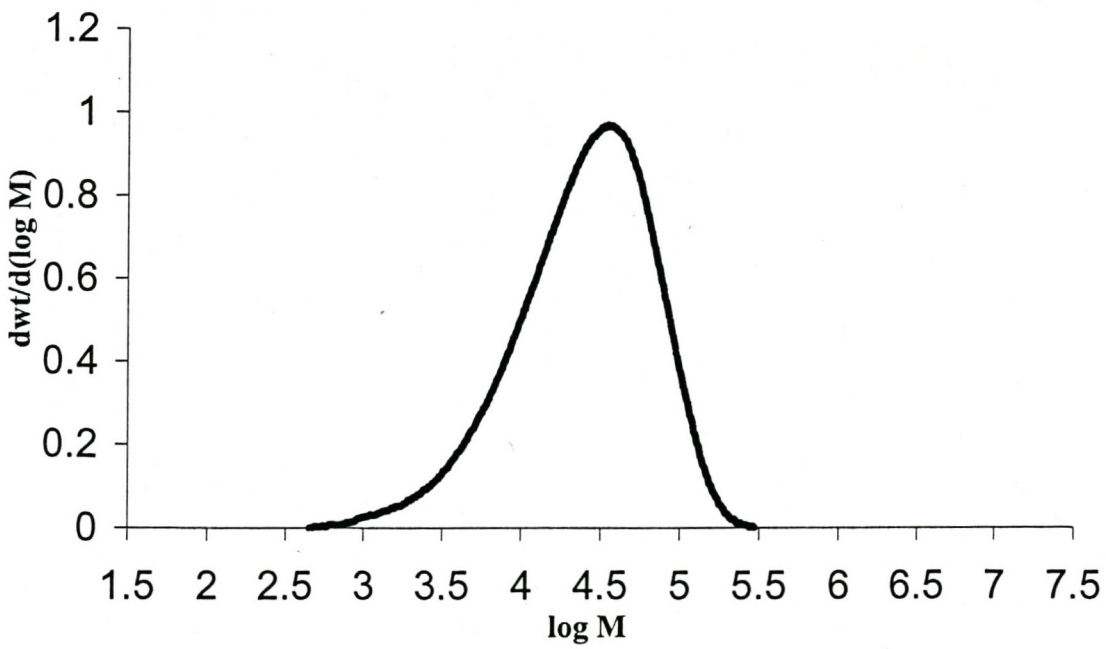

Propylene/1-octene copolymer (A8, 3.89% 1-oct.)

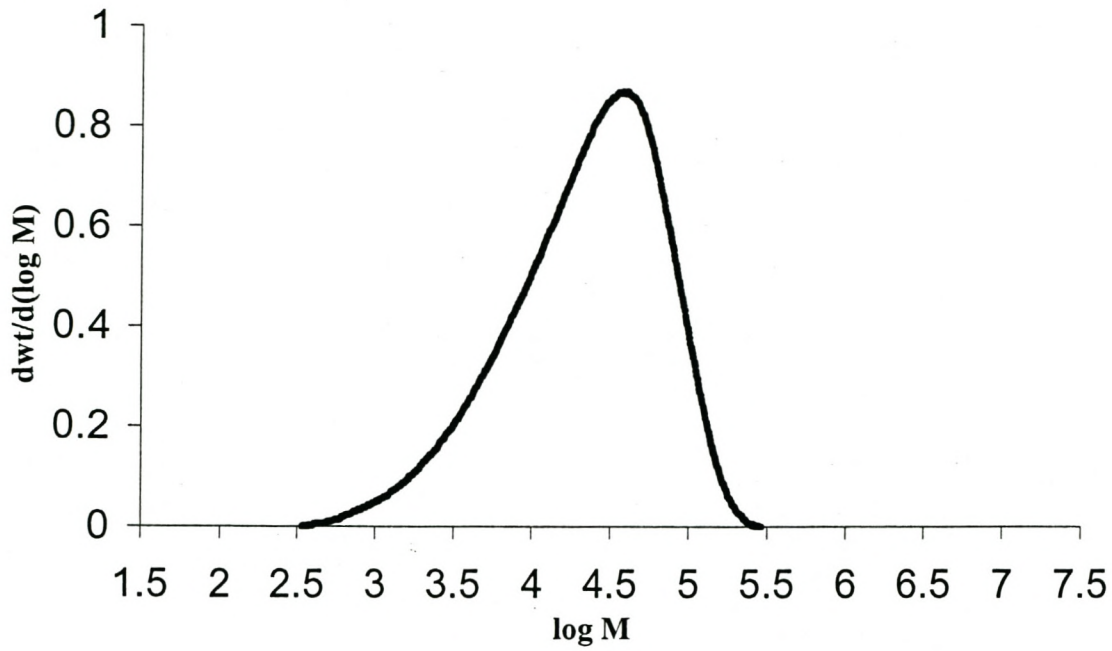

Propylene/1-octene copolymer (A9, 5.40% 1-oct.)

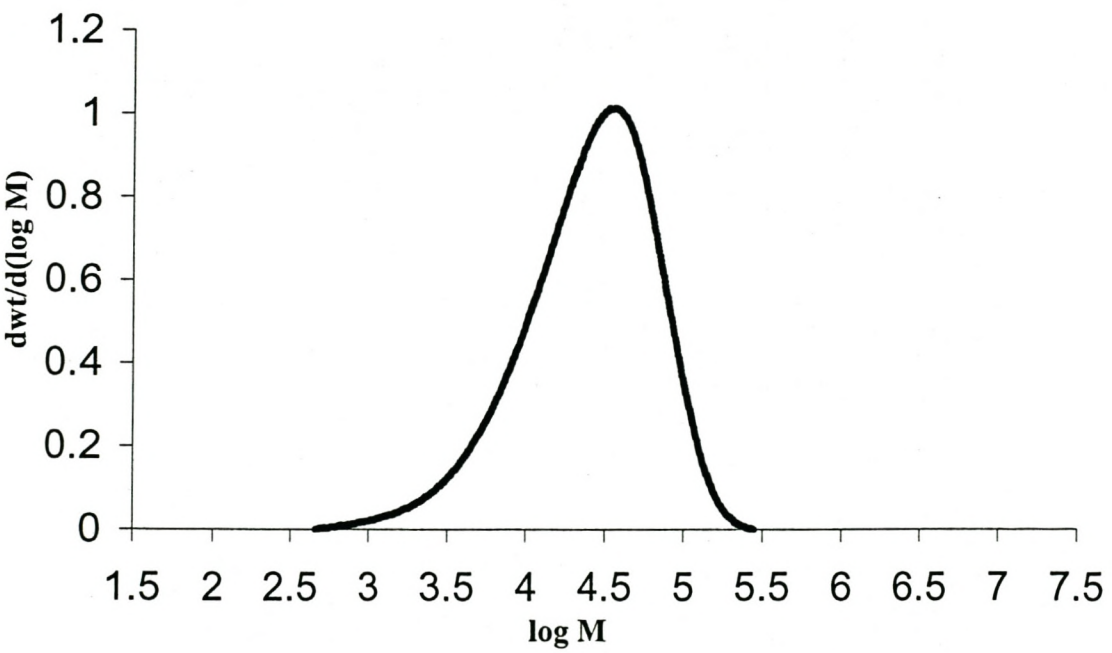

Propylene/1-octene copolymer (A10, 6.32% 1-oct.)

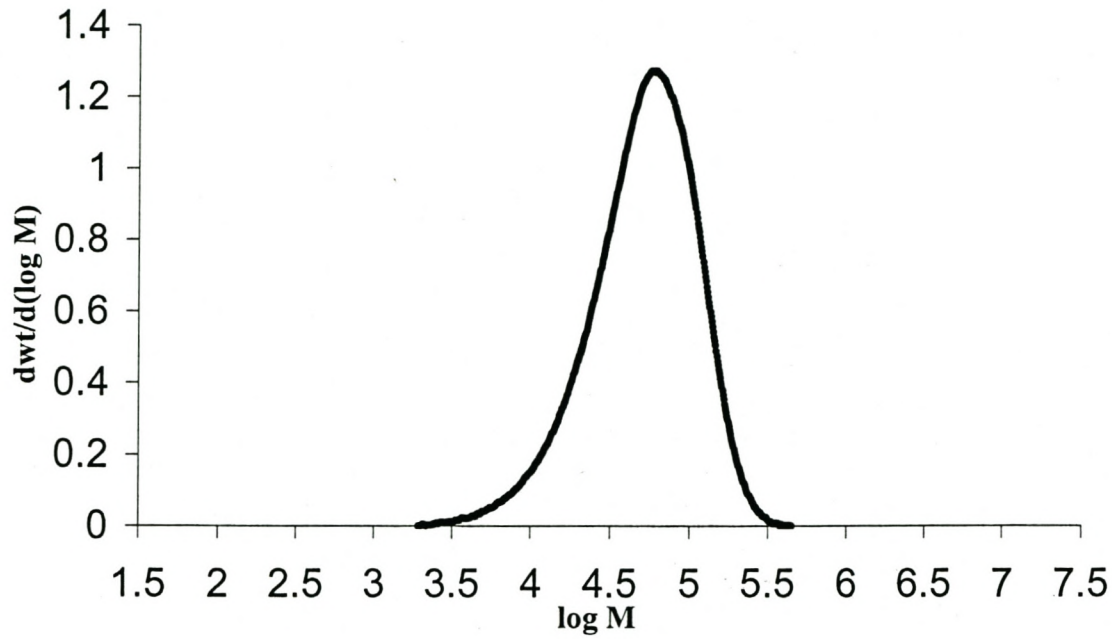

Propylene/1-octene copolymer (A11, 7.08% 1-oct.)

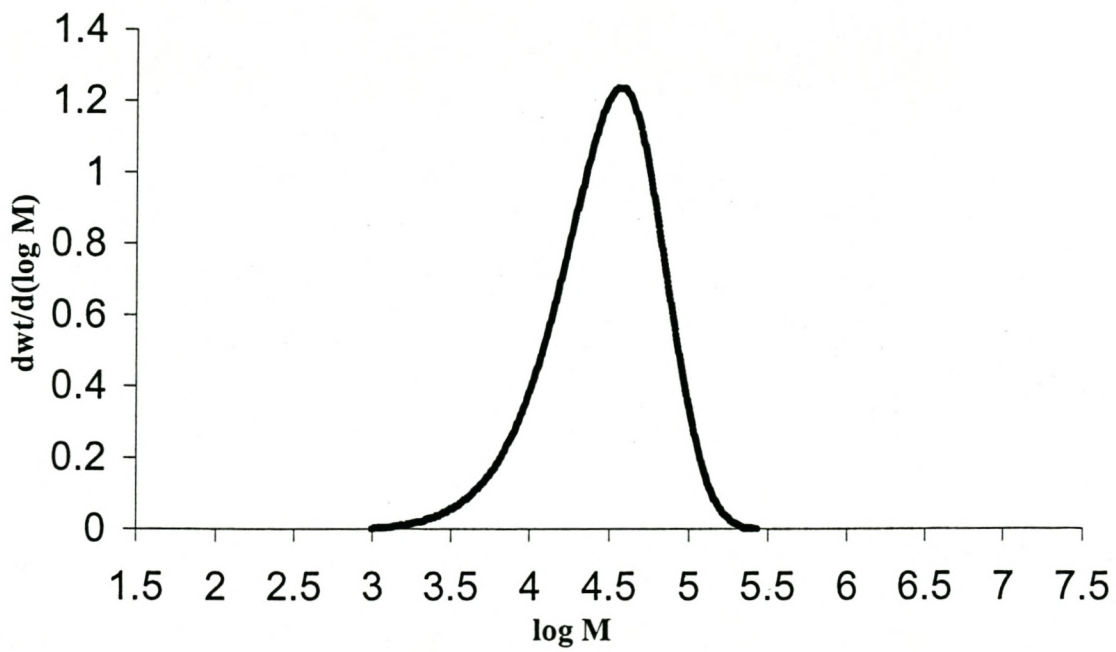

Propylene homopolymer (B1)

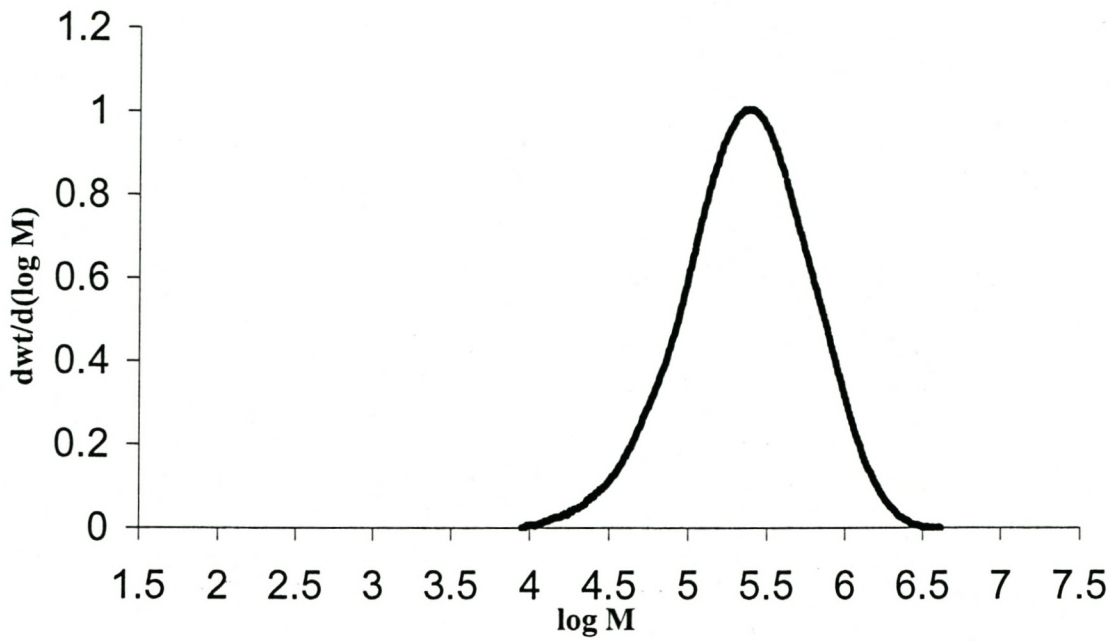

Propylene/1-hexene copolymer (B2, 4.42% 1-hex.)

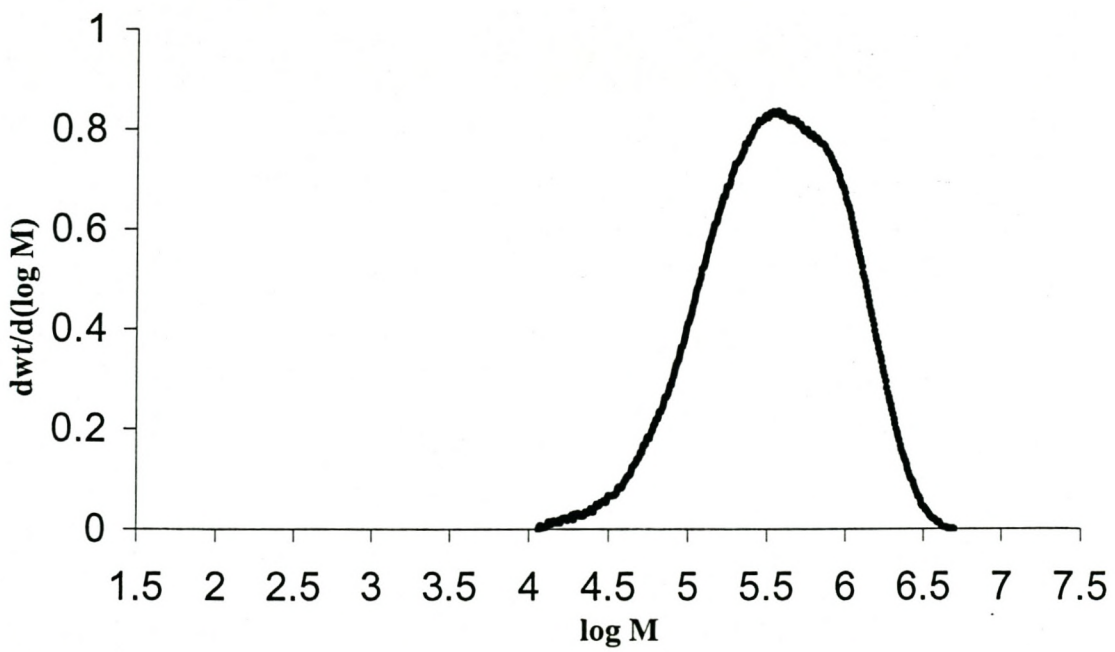

Propylene/1-hexene copolymer (B3, 5.73% 1-hex.)

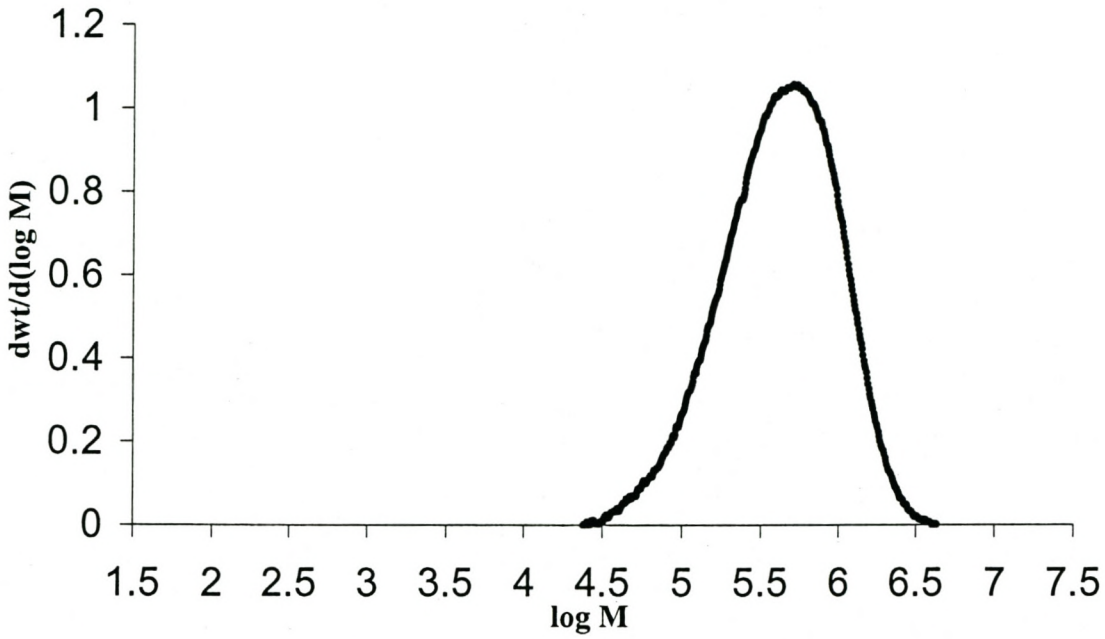

Propylene/1-octene copolymer (B4, 4.07% 1-oct.)

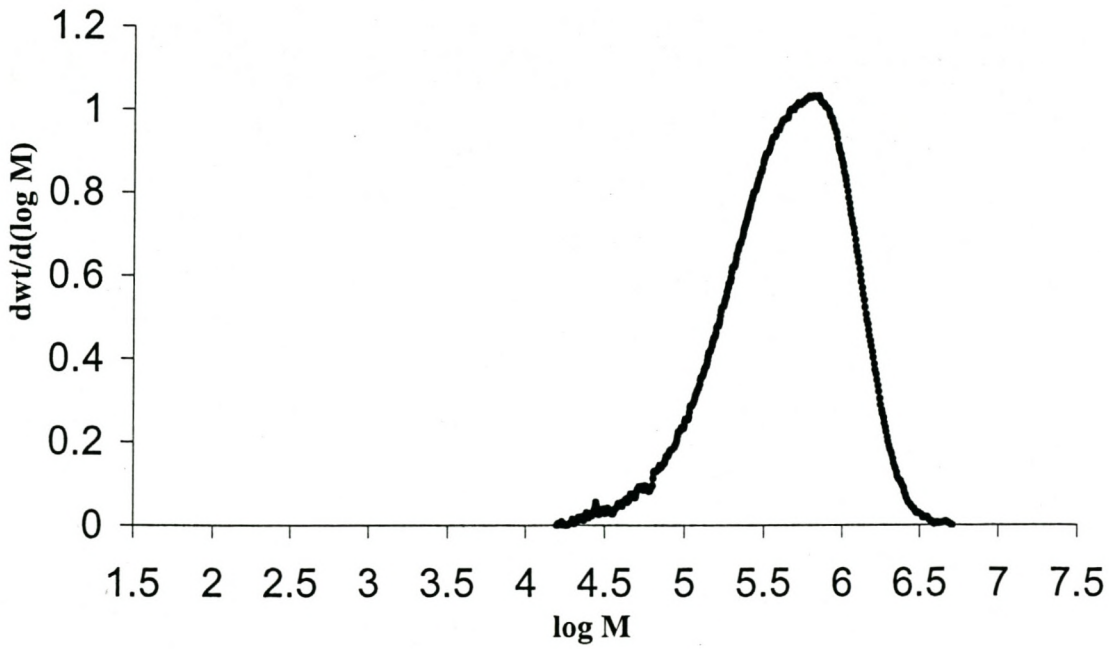

Propylene/1-octene copolymer (B5, 4.70% 1-oct.)

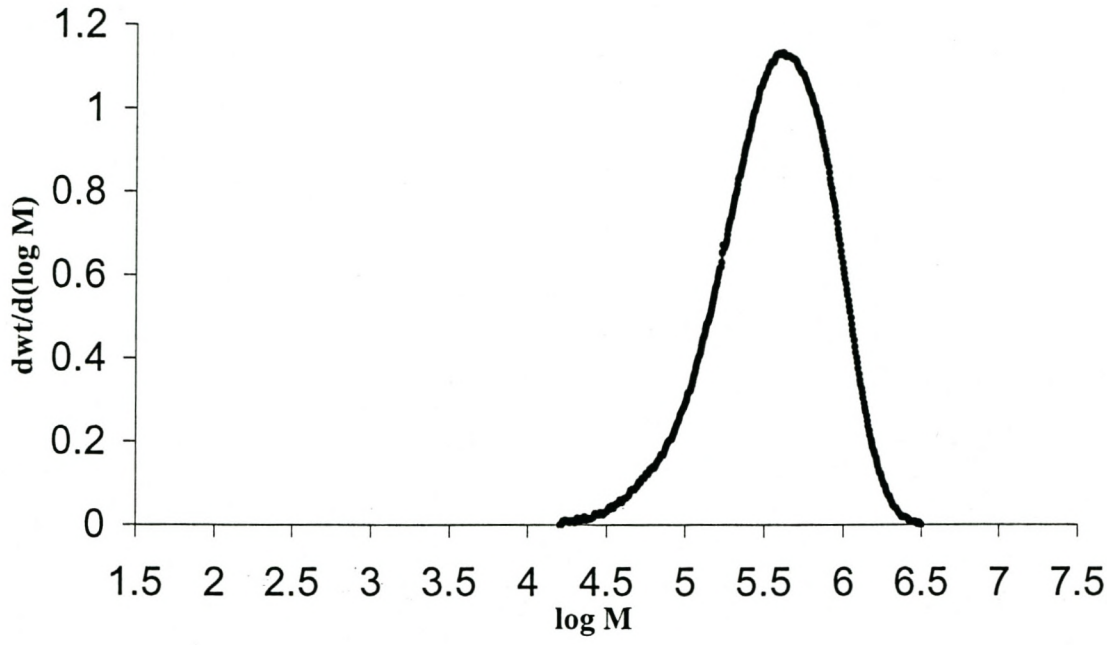

Propylene/1-heptene copolymer (B6, 1.03% 1-hept.)

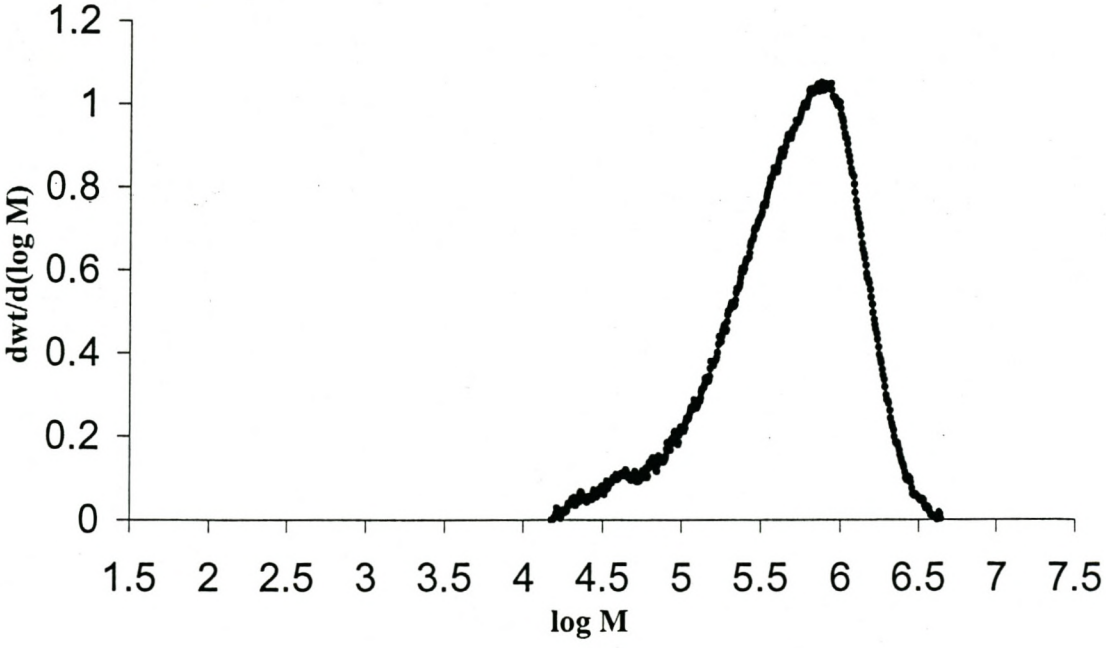

Propylene/1-heptene copolymer (B8, 5.19% 1-hept.)

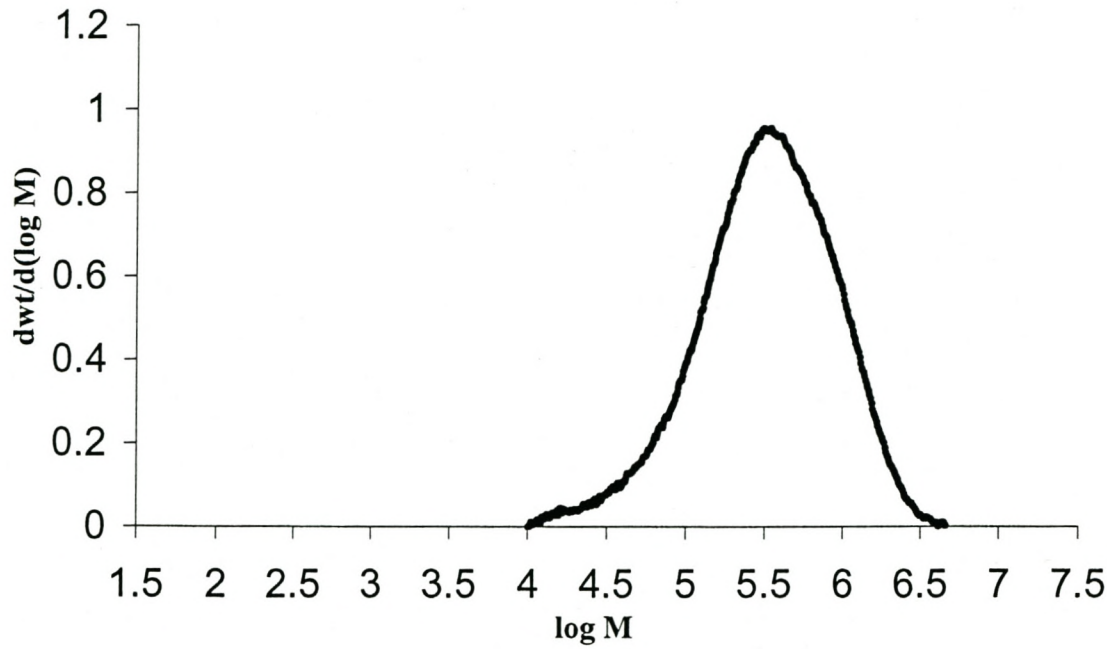

Propylene/1-heptene copolymer (B9, 5.79% 1-hept.)

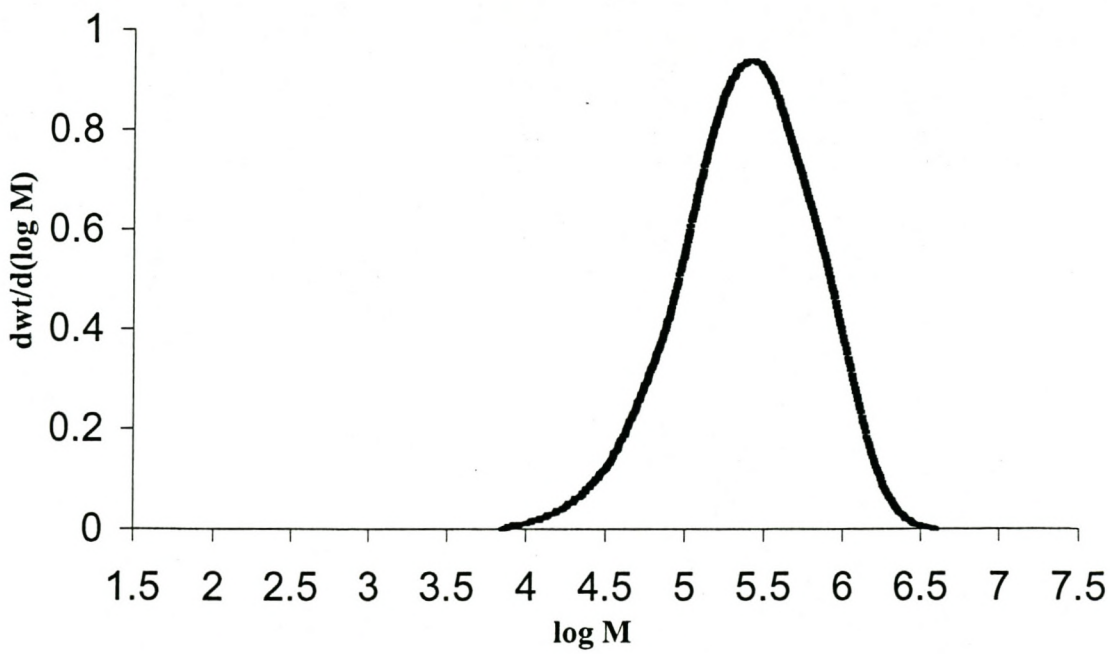

Propylene/1-heptene copolymer (B10, 7.58% 1-hept.)

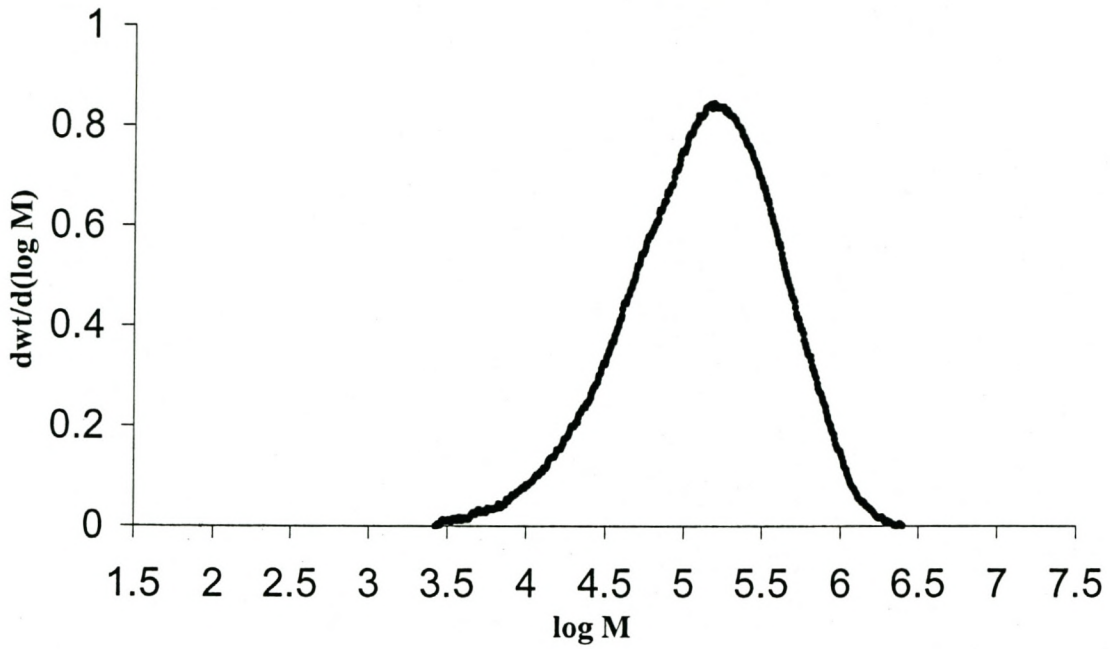

Propylene/1-heptene copolymer (Z1, ≈1.00% 1-hept.)

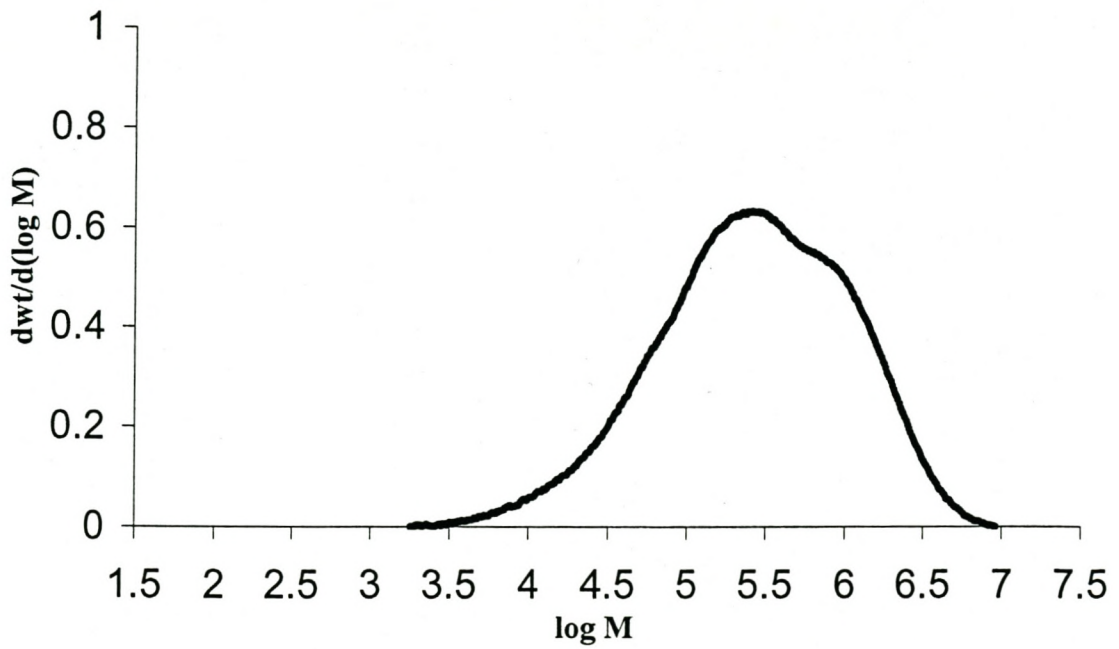

APPENDIX C
(DSC Spectra)

Propylene homopolymer (A1)

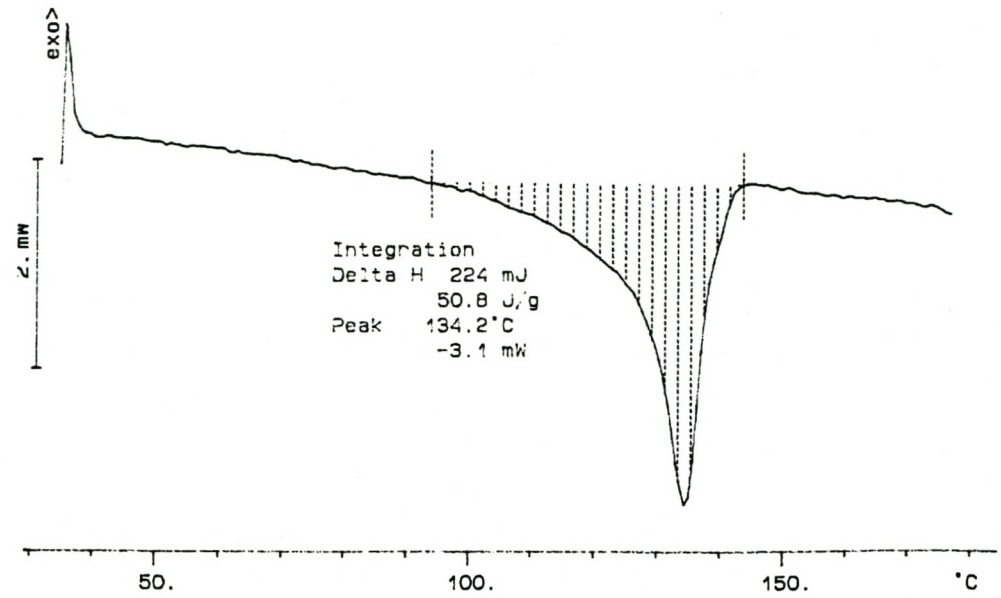

Propylene/1-hexene copolymer (A3, 2.51% 1-hex.)

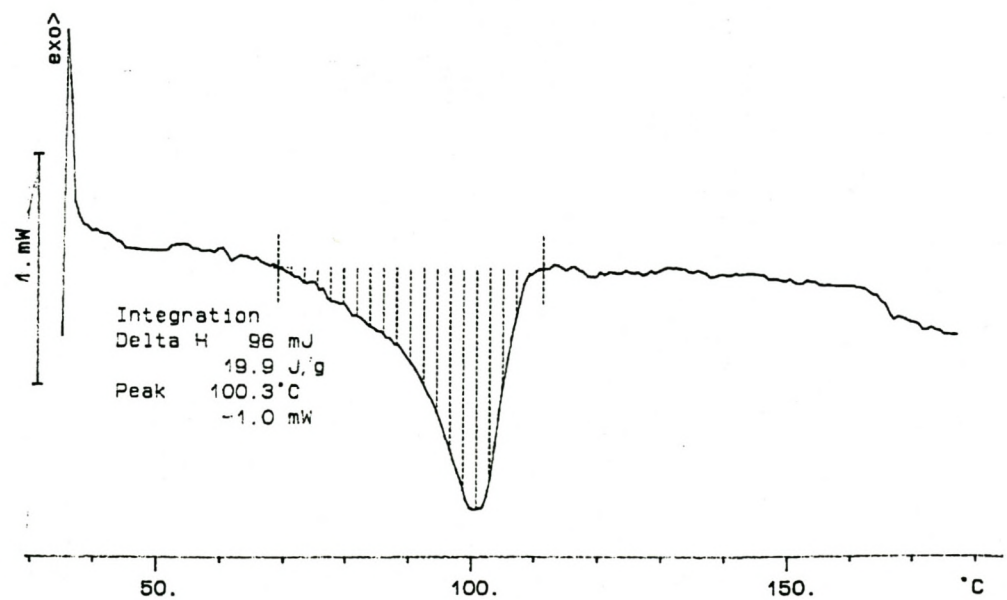

Propylene/1-hexene copolymer (A4, 3.53% 1-hex.)

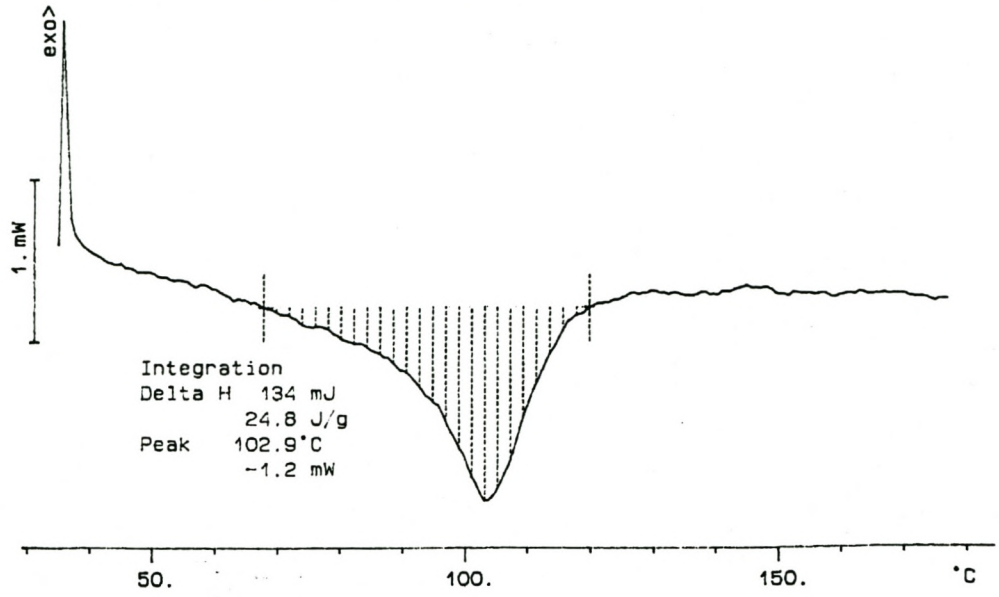

Propylene/1-hexene copolymer (A5, 4.10% 1-hex.)

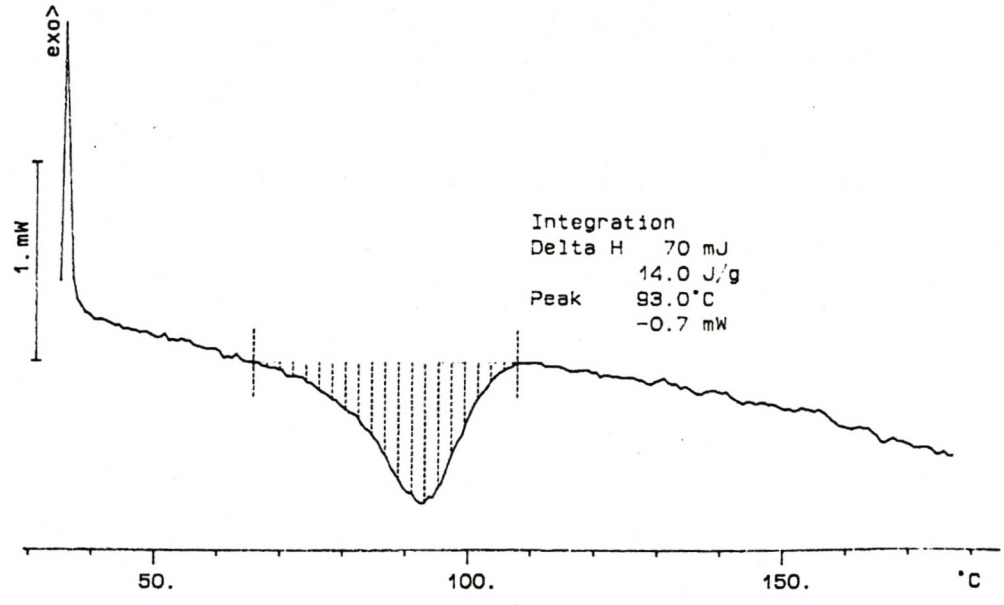

Propylene/1-octene copolymer (A7, 2.16% 1-oct.)

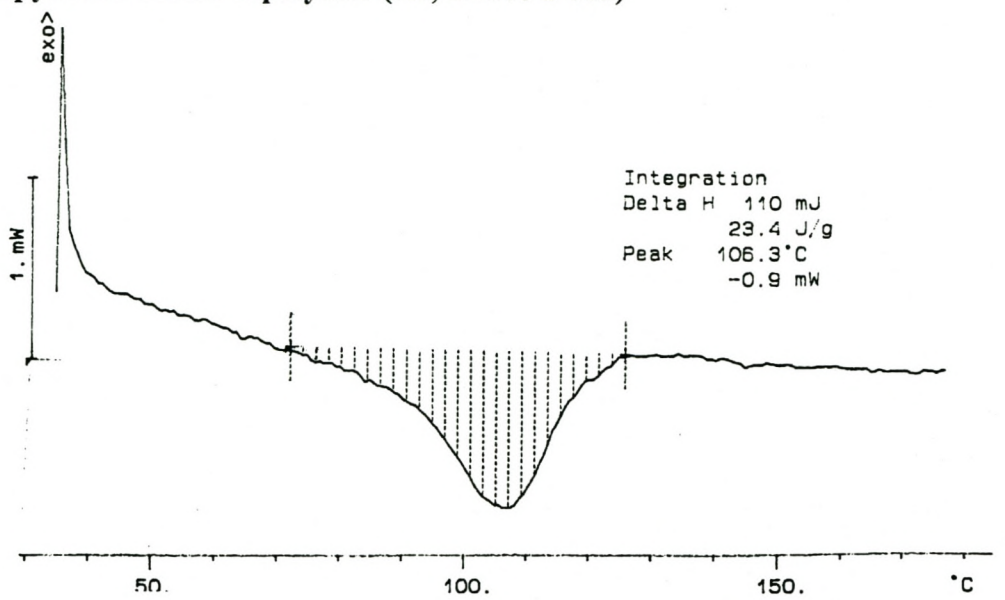

Propylene/1-octene copolymer (A8, 3.89% 1-oct.)

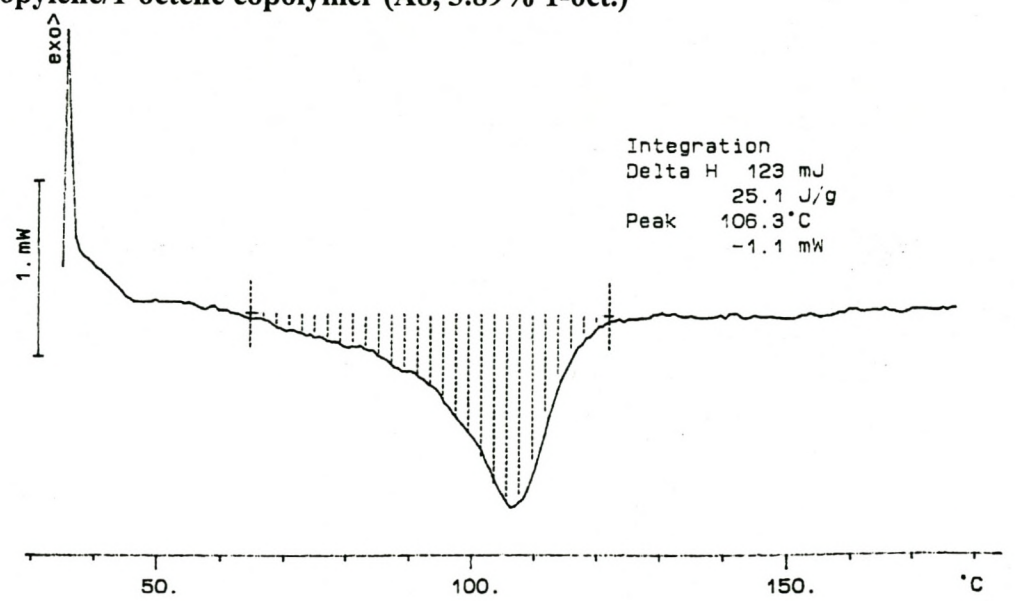

Propylene/1-octene copolymer (A9, 5.40% 1-oct.)

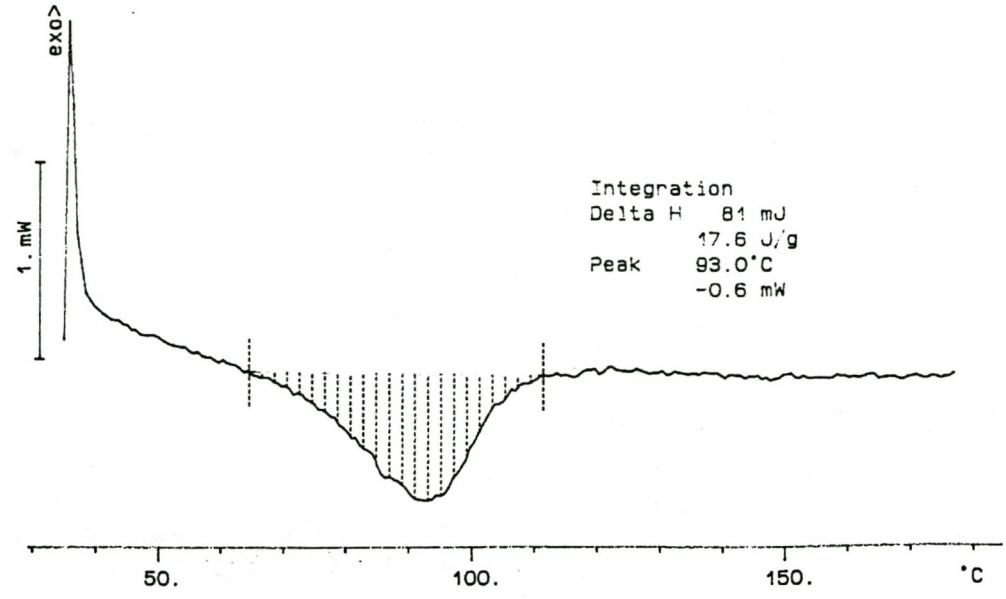

Propylene/1-octene copolymer (A10, 6.32% 1-oct.)

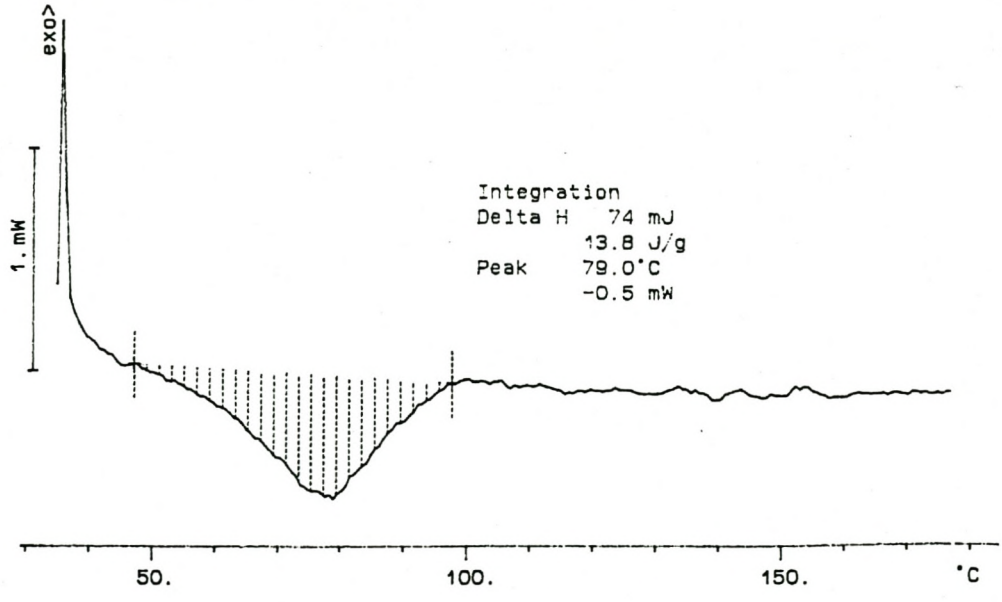

Propylene/1-octene copolymer (A11, 7.08% 1-oct.)

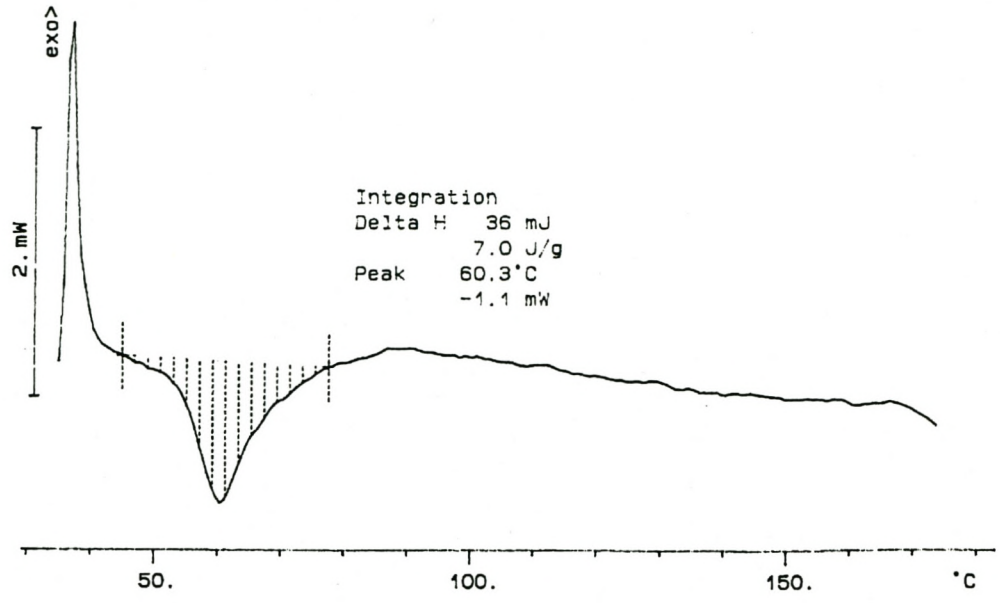

Propylene homopolymer (B1)

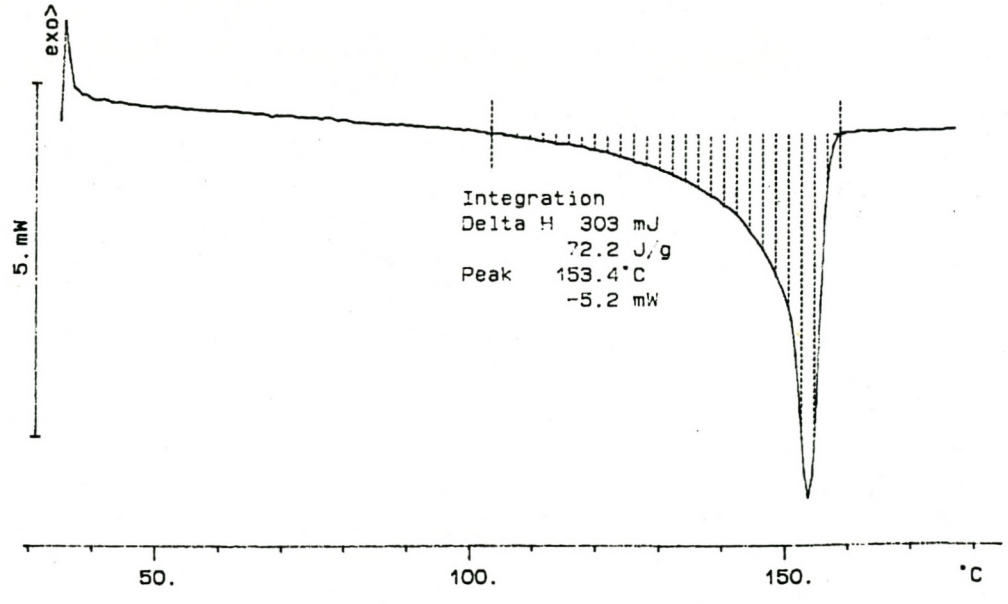

Propylene/1-hexene copolymer (B2, 4.42% 1-hex.)

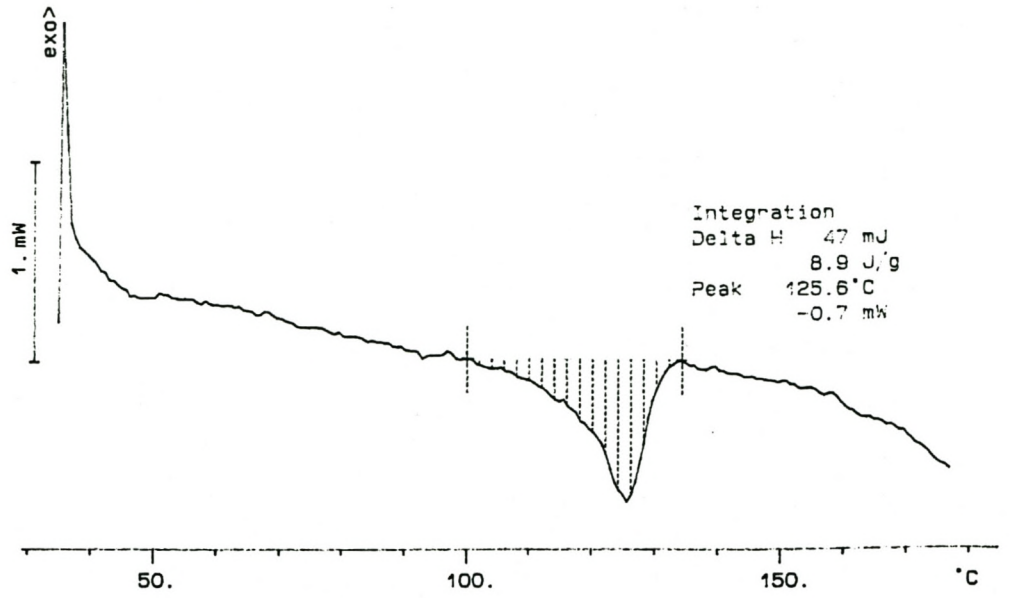

Propylene/1-hexene copolymer (B3, 5.73% 1-hex.)

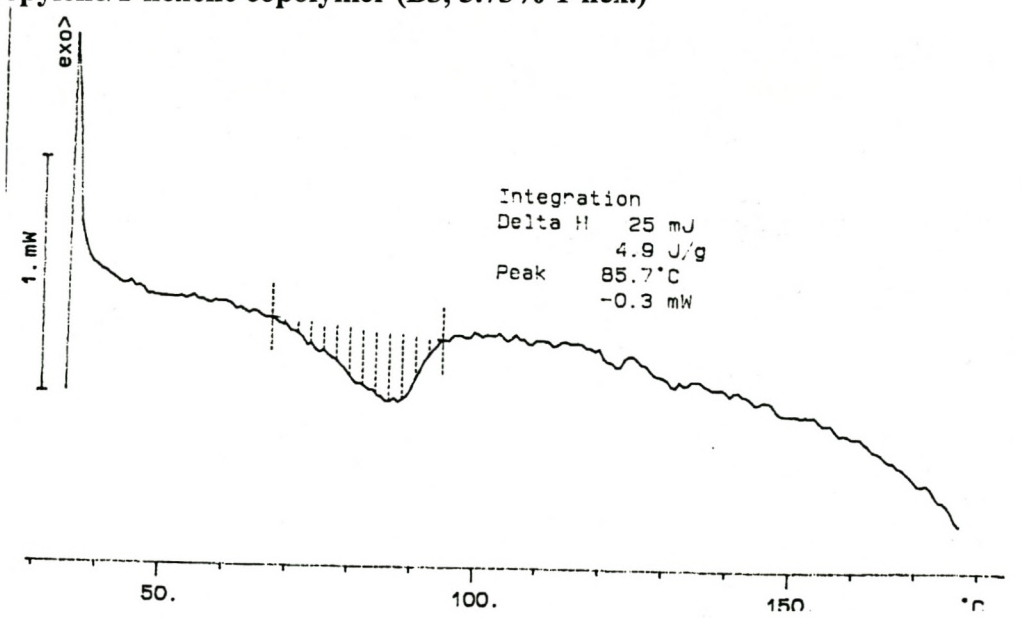

Propylene/1-octene copolymer (B4, 4.07% 1-oct.)

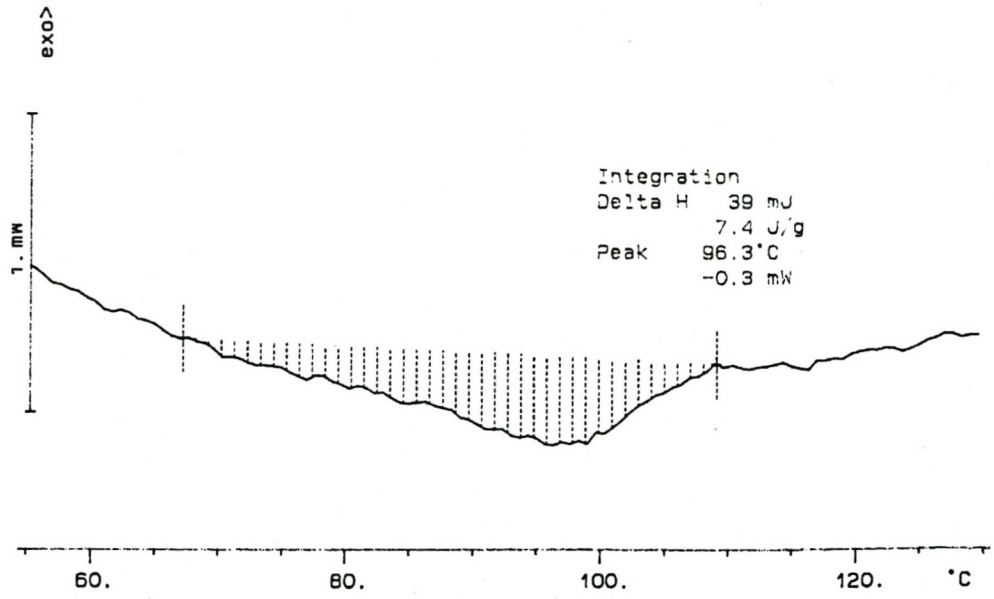

Propylene/1-octene copolymer (B5, 4.70% 1-oct.)

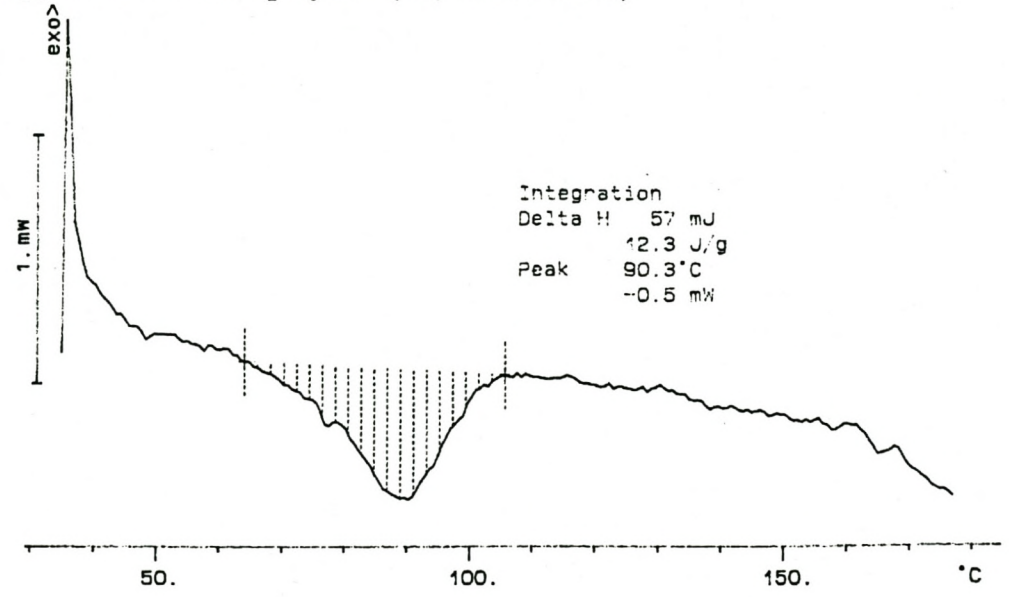

Propylene/1-heptene copolymer (B6, 1.03% 1-hept.)

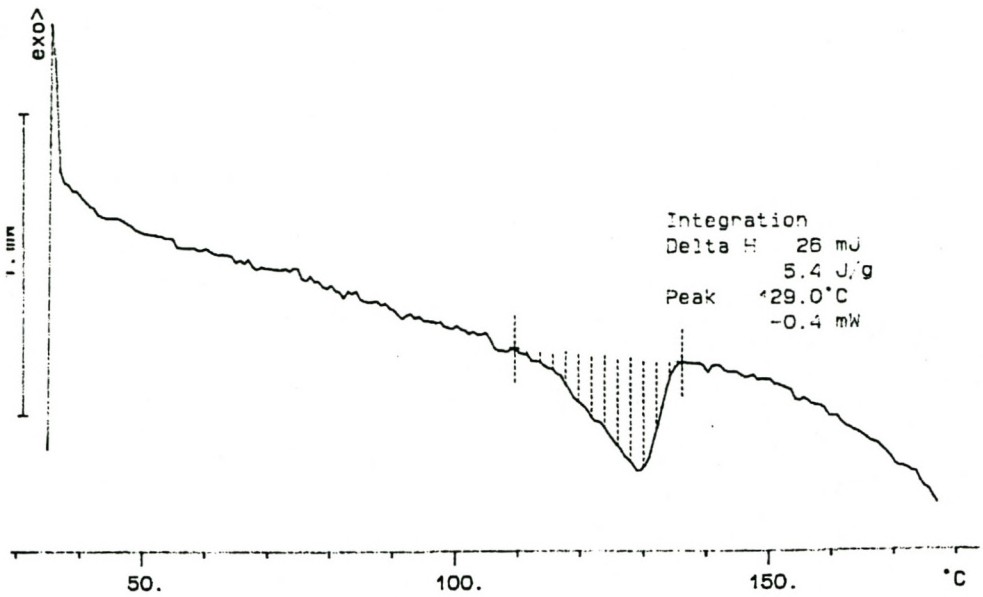

Propylene/1-heptene copolymer (B7, 3.98% 1-hept.)

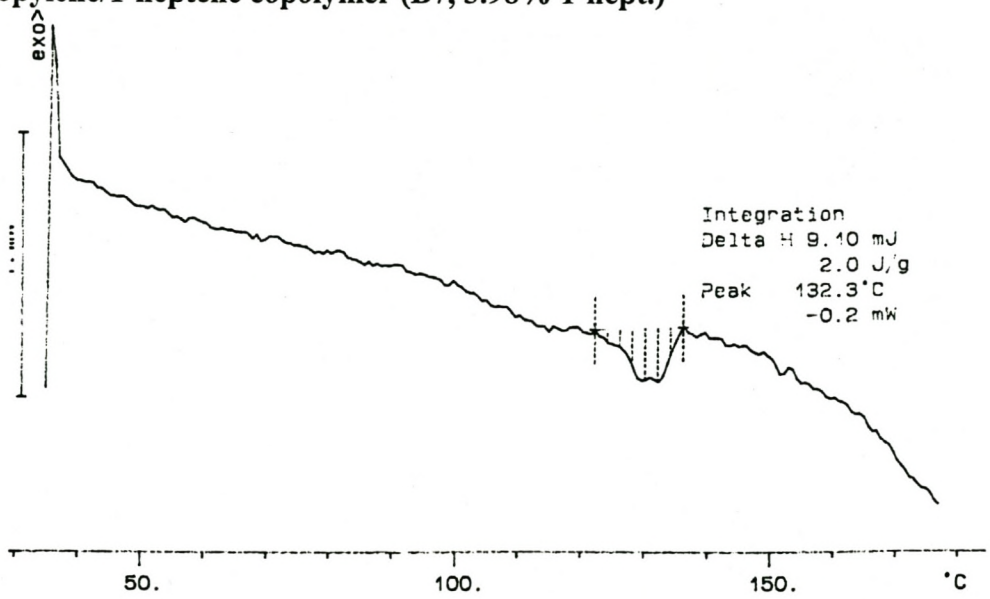

Propylene/1-heptene copolymer (B8, 5.19% 1-hept.)

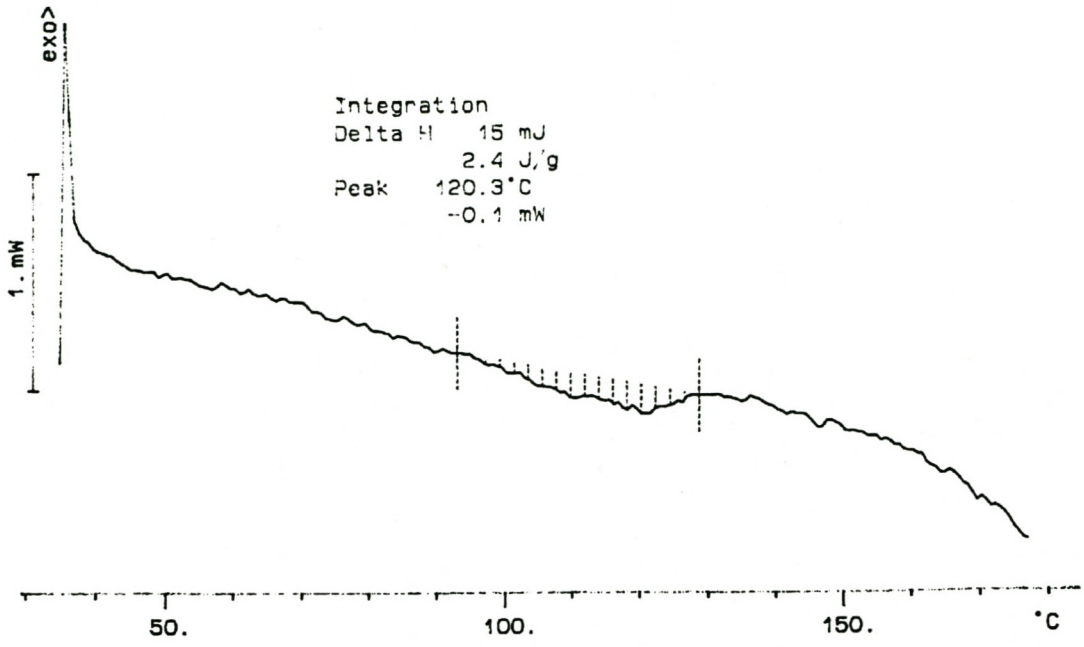

Propylene/1-heptene copolymer (B9, 5.79% 1-hept.)

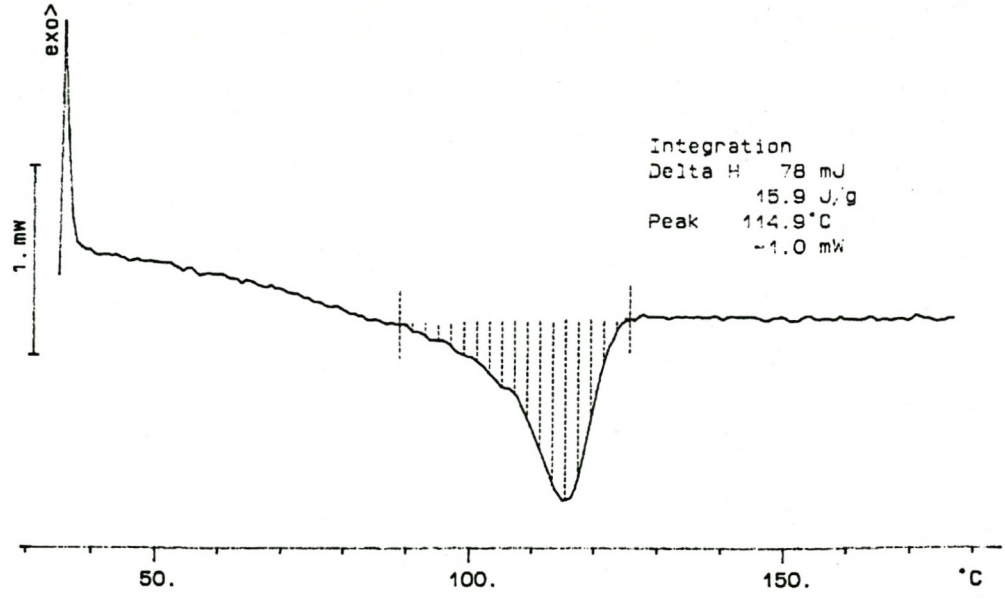

Propylene/1-heptene copolymer (B10, 7.58% 1-hept.)

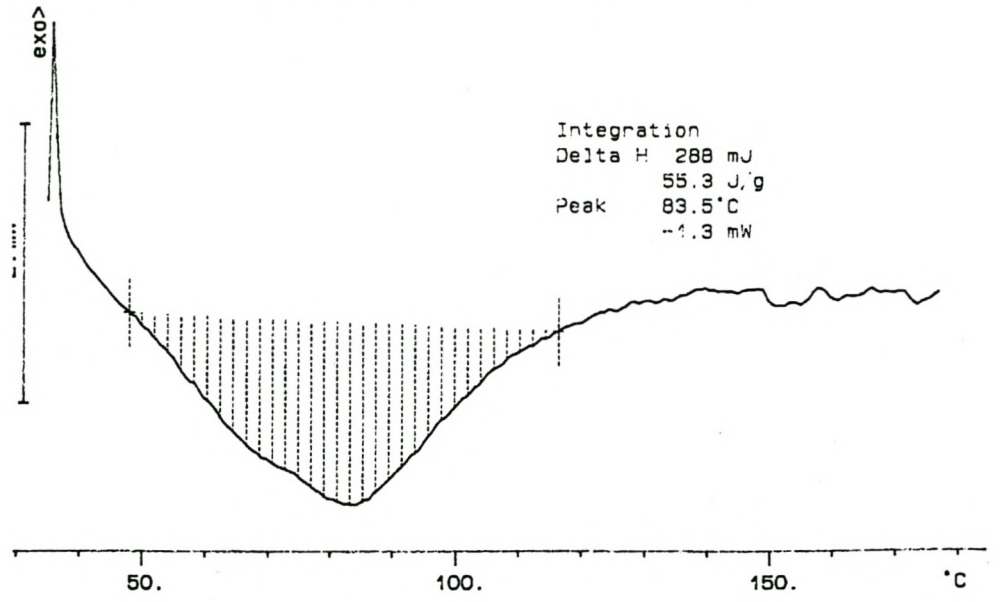

Propylene/1-heptene copolymer (Z1, ≈1.00% 1-hept.)

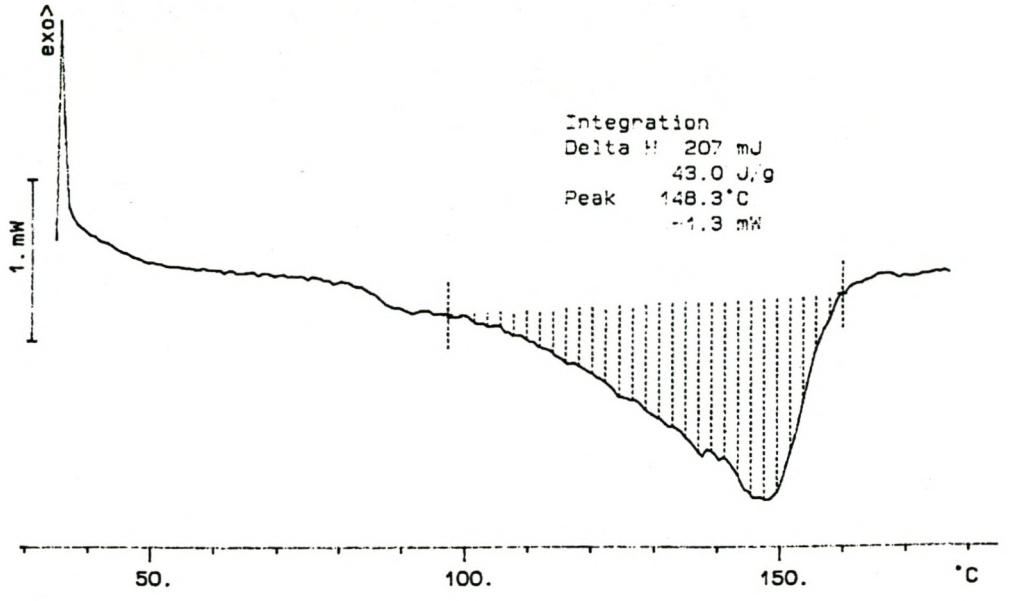

APPENDIX D
(DMA Spectra)

Propylene/1-hexene copolymer (A6, 6.36% hex)

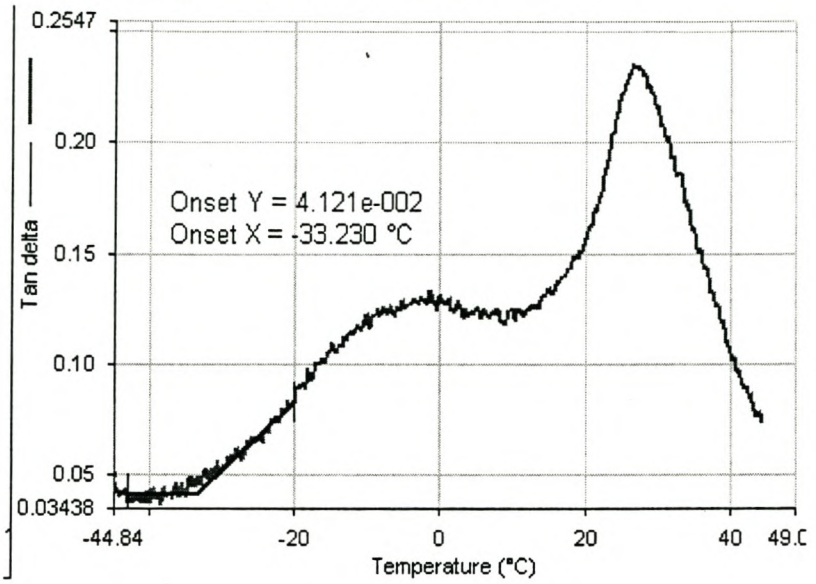

Propylene/1-octene copolymer (A10, 6.32% 1-oct.)

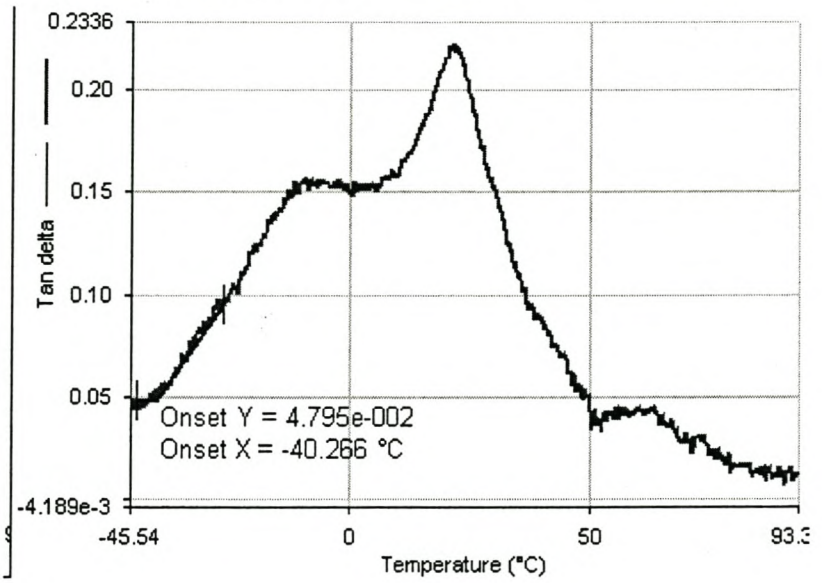

Propylene/1-hexene copolymer (B2, 4.42% 1-hex.)

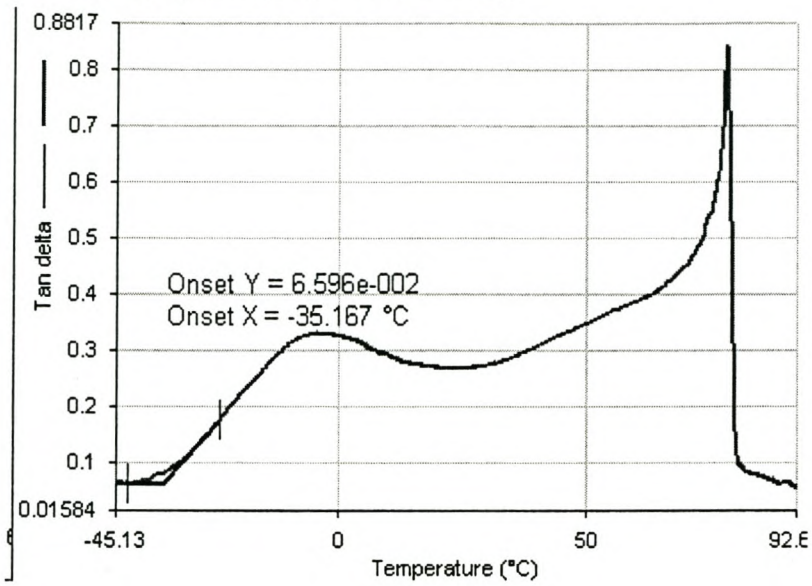

Propylene/1-octene copolymer (B4, 4.07% 1-oct.)

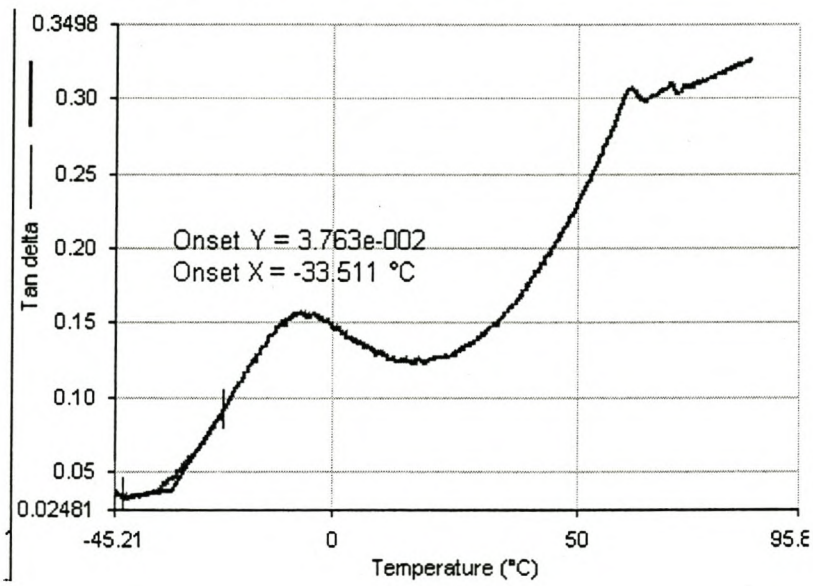

Propylene/1-heptene copolymer (B7, 3.98% 1-hept.)

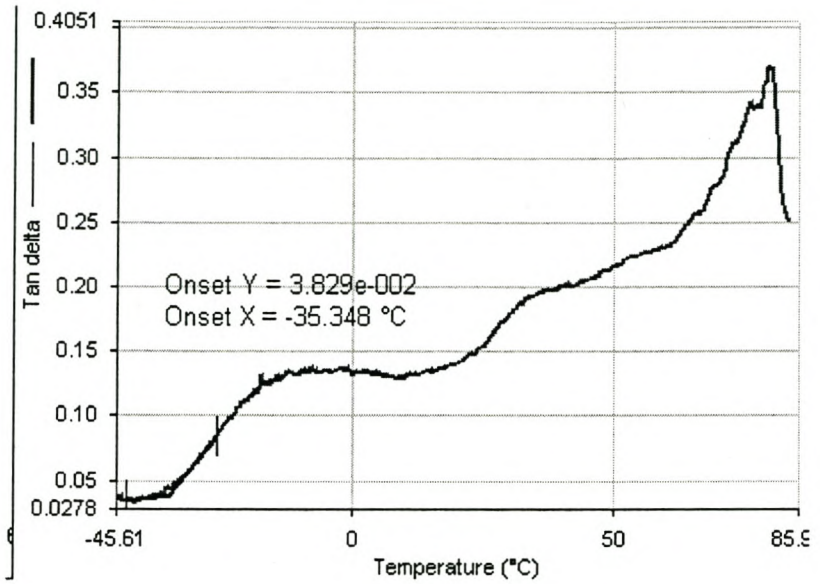

Propylene/1-heptene copolymer (B8, 5.19% 1-hept.)

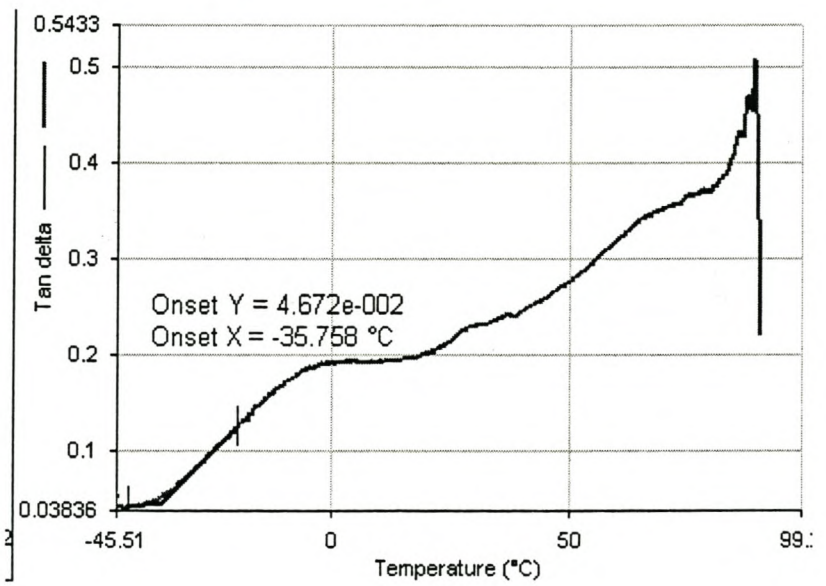

Propylene/1-heptene copolymer (B9, 5.79% 1-hept.)

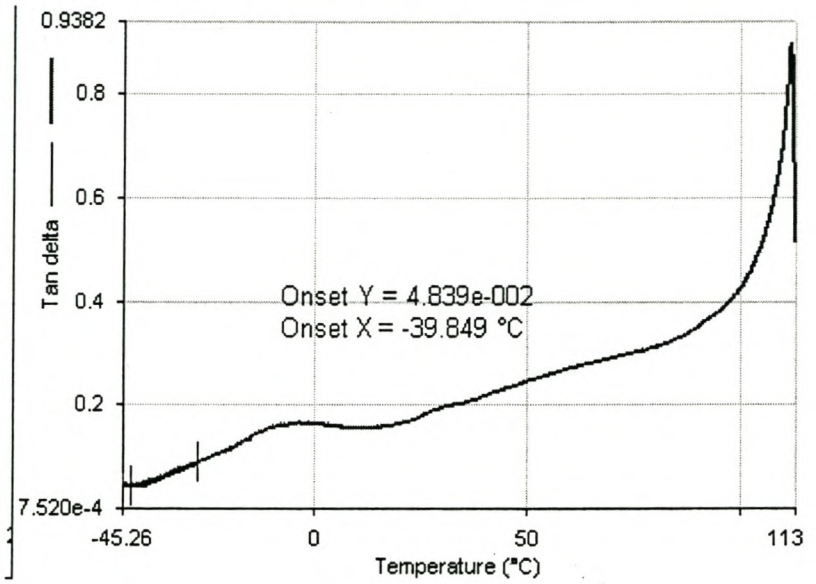

Propylene/1-heptene copolymer (B10, 7.58% 1-hept.)

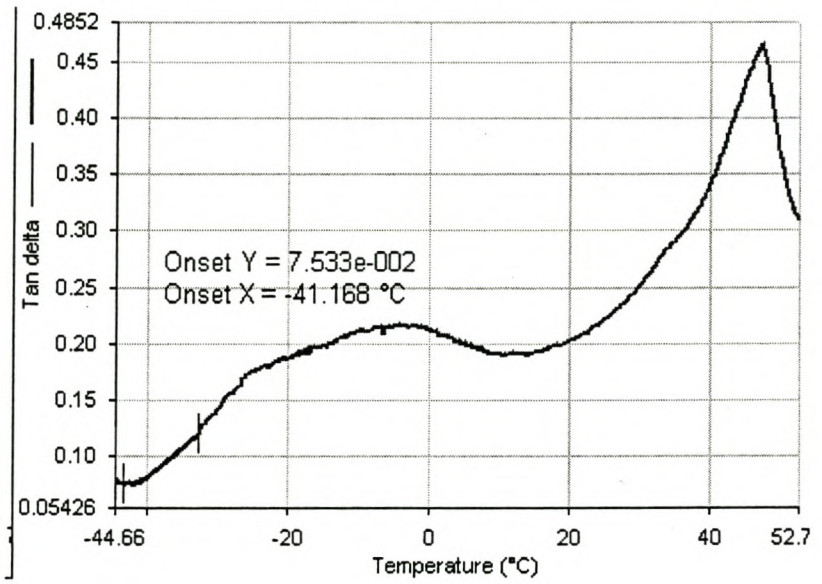

Propylene/1-heptene copolymer (Z1, ≈1.00% 1-hept.)

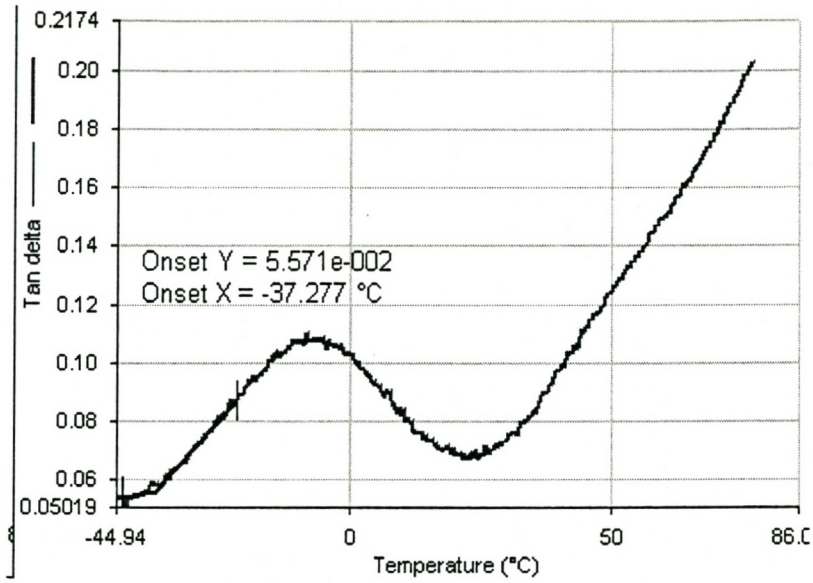

APPENDIX E
(CRYSTAF Spectra)

Propylene/1-hexene copolymer (A2, 1.20% 1-hex.)

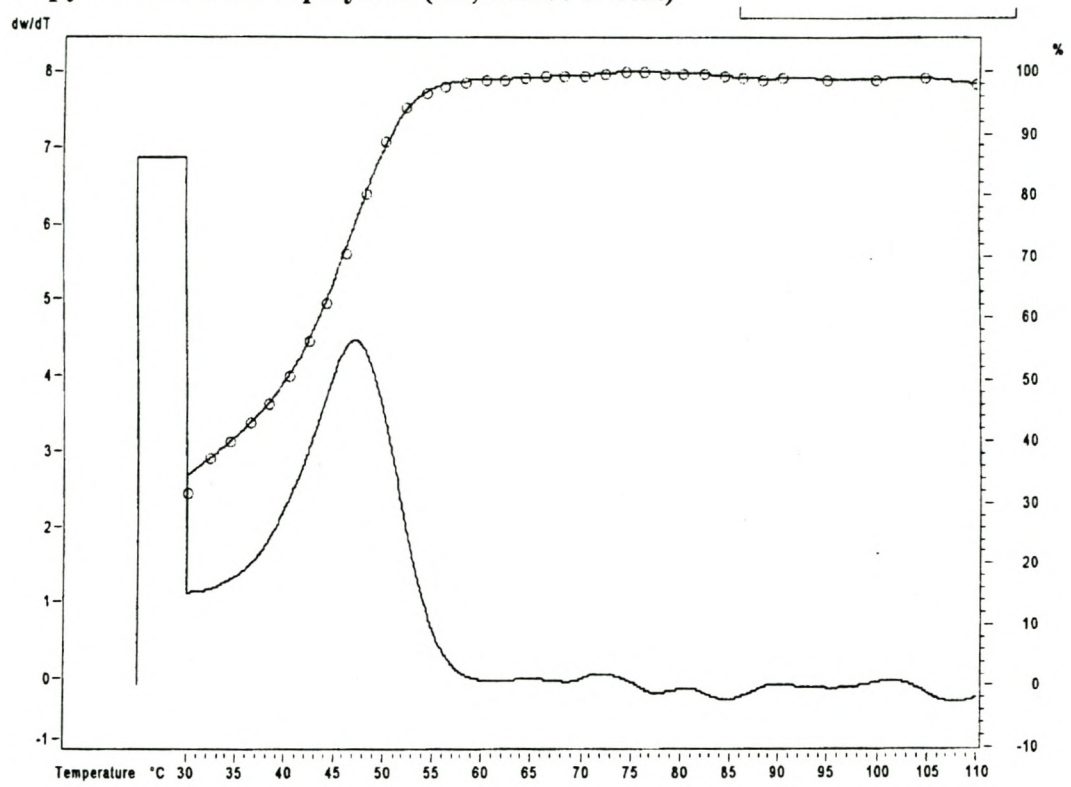

Propylene/1-hexene copolymer (A3, 2.51% 1-hex.)

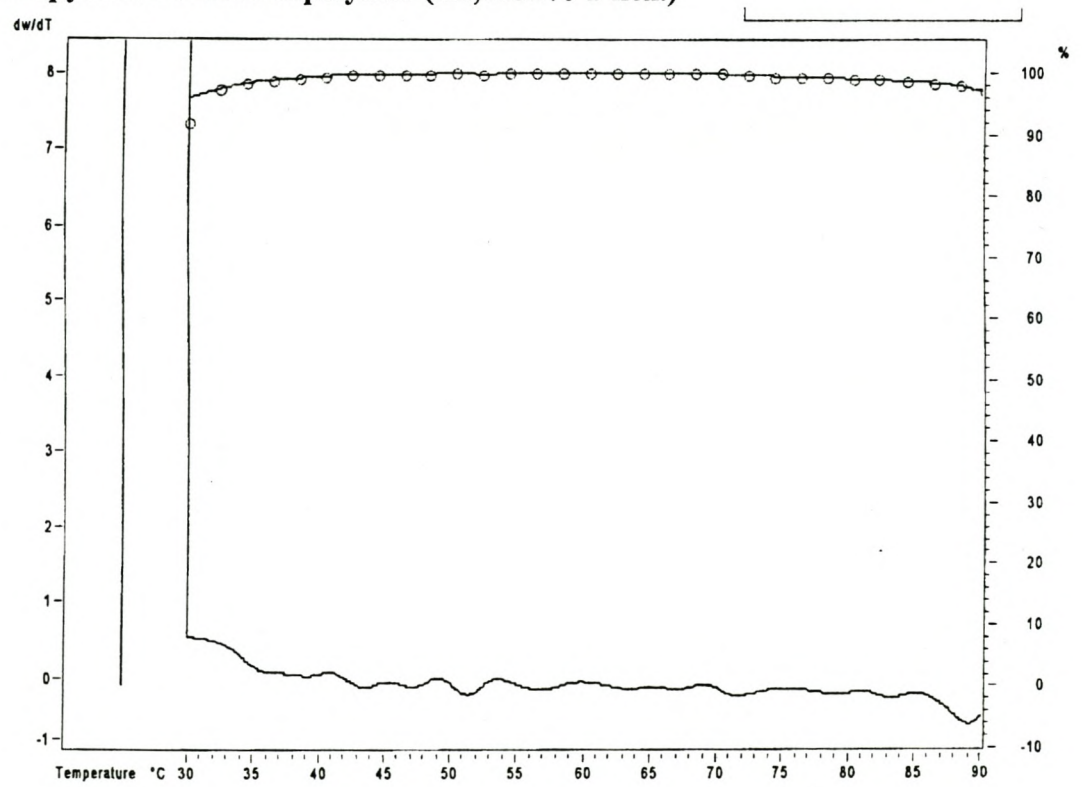

Propylene/1-hexene copolymer (A4, 3.53% 1-hex.)

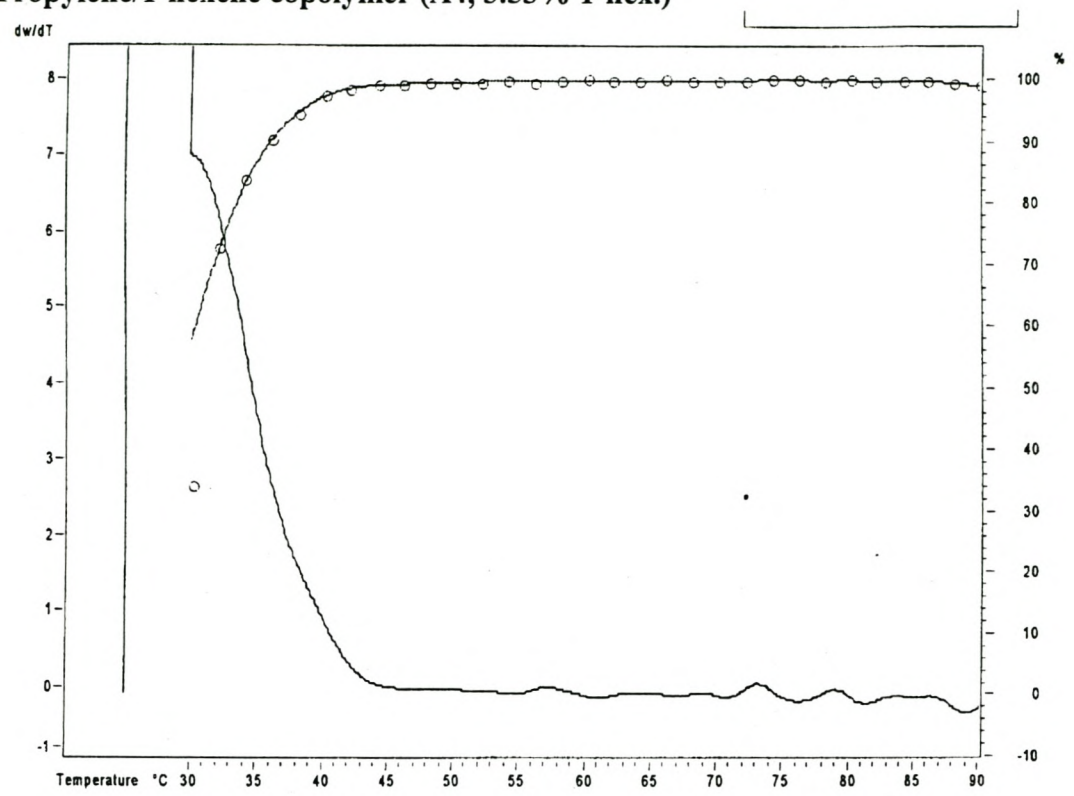

Propylene/1-hexene copolymer (A5, 4.10% 1-hex.)

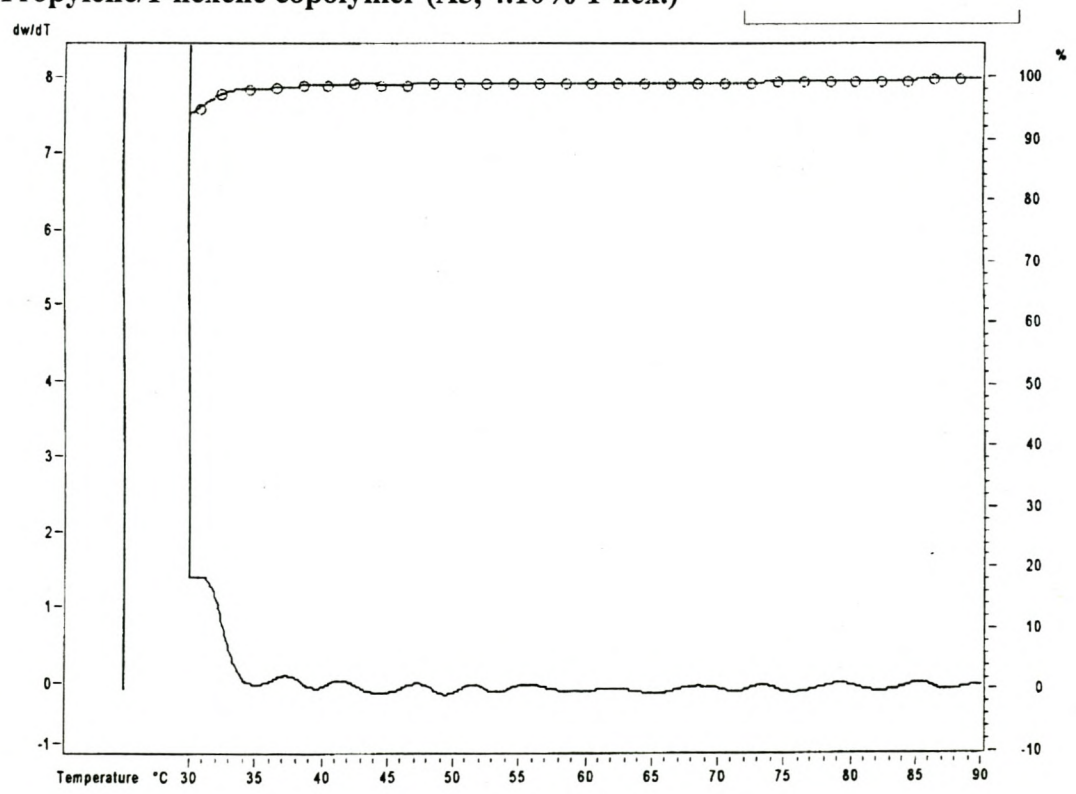

Propylene/1-hexene copolymer (A6, 6.36% 1-hex.)

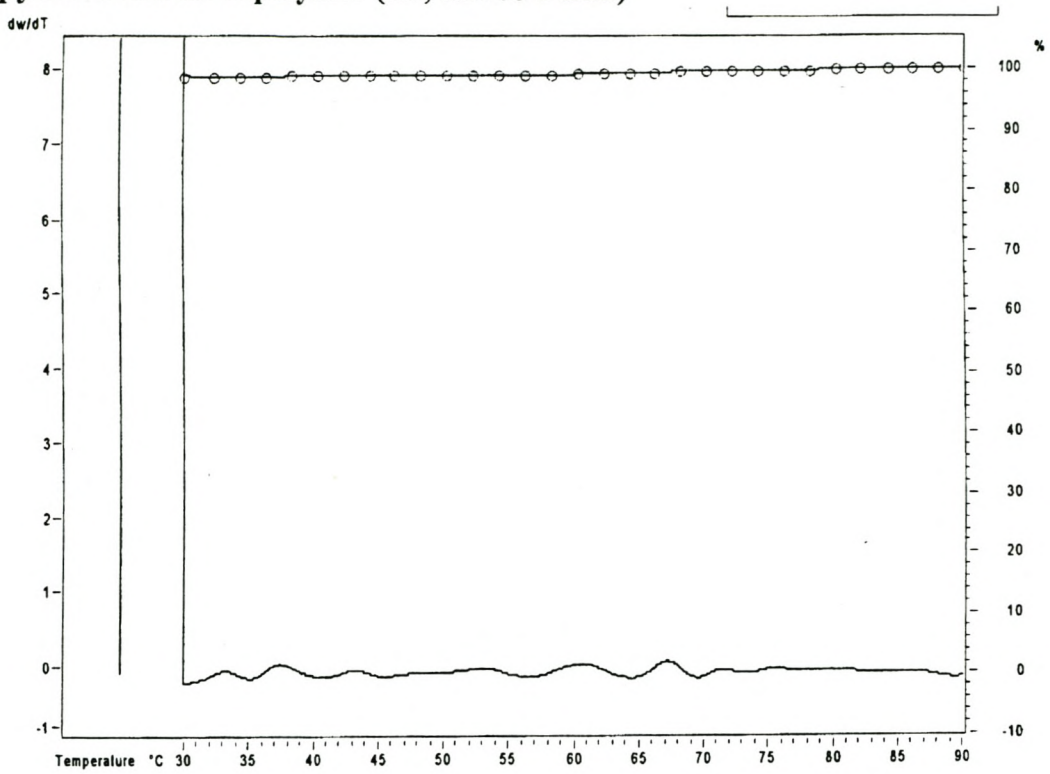

Propylene/1-octene copolymer (A7, 2.16% 1-oct.)

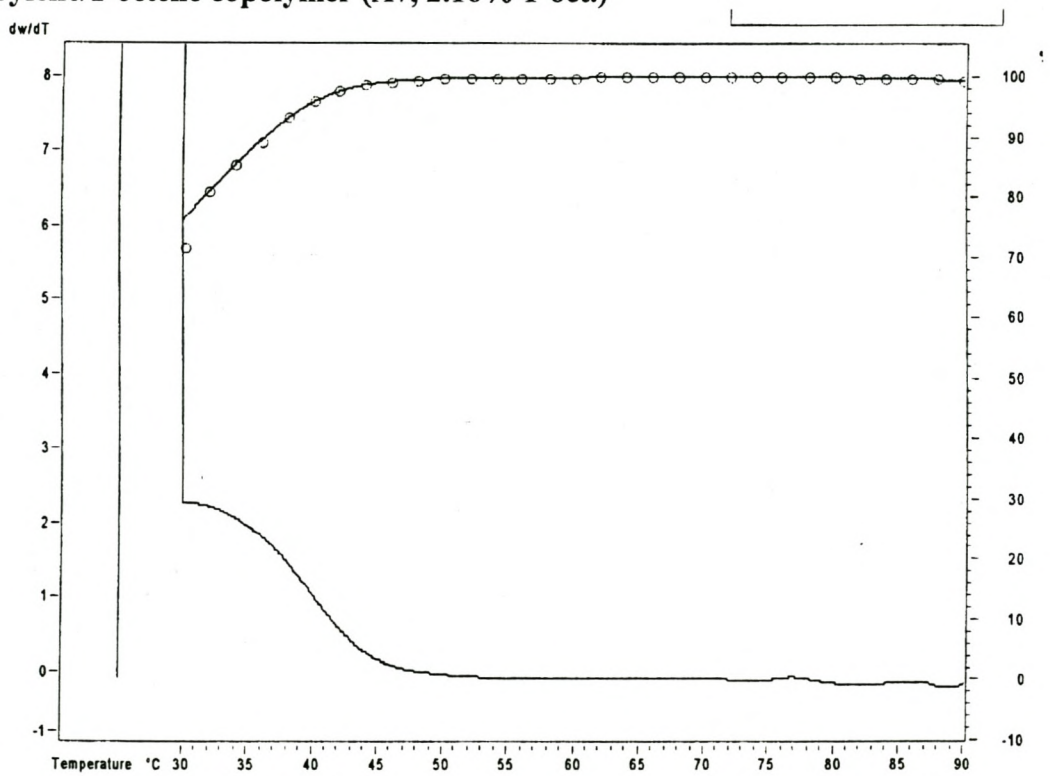

Propylene/1-octene copolymer (A8, 3.89% 1-oct.)

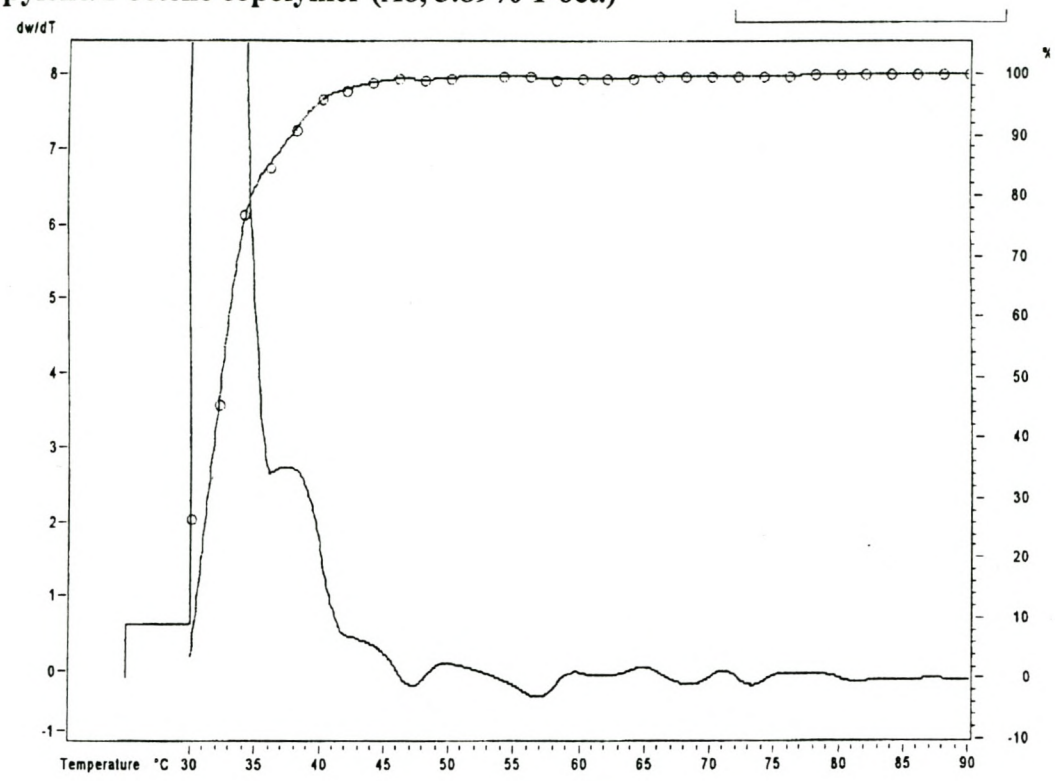

Propylene/1-octene copolymer (A9, 5.40% 1-oct.)

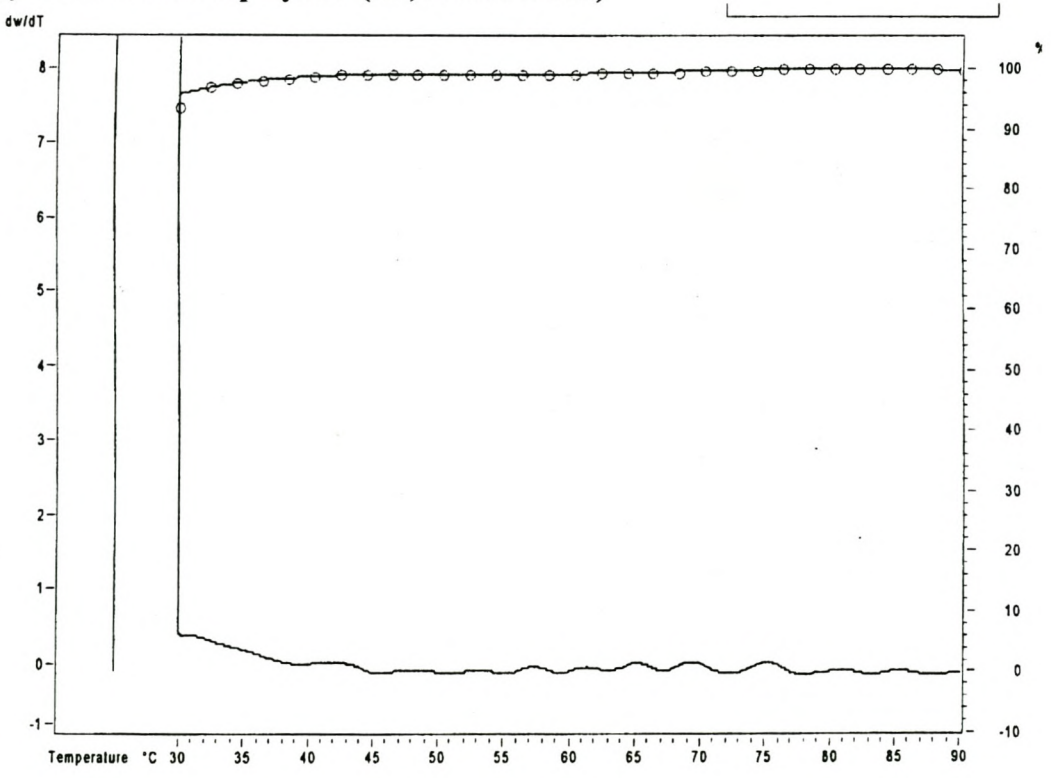

Propylene/1-octene copolymer (A10, 6.32% 1-oct.)

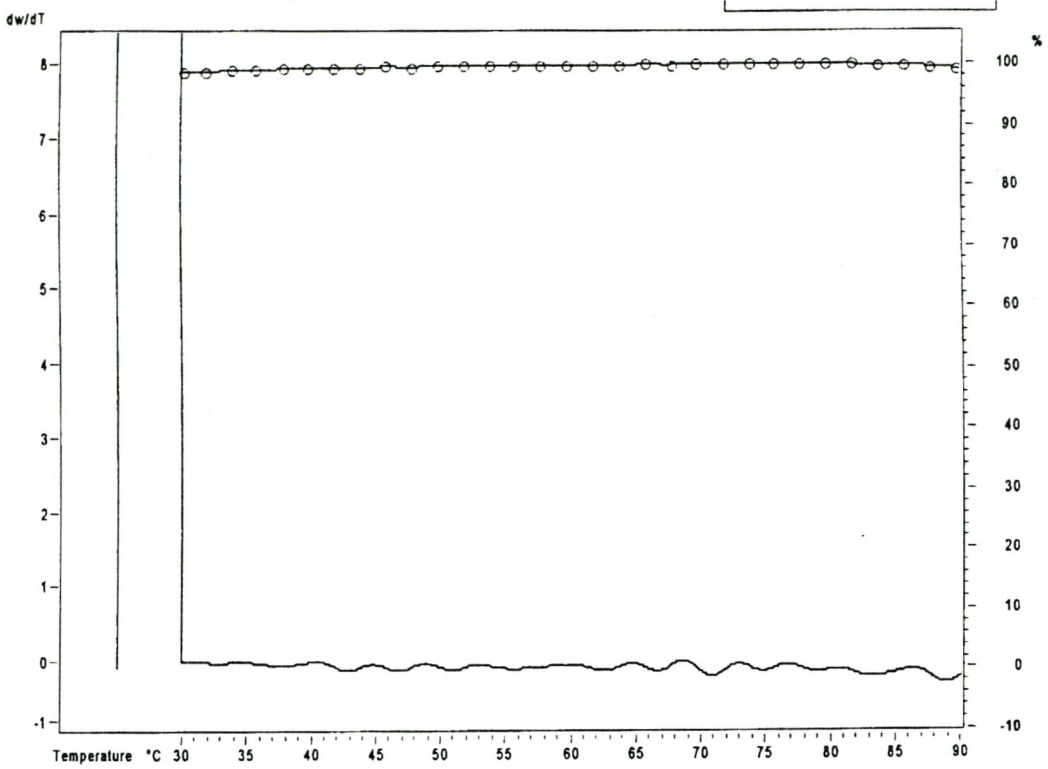

Propylene/1-octene copolymer (A11, 7.08% 1-oct.)

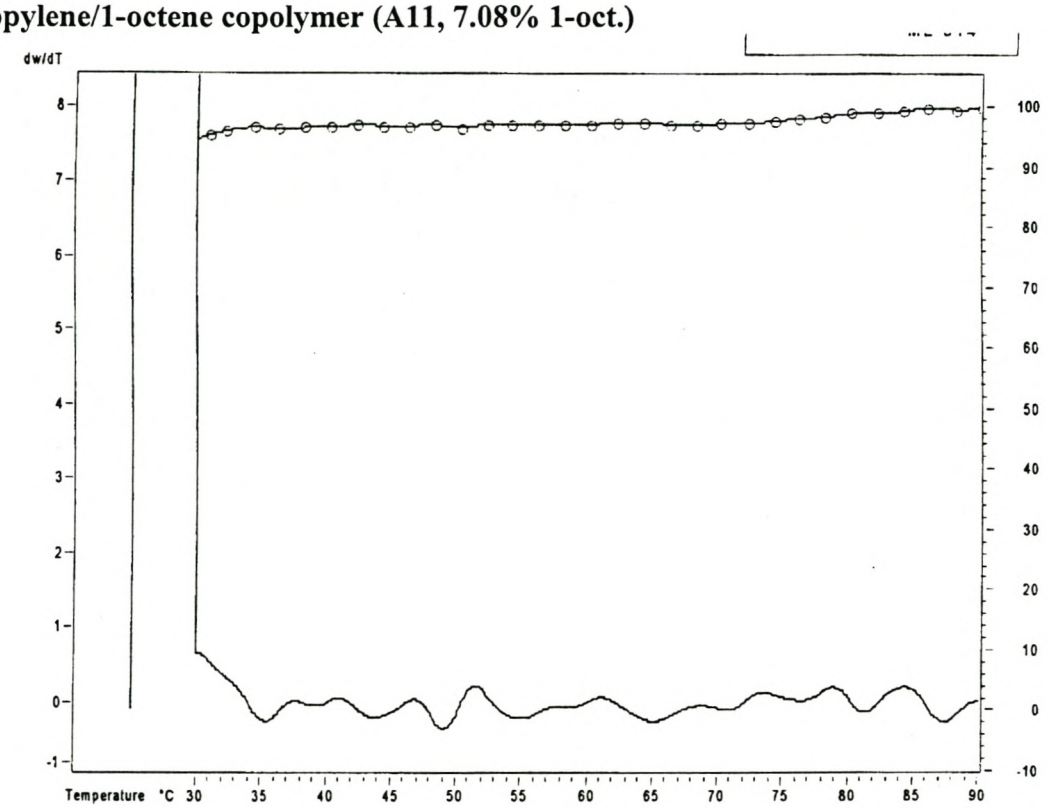

Propylene homopolymer (B1)

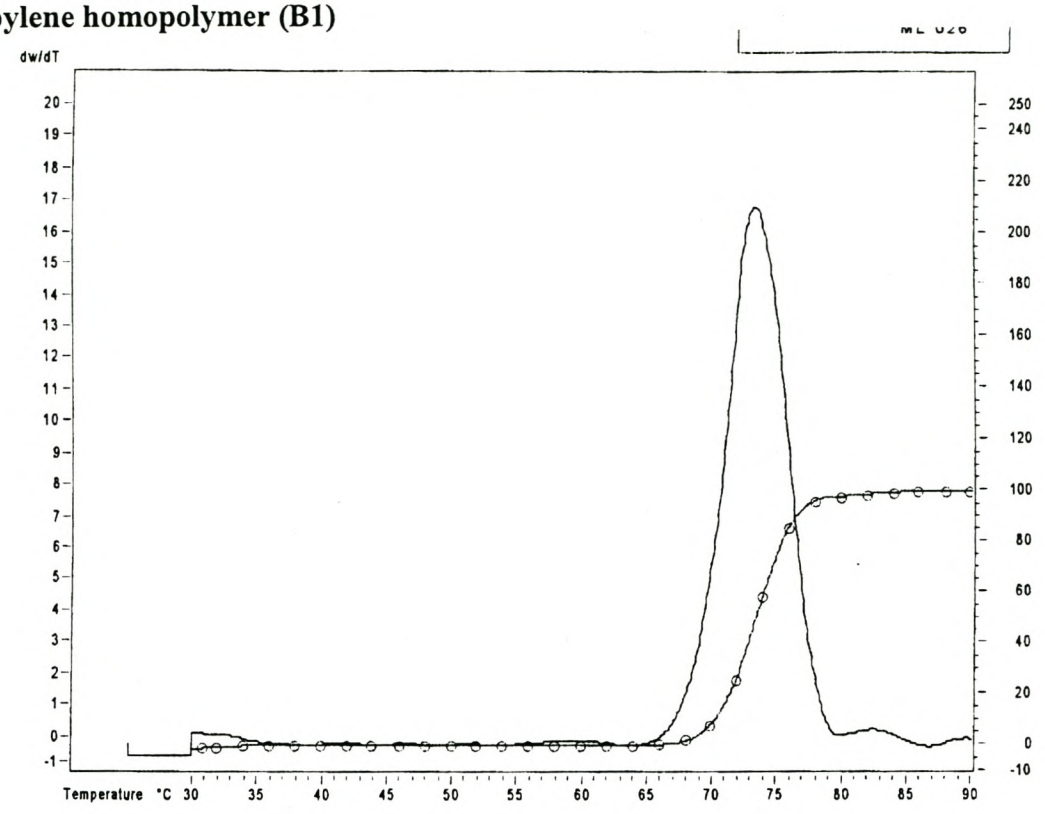

Propylene/1-hexene copolymer (B3, 5.73% 1-hex.)

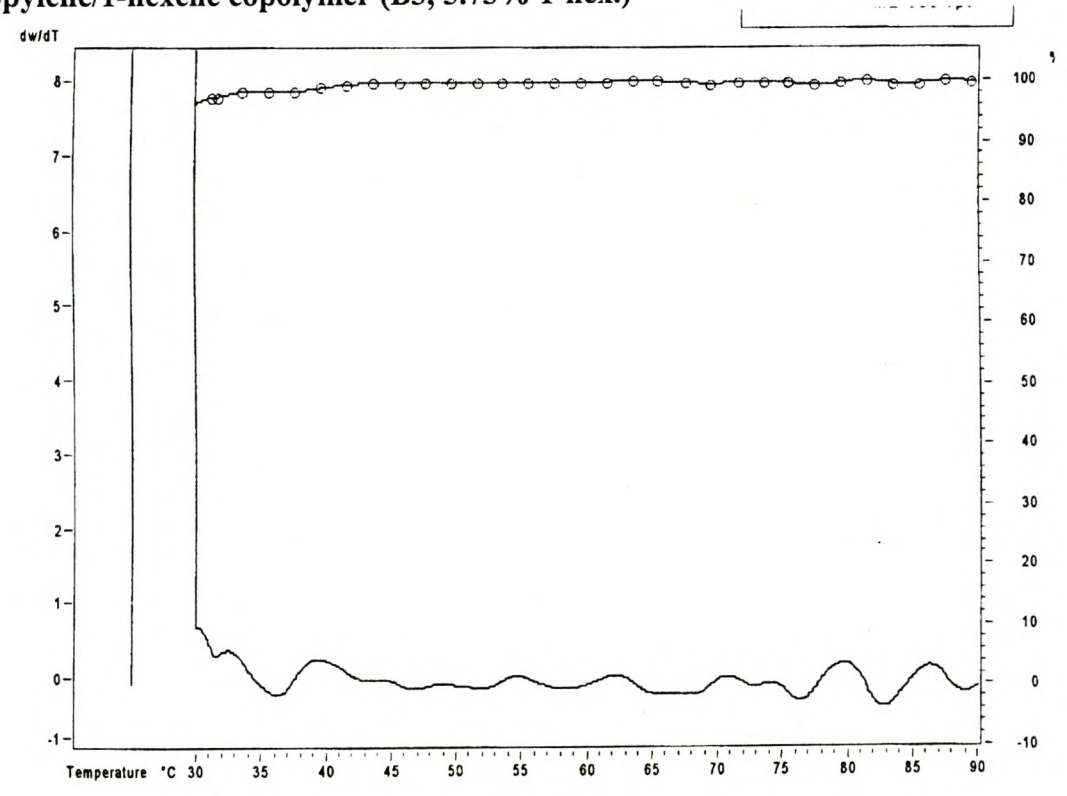

Propylene/1-octene copolymer (B4, 4.07% 1-oct.)

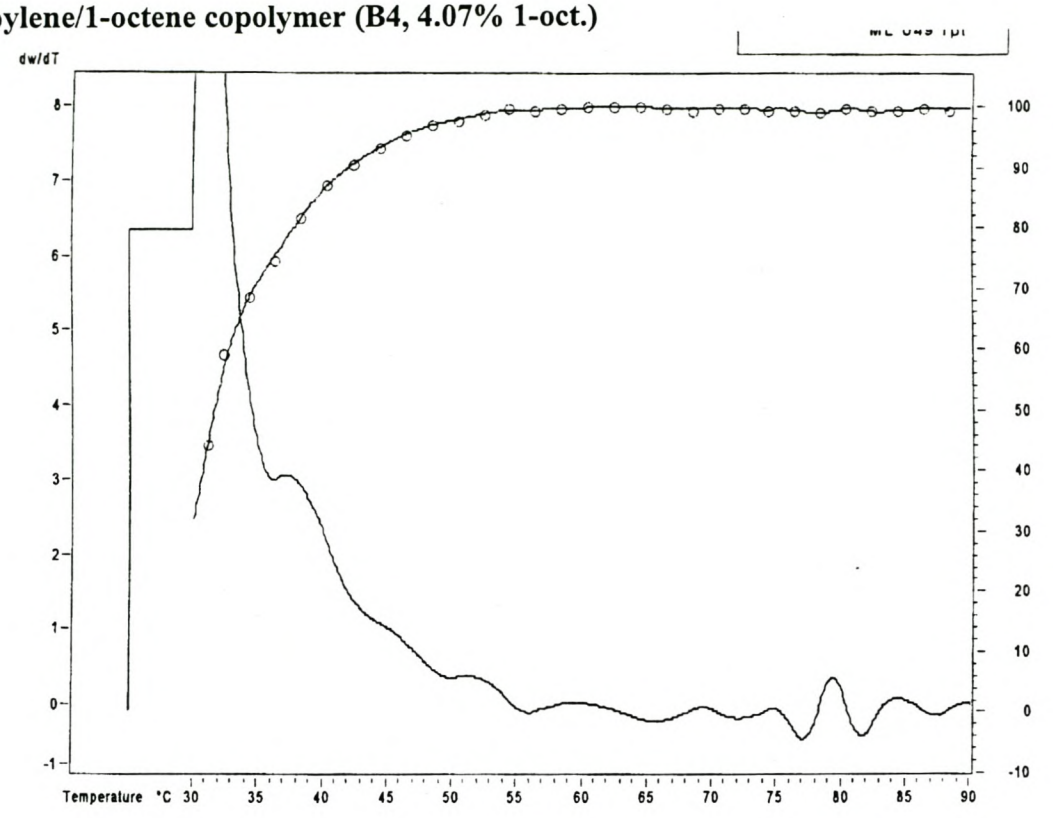

Propylene/1-heptene copolymer (B6, 1.03% 1-hept.)

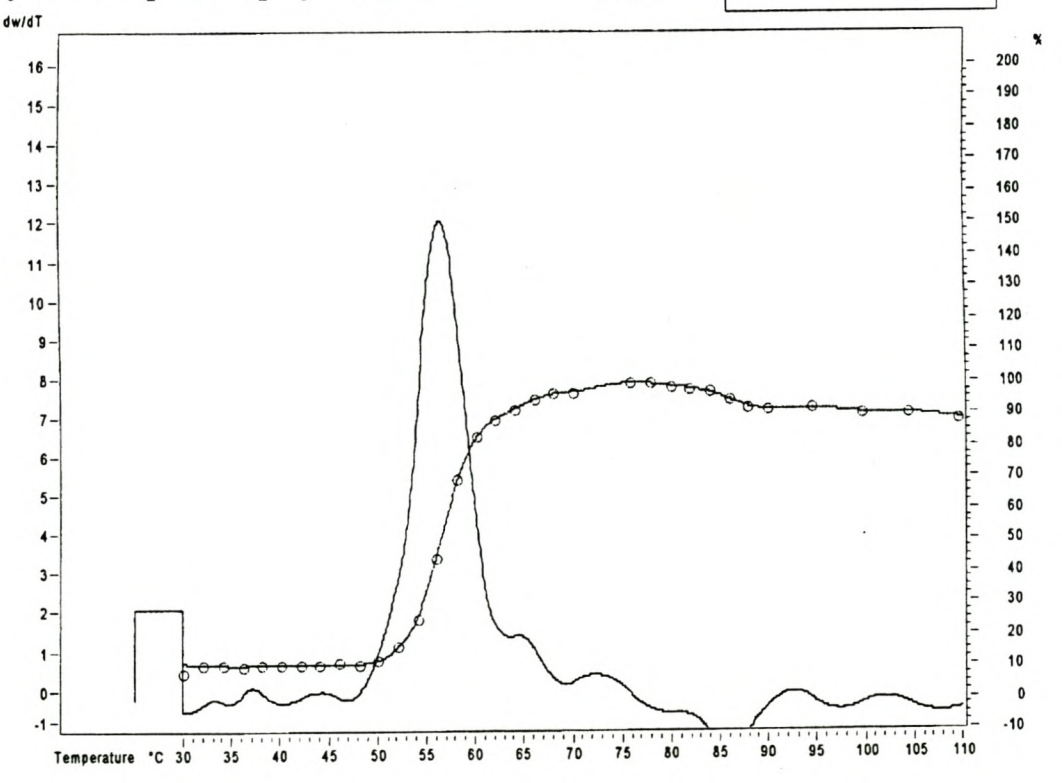

Propylene/1-heptene copolymer (B7, 3.98% 1-hept.)

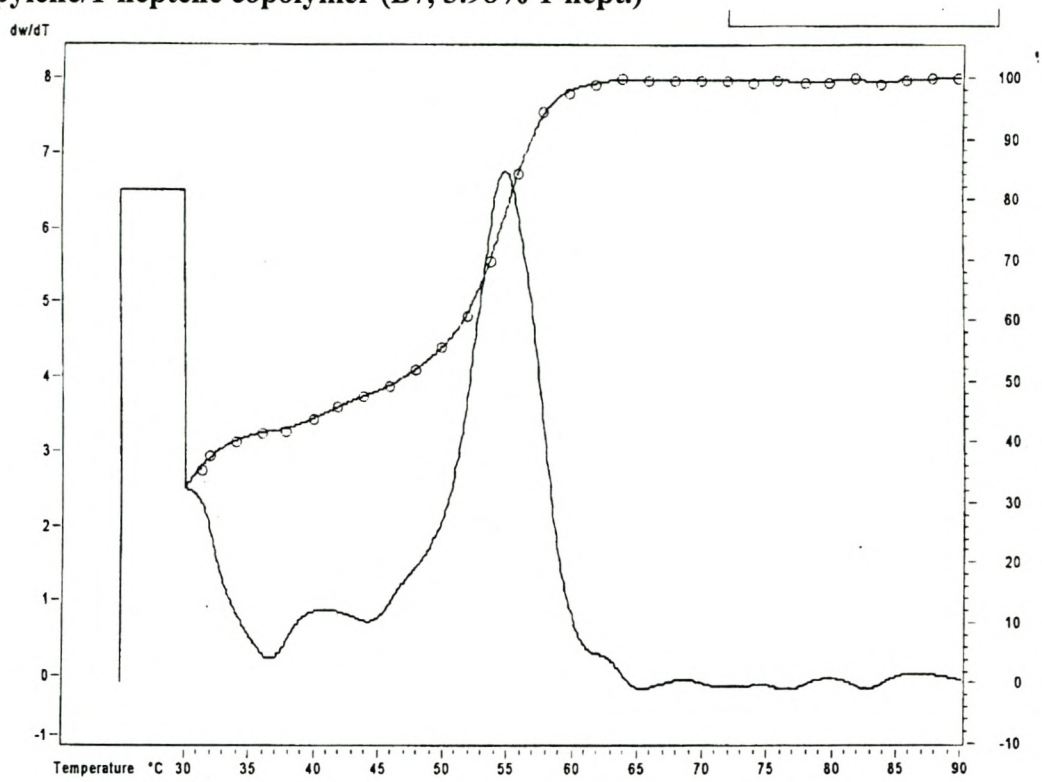

Propylene/1-heptene copolymer (B8, 5.19% 1-hept.)

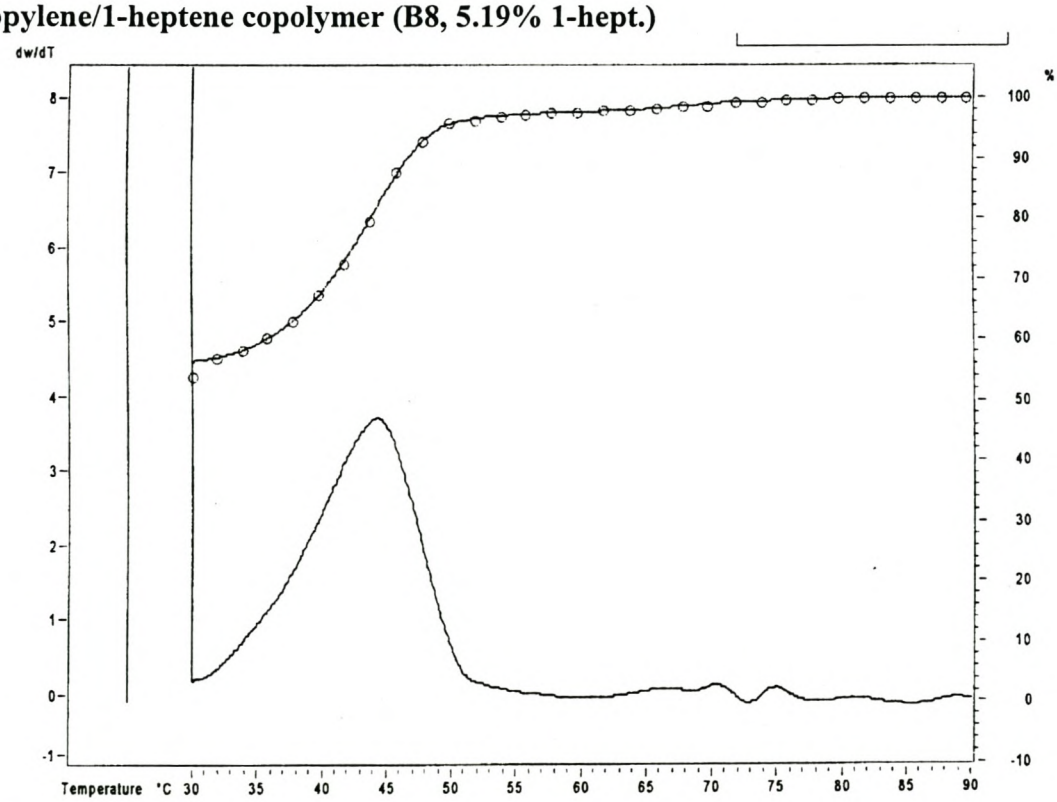

Propylene/1-heptene copolymer (B10, 7.58% 1-hept.)

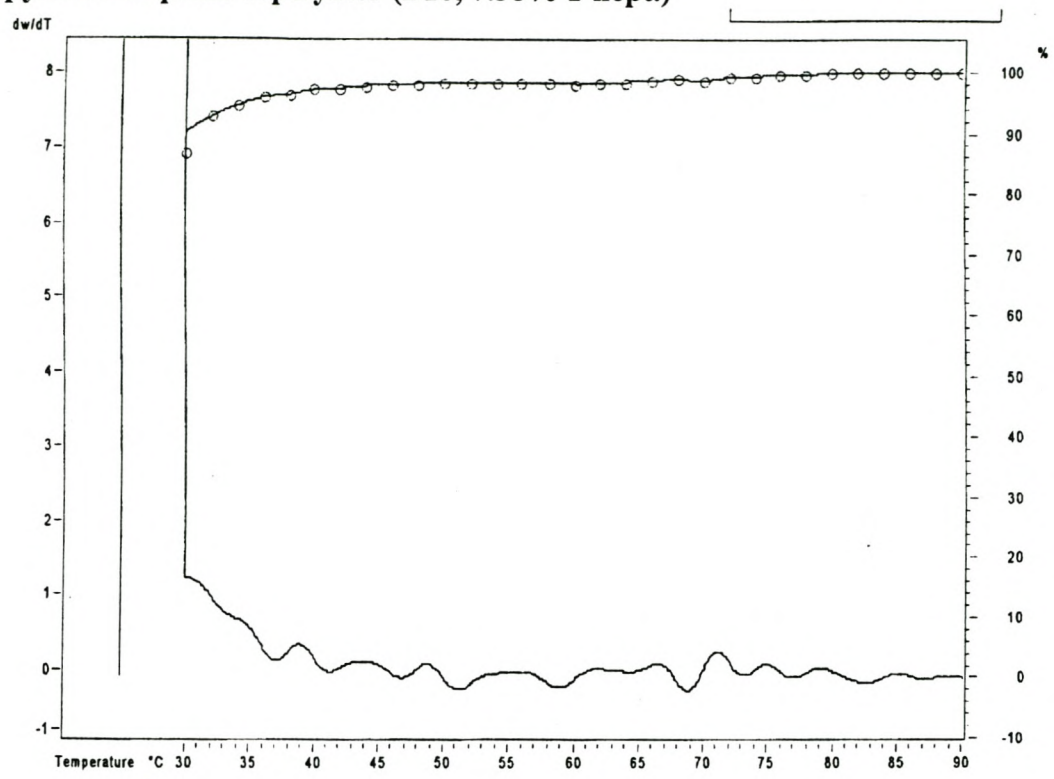

Propylene/1-heptene copolymer (Z2, 1.66% 1-hept.)